JOURNAL OF GEOPHYSICAL RESEARCH

The continuation of

ESTRIAL MAGNETISM AND ATMOSPHERIC ELECTRICITY

(1896-1948)

An International Quarterly

UME 56 June, 1951 NUMBER 2

CONTENTS

(Contents concluded on outside back cover)

PUBLISHED BY

THE WILLIAM BYRD PRESS, INC.

P. O. Box 2-W—Sherwood Ave. and Durham St., Richmond 5, Virginia

FOR THE JOHNS HOPKINS PRESS, BALTIMORE 18, MARYLAND

EDITORIAL OFFICE:

5241 Broad Branch Road, Northwest, Washington 15, D.C., U.S.A.

HREE DOLLARS AND FIFTY CENTS A YEAR SINGLE NUMBERS, ONE DOLLAR

JOURNAL OF GEOPHYSICAL RESEARCH

The continuation of

Terrestrial Magnetism and Atmospheric Electricity

(1896-1948)

An International Quarterly

Founded 1896 by L. A. BAUER *Continued 1928–1948 by* J. A. FLEMING

Fields of Interest

Terrestrial Magnetism
Atmospheric Electricity
The Ionosphere
Solar and Terrestrial Relationships
Aurora, Night Sky, and Zodiacal Light
The Ozone Layer
Meteorology of Highest Atmospheric Levels
The Constitution and Physical States of t Upper Atmosphere
Special Investigations of the Earth's Cru and Interior, including experimental seism waves, physics of the deep ocean and oce bottom, physics in geology
And similar topics

This Journal serves the interests of investigators concerned with terrestrial magnetism and el tricity, the upper atmosphere, the earth's crust and interior by presenting papers of new analy and interpretation or new experimental or observational approach, and contributions to int national collaboration. It is not in a position to print, primarily for archive purposes, extens tables of data from observatories or surveys, the significance of which has not been analyzed

Forward *manuscripts* to the editorial office of the Journal at 5241 Broad Branch Road, Northwe Washington 15, D. C., U.S.A., or to one of the Associate Editors. It is preferred that manuscri be submitted in English, but communications in French, German, Italian, or Spanish are a acceptable. A brief abstract, preferably in English, must accompany each manuscript. A *publi tion charge* of $4 per page will be billed by the Editor to the institution which sponsors the work any author; private individuals are not assessed page charges. Manuscripts from outside United States are invited, and should not be withheld or delayed because of currency restricti or other special difficulties relating to page charges. Costs of publication are roughly twice total income from page charges and subscriptions, and are met by subsidies from the Carne Institution of Washington and international and private sources.

Back issues and *reprints* are handled by the Editorial Office, 5241 Broad Branch Road, N. Washington 15, D.C., U.S.A.

Subscriptions are handled by The Johns Hopkins Press, Baltimore 18, Maryland, U.S.A.

THE JOHNS HOPKINS PRESS

Baltimore 18, Maryland

Entered as second-class matter at the Post Office at Richmond, Virginia, under the act of March 3, 1879.

Journal of

GEOPHYSICAL RESEARCH

The continuation of

Terrestrial Magnetism and Atmospheric Electricity

VOLUME 56 JUNE, 1951 No. 2

RESULTS OF SEISMIC OBSERVATIONS IN GERMANY ON THE HELIGOLAND EXPLOSION OF APRIL 18, 1947

BY H. REICH, O. FOERTSCH, AND G. A. SCHULZE

Institut für Angewandte Geophysik der Universität, München, and Gewerkschaft Brigitta, Hannover, Germany

(Received February 12, 1951)

ABSTRACT

Seismic recording of the Heligoland explosion of April 18, 1947, provided important evidence on the structure of the continental shield, especially so since the region of the German bay around which most of the stations were located is well defined geologically. The depths and velocities of the three layers are discussed and comparisons are made with the interpretations of others. The velocities of the seismic waves inferred from the summarized observations are 5.4 km/sec in the upper layer (granitic), 6.18 and 6.6 km/sec in the middle layer (gabbroic), and 8.32 and 8.19 km/sec in the lowest one (peridotitic). The observational data indicate the discontinuous character of the stratification of the crust; that the granitic and gabbroic layers are not horizontal but variable in depth. When consideration is taken of possible factors involved, such as non-uniform elastic properties of the sedimentary layer and inclination along profiles, a more uniform depth is found.

British military authorities made arrangements for the geophysicists in Western Europe to observe the seismic effects of the Heligoland explosion. In this paper, the observations in Germany shall be discussed, and the results derived by several authors shall be compared.

FIG. 1—Map of German stations where readable seismograms of the Heligoland explosion were obtained.

Figure 1 shows a map of the stations. At Göttingen, Leipzig, Jena, and Stuttgart, the station instruments were used, some of them with increased magnification by optical registration. The other stations were temporary field-stations, equipped

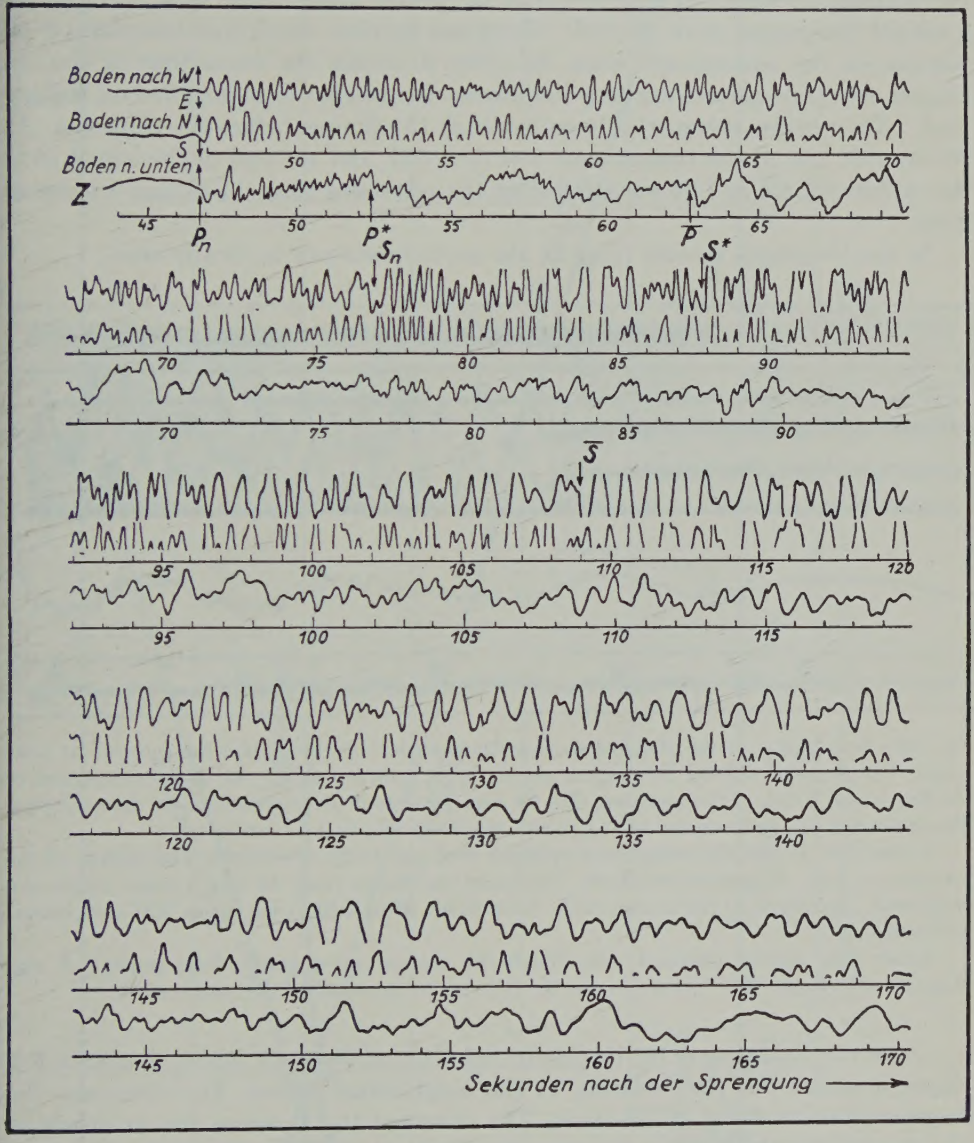

FIG. 2A—Seismogram of the Heligoland explosion recorded by the station instruments at Göttingen. Tracing of the complete records of the 17-ton pendulum, components EW and NS, and of the vertical Z-pendulum. Times are counted from the explosion instant.

with small transportable vertical seismographs. Of the 17 field-stations equipped by the Geophysikalisches Institut of Göttingen, 13 had the Wiechert-Angenheister type of instrument, three had piezoelectric acceleration recorders built by Electro-

akustik (Kiel), and one Geophones (carbon microphones of Siemens, Berlin). The firm Seismos (Hannover) observed at four stations with Mintrop pendulums, and the Gesellschaft für praktische Lagerstättenforschung (Hannover) recorded at two stations with dip coil receivers after Dr. Zettel. Exact times were provided by a special time-signal from the BBC European Service, which was recorded by all stations on the seismograph films. In order to obtain the exact time of the explosion, two transmitters working on different frequencies were installed on Heligoland. They began automatically to transmit 15 minutes before the explosion. At Altenwalde, one of the transmitters was recorded, and the end of the signal gave the explosion time as 1.61 seconds before the scheduled time, 11 o'clock Universal Time.

In the Göttingen records (Fig. 2), the main onsets can be clearly seen.

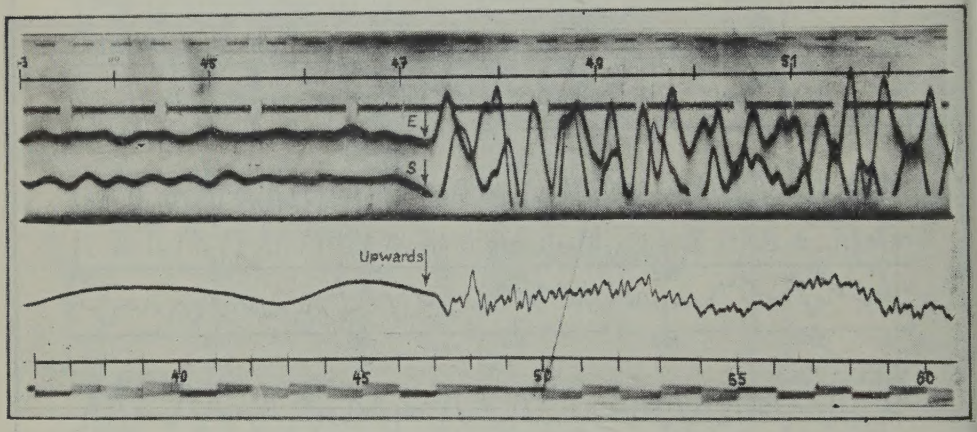

FIG. 2*B*—Seismogram of the Heligoland explosion recorded by the station instruments at Göttingen. Photographic copy of the original photographic records to show the distinct character of the first onset. Width of the recording film 60 mm. Time-scale gives seconds after the explosion. The upper film ran with a speed of 31 mm/sec, the lower film with 11 mm/sec.

Upper film: Horizontal components recorded with the 17-ton pendulum. Free period of the pendulum 1.4 sec. Magnification 60,000. The upper film shows, from the top, 1/5-sec marks of a clockwork, 1-sec marks of the station clock, 1-sec marks of the BBC transmitter, EW-component, NS-component.

Lower film: Record obtained with Wiechert's vertical seismograph. Free period 4.5 sec. Magnification 45,000. The film shows also the time-marks (seconds) of the station clock.

From the discussion of the records by Schulze and Foertsch (abbreviated S.a.F.), Figure 3 shows the part relating to the longitudinal waves. For clearness, the diagram shows reduced travel-times. The onsets of the P_n wave are, at distances of over 100 km, the first to arrive; on the whole profile, they fit well two straight lines, corresponding to velocities of 8.32 and 8.14 km/sec, and intersecting near Göttingen. Comparing with the results of the Haslach explosion in the Black Forest, agreement is reached by assuming that the velocity in the peridotitic layer is about 8.2 km/sec, and that this layer is nearly horizontal in northwest Germany. Appreciable deviations from the straight lines occur for the stations of Westerholz (96.5 km) and Jübeck (106.3 km); the waves arrive too early. These two stations

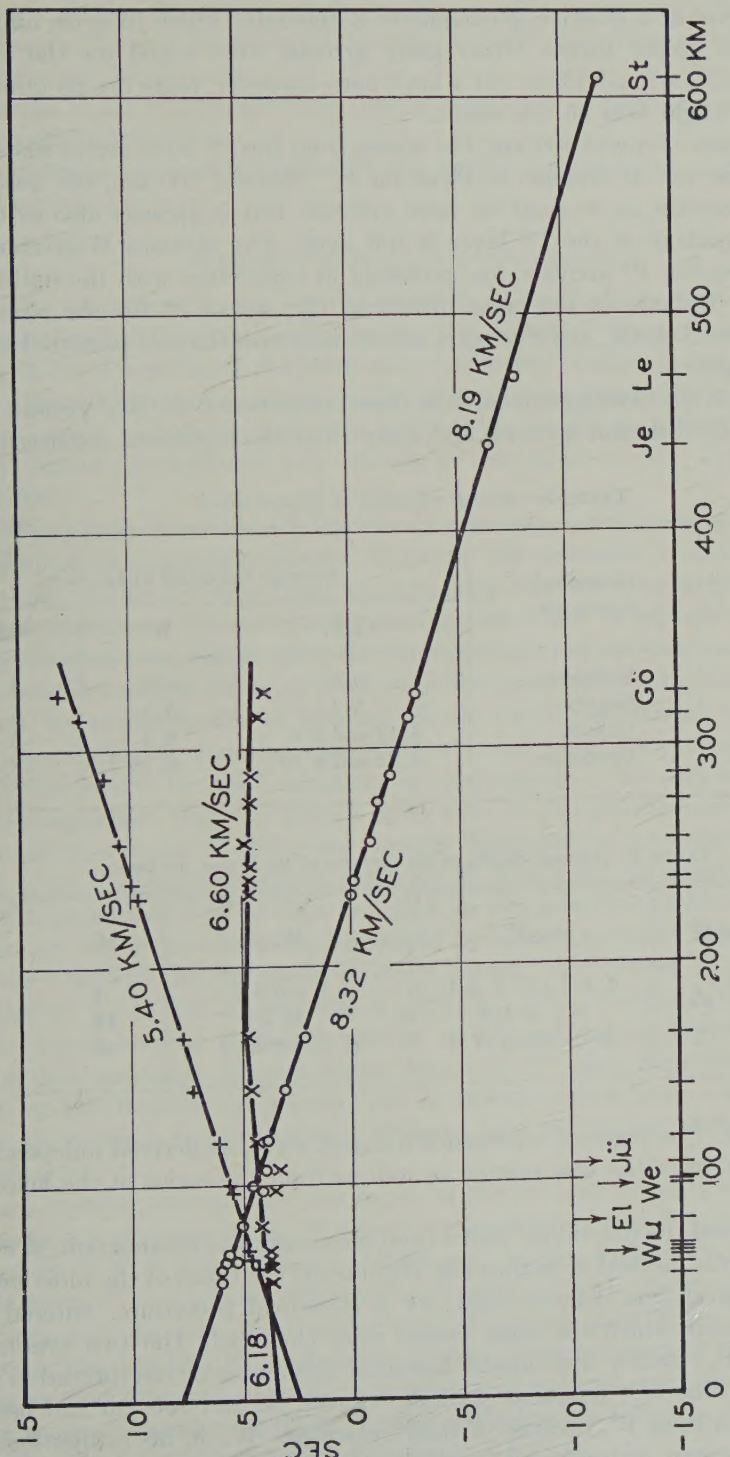

FIG. 3—Reduced travel-time curves of the longitudinal waves for the Heligoland explosion. [Reduced travel-time] = [Measured travel-time] minus [Distance/6.5 km/sec].

lie in the region of a positive geomagnetic Z-anomaly, which likewise hints at a local uplift of deeper layers. Other early arrivals were noted for the stations Wurfreihe (65.7 km) and Ellens (81.4 km); here, however, there are no other facts known which might bear on this result.

To a distance of about 100 km, the onsets from the P* layer arrive first. Their travel-times are not as uniform as those for P_n . Beyond 100 km, the onsets are somewhat uncertain, as is usual for later arrivals. But it appears also as though the upper boundary of the P* layer is not even. The stations Westerholz and Jübeck show earlier P* arrivals, too, probably in connection with the uplift mentioned above. Because of the great distances, the onsets P* for the permanent stations of Jena, Leipzig, and Stuttgart are so uncertain that we preferred to omit them from Figure 3.

According to the Göttingen records in three components, the first ground movement was in the direction upward, and away from the explosion, consistent with

TABLE 1—*Average velocities of seismic waves*

Onset	Geological description	Average velocities in km/sec		
		S.a.F.	W.	M.
(1) P_s	Sediment	3.6	4.4	3.5
(2) P_g	Granite	5.4	5.5	5.2
(3) P^*	Gabbro	6.18 and 6.6	6.5	6.4
(4) P_n	Peridotite	8.32 and 8.19	8.18	8.1

TABLE 2—*Average depths of the surfaces of the layers (in km)*

Onset	S.a.F.	W.	M.
(1) P_g	6 ± 1 and 5 ± 1	5.9 and 6.7	4
(2) P^*	9.3 ± 1.5	14.2	13
(3) P_n	26 ± 2 and 27.4	27.4 and 29.9	28

a push (Fig. 2). The angles of emergence for each wave, as derived independently from the direction of the first motion as well as from the ratios of the velocities, agree well.

S.a.F. followed the individual waves from seismogram to seismogram. Willmore applied a different method of evaluation. He entered the times of the most marked onsets in a travel-time diagram and, by a statistical procedure, entered such straight lines near which the most onsets were clustered. The two evaluations agree well for P_n , mostly first onsets. Essential differences of interpretation occur for P_g and P*. The first onsets at stations between 50 and 100 km had been interpreted by S.a.F. as P*, because of their velocities. W., in his evaluation, considered non-German stations and, particularly, observations near Soltau in the

Lüneburger Heide, and arrives at the conclusion that those onsets are P_g waves. He evaluates P* waves for more distant stations only, but does not mention them in the main part of his paper.

Mintrop, in his papers, gave the depths calculated by him, without details as to the method applied.

The geologist is most interested in the depths for the layers calculated from these observations.

Discussion of the depth determinations

(1) The agreement is best for the depth h_n of the P_n layer (peridotitic). This is the most essential and important result of these rather exact observations. The velocity in the lowest layer is known most accurately; intercept times can, therefore, be derived with great certainty. The average velocities in the covering layers are also known sufficiently well; the results with regard to h_n differ little when different values for thickness and velocity in the layers for P_s, P_g, and P* are considered.

(2) The depth h^* of the P* layer is known with less certainty, the more so since Willmore's evaluation throws doubt on the existence of that layer. Geophysical occurrence of gradual data must be supplemented by geological considerations; the transitions between granite and gabbro must be regarded as an established geological fact. But it must not be forgotten that the great mass of known plutons and crystalline slates have elastic properties approaching those of granite, and that the predominance of basaltic effusions in the vulcanites occurring near the surface indicates that the masses below, from which they come, are mostly of gabbroid nature. Detailed variations in the chemism or the mineral content are here less important than the known mass ratio of the granitic and the gabbroic groups. In fact, rocks of these two families dominate in the composition of the earth's crust. For the integrating methods of geophysics, it is less important to stress the transitions, real as they are, than to recognize the depth region of these two groups, which are distinctly separated by their velocities. This statement is definitely supported by the observations of natural earthquakes, in which the two velocities of 5.5 to 5.6 km/sec and 6.5 km/sec occur. Similarly, the Heligoland records permit keeping these two groups of 5.5 and 6.5 km/sec separated with more or less certainty. Intense onsets from the P* layer occurred again in the records of the Haslach detonation, and of recent quarry blasts near Würzburg. They proved again the pronounced division, into two layers, of the crust below the sediments.

It is, however, certain that the depth of the P* layer is quite different at the various points of observation. Wiechert, Angenheister, and Brockamp found an average depth $h^* = 8 \pm 2$ km near Göttingen. In the northwest profile of Soltau, we calculated $h^* = 6.35$ km. The Haslach detonation led to the much bigger depth of 18 km, and the new observations near Würzburg gave $h^* = 4.5$ km. These changes in the depth of P* may also be inferred from gravimetric results, as Willmore does, and the great magnetic anomalies will have no other reason. In a deep bore-hole near Johannisburg (East Prussia), drilled to find the cause of the magnetic anomalies, these rocks were found in a depth of 1.2 km.

All this shows that the surface of the P* layer is not horizontal, but variab in depth, just as S.a.F. considered probable. This again entails that velocitie inferred from summarized observations along profiles or in areas may show a parent changes in velocity due to inclinations. This should be taken into accou with all depth determinations. Assuming uniform velocities in the layers P_g an P*, the depths given by S.a.F. appear most probable. Thereby, the smaller depth of the P* layer must be considered as proved, of 5 to 6 km in Schleswig-Holste (and in Denmark, too), of 6.35 km under the magnetic anomaly of Sittensen t the south of Hamburg (Soltau records), and of 8 ± 2 km near Göttingen.

(3) The difficulties discussed for P* are similar for P_g. For reasons given belo the depths given by Willmore seem, to us, to refer to other boundary layers tha that geologically defined as granite or crystalline (basement). As W. remark these determinations are made difficult by the lack of seismic stations within distance of 50 km from Heligoland. However, that region of the German ba around which most of the observations were made is well known, not only fro seismic observations, but also from many borings, two of which were more tha 3.8 km deep. From these data, a mean velocity in the sedimentary layer down t about 6 km can be deduced—3.5 km according to Mintrop and Reich, 3.6 k according to S.a.F.

In that connection, it must be remembered that the sedimentary layer is no composed of layers of uniform elastic properties. Over short distances, these layer will show with their individual velocities. For greater distances, each layer wit high velocities, by wedging out or by tectonic disturbances, will act as though i is interrupted, so that an average velocity for the whole sedimentary layer wi be effective. Below northwest Germany, there are at least two, perhaps even thre layers of sediments with velocities over 5 km/sec, which, considered by thei velocities, may be mistaken for the upper boundary of the granite; namely, th Upper Cretacean (limestone), the "Muschelkalk" in the Triassic, and the Permia with its great deposits of anhydrite and salt. These layers are certainly interrupte near the mouth of the Elbe River. On the other hand, the uninterrupted conductio of seismic waves in the Permian appears possible toward the Netherlands an toward Denmark. The extent of the sedimentary sheets cannot be given wit certainty.

If this fact is taken into account and the velocities calculated by us for th covering layer are assumed, a much more uniform depth of the crystalline is foun for the whole region of observation. The observations around Soltau, obtained i rather small distances, may show onsets from the Cretacean, the "Muschelkalk, and the Permian, all belonging to the level of the sediments, but possibly observe with velocities which, for longer distances, are observed in the granite only. those onsets are ascribed to granite, a much too small depth for that layer obtained. This seems to have occurred in W.'s calculations for the west profile Soltau; the well-known geological results are incompatible with such small dept as 2.8 or 3.3 km for the upper boundary of granite. That depth can only be inte preted as the upper boundary of the Permian; our own calculations lead to th true depth of the crystalline in about 5 km.

Likewise, the very small depths (-0.9 and 3.2 km) for Denmark and par

of Schleswig-Holstein must be explained otherwise, since the results of deep borings are quite inconsistent with such depths. The smaller travel-times actually observed there lead, with a schematic evaluation and use of a uniform velocity as for stations with normal granitic basis, to smaller depths. But such extremely high situations of the granite give less likely explanations of these small travel-times than the higher situation of the P* layer (gabbroic), which is proved by the high observed apparent velocities. Our calculations for that region gave a depth of the gabbroic layer of 5 to 6 km, which, however, may be covered by a granitic layer of unknown thickness.

With respect to later arrivals, we do not share the conception of Mintrop (1949), who—particularly in the records of the station Wurfreihe (66 km distant from Heligoland)—believes he recognized reflections from deeper parts of the earth's crust, coming from a plastic layer (magma). In another paper (1947), Mintrop believes he traced the transition of the solid into the liquid phase at four further depths—170, 350, 410, and 610 km. This hypothesis appears to us not well established. Since the Heligoland explosion has not been recorded with reflection apparatus, the apparent velocities of the onsets which Mintrop interprets as reflections cannot be given with certainty. From the observed times and the distances from Heligoland, an average velocity of about 1.43 to 1.53 km/sec is obtained—of the order of longitudinal waves in water. Since most of the distance between Heligoland and these stations lies across the North Sea, these onsets may perhaps be conceived as due to waves which had run near the surface, and mostly in water. The seismogram of Wurfreihe, on which Mintrop bases his theory, exhibits friction of the seismograph, which explains the form of the onsets considered by Mintrop. Those onsets are not shown in the records of stations near Wurfreihe either.

The contributions of Gutenberg and Richter which Mintrop cites in support of his views are based on a much more extended material. We regard these papers as essential discussions on the problem concerned, although we believe that they may not yet be valid for the whole earth.

LITERATURE

Brockamp, B. Seismische Beobachtungen bei Steinbruchsprengungen. Zs. Geophysik, Braunschweig, **7**, S.295 (1931).

Brockamp, B., and K. Wölcken. Bemerkungen zu den Beobachtungen bei Steinbruchsprengungen. Zs. Geophysik, Braunschweig, **5**, S.163 (1929).

Charlier, Ch. Premiers résultats des observations séismologiques faites à Uccle de l'explosion d'Heligoland (1947).

Mintrop, L. Göttingen, Nachr. Akad. Wiss., Math.-Phys. K1 (1947).

Mintrop, L. Geophysics, **14**, 321-336 (1949).

Reich, H. Geologische Ergebnisse der seismischen Beobachtungen der Sprengung auf Helgoland. Geol. Jahrb., Hannover/Celle, **64**, 243-266 (1950).

Reich, H., G. A. Schulze, and O. Förtsch. Das geophysikalische Ergebnis der Sprengung von Haslach im südlichen Schwarzwald am 28. und 29. April 1948. Geol. Rdsch., **36**, 85-95 (1948).

Schulze, G. A., and O. Förtsch. Die seismischen Beobachtungen bei der Sprengung auf Helgoland am 18.April 1947 zur Erforschung des tieferen Untergrundes. Geol. Jahrb., Hannover/Celle, **64**, 204-242 (1950).

Visser, S. W., and J. Veldkamp. De Nederlandse Waarnemingen van de Explosie op Helgolan Hemel en Dampkring.

Wiechert, E. Seismische Beobachtungen von Steinbruchsprengungen. Zs. Geophysik. Braun schweig, 5, S.159 (1929).

Willmore, P. L. Seismic experiments on the North German explosions, 1946 to 1947. Phil. Tran R. Soc., A, 242, 123-151 (1949).

SEISMISCHE GESCHWINDIGKEITSMESSUNG IM KARBONGESTEIN UNTER TAGE*

Von Heinrich Baule

Westfälische Berggewerkschaftskasse, Geophysikalische Abteilung, Bochum, Germany

(Received February 12, 1951)

ABSTRACT

The travel-times of longitudinal waves in sandstone were measured with high accuracy in a mine over distances of 5 to 100 meters; 0.1 mm on the recording film represented 1/50,000 second. The travel-time curves, which reflect the geological particularities in the profile, gave velocities of 4,240 and 4,100 m/sec. The frequencies of the vibrations were between 100 and 500 cycles/sec. The "frequency of the first onset" decreased with increasing distance, from 300 cycles/sec at 5 meters to 180 cycles/sec at 95 meters. Travel-time measurements made in the laboratory with large blocks of rock gave the following average velocities: A rock-salt block, 4,400 m/sec; two coal-blocks, 670 and 450 m/sec; a bore-core of coarse-grained sandstone, 2,800 m/sec.

ZUSAMMENFASSUNG

Die Laufzeiten longitudinaler Wellen wurden im Sandgestein unter Tage über Messtrecken von 5 m bis 100 m mit hoher Genauigkeit gemessen; auf dem Registrierfilm entsprach 0.1 mm einer 1/50,000 s. Aus den Laufzeitkurven, in denen sich die geologischen Besonderheiten des Profils widerspiegeln, ergab sich die Ausbreitungsgeschwindigkeit zu 4,240 m/s bzw. 4,100 m/s. Die Frequenzen der Erschütterungen lagen zwischen 100 und 500 Hz. Die "Frequenz des ersten Einsatzes" nahm mit zunehmender Entfernung ab, und zwar von 300 Hz bei 5 m auf 180 Hz bei 95 m. Laufzeitmessungen, die im Laboratorium an grossen Gesteinsblöcken vorgenommen wurden, ergaben für einen Steinsalzblock eine mittlere Geschwindigkeit von 4,400 m/s, für zwei Kohleblöcke 670 m/s bzw. 450 m/s und für einen Bohrkern aus grobkörnigem Sandstein 2,800 m/s.

Wenn man die Tektonik unter Tage mit seismischen Mitteln, etwa nach dem Refraktions- oder Reflexionsverfahren, erfassen will, so ist die Messung der longi-

*Auszug aus dem Vortrag auf der Tagung der Deutschen Geophysikalischen Gesellschaft am 23. 10. 1950 in Hamburg.

tudinalen Wellengeschwindigkeiten und ihrer Änderungen im anstehenden Gebirge notwendig. Solche Geschwindigkeitsmessungen stellen bei kurzen Profillängen bis zu rd. 100 m—entsprechend den Verhältnissen unter Tage—sehr hohe Anforderungen an die Messtechnik, wenn eine befriedigende Messgenauigkeit erreicht werden soll.

Im folgenden werden die Ergebnisse beschrieben, die sich aus Messungen an einem 100 m langen Profil am Stoss entlang (d.h. an der Stollenwand) in einem 350 m tiefen Hauptquerschlag des Karbons ergaben. Es handelt sich bei diesem Querschlag um eine standfeste Strecke ohne Ausbau im Sandgestein auf der 4. Sohle der Versuchsgrube Tremonia—Dortmund. An den beiden Schusspunkten am Anfang und Ende der Messtrecke wurden jeweils etwa 50 bis 100 g Wettersprengstoff 1 m tief im Stoss so gezündet, dass das Gestein nicht zerstört wurde. Mit empfindlichen piezoelektrischen Erschütterungsmessern hoher Eigenfrequenz [1, 2] und einem selbstgebauten Oszillographen mit Siemens-Messchleifen wurden die Erschütterungen der kleinen Sprengungen aufgezeichnet. Die erforderliche hohe Ablaufgeschwindigkeit des Registrierpapiers von ca. 5 m/s wurde dadurch erreicht, dass ein 1.20 m langes Filmstück sehr schnell von einem kleinen Elektromotor durch die Kassette hindurchgezogen wurde. Die Zündung der Ladung wurde durch einen elektrischen Kontakt an der Kassette ausgelöst.

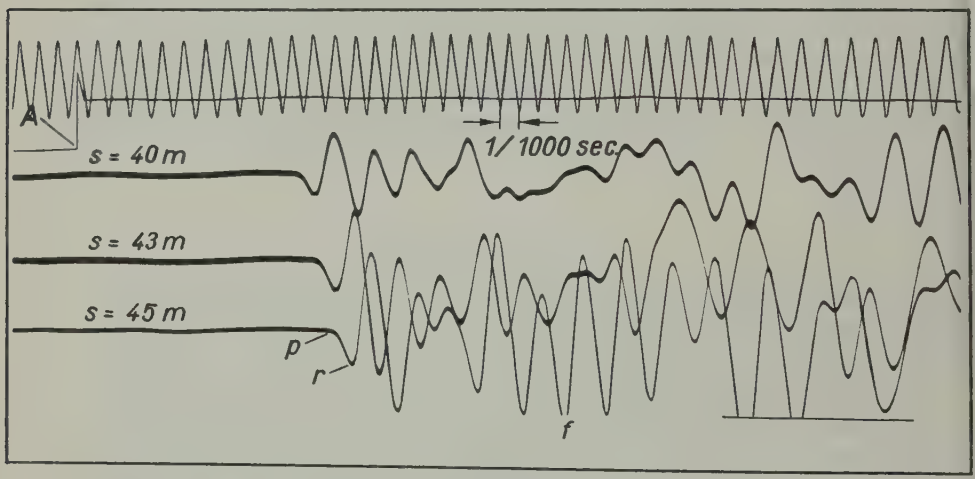

Fig. 1— Aufzeichnung einer Erschütterung im Sandstein Versuchsgrube Tremonia, Teufe 350 m

Ein Ausschnitt aus einer solchen Erschütterungsaufzeichnung ist in Abb. 1 wiedergegeben. Die Spuren bedeuten von oben nach unten: Zeitmarke von 1000 Hz; Abriss "*A*" zur Festlegung des Sprengmomentes, drei Seismogramme in Entfernungen von rd. 40, 43 und 45 m. Besonders zu beachten sind die hohen Frequenzen der Erschütterungen; sie betragen z.B. im unteren Kurvenzug bei "*f*" etwa 450 Hz. Bei zahlreichen weiteren Sprengversuchen über Entfernungen bis zu 300 m lagen die Frequenzen der Erschütterungen des Gebirges zwischen 500 und 100 Hz [3].

Für die Laufzeitkurven wurde im allgemeinen der in Abb. 1 mit "*p*" bezeich-

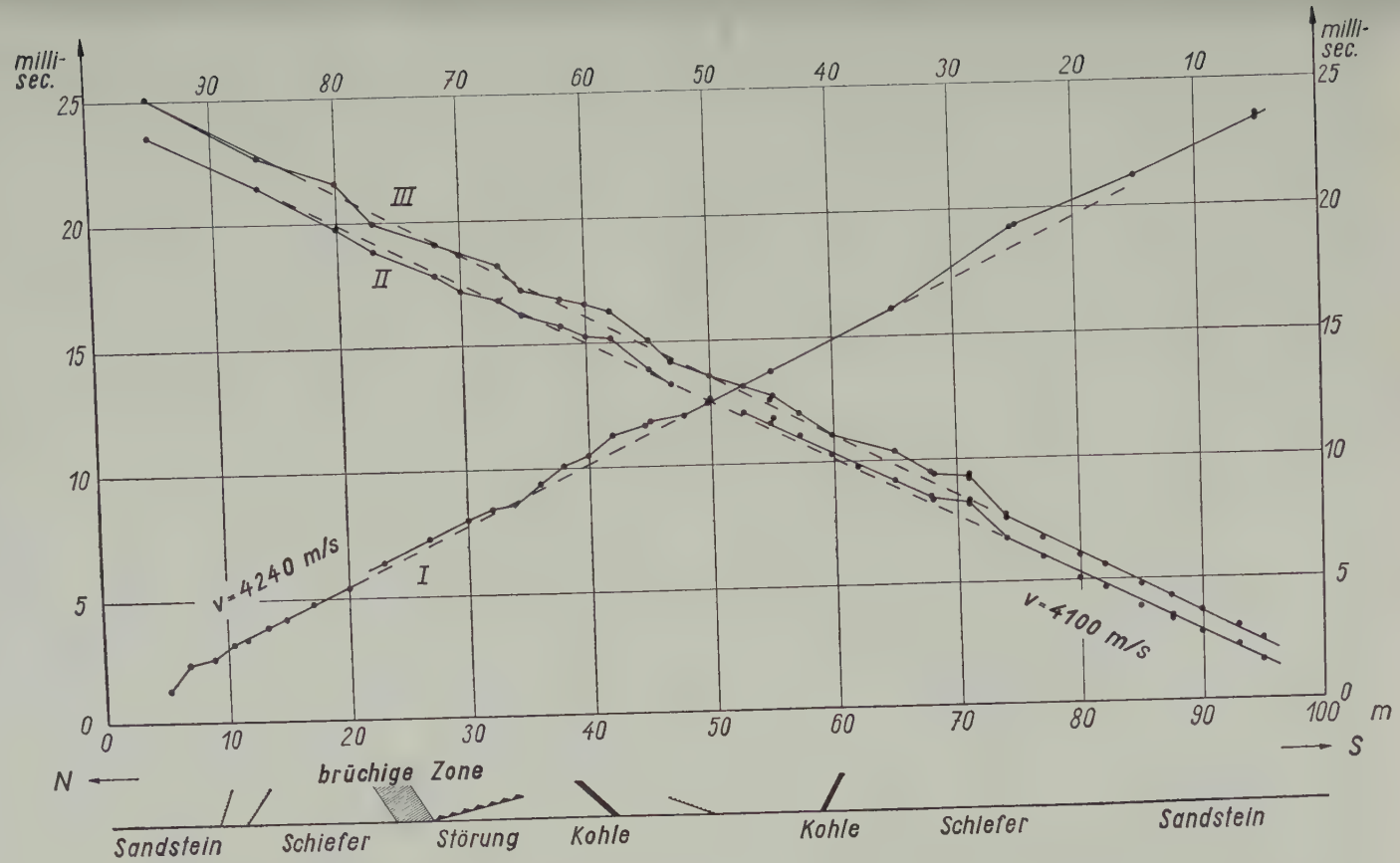

Fig. 2—Laufzeitkurven für Sandstein mit Schiefer.
Versuchsgrube Tremonia, 4. Sohle, Teufe=350m

nete erste Einsatz, der Augenblick des Abbiegens aus der Nullage, benutzt. Für eine Kurve wurde ausserdem der in den Seismogrammen mit "r" bezeichnete erste Umkehrpunkt mit herangezogen.

In Abb. 2 sind die Laufzeitkurven wiedergegeben. Bei der im Bilde von links unten nach rechts oben verlaufenden Kurve I in der Profilrichtung nach Süden beträgt die mittlere Geschwindigkeit 4,240 m/s; aus der Neigung der Gegenprofilkurve II ergibt sich eine Geschwindigkeit von 4,100 m/s. Zu beachten ist die Parallelversetzung einiger Kurvenabschnitte, z.B. in Kurve I ab 23 m. Von diesem Punkt an kommen die Erschütterungswellen um etwa 0.3 ms später an als vorher. Weiter fällt in Kurve I und auch in II der Bereich zwischen 34 m und 48 m ins Auge. Dort ist ein allmählich wachsendes Nacheilen und Wiedereinmünden in die Hauptkurve festzustellen. Mehrfache Wiederholungen der Messungen zeigten, dass es sich um echte Verspätungen handelt.

Bei dem Versuch, solche Kurven geologisch zu deuten, lassen sich m. E. die Deutungsverfahren der Übertageseismik nur ganz bedingt auf den von Hohlgängen durchzogenen, mit schnellwechselnden und z.T. gestörten und besonders steilen Lagerungsverhältnissen gekennzeichneten Vollraum unter Tage anwenden. Das geologische Profil, das unter die Abszissenachse gezeichnet ist, zeigt einen Wechsel vom reinen Sandstein—an beiden Profilenden—über vornehmlich Schiefer und wieder zum Sandstein mit einer Mulde in der Profilmitte. Damit verbunden ist ein Wechsel im Einfallen der Schichten. Mit Sicherheit lässt sich folgendes feststellen:

(1) Der Kurvensprung bei 23 m tritt beim Überschreiten einer stark gebrächen Gesteinszone auf, die als weiches Polster eine Nacheilung der Laufzeiten hervorruft.

(2) Die Verspätung der Erschütterungen im Bereich zwischen 34 und 38 m entspricht dem Störungsgebiet mit den weichen Schichten aus Schiefer, Wurzelboden und Flöz auf dem Nordflügel der Mulde bis zur Störung im Muldentiefsten. Für die plötzliche Abweichung bei 70 m in Kurve II sind keine am Stoss sichtbaren geologischen Besonderheiten festzustellen.

Es sei noch kurz auf die Laufzeitkurve III eingegangen, die aus den Ankunftszeiten der ersten Umkehrpunkte "r" im Seismogramm ermittelt wurde. Diese Kurve III ist der Hauptkurve II im wesentlichen ähnlich, unterscheidet sich aber von ihr durch eine etwas grössere Steilheit. Der Laufzeitabstand zwischen beiden Kurven beträgt bei 5 m Entfernung vom Schusspunkt rd. 0.8 ms und bei 95 m etwa 1.5 ms. Das entspricht einer Abnahme der Frequenz des ersten Einsatzes mit zunehmender Entfernung. Zur Bestimmung der Frequenz wurde hierbei im Seismogramm der Kurvenabschnitt vom Auslenken aus der Nullage bis zum ersten Umkehrpunkt —also $p - r$ in Abb. 1—als eine Viertelschwingung betrachtet. Nach den Ausmessungen auf den Filmen sinkt diese Frequenz von rd. 300 Hz bei 5 m auf 180 Hz bei 95 m Entfernung herab.

Mit der hier benutzten Messapparatur, bei der 0.1 mm auf dem Film 1/50,000 s entspricht, wurden u. a. die Longitudinalgeschwindigkeiten im dem etwa 1/3 m^3 grossen Magerkohlenblock und dem etwa gleich grossen Steinsalzblock, die seit vielen Jahren in der Bergschule Bochum ausgestellt sind, gemessen. Es wurde

für Steinsalz, ... $v = 4{,}400$ m/s
für den Kohleblock, ... $v = 670$ m/s
für einen weiteren Kohleblock, ... $v = 450$ m/s
für einen Bohrkern aus grobkörnigem
Sandstein, ... $v = 2{,}800$ m/s ermittelt.

Bei diesen seismischen Kurzzeitmessungen im Laboratorium über sehr kleine Entfernungen von rd. 1 m konnte zunächst allerdings nur eine Genauigkeit von etwa $\pm 5\%$ erreicht werden.

Schrifttum

[1] H. Köhler, Neuere Erschütterungsmesser mit elektrischer Anzeige, Elektrotechnik, **3**, S. 307 (1949).
[2] H. Baule, Seismische Instrumente. Naturforschung u. Medizin in Deutschland (Fiat Review), **18**, Teil II, S. 61/62 (1948).
[3] H. Baule, Seismische Untersuchungen unter Tage, Bergmännische Zs. Glückauf, **85**, S. 161 (1949).

Journal of Geophysical Research Volume 56, No. 2 June, 1951

NOMOGRAM AND SLIDE-RULE FOR SOLUTION OF SPHERICAL TRIANGLE PROBLEMS FOUND IN RADIO COMMUNICATION

By David V. Dickson

Defense Research Telecommunications Establishment, Defense Research Board, Ottawa, Canada

(Received February 27, 1951)

ABSTRACT

The nomogram and slide-rule, based on Napier's proportions, solve all unknowns in any spherical triangle, given three known adjacent parts. The design of a slide-rule based on Napier's proportions has been included as a speedy means of obtaining a fairly accurate answer.

INTRODUCTION

Many nomograms have been published, of which some give a speedy solution for a specific part of a spherical triangle [see 1 of "References" at end of paper], while others give a solution for several parts [2]. The formulae for these nomograms cannot be used efficiently on a slide-rule. Even the polar cosine formula, which gives a complete solution of a spherical triangle, cannot be used on a slide-rule without two linear reference scales and four settings of the slide for each side or angle required. Also, the sine and cosine scales are compressed near 90°, and 0° and 180°, respectively, so that inaccurate readings would be obtained in these regions.

The nomogram described herein gives a complete solution for any spherical triangle by a quite different method from the polar cosine formula, which enables it to reach some answers more quickly. Also, the equation is such that its adaption to a slide-rule is simple. The rare cases of describing spherical triangles by three angles or three sides are left unsolved, as they seldom appear in communication problems.

This work has been undertaken as an aid to a project of J. H. Meek in the prediction of communication frequencies. These frequencies are dependent upon conditions in the ionosphere which vary, not only with latitude, but also with longitude. Thus, it is essential to have a speedy means of locating geographically all points in the ionosphere which affect each communication route. The application of the nomogram to radio direction finding is evident [3]. Without modification, a fix from the bearings taken by two stations a known distance apart can be obtained very quickly. Speed in finding a fix is extremely important in locating a fast-moving aircraft or surface craft.

This nomogram can be used to find the point, by latitude and longitude, where a great circle path intersects a second great circle. In drawing a path which is partially on two or more gnomonic charts, one determines by this nomogram where the path cuts the edge of each chart, so that the path is found by joining these intersection points to each other or to the station on the chart. The full importance of these intersection points may not be realized until one has to draw a route across several gnomonic charts.

THE NOMOGRAM EQUATIONS

Nomograms are generally considered to be a part of higher mathematics, but with a small amount of study any person can use them after their construction. The general equation of a nomogram is shown here.

$$X_1Y_2 + X_2Y_3 + X_3Y_1 - X_3Y_2 - X_2Y_1 - X_1Y_3 = 0$$

In determinant form, the requirement that three points, (X_1Y_1), (X_2Y_2), and (X_3Y_3), be collinear is satisfied when the factors in the last column are all one.

$$\begin{vmatrix} X_1 & Y_1 & 1 \\ X_2 & Y_2 & 1 \\ X_3 & Y_3 & 1 \end{vmatrix} = 0$$

If X_1 , X_2 , and X_3 are plotted on the abscissa on linear coordinate graph paper and Y_1 , Y_2 , and Y_3 are plotted on the ordinate, a nomogram is constructed. Placing a straight-edge on the chart so that it passes through two points deter-

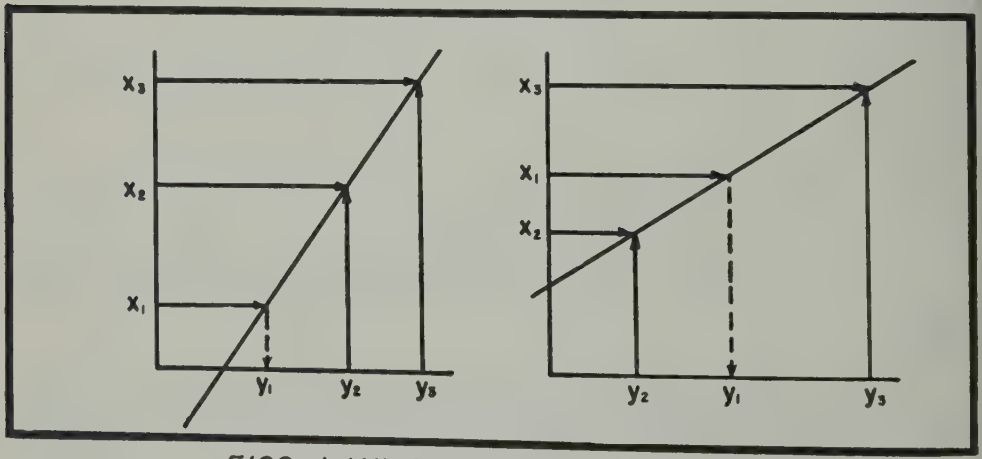

FIGS. 1 AND 2—TYPICAL NOMOGRAMS

mined by the corresponding coordinates, the proportion of the other pair of values is given and, knowing one of these values, the value of the second is given immediately (see Figures 1 and 2).

As an example, let us suppose we know X_1 , X_2 , X_3 , Y_2 , and Y_3 , and we wish

to find Y_1 . To solve the algebraic equation would require considerable accurate work. The nomographic solution requires only a few seconds and can be repeated many times for varying values of the knowns.

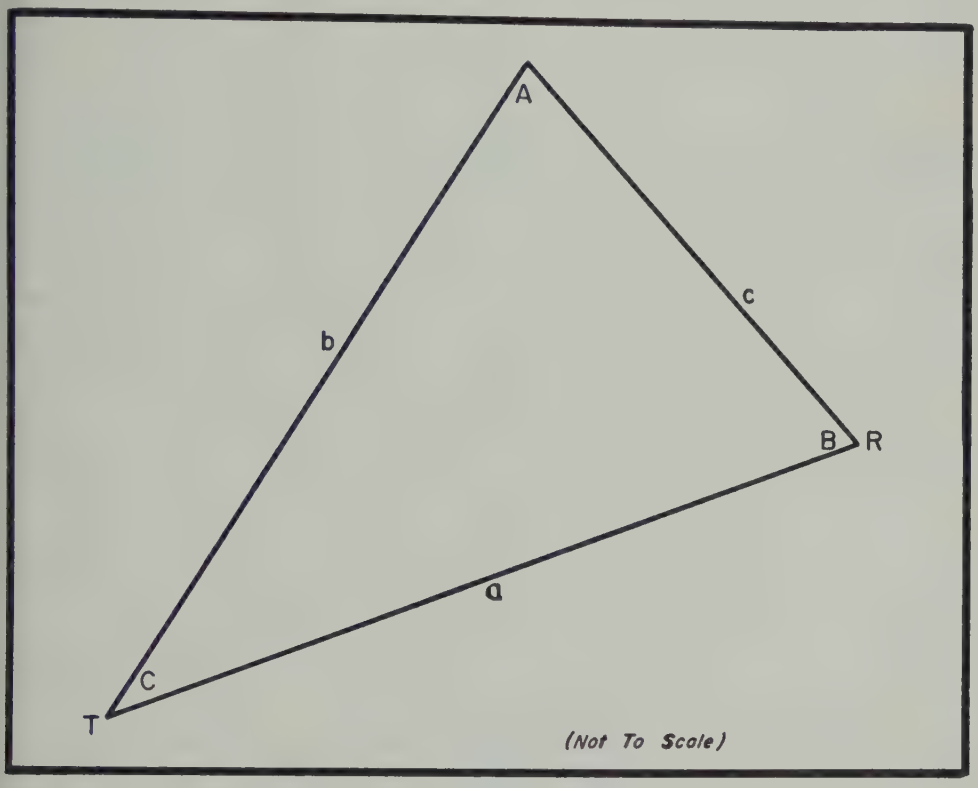

FIG. 3—POLAR GNOMONIC PROJECTION OF SPHERICAL TRIANGLE

The nomogram giving solution for all spherical triangles is based on four of Napier's proportions, as follows:

$$(1) \qquad \tan \tfrac{1}{2}(a + b) = \frac{\cos \tfrac{1}{2}(A - B)}{\cos \tfrac{1}{2}(A + B)} \tan \tfrac{1}{2}c$$

$$(2) \qquad \tan \tfrac{1}{2}(a - b) = \frac{\sin \tfrac{1}{2}(A - B)}{\sin \tfrac{1}{2}(A + B)} \tan \tfrac{1}{2}c$$

$$(3) \qquad \tan \tfrac{1}{2}(A + B) = \frac{\cos \tfrac{1}{2}(a - b)}{\cos \tfrac{1}{2}(a + b)} \cot \tfrac{1}{2}C$$

$$(4) \qquad \tan \tfrac{1}{2}(A - B) = \frac{\sin \tfrac{1}{2}(a - b)}{\sin \tfrac{1}{2}(a + b)} \cot \tfrac{1}{2}C$$

Using either pair of these four equations gives the two sides opposite two known angles and one known contained side, or the two angles opposite any known sides and known contained angle (see Figure 3).

The four determinants from these four equations are

$$(1)\qquad \begin{vmatrix} \tan \tfrac{1}{2}(a+b) & \cos \tfrac{1}{2}(A-B) & 1 \\ \tan \tfrac{1}{2}c & \cos \tfrac{1}{2}(A+B) & 1 \\ 0 & 0 & 1 \end{vmatrix} = 0$$

$$(2)\qquad \begin{vmatrix} \tan \tfrac{1}{2}(a-b) & \sin \tfrac{1}{2}(A-B) & 1 \\ \tan \tfrac{1}{2}c & \sin \tfrac{1}{2}(A+B) & 1 \\ 0 & 0 & 1 \end{vmatrix} = 0$$

$$(3)\qquad \begin{vmatrix} \tan \tfrac{1}{2}(A+B) & \cos \tfrac{1}{2}(a-b) & 1 \\ \cot \tfrac{1}{2}C & \cos \tfrac{1}{2}(a+b) & 1 \\ 0 & 0 & 1 \end{vmatrix} = 0$$

$$(4)\qquad \begin{vmatrix} \tan \tfrac{1}{2}(A-B) & \sin \tfrac{1}{2}(a-b) & 1 \\ \cot \tfrac{1}{2}C & \sin \tfrac{1}{2}(a+b) & 1 \\ 0 & 0 & 1 \end{vmatrix} = 0$$

THE NOMOGRAM

A moment's inspection shows that, since the sine and cosine values occur on the same ordinate, the cosine may be plotted as the complement of the sine. By the same reasoning, the cotangent may be plotted as the complement of the tangent. Thus, these four nomograms may be plotted on one grid. One must keep in mind that, while the change of longitude gives the angle subtended by the path at the pole, the latitudes must be converted to colatitudes or distances from the pole by adding to or subtracting from 90°.

The nomogram is shown in Figure 4. The tangent and cotangent scales are plotted along the horizontal axis; the cotangent values are in parentheses. The sine and cosine values are plotted on the vertical axis and the cosine values are in parentheses. Only one-quarter of the complete nomogram is shown, but it is the part which is used for approximately 98 per cent of the work. Enlarging this section has increased the accuracy of the nomogram. The origin lies at the lower left corner of the chart. An alignment rule may be pivoted from the origin to increase the speed and accuracy of the work. The tangent scale from 0° to 65° is plotted along the lower edge of the chart, and it is from this scale that the grid is constructed. A second tangent scale from 0° to 80° is marked along the 45° sine value. Since the tangent and cotangent functions are independent of the other scales, any convenient range of values may be used on the abscissa.

THE SLIDE-RULE

The simplicity of the four equations and the fact that only two scales are necessary make the construction of a slide-rule an easy task. By putting two ranges of tangent values on a 20-inch slide-rule, excellent accuracy can be obtained. One must remember that 0° to 90° on the sine and cosine scale must be

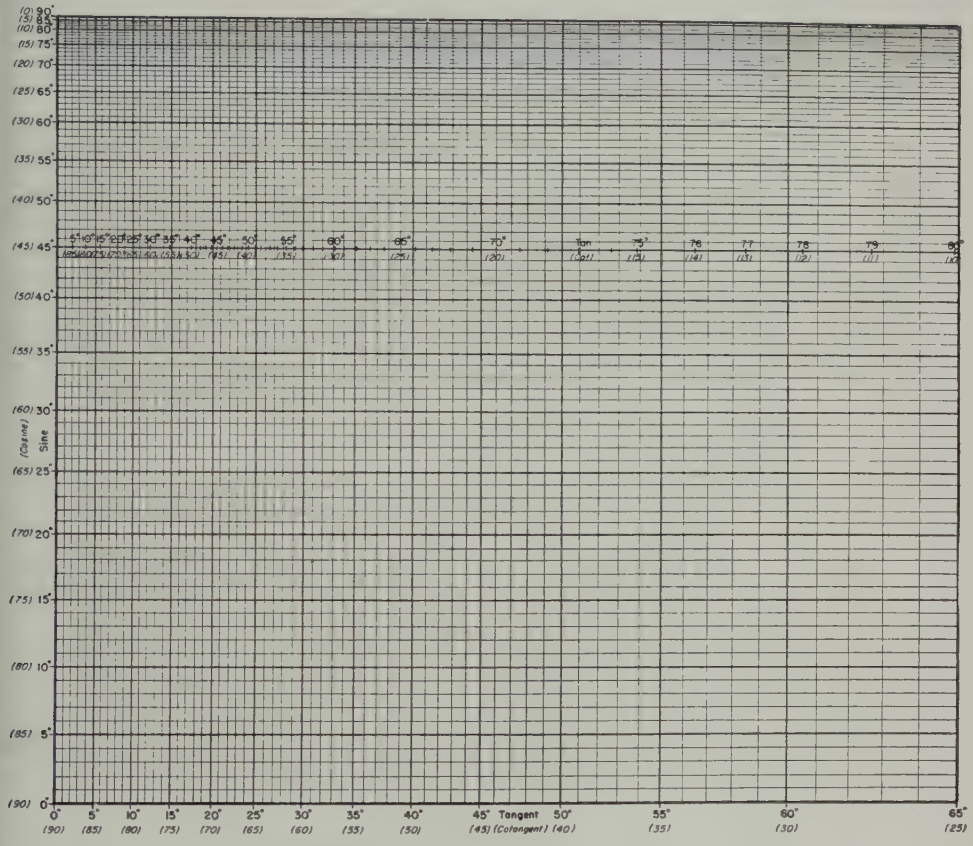

FIG. 4—NOMOGRAM FOR SPHERICAL TRIGONOMETRY

equal in length to the range from 0° to 45° on the tangent scale. Since each scale is plotted logarithmically on a slide-rule, the zeros disappear from the scales and the functions cover the centre range very well. The accuracy of the sine values is reduced near 90°, but this is unimportant since the result of each setting of the slide is read on the tangent scale. This slide-rule is shown in Figure 5.

To use the slide-rule, the average sum of the sides (or angles) on the sine scale is set opposite one-half the angle (or side) on the cotangent (or tangent) scale. The average difference of the required angles is read directly on the tangent scale opposite the average difference of the sides on the sine scale. The average sum of the required sides is found by making the setting and readings from the cosine scale instead of the sine scale.

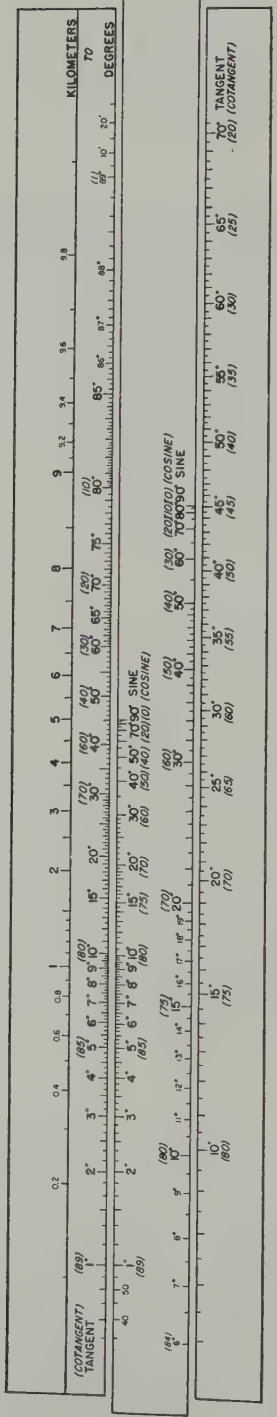

FIG. 5—SLIDE-RULE FOR SPHERICAL TRIGONOMETRY

APPLICATIONS

For an example, let us examine the path from station T at 137° west and 30° north to station R at 27° west and 60° north. The change of longitude is $A = 110°$, the colatitude of station T is $b = 60°$ and the colatitude of station R is $c = 30°$.

The spherical triangle is shown in Figure 6 with the requirements drawn in. We need the path length a, the change of longitude of mid-point A_1 , and the colatitude d_1 . On a long transmission, the first control point is 18° from each end. Let the change of longitude of the control point closer to station T be A_3 and the colatitude be d_3 . Correspondingly, let the change of longitude and the colatitude of the control point 18° from station R be A_4 and d_4 .

GREAT CIRCLE BEARINGS AND PATH LENGTH

The spherical triangle shown in Figure 3 is simpler to follow for this detailed example and it has the same labeling as Figure 6. First we must find angles B and C, which are the great circle bearings of the stations from each other. Ap-

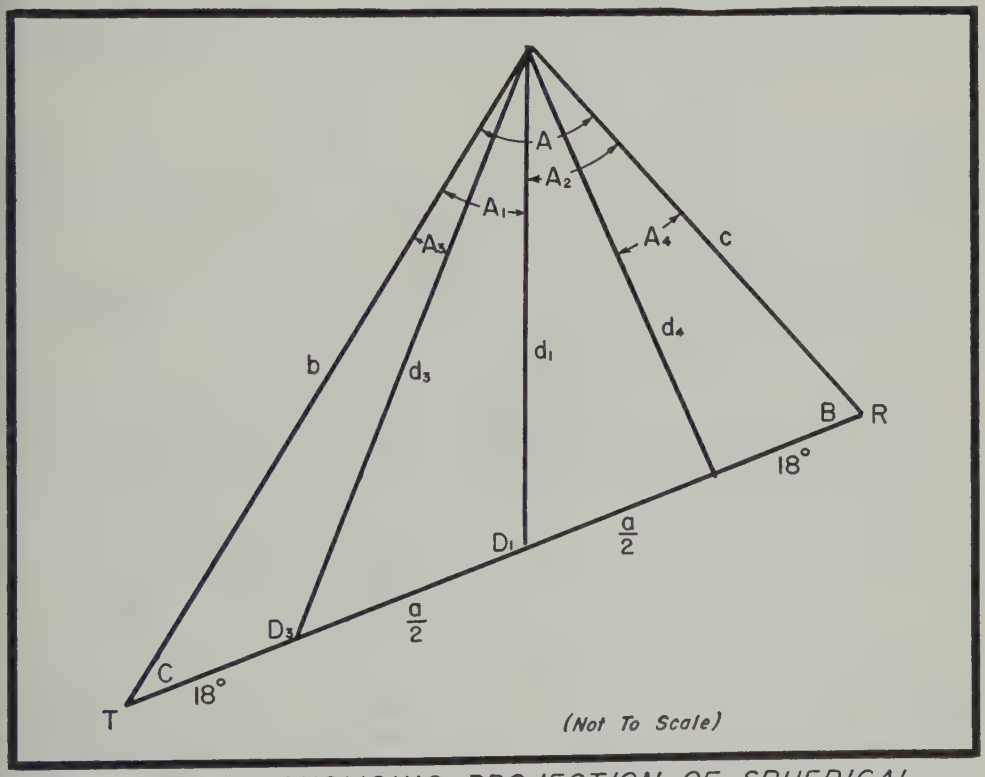

FIG. 6—POLAR GNOMONIC PROJECTION OF SPHERICAL TRIANGLE SHOWING MID-POINT AND CONTROL POINTS

plying equations (3) and (4) to the nomogram, we find $\frac{1}{2}(B - C) = 14\frac{1}{4}°$ and $\frac{1}{2}(B + C) = 43\frac{3}{4}°$, from which $B = 58°$ and $C = 29\frac{1}{2}°$. Applying equation (2), the nomogram gives $\frac{1}{2}(a - b) = 6\frac{3}{4}°$, from which the path length $a = 73\frac{1}{2}°$. Re-

checking with equation (1) gives $\frac{1}{2}(a + b) = 66\frac{3}{4}°$ and $b = 60°$. To follow through these two moves in detail, we align with our straight-edge the point $\frac{1}{2}(b + c)$, which is 45° on our cosine scale and $\frac{1}{2}A$ or 55° on our cotangent scale, with the origin. Then we move horizontally across our grid from $\frac{1}{2}(b - c)$ or 15° on our cosine scale until we reach the aligning edge of our straight-edge. By dropping straight down to our tangent scale, we find our angle of $\frac{1}{2}(B + C) = 43\frac{3}{4}°$. Aligning $\frac{1}{2}(b + c)$ on the sine scale and $\frac{1}{2}A$ on the cotangent scale with the point 0, 0, and proceeding from $\frac{1}{2}(b - c)$ on our sine scale, we obtain $\frac{1}{2}(B - C) = 14\frac{1}{4}°$. Thus $B = 58°$ and $C = 29\frac{1}{2}°$. Similarly, by aligning sine $\frac{1}{2}(A + B)$ or 84° and tan $\frac{1}{2}c$ or 15° with 0, 0, and using $\frac{1}{2}(A - B) = 26°$, we obtain $\frac{1}{2}(a - b) = 6\frac{3}{4}°$, from which $a = 73\frac{1}{2}°$. This gives a path length of 8,167 km by multiplying the $73\frac{1}{2}°$ by the factor of 1,000/9 or 111.11 to give kilometers.

As an orderly way to attain the required answers, let us make up a table of values:—

Given			*Use*			*Find*			
A	b	c	$\frac{A}{2}$	$\frac{1}{2}(b + c)$	$\frac{1}{2}(b - c)$	$\frac{1}{2}(B + C)$	$\frac{1}{2}(B - C)$	B	C
110°	60°	30°	55°	45°	15°	$43\frac{3}{4}°$	$14\frac{1}{4}°$	58°	$29\frac{1}{2}°$
c	A	B	$\frac{c}{2}$	$\frac{1}{2}(A + B)$	$\frac{1}{2}(A - B)$	$\frac{1}{2}(a + b)$	$\frac{1}{2}(a - b)$	a	b
30°	110°	58°	15°	84°	26°	$66\frac{3}{4}°$	$6\frac{3}{4}°$	$73\frac{1}{2}°$	60°

MID-POINT

The latitude and longitude of the mid-point of the path is of great importance to communications.

Given			*Use*			*Find*			
C	b	$\frac{a}{2}$	$\frac{c}{2}$	$\frac{1}{2}\left(b + \frac{a}{2}\right)$	$\frac{1}{2}(b - a)$	$\frac{1}{2}(D_1 + A_1)$	$\frac{1}{2}(D_1 - A_1)$	A_1	D_1
$29\frac{1}{2}°$	60°	$36\frac{3}{4}°$	$14\frac{3}{4}°$	$48\frac{3}{8}°$	$11\frac{5}{8}°$	80°	46°	34°	126°
b	c	A_1	$\frac{b}{2}$	$\frac{1}{2}(A_1 + C)$	$\frac{1}{2}(A_1 - C)$	$\frac{1}{2}\left(\frac{a}{2} + d_1\right)$	$\frac{1}{2}\left(\frac{a}{2} - d_1\right)$	d_1	$\frac{a}{2}$
60°	$29\frac{1}{2}°$	34°	30°	$31\frac{3}{4}°$	$2\frac{1}{4}°$	34°	$2\frac{1}{2}°$	$31\frac{1}{2}°$	$36\frac{1}{2}°$

Thus, the mid-point of the path is found at 103° west and $58\frac{1}{2}°$ north.

CONTROL POINT

The first control point, or the location of the reflection of a radio wave which leaves or arrives at zero angle of elevation above the horizon, on a long distance transmission is 18° from each end of path.

Given			*Use*			*Find*			
C	b	18°	$\frac{C}{2}$	$\frac{1}{2}(b + 18°)$	$\frac{1}{2}(b - 18°)$	$\frac{1}{2}(D_3 - A_3)$	$\frac{1}{2}(D_3 + A_3)$	A_3	D_3
$29\frac{1}{2}°$	60°	18°	$14\frac{3}{4}°$	39°	21°	$65\frac{1}{2}°$	$77\frac{3}{4}°$	$12\frac{1}{4}°$	$143\frac{1}{4}°$
b	C	A_3	$\frac{b}{2}$	$\frac{1}{2}(C + A_3)$	$\frac{1}{2}(C - A_3)$	$\frac{1}{2}(d_3 + 18°)$	$\frac{1}{2}(d_3 - 18°)$	d_3	18°
60°	$29\frac{1}{2}°$	$12\frac{1}{4}°$	30°	$20\frac{7}{8}°$	$8\frac{5}{8}°$	$31\frac{1}{2}°$	$13\frac{1}{2}°$	45°	18°

The first control point from station T is located at $124\frac{3}{4}°$ west and 45° north. The values A_4 and d_4 are found in a similar manner.

POSITION FROM RADIO BEARINGS

In finding a D/F fix, two angles and the contained side of a spherical triangle would be known. As an example, let us take one D/F station B_1 at 70° west and 30° north, and a second station B_2 at 118° 13′.0 west and 5° 33′.4 south. In Figure 7, angles K_2 and K_3 and side k_1 would describe the first triangle. When $K_2 = 20°$ and $K_3 = 80°$, one-half the sum of these angles is 50° and one-half the difference is 30°. The contained side is 70° in length and one-half of this is 35°, to be found on the tangent scale, since it is a side and not an angle. By aligning with a straightedge one-half the sum of the angles, on the sine scale, and one-half the side, on the tangent scale, with the origin and reading opposite one-half the difference on the sine scale, one finds one-half the difference of the required angles on the tangent scale. Using the cosine scale instead of the sine scale for one-half the sum and one-half the difference gives one-half the sum of the required angles, and adding and subtracting these two newly found values give the required sides separately.

Given			*Use*			*Find*			
k_1	K_2	K_3	$\frac{k_1}{2}$	$\frac{1}{2}(K_3 + K_2)$	$\frac{1}{2}(K_3 - K_2)$	$\frac{1}{2}(k_3 + k_2)$	$\frac{1}{2}(k_3 - k_2)$	k_3	k_2
70°	20°	80°	35°	50°	30°	$43\frac{1}{4}°$	$24\frac{1}{2}°$	$67\frac{3}{4}°$	$18\frac{3}{4}°$

To solve this problem with the slide-rule, set 50° on the sine scale opposite 35° on the tangent scale and read $24\frac{1}{4}°$ on the tangent scale opposite 30° on the sine scale. Then set 50° on the cosine scale opposite 35° on the tangent scale, and opposite 30° on the cosine scale read $43\frac{1}{4}°$ on the tangent scale. The sides b and c are obtained by addition and subtraction as before.

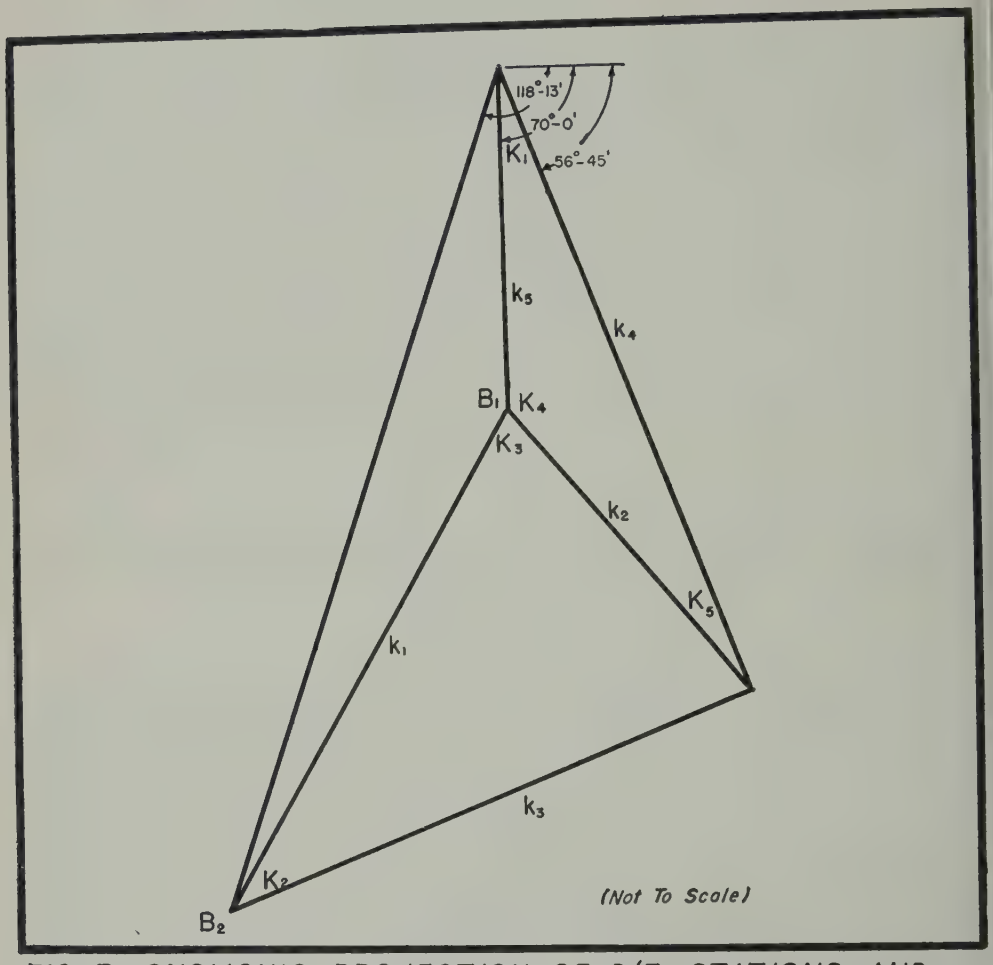

FIG. 7—GNOMONIC PROJECTION OF D/F STATIONS AND BEARINGS ON POSITION

This gives the distance from each observing station to the point in question. To find the latitude and longitude of the position, the change of longitude from the nearer observing station is found first.

Given			*Use*			*Find*			
K_4	k_2	k_5	$\frac{K_4}{2}$	$\frac{1}{2}(k_5 + k_2)$	$\frac{1}{2}(k_5 - k_2)$	$\frac{1}{2}(K_5 - K_1)$	$\frac{1}{2}(K_5 + K_1)$	K_5	K_1
150°	20°	30°	75°	25°	5°	$3\frac{1}{4}$°	$16\frac{1}{2}$°	$19\frac{1}{2}$°	$13\frac{1}{4}$°

Using the colatitude of the nearer station and the newly found change of longitude, the colatitude of the position is attained.

Given			*Use*			*Find*			
k_5	K_4	K_1	$\frac{k_5}{2}$	$\frac{1}{2}(K_4 + K_1)$	$\frac{1}{2}(K_4 - K_1)$	$\frac{1}{2}(k_4 + k_2)$	$\frac{1}{2}(k_4 - k_2)$	k_4	k_2
30°	150°	$13\frac{1}{4}°$	15°	$81\frac{1}{2}°$	$68\frac{1}{4}°$	34°	$14\frac{1}{4}°$	$48\frac{1}{4}°$	$19\frac{3}{4}°$

Thus the position is at $56\frac{3}{4}°$ west and $41\frac{3}{4}°$ north.

PATH ACROSS TWO OR MORE GNOMONIC PROJECTIONS

In drawing a path across gnomonic projections, the latitude and longitude of the intersection of the path with the great circle which forms the boundary of the chart are necessary. Generally, four equatorial gnomonic charts surround a sphere at the equator and one polar gnomonic is placed at each pole. These gnomonic projections are 90° in width or 45° of distance from the point of contact to the boundary in an east-west or north-south direction.

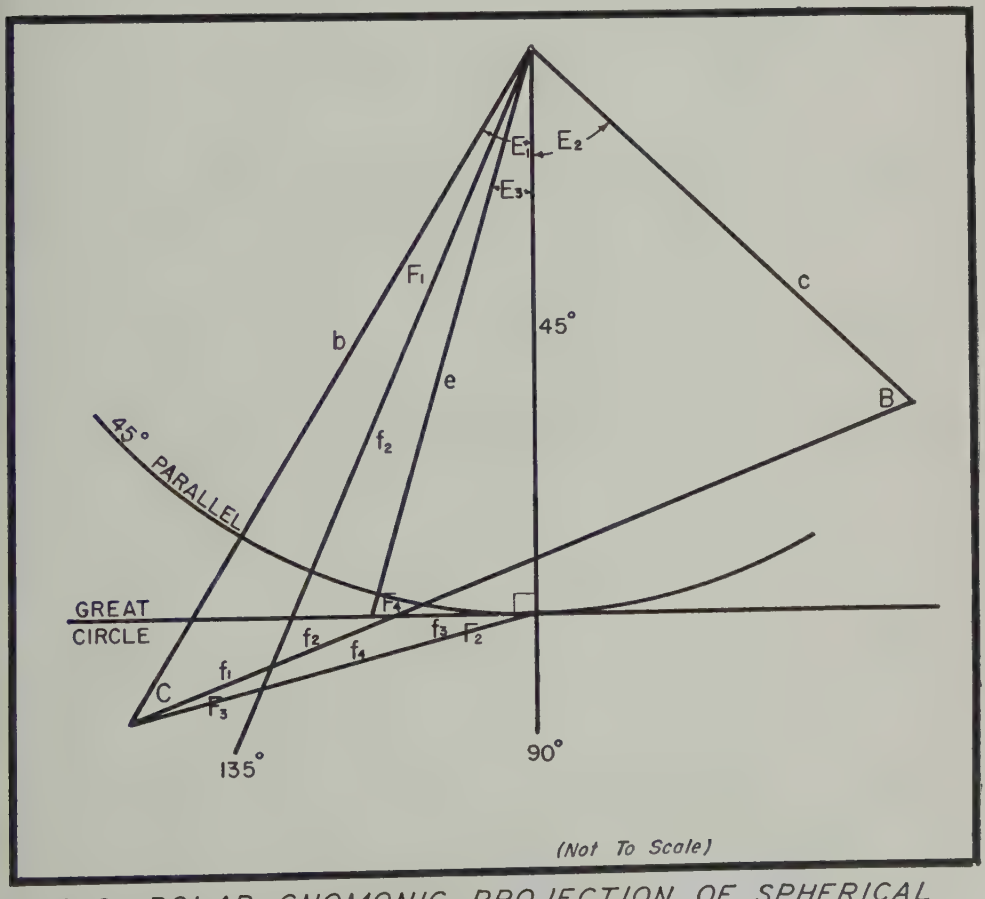

FIG. 8—POLAR GNOMONIC PROJECTION OF SPHERICAL TRIANGLE SHOWING BOUNDARIES OF THREE CHARTS

Given			*Use*			*Find*			
E_1	b	$45°$	$\frac{E_1}{2}$	$\frac{1}{2}(b + 45°)$	$\frac{1}{2}(b - 45°)$	$\frac{1}{2}[90° + F_2 + (C + F_3)]$	$\frac{1}{2}[90° + F_2 - (C + F_3)]$	F_2	F_3
$47°$	$60°$	$45°$	$23\frac{1}{2}°$	$52\frac{1}{2}°$	$7\frac{1}{2}°$	$75°$	$20\frac{3}{4}°$	$5\frac{3}{4}°$	$25°$
b	$C + F_3$	E_1	$\frac{b}{2}$	$\frac{1}{2}[E_1 + (C + F_3)]$	$\frac{1}{2}[E - (C + F_3)]$	$\frac{1}{2}(45° + f_4)$	$\frac{1}{2}(45° - f_4)$	$45°$	f_4
$60°$	$54\frac{1}{4}°$	$47°$	$30°$	$50\frac{3}{4}°$	$3\frac{3}{4}°$	$42\frac{1}{4}°$	$2\frac{3}{4}°$	$45°$	$39\frac{1}{4}°$
f_4	F_3	F_2	$\frac{f_4}{2}$	$\frac{1}{2}(F_3 + F_2)$	$\frac{1}{2}(F_3 - F_2)$	$\frac{1}{2}[f_3 + (f_1 + f_2)]$	$\frac{1}{2}[f_3 - (f_1 + f_2)]$	$f_1 + f_2$	f_3
$39\frac{1}{4}°$	$25°$	$5\frac{3}{4}°$	$19\frac{3}{4}°$	$15\frac{1}{2}°$	$9\frac{1}{2}°$	$20\frac{1}{4}°$	$12\frac{1}{2}°$	$7\frac{3}{4}°$	$32\frac{3}{4}°$
$90°$	$45°$	f_3	$\frac{90°}{2}$	$\frac{1}{2}(45° + f_3)$	$\frac{1}{2}(45° - f_3)$	$\frac{1}{2}(F_4 + E_3)$	$\frac{1}{2}(F_4 - E_3)$	F_4	E_3
$90°$	$45°$	$32\frac{3}{4}°$	$45°$	$39°$	$6°$	$52°$	$9\frac{1}{2}°$	$61\frac{1}{2}°$	$42\frac{1}{4}°$

The path used in the first examples lies on three gnomonic projections. Proceeding from station T, we must find first the latitude at which the path cuts the meridian at 135° west longitude. A polar gnomonic projection of this triangle is shown in Figure 8.

Given			*Use*		*Find*			
b	F_1	C	$\frac{b}{2}$	$\frac{1}{2}(C + F_1)$ $\frac{1}{2}(C - F_1)$	$\frac{1}{2}(f_2 - f_1)$	$\frac{1}{2}(f_2 + f_1)$	f_2	f_1
60°	2°	29½°	30°	15¾° 13¾°	26¾°	30¼°	57°	3½°

Now station T may be joined to the point at 135° west and 35° north to show the path across the first gnomonic.

To find the longitude from intervals of 90° at which a great circle path intersects the edge of a polar gnomonic projection of 45° width from point of contact, four steps are used.

The path is drawn on the second equatorial gnomonic by joining 135° west 35° north to 132° west on the great circle boundary of chart. Finally, join 132° west to station R.

ACKNOWLEDGMENT

The valuable advice and guidance of Mr. James C. W. Scott in the preparation of this publication are sincerely appreciated.

References

[1] J. C. W. Scott, Nomogram for ionosphere control points, Proc. Inst. Radio Eng., **37**, 821-824 (1949).

[2] Basic radio propagation predictions, Central Radio Propagation Laboratory, Nation. Bur. Stand., Washington, D. C. (Aug. 1947).

[3] L. S. Prior, A method of making rapid D/F position fixes, Radio Research Board, Univ. Sydney, N.S.W., Australia.

SUDDEN COMMENCEMENTS AND SUDDEN IMPULSES IN GEOMAGNETISM: THEIR HOURLY FREQUENCY AT CHELTENHAM (MD.), TUCSON, SAN JUAN, HONOLULU, HUANCAYO, AND WATHEROO

By V. C. A. Ferraro, W. C. Parkinson, and H. W. Unthank

University College, Exeter, Devon, England (1, 3) and
Department of Terrestrial Magnetism,
Carnegie Institution of Washington, Washington, D.C. (2)

(Received March 1, 1951)

ABSTRACT

The diurnal variation in the frequencies of sudden commencements of magnetic storms (SCs) and sudden impulses (SIs), defined in Section 1, is examined at six stations, Cheltenham, Tucson, San Juan, Honolulu, Huancayo, and Watheroo. The data for SCs and SIs are analysed separately for the period 1926-1946, which is common to all six stations. The results show that any local time variation in the hourly frequency of SCs seems likely to be small, and it is suggested that SCs may be more frequent in the afternoon hours, with a maximum around 13^h local time, in agreement with the observation made by Moos from his analysis of the Bombay SCs.

The hourly frequency of SIs for the six stations considered separately do not exhibit any marked local time effect. Indeed, their U.T. hourly frequencies are not greatly different from one another. When the local mean hourly frequency for the combined data at the six stations is considered, this curve shows similarities to the curve obtained by Newton in his analysis of the Greenwich records, with minima around 08^h and 20^h local time, this second minimum being much more pronounced than the Greenwich one. Much the same variation is obtained when the ratios of the observed frequencies of SIs at any one station to the greatest frequency at each U.T. are arranged according to local time and the local time mean plotted. The curve exhibits a variation which is very nearly semi-diurnal. It is suggested that there is an essential difference between SCs and SIs in spite of the similarity of their appearance on the magnetic traces.

The diurnal variations in the frequency of sudden commencements and sudden impulses with a preliminary movement in the opposite direction (SCs* and SIs*) exhibit a local time effect and they appear to be most frequent in the afternoon. The frequency

of occurrence of SCs* and SIs* may also depend on the longitude of the particular station, though this dependence may be more complex than the one suggested in [6].

The curves for the annual mean number of SCs and SIs (combined) and the curve giving the annual mean sunspot numbers show striking similarities.

§1—*Introduction: Definition of "sudden commencements" and "sudden impulses"*

The term "sudden commencement" (SC) is usually applied to the abrupt beginning of a great magnetic disturbance. SCs are found to be nearly simultaneous at all magnetic observatories to within one minute of time (see also Section 7). More recently the term has been applied to denote all rapid movements simulating a sudden commencement of a magnetic storm, whether or not followed by a disturbance.

Thus, an SC has been defined by McNish [see 1 of "References" at end of paper] as an abrupt movement in all three elements, usually H, D, Z (the principal one in the horizontal force, H, being an increase), the period preceding the movement being relatively quiet. Presumably SCs may occur during disturbed magnetic periods, but they would generally be difficult to recognize.

Newton [5] has given a useful classification of SCs, whether followed by a storm or not, of which, he considers, there are three main types†—(*i*) the ordinary SC, shown in Figure 1*A*, in which the sudden change in H is an increase; (*ii*) the SC*, shown in Figure 1*B*, which is characterized by a small preliminary movement in the opposite direction and is immediately followed by the main impulse, as in the ordinary SC; and (*iii*) the inverted SC, shown in Figure 1*C*, in which the movement in H is a decrease. There are also, occasionally, inverted SCs* (Figure 1*D*).

In this paper the term SC will be restricted to a sudden movement followed by a magnetic storm, and SI (sudden impulse) will be used for sudden movements simulating SCs but not followed by magnetic storms. The importance of drawing this distinction was suggested by S. Chapman in a private communication to one of us (V.C.A.F.).

The first mention in the literature of a possible local time effect in the hourly frequencies of SCs appears to be the remark made by N. A. F. Moos in 1910 [2] that the SCs of 113 magnetic storms recorded at Bombay for the period 1846-1905 showed a slight tendency to occur more frequently at about 13^h local time. He thought that this effect was probably spurious and that the occurrence of SCs was fairly evenly distributed over all hours of the day. Thereafter, several analyses of SCs and SIs (not distinguished) were made.

L. Rodés [3] in 1932, analysing the records at Ebro for the period 1905-1931, found that the hourly frequency of 218 such sudden movements had a pronounced minimum around 08^h local time, and a secondary minimum between 17^h and 21^h

†An SC must be distinguished from a magnetic crochet associated with solar flares. According to Newton, what appears to be the complete SC is the SC* (Fig. 1*B*) and he suggests that though the absence of the small preliminary movement may be radical, it appears likely that the solar time may be a determining factor. This is supported by the analysis presented here (Section 6).

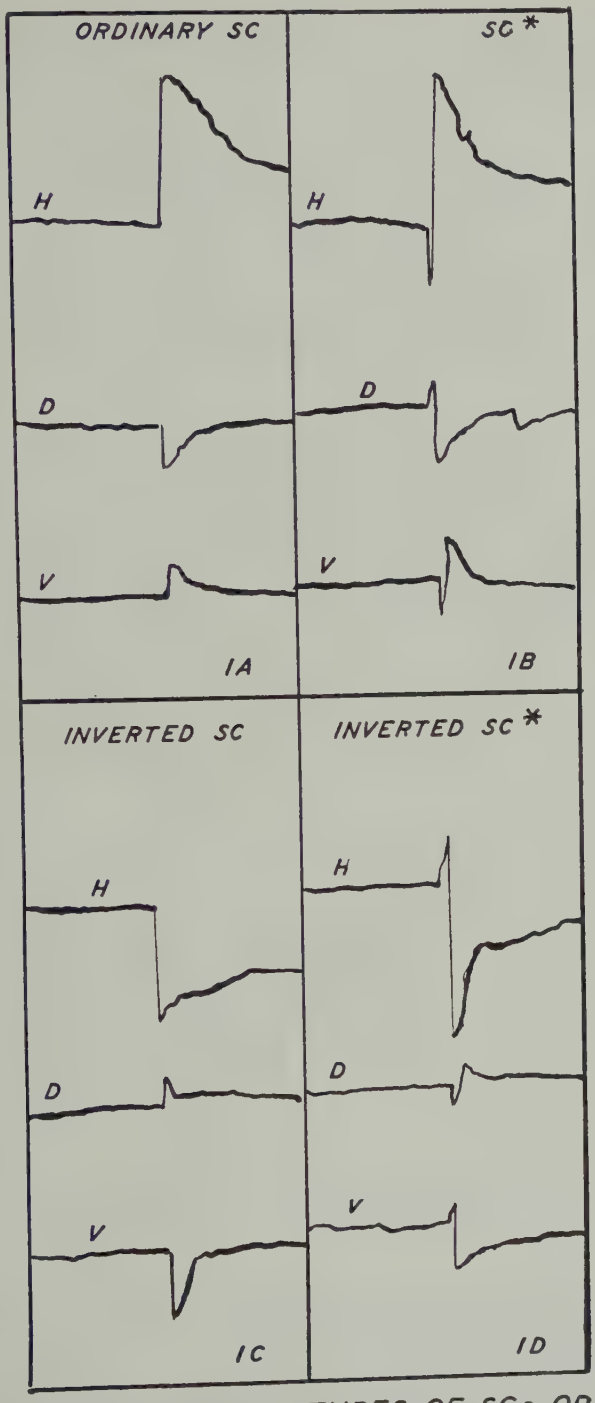

FIGS. IA TO ID— TYPES OF SCs OR SIs

local time. He found that much the same diurnal variation resulted when he considered only those SCs which were followed by great perturbations. A. G. McNish, in 1933 [4], likewise found a local time effect in the hourly frequency of SCs and SIs (undistinguished) at Watheroo, with a forenoon minimum and an afternoon maximum. H. W. Newton, in 1948 [5] discussed at length the records of 681 sudden movements at Greenwich for the period 1874-1944. He refers to these as "sudden commencements" in his paper but, like McNish and Rodés, he does not draw a distinction between SCs and SIs. He finds that the hourly frequency of these sudden movements has a broad minimum around 08^h, and an afternoon and night maximum, broken by a second minimum around 18^h, as was found by Rodés at Ebro but, as Newton remarks, the almost identical longitudes of Greenwich and Ebro make it impossible to decide whether this effect is a local time one or one depending on U.T.

Nevertheless, these results, taken with some records for other stations considered by Newton, seem to point to a local time effect in the hourly frequency of such sudden movements, and to a minimum in the local forenoon. As Newton remarks in his paper, there is a difficulty in accepting a marked local time effect in a phenomenon which is essentially world-wide, and it is of interest to examine the records of other observatories not only for such a local time effect but also to investigate the differences in the results obtained for SCs and SIs. We have made

Table 1—*Geographic and geomagnetic latitudes and longitudes of the six stations (arranged in order of decreasing latitudes) whose records are here examined*

Observatory	Period	Geographic		Geomagnetic	
		Lat.	Long.†	Lat.	Long.†
		°	°	°	°
(1) Cheltenham (CH)	1922–46	38.7 N	283.2	50.1 N	350.5
(2) Tucson (TU)	1910–46	32.2 N	249.2	40.4 N	312.2
(3) San Juan (SJ)	1926–46	18.4 N	293.9	29.9 N	3.2
(4) Honolulu (HO)	1902–46	21.3 N	201.9	21.1 N	266.5
(5) Huancayo (HU)	1922–46	12.0 S	284.7	0.6 S	353.8
(6) Watheroo (WA)	1919–46	30.3 S	115.9	41.8 S	185.6

†All longitudes are east.

a beginning by examining the magnetic traces from six observatories, considering separately the data for SCs and SIs for the period 1926-1946, common to all six stations.

We hope that similar analyses will be made, making use of data from other observatories, in order to gain a better insight into what is undoubtedly a very complex phenomenon.

The geographic and geomagnetic latitudes and longitudes of the six observatories are given in Table 1, which also gives the length of the period of the records examined. Their locations are shown on the map in Figure 2.

FIG. 2—GEOGRAPHICAL DISTRIBUTION OF OBSERVATORIES WHOSE RECORDS WERE EXAMINED

The magnetic traces for observatories 1 to 4 were kindly made available by the Director of the United States Coast and Geodetic Survey for the purpose of the analysis, and those for observatories 5 and 6 by the Director of the Department of Terrestrial Magnetism, Carnegie Institution of Washington, under whose auspices these observatories were operated during the period examined.

§2—*The measurement of the magnetic traces*

The data collected for this paper have been obtained from the records of the horizontal force, H, declination, D, and vertical force, Z (measured positively upwards) at observatories 1 to 6 (Table 1). The traces were all measured by one of us (W.C.P.), the time of occurrence of an SC or SI being measured to the nearest minute. In selecting an SC or SI, we followed Newton in choosing no abrupt movement as an SC or SI unless this occurred in two of the three elements.

One characteristic feature of SCs and SIs is that they are not always detected at a particular station. This may be partly due to the fact that the movement may be too small to be distinguished from neighbouring movements on the traces.

Very few "inverted SCs" were recorded at any one of the six stations, eight being recorded at Watheroo, two at Honolulu, and one at the remaining stations, excepting San Juan, where none were recorded, making a total of 13—too few to be analyzed here.

§3—*The hourly frequency of SCs at the various stations*

We now consider the local time hourly frequency of SCs. These were selected from the period 1926-1946, this being common to all six stations. This selection was bound to be arbitrary to some extent, since it depends on a particular selection of storms preceded by an SC. It was decided to select all magnetic storms recorded at Watheroo (given in Vols. VII-A and VII-B of the Researches of the Department of Terrestrial Magnetism, Carnegie Institution of Washington) which were preceded by an SC at *at least one* of the six stations. In this way, we divided our data into a group of 141 SCs and a group of 338 SIs, giving a proportion of SCs to SIs of nearly 2 to 5.

Combining the local time hourly values of the number of SCs at the six stations, we plotted the mean percentage for each local hour. The result is shown in Figure 3*A*, and it is seen that the curve bears little resemblance to the curve of hourly frequencies obtained by Newton at Greenwich; also, that SCs appear to be slightly more frequent over the P.M. hemisphere. In order to test whether these variations were significant, we analysed the local time hourly frequency of SCs into diurnal and semi-diurnal harmonic terms; that is, we assumed that the number of SCs recorded at each local hour, t, of the day could be expressed in the form

$$a + b \cos(\theta - \alpha) + c \cos 2(\theta - \beta)$$

where $\theta = (t + \frac{1}{2}) \times 15°$.

After expressing the hourly values as percentages, we obtained the following expression

$$4.17 - 0.30 \cos(\theta - 63°) + 0.10 \cos 2(\theta - 7\tfrac{1}{2}°) \quad \ldots\ldots\ldots\ldots (1)$$

The probable error is 0.12 for each of the two amplitudes and 22° and 66° for the phases of the diurnal and semi-diurnal terms. The mean residual, 0.43, is large

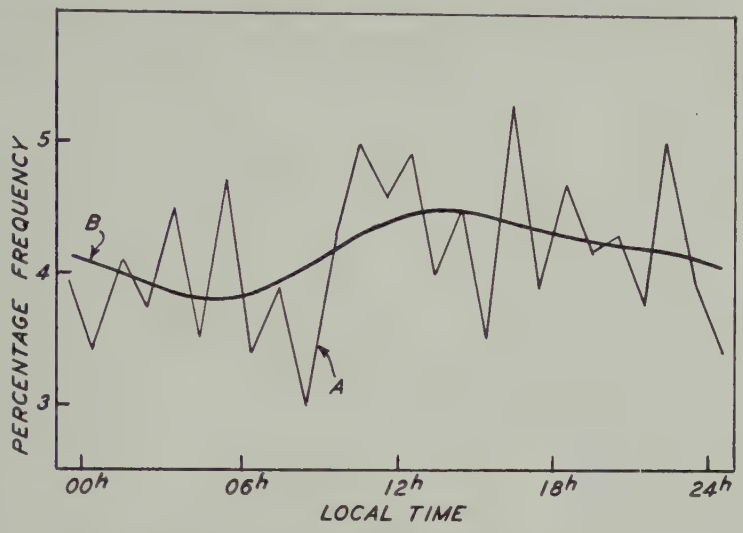

FIG. 3—LOCAL TIME AND SMOOTHED HOURLY FREQUENCIES OF SCs FROM COMBINED DATA

compared with either amplitude. The graph of (1) is shown in Figure 3*B*. When the third harmonic is included, the mean residual is reduced only slightly, its value being 0.42.

The results suggest that the variations are unlikely to be significant and, at best, the analysis would seem to lend support to Moos' remark (Section 1) that SCs have a slight tendency to be more frequent at about 13^h. *The smallness of the amplitudes of the two harmonics, however, shows that even if the variations were significant and are attributed to a local time effect, this must be small.*

§4—*The hourly frequency of SIs at the various stations*

The local time hourly frequencies for the SIs at the separate stations show no great similarity. Indeed, *better agreement is shown by the curves giving the U.T. hourly frequencies*, suggesting that *any local time effect on the hourly frequency of SIs* at any station is *comparatively* small. In order to trace any possible local time effect it was decided to combine the data for all six stations.

After combining the local time hourly frequencies for SIs for the six stations, we plotted the mean percentage for each local hour; the result is shown in Figure 4*A*. It will be seen that it bears some resemblance to the curve obtained by Newton. The analysis of the hourly values into diurnal and semi-diurnal harmonic terms (as in Section 3) gives

$$4.17 + 0.33 \cos(\theta + 43°) + 0.71 \cos 2(\theta - 34°) \cdots\cdots\cdots (2)$$

for the percentage hourly frequency, where $\theta = (t + \frac{1}{2}) \times 15°$, as before. The graph of this function is shown in Figure 4*B*.

The probable errors are 0.16 for the two amplitudes and 28° and 7° for the phases of the diurnal and semi-diurnal terms, respectively. The mean residual is 0.62 and so comparable with the amplitudes of the harmonic terms.

It will also be seen that the amplitude of the semi-diurnal term in (2) is nearly double that of the diurnal term, suggesting that any local time effect is likely to be semi-diurnal. This fact emerges more clearly from the analysis of the next section.

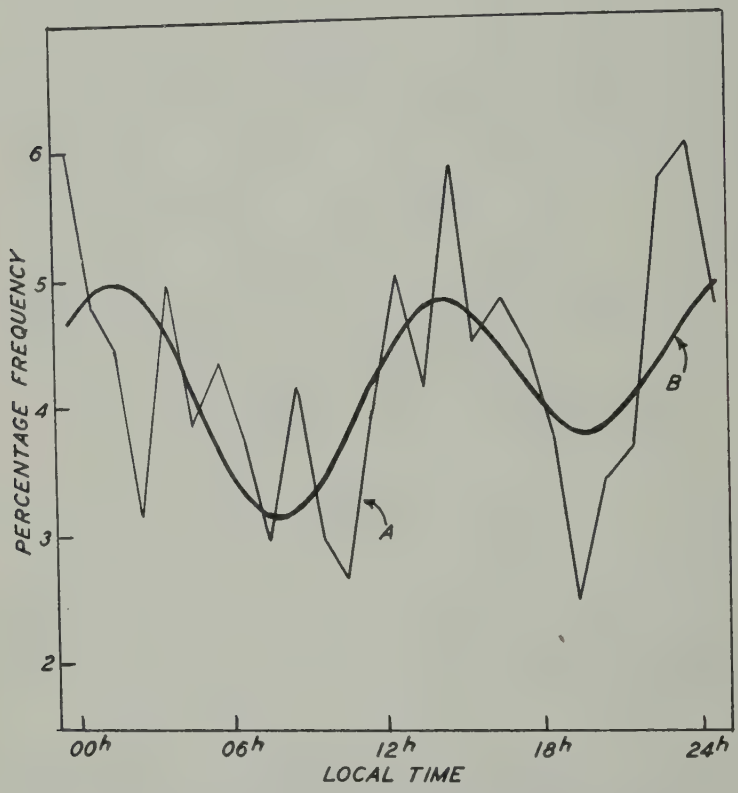

FIG. 4—LOCAL TIME AND SMOOTHED HOURLY FREQUENCIES OF SIs FROM COMBINED DATA

The above analysis does not take into account the fact that the greatest number of SCs (or SIs) recorded at any one U.T. hour of the day may not be uniform over the whole day for the comparatively short period of time here examined. For the six stations here examined, the greatest numbers of SCs recorded at each U.T. hour beginning at 00^h are as follows:

3, 5, 6, 8, 5, 6, 8, 7, 7, 4, 6, 3, 3, 4, 6, 5, 7, 7, 5, 3, 4, 6, 5, 11

and the greatest numbers of SIs recorded at each U.T. hour beginning at 00^h are likewise

4, 5, 8, 10, 10, 14, 5, 5, 8, 8, 15, 7, 7, 7, 5, 6, 5, 6, 4, 14, 11, 8, 6, 9

It will be seen that these hourly values are less uniform than might have been supposed and this non-uniformity must be reflected to some extent in the local time hourly values of the number of SCs and SIs. A more reliable index of a possible local time effect must be sought in this case. One such index is obtained by forming for each station the ratio n/N, where n is the observed frequency and N is the greatest frequency recorded for each U.T. hour, rearranging according to local time and taking the mean for the six stations for each local hour of the day. The mean so formed will be called the index I.

In the next two sections we have analysed the data for SCs and SIs using this index,

§5.1—*The variation of the index I with local time for SCs*

Figure 5*A* gives the local hourly values of the index I for SCs, and it will be seen that, as for the mean hourly values at all six stations, the variations from the mean are small and, hence, so is any likely local time effect. It will also be noted that this curve differs considerably from Figure 3*A* giving the mean hourly

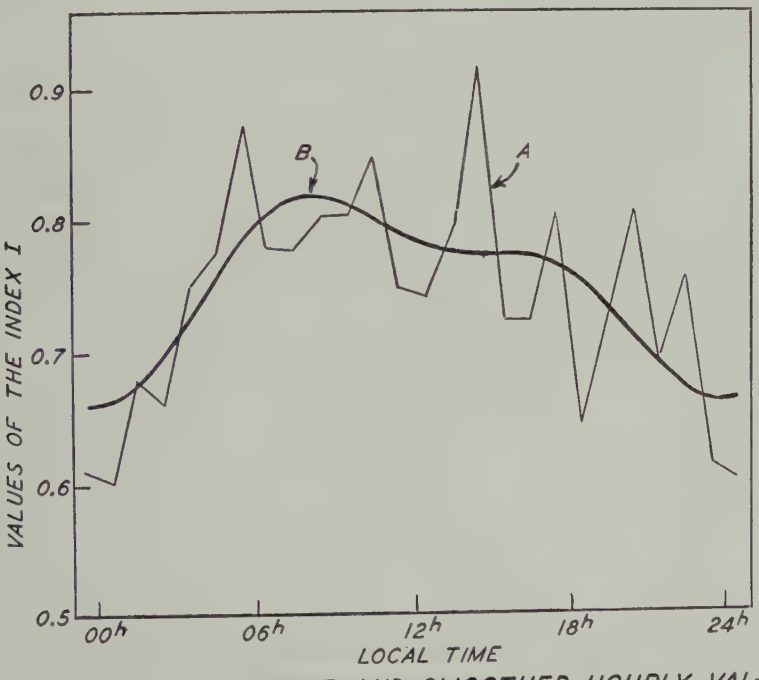

FIG. 5—LOCAL TIME AND SMOOTHED HOURLY VALUES OF INDEX I FOR SCs FROM COMBINED DATA

frequency of SCs, and suggests that the local time effect is greatest around local midnight and least around local noon.

The harmonic analysis similar to that in Sections 3 and 4 gives

$$0.752 - 0.066 \cos(\theta + 9\tfrac{1}{2}^\circ) - 0.029 \cos 2(\theta + 14^\circ) \quad \ldots\ldots\ldots (3)$$

for the hourly values of the index I, where $\theta = (t + \frac{1}{2}) \times 15°$, as before. The probable error for the two amplitudes is 0.013, and 11° and 13° for the phases of the diurnal and semi-diurnal terms. The mean residual is 0.046. It will be seen from this analysis also that the local time effect is small. The graph of (3) is shown in Figure 5*B*.

§5.2—*The variation of the index I with local time for SIs*

Figure 6*A* shows the local hourly values of the index I for SIs. It is seen to be greatly different from Figure 5*A* but bearing some resemblance to Figure 4*A* giving the mean hourly frequencies of SIs. The harmonic analysis into diurnal and semi-diurnal terms gives

$$0.693 + 0.020 \cos (\theta - 88°) + 0.095 \cos 2 (\theta - 26°) \ldots\ldots\ldots (4)$$

for the hourly values of the index I, where $\theta = (t + \frac{1}{2}) \times 15°$, as before. The graph of this function is shown in Figure 6*B*. The probable error is 0.019 for the

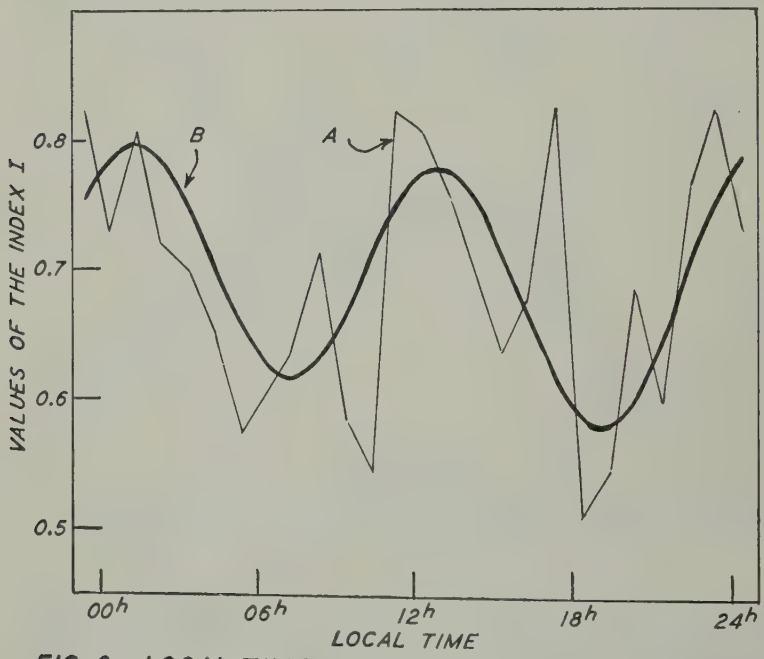

FIG. 6—LOCAL TIME AND SMOOTHED HOURLY VALUES OF INDEX I FOR SIs FROM COMBINED DATA

two amplitudes, and 54° and 6° for the phases of the diurnal and semi-diurnal terms, respectively. The mean residual is 0.067.

It will be seen from (4) that *the curve is very nearly semi-diurnal*, the amplitude of the semi-diurnal term being nearly five times as large as that of the diurnal term. Again, since the amplitudes of the two harmonic terms are small compared with the mean value, the analysis suggests that any local time effect on the fre-

quency of occurrence of SIs for the six stations is likely to be small. This seems also supported by the analysis of Section 4.

We note also that the phase of the semi-diurnal term (26°) is comparable with the phase of the corresponding term in the harmonic analysis of the mean hourly frequency, equation (2), namely, 34°.

TABLE 2—*Showing the (local) hourly frequencies of SC* and SI* at the various stations for the complete period examined in each case*

(Totals in the last two columns are for the six stations combined)

Local time	Hourly frequencies											
	Wa		SJ		Hu		Ch		Tu		Totals	
	SC*	SI*	SC*	SI*	SC*	SI*	SC*	SI*	SC*	SI*	SC*	SI*
hours												
0– 1	2	1	0	1	0	0	1	0	0	1	3	3
1– 2	0	0	0	2	1	0	0	0	1	1	2	3
2– 3	0	1	1	1	0	0	1	0	0	1	2	3
3– 4	0	0	1	0	0	1	1	0	0	0	2	1
4– 5	0	0	1	0	0	0	0	0	0	0	1	0
5– 6	0	0	2	1	2	0	1	0	0	0	5	1
6– 7	0	0	1	0	0	2	0	0	0	0	1	2
7– 8	0	0	1	0	2	4	0	0	0	0	3	4
8– 9	0	0	1	0	2	7	0	0	0	0	3	7
9–10	0	0	2	0	3	3	0	1	0	0	5	4
10–11	0	0	2	0	3	3	1	1	0	0	6	4
11–12	1	6	2	1	1	5	2	2	0	2	6	16
12–13	0	4	3	1	3	3	2	2	0	3	8	13
13–14	2	2	2	3	2	1	1	1	2	2	9	9
14–15	5	2	3	4	1	5	3	9	1	8	13	28
15–16	2	2	1	6	1	4	2	4	2	2	8	18
16–17	0	4	2	1	1	1	3	8	1	6	7	20
17–18	2	3	1	8	1	0	5	5	1	3	10	19
18–19	3	4	1	1	1	0	2	3	3	1	10	9
19–20	1	0	3	0	0	1	1	1	2	0	7	2
20–21	0	2	1	1	0	0	1	2	1	3	3	8
21–22	2	2	1	1	0	1	2	1	0	5	5	10
22–23	1	1	1	0	0	0	4	2	0	0	6	3
23–24	1	1	1	3	1	1	0	1	1	0	4	6
Totals	22	35	34	35	25	42	33	43	15	38		

The minima in the curve for the index I occur at $7\frac{1}{2}^{h}$ and $19\frac{1}{2}^{h}$ (local time), respectively. These coincide approximately with the minima found by Newton in his analysis of the Greenwich data, though the second minimum in his graph is not so pronounced as that shown in Figures 5*A* and 6*A*. This may be accounted

for by the fact that Newton did not eliminate the SCs from his data; but this seems to a great extent to have been counteracted by the fact that he was dealing with a long series of records in which SIs were probably more numerous than SCs.

§6—*The hourly frequency of SCs* and SIs* at the various stations and its possible dependence on geomagnetic longitude*

The local time hourly frequencies of SCs* and SIs* are given in Table 2 for each of the above stations with the exception of Honolulu. The number of SCs* at this station are too few to be included. It will be seen that, except for Huancayo, the SCs* appear most frequently in the late morning and afternoon hours, and that SIs* appear to be most frequent from about 11^h to 17^h. These results appear to support Newton's suggestion that local solar time is a determining factor in the appearance of an SC* (or SI*); page 163 of [5].†

In Table 3 we give the total of SCs and SCs*, and also of SIs and SIs*, recorded at all stations other than Honolulu, and the ratio, f, of the total number of SCs* (or SIs*) to the number of SCs (or SIs) of all types. It will be seen that the ratios for SCs and SIs at any one station are very nearly the same (Table 3), and it

TABLE 3—*Showing for the period examined the total number of SCs (or SIs) of all types recorded at each station (N_{SC} or N_{SI}); total number of SCs* (or SI*s) recorded at each station (n_{SC*} or n_{SI*}); and the proportion of SCs* (or SIs*) recorded at each station (f_{SC} or $f_{SI} = n/N$)*

Station	N_{SC}	n_{SC*}	$f_{SC} = n_{SC*}/N_{SC}$	N_{SI}	n_{SI*}	$f_{SI} = n_{SI*}/N_{SI}$
Watheroo	119	22	0.18	196	35	0.18
San Juan	102	34	0.33	124	35	0.28
Huancayo	86	25	0.29	114	42	0.37
Cheltenham	99	33	0.33	128	43	0.34
Tucson	134	15	0.11	276	38	0.14

is interesting to note that the values of f for Cheltenham, San Juan, and Huancayo, which have approximately the same longitude, are comparable. Moreover, as for the combined data of SCs and SIs discussed in [6], when the ratio f for SCs and SIs is plotted against geomagnetic longitude, the points lie on regular curves (Figure 7). [Explanation of Figure 7: The points marked "x" or "o" refer to values of the ratios f_{SC} and f_{SI}, respectively, at stations other than Greenwich and Honolulu, where the "o" refers to the ratio for the combined data. The points marked "⊗" and "◎" refer to the values of f_{SC} and f_{SI} at Huancayo, in order to distinguish them from the values for Cheltenham on the same meridian.] This fact suggested the possibility that the frequency of occurrence of SCs* and SIs* might depend on geomagnetic longitude or possibly U.T., though, as was stressed in our letter to *Nature* [6], the data from many other stations in Europe and Asia

†In a recent letter to *Nature* [6] by two of us (V.C.A.F. and W.C.P.), it was stated that SCs* and SIs* occur most frequently after 12^h U.T. Further analysis of two other stations has shown that this is unlikely to be the case.

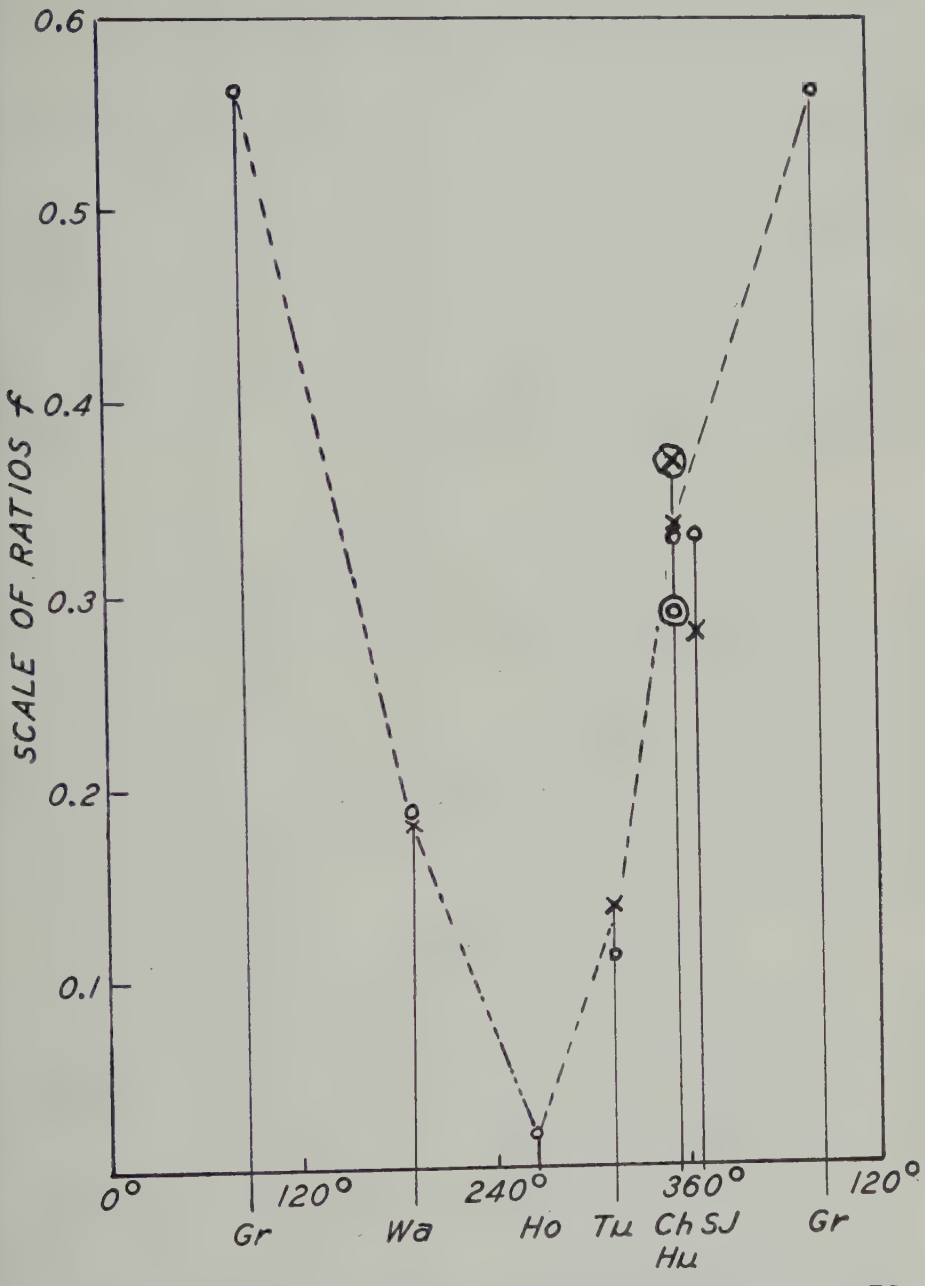

FIG. 7—RATIO f FOR SCs AND SIs PLOTTED AGAINST GEOMAGNETIC LONGITUDE

would need to be analysed before the suggested dependence on longitude could be established. Recent investigations, however, appear to be conflicting on this point. Thus, Watson and McIntosh [7] find that at Lerwick for the period 1934-1949, the value of the ratio f for SCs and SIs combined (including the "inverted" SCs or SIs) is 0.48, which is close to the value suggested on the basis of magnetic longitude. On the other hand, Jackson [8] casts doubt on the suggestion. On examining the records from Sitka for the three years 1946-1948, he finds that the ratio f is closer to the value for Abinger, though the longitude would indicate a value similar to that for Honolulu. However, as Jackson points out, no great weight can be placed on results obtained from only three years of magnetograms; it is also possible that Sitka is an anomalous station.

Again, Chakrabarty [9] has recently analysed the Alibag records of SCs and SIs for the period 1905-1944 and does not find a single SC* or SI*; in this the station resembles Honolulu. This result for Alibag must be taken as contradicting the simple relation suggested in [6].

§7—*Simultaneity of sudden commencements*

The data available would appear to afford a basis for an attempt to find out how far observations of the same SC made at different places fail to be simultaneous. The procedure described by Chapman [10] was applied to records of 40 SCs observed at the six stations, residuals from the mean recorded time (U.T.) being tabulated (Table 4).

Observations which would have given residuals exceeding two minutes were rejected (shown in parentheses) as probably recording a movement not strictly identical with the SC. In addition to mean residuals for each station and for each storm, totals and means were found for observations in each "quadrant" of local time; namely, Night P.M. (18^h to $23^h\ 59^m$), Night A.M., Day A.M., Day P.M. Means were also found for all P.M. and all A.M. observations, and for Night and Day observations.

(Units are 0.1 minute unless otherwise stated)

No. of Night A.M. residuals = 57 having total 28 and mean 0.49 = 2.9 sec
No. of Day A.M. residuals = 43 having total −140 and mean −3.26 = −19.6 sec
No. of Day P.M. residuals = 55 having total −29 and mean −0.53 = −3.2 sec
No. of Night P.M. residuals = 70 having total 139 and mean 1.99 = 11.9 sec

Mean P.M. residual = 0.88 Mean A.M. residual = −1.12
Difference P.M. − A.M. = 2.00 = 12.0 sec
Mean Night residual = 1.31 Mean Day residual = −1.72
Difference Night − Day = 3.03 = 18.2 sec

The Day P.M. residual found, −3.2 sec, is in agreement with the value found by Chapman, −2.6 sec. For the other quadrants, our values differ in sign from Chapman's, are numerically more than three times as large, and decrease steadily (from 18^h to the following 12^h) while Chapman's increase. The difference, P.M.—A.M., and Night—Day, are both opposite in sign to Chapman's figures (−5.3 sec, −3.3 sec,) and numerically larger. The probable errors of these differences appear to be about 48 sec, and those of the means of quadrants from 32 to 36

TABLE 4—*Showing residuals from the mean recorded time (U.T.) for 40 SCs observed at all six stations*

Date	Mean U.T.	Residuals						Mean numerical residual
		Wa	SJ	Hu	Ch	Tu	Ho	
	h m							
1926 Mar. 5	10 03.8	2	−18	2	2	2	12	6
May 3	21 13.4	6	(−24)	6	6	− 4	−14	7
Sep. 14	8 44.8	12	− 8	2	2	− 8	(−28)	6
Oct. 13	19 24.4	6	6	6	−14	− 4	(−34)	7
1927 Apr. 13	23 48.0	0	−10	0	10	0	0	3
Oct. 12	10 24.5	15	−15	5	−15	5	5	10
Oct. 22	6 39.2	8	−12	−12	8	8	− 2	8
1928 Sep. 24	16 23.4	− 4	(−34)	− 4	6	6	− 4	5
Oct. 18	7 24.5	5	− 5	− 5	15	5	−15	8
1929 Mar. 11	13 52.7	13	−17	3	− 7	− 7	13	10
1930 Dec. 3	1 06.8	2	− 8	2	2	2	(52)	3
1934 Jul. 30	3 18.4	− 4	16	− 4	(26)	− 4	− 4	6
1935 Jul. 7	21 08.5	− 5	−15	5	5	− 5	15	8
Oct. 24	6 39.0	−10	0	0	10	10	−10	7
1936 Oct. 31	1 24.3	−13	− 3	− 3	7	7	7	7
Nov. 28	23 36.8	2	2	2	− 8	12	− 8	6
Dec. 27	3 27.2	8	−12	8	− 2	(28)	− 2	6
1937 Jan. 27	8 37.2	−12	− 2	− 2	8	− 2	8	6
Mar. 26	20 55.7	3	−17	13	3	− 7	3	8
Apr. 24	12 00.7	3	−17	13	− 7	− 7	13	10
Sep. 30	13 45.3	7	−13	7	− 3	− 3	7	7
1938 Aug. 3	21 35.5	− 5	5	− 5	15	− 5	− 5	7
Sep. 13	18 37.2	−12	− 2	− 2	18	−12	8	9
1939 Apr. 17	1 57.3	− 3	− 3	7	7	7	−13	7
Jul. 21	9 58.7	−17	3	3	13	13	−17	11
Aug. 12	1 39.8	2	− 8	2	2	2	2	3
Oct. 13	2 05.4	−14	− 4	6	6	6	(−24)	7
1940 Apr. 25	2 04.3	−13	− 3	17	7	7	−13	10
May 23	17 54.2	−12	− 2	− 2	8	8	(−32)	6
Jun. 25	2 54.4	−14	− 4	6	6	6	(−24)	7
1941 Mar. 1	3 57.2	− 2	− 2	− 2	8	8	−12	6
Aug. 4	1 28.4	−14	− 4	6	6	6	(−24)	7
Oct. 31	3 41.2	−12	− 2	8	8	8	−12	8
1944 Dec. 15	18 52.4	− 4	− 4	− 4	6	6	(−24)	8
1946 Jan. 3	8 10.4	− 4	6	(−34)	16	− 4	−14	9
Mar. 28	6 36.0	0	0	−10	10	10	−10	7
Apr. 22	6 59.4	6	− 4	−14	6	6	(−24)	7
Jul. 26	18 46.0	10	−10	10	0	0	−10	7
Nov. 5	9 22.8	12	− 8	2	2	12	−18	9
Nov. 24	3 45.4	6	− 4	−14	6	6	(−34)	7
Mean residual		− 1.2	− 5.0	1.4	4.4	2.4	− 3.0	
Mean numerical residual		7.6	7.2	5.7	7.5	6.2	9.2	

sec; only in the case of the Day A.M. quadrant is the probable error less than twice the calculated mean residual.

In view of the relatively high probable error (estimated from standard deviations), no great value can be attached to the results obtained. For several reasons,

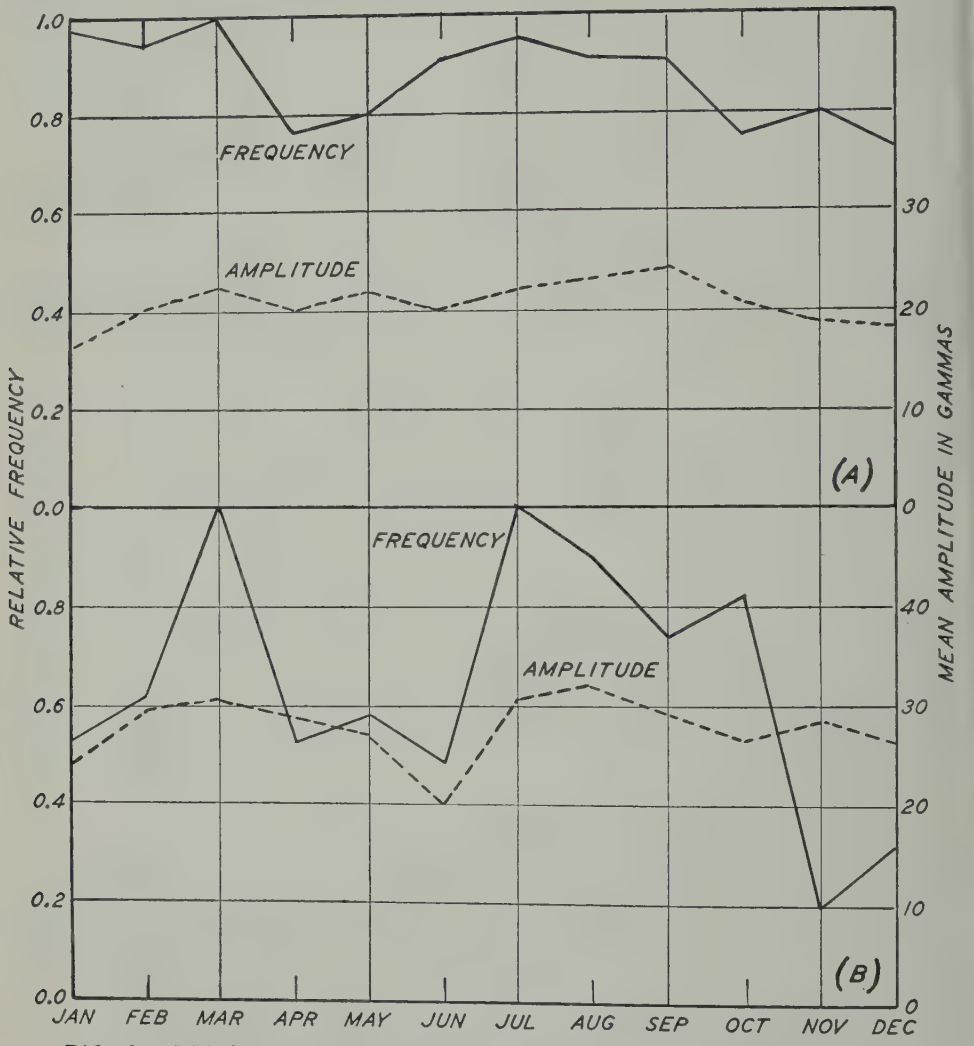

FIG. 8—RELATIVE MONTHLY FREQUENCIES AND MEAN AMPLITUDES AT HONOLULU, 1902–1946: (A) SCs AND SIs COMBINED; (B) SCs FOLLOWED BY DISTURBANCE

one might expect them to be less reliable than Chapman's figures, which the author did not regard as very satisfactory. Our times were given to the nearest minute by six stations, of which four had geographical longitudes within a range of 45°, while Chapman's were given by 32 stations, covering the world, most of which attempted greater precision. Several "runs" of + or of − for one station

occur in our Table and strongly suggest systematic errors persisting with the same sign but perhaps varying magnitude for seven years or longer. Such errors must have far too great effect on the means calculated if the number of stations is as small as six. In the course of the work it became obvious that the means might be appreciably changed by the inclusion or rejection of three or four SCs (for example, by variation of the date limits, January 1926 to December 1946).

§8—*Seasonal variation of SCs and SIs (combined data) at Honolulu*

The long series of records at Honolulu, from 1902 to 1946, provides an opportunity of comparing the seasonal variations at this station with that found by Newton at Greenwich. The results are shown in Figure 8*A*, which gives the monthly frequency (full line) and mean amplitude (dotted line) of the combined data for SCs and SIs. Figure 8*B* shows the corresponding frequencies for those SCs which are followed by storms. The curves for Greenwich and Honolulu differ only in the higher proportions of SCs and SIs during January and February at Honolulu. *But this difference disappears when only SCs (followed by large or moderate disturbance) are considered,* also suggesting a fundamental difference between SCs and SIs.

§9—*Annual variation in the number of SCs and SIs (combined data)*

Figure 9 shows the annual relative sunspot number (dotted line) from 1902 to 1946, slightly more than four sunspot cycles. Below we give the annual total number of SCs and SIs combined for each observatory. Apart from the general agreement of the cycles in sunspots and SCs and SIs, there are points of similarity between the SC and SI curves themselves, the most prominent of these being the decrease in their number during 1925. There is also a slight departure from a smooth curve in 1941. These effects are perhaps exaggerated by the large scale on which SCs and SIs are drawn, but there can be little doubt that they are real. Considering the sunspot curve, it will be seen that the mean values in the sunspot numbers during 45 years show a small steady increase and a similar increase is shown in the long series of Honolulu traces examined.

§10—*Discussion*

(1) The results of the analysis for the six stations considered here show that, as suggested by Chapman, a distinction should be drawn between sudden commencements of magnetic storms (SCs) and sudden impulses (SIs). Thus, the curve showing the hourly frequency of SCs for the combined data at all six stations shows little resemblance to the curve for the hourly frequency found by Newton at Greenwich. Any local time effect in the hourly frequency of SCs seems likely to be small, if it exists at all, and at best the analysis suggests that SCs may possibly be slightly more frequent in the local afternoon hours.

The hourly frequency of the combined data for SIs at all six stations is similar to Newton's curve of hourly frequency of SCs and SIs (combined) for Greenwich, but the second minimum around 20^h is somewhat deeper for the SIs. This difference may be ascribed to the fact that SCs, which seem to be more frequent in the local afternoon hours, are included in Newton's analysis.

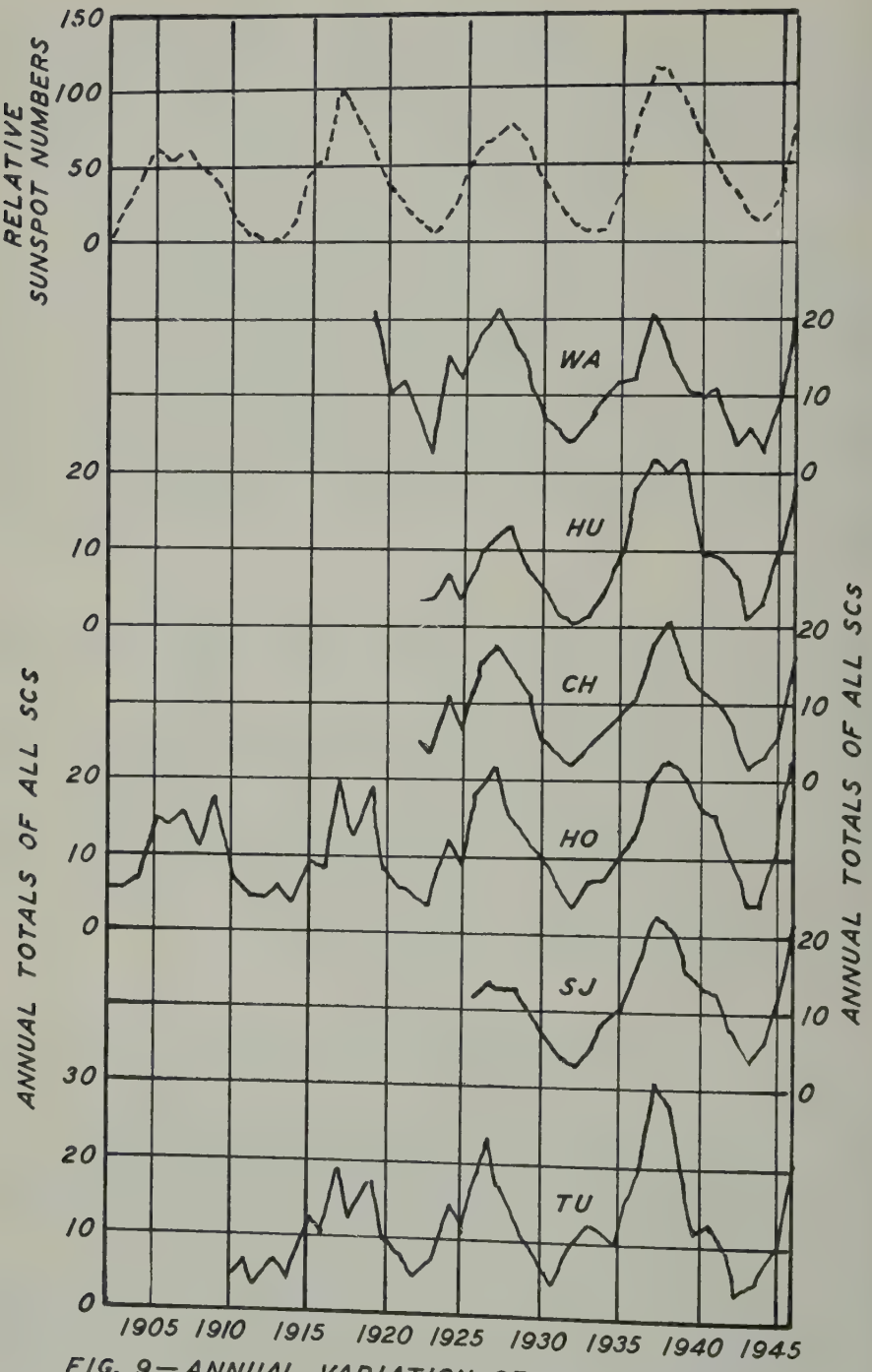

FIG. 9—ANNUAL VARIATION OF SCS AND SIS FOR ALL TYPES AND RELATIVE SUNSPOT NUMBERS

There is undoubtedly a local time effect in the hourly frequency of SIs and the harmonic analysis of Sections 4 and 5.2 suggests that this daily variation in the frequency may be very nearly semi-diurnal, with minima at 08^h and 20^h (approximately) local time. Any such local time effect may well be attributed to causes of terrestrial origin, but the fact that the variation is approximately semi-diurnal does not seem to lend much support to the suggestion that one such cause may be the electromagnetic shielding of the ionosphere.

(2) The daily variation of the frequency of SCs* and SIs* differs essentially from that found for ordinary SIs. There is a dependence on *local* solar time but the variation is simpler, both SCs* and SIs* occurring more frequently during the local afternoon hours. Further, the frequency of occurrence of both SCs* and SIs* for the six stations suggests a possible dependence on longitude (geographic or geomagnetic), though recent investigations would not seem to support this possibility [9]. The frequency of occurrence of SCs* and SIs* would now appear to be due to local conditions; and the fact that both SCs* and SIs* occur most frequently in the local afternoon hours at the stations here considered lends support to this view and suggests that the preliminary movement opposite to the direction of the main impulse may well be of atmospheric origin.

(3) The stations whose records have so far been examined are too few in number for definite conclusions to be reached regarding the nature of SCs and SIs. For this reason, we again urge that a synoptic study of SCs and SIs be facilitated by observatories analysing their own data for hourly frequencies, diurnal variation of mean amplitude in the horizontal force, seasonal variation, and variation with the 11-year solar cycle. What Newton calls SCs* and inverted SCs should also be studied synoptically.

We should like to express our thanks for criticisms and advice which we have received from the Astronomer Royal, Messrs. H. W. Newton and J. Jackson, and especially to Prof. S. Chapman, who first suggested that there might be a real difference between SCs and SIs.

References

[1] A. G. McNish, Res. Dep. Terr. Mag., Carnegie Inst. Wash., Pub. 175, **7-B**, 17 (1947).
[2] N. A. F. Moos, Colaba magnetic data, 1846 to 1905, Bombay (1910).
[3] L. Rodés, Terr. Mag., **37**, 273 (1932).
[4] A. G. McNish, Assemblée Lisbonne, Union Géod. Géophys. Internat., Ass. Mag. Electr. Terr., Bull. No. 9, 234 (1934).
[5] H. W. Newton, Mon. Not. R. Astr. Soc., Geophys. Sup., **5**, 159 (1948).
[6] V. C. A. Ferraro and W. C. Parkinson, Nature, **165**, 243 (1950).
[7] R. A. Watson and D. H. McIntosh, Nature, **165**, 1018 (1950).
[8] W. Jackson, Nature, **166**, 691 (1950).
[9] S. K. Chakrabarty, Nature, **167**, 31 (1951).
[10] S. Chapman, Proc. Phys. Soc., **30**, 205 (1918).

JOURNAL OF GEOPHYSICAL RESEARCH VOLUME 56, No. 2 JUNE, 1951

WAVE PACKETS, THE POYNTING VECTOR, AND ENERGY FLOW: PART II—GROUP PROPAGATION THROUGH DISSIPATIVE ISOTROPIC MEDIA

By C. O. Hines

Radio Physics Laboratory, Defense Research Board, Ottawa, Canada

(Received March 1, 1951)

ABSTRACT

An investigation of electromagnetic energy flow in complex media was initiated in Part I of the present series [see 1 of "References" at end of Part III], where non-dissipative anisotropic media were considered. Before a corresponding treatment in cases of dissipative media can be carried out, it is necessary to find expressions for the velocity of a wave packet in such media. In the present paper, an intermediate step of some general applicability is taken—that of finding the group speed in a dissipative isotropic medium. It is found that the most appropriate expression for this is $c/(\mathrm{d}kn_1/\mathrm{d}k)$, where n_1 is the real part of the refractive index at frequency $kc/2\pi$. In the course of the development, a common laxity in the formulation of the group is corrected, and also expressions are obtained which are applicable to the transmission of pulses through slabs of material.

1—*Introduction*

The concept of group speed in a dispersive medium is an important one, since it gives the speed of a signal much more accurately than does the phase speed. For non-dissipative media, which have a real refractive index, the development is fairly simple and may be made in various ways. Most suitable for our purposes, since it corresponds most closely to experimental conditions when pulses are transmitted, is a treatment in which a wave group is built up mathematically by the superposition of waves of varying frequencies traveling in the same direction. A common development is given below; it will be criticized later in this paper. (Comparison may be made with the treatment given by Stratton [2] for example; they are essentially the same.)

The group we shall consider consists of waves of frequency $kc/2\pi$ having unit amplitude if $|k - k_0| < K$ and zero amplitude otherwise. The resulting field is given in complex form by

$$F = \int_{k_0-K}^{k_0+K} \epsilon^{ik(nz-ct)}\,\mathrm{d}k \qquad (1)$$

for propagation in the z-direction through a medium having refractive index n (real). Assuming $n = n(k)$ to be a continuous function of k in the neighborhood of k_0, and taking K sufficiently small, (1) approximates to

$$f = \epsilon^{ik_0(nz-ct)} \int_{-k}^{k} \epsilon^{i(\dot{k}nz-ct)\kappa} \, d\kappa \quad \ldots\ldots\ldots\ldots\ldots\ldots (2)$$

where

$$\dot{k}n = \left(\frac{dkn}{dk}\right)_{k=k_0} \qquad \kappa = k - k_0 , \qquad \text{and} \qquad n = n(k_0),$$

This expression integrates to

$$f = 2\epsilon^{ik_0(nz-ct)} \frac{\sin [K(\dot{k}nz - ct)]}{\dot{k}nz - ct} \quad \ldots\ldots\ldots\ldots\ldots\ldots (3)$$

which has amplitude squared

$$f\tilde{f} = 4\left[\frac{\sin [K(\dot{k}nz - ct)]}{\dot{k}nz - ct}\right]^2 \quad \ldots\ldots\ldots\ldots\ldots\ldots (4)$$

a well-known function. This has its principal maximum where

$$\dot{k}nz - ct = 0 \ldots\ldots\ldots\ldots\ldots\ldots\ldots\ldots (5)$$

which leads to the expression for the group speed

$$u = c/\dot{k}n \ldots\ldots\ldots\ldots\ldots\ldots\ldots\ldots (6)$$

in non-dissipative media. The generalization of this expression for cases when absorption occurs is the problem of the present paper.

2—*Formal generalizations*

It will be seen that the mathematical development given above leads to the same result as the "stationary phase" rule. This rule, which says that the pulse maximum will be where the first-order variation of phase with frequency shall vanish, that is, $d(knz - kct)/dk = 0$, may be based on the physical picture of interfering waves.

Booker [3] has used this rule to locate the group maximum even when absorption occurs ($n = n_1 + in_2$ is complex), taking as "the phase" the whole of the complex expression

$$\Phi \equiv knz - kct \ldots\ldots\ldots\ldots\ldots\ldots\ldots\ldots (7)$$

The group speed obtained is then formally the same, $c/\dot{k}n$. This is a complex quantity (if k is real), unfortunately, and so is physically inadmissible as a true speed. Because of this, Booker has subjected the result to a reinterpretation. His suggestion is that, for a group to have a real speed, k must be complex. Nevertheless, it is here maintained that if we *have* a group made up of waves with real k, then that group must, on physical grounds, continue to exist and so must be located somewhere, at least for some time, however short. Actually, there is a breakdown of the concepts involved in formulating the rule of stationary phase when n (not to mention k) becomes complex, hence there is no real reason for expecting it to give a physically valid result.

Instead of basing our formulae on the semi-empirical stationary phase rule, we shall continue with the development given in section 1. Moreover, we shall insist on keeping k, z, and t real. The group may be built up as before, and the approximation (3) is as valid as before. However, the amplitude squared is now given by

$$f\tilde{f} = 4\epsilon^{-2kn_2z}\frac{\sin[K(kn z - ct)]\sin[K(k\tilde{n}z - ct)]}{(kn z - ct)(k\tilde{n}z - ct)} \quad \ldots\ldots\ldots\ldots (8)$$

$$= 2\epsilon^{-2kn_2z}\frac{\cosh[2Kkn_{2z}] - \cos[2K(kn_1z - ct)]}{(kn_2z)^2 + (kn_1z - ct)^2} \quad \ldots\ldots\ldots\ldots (9)$$

Writing $\partial f\tilde{f}/\partial z$ as a quotient, it can be shown that the numerator vanishes if $kn_2z = kn_1z - ct = 0$, which corresponds to the condition (5) for the principal maximum in the non-dissipative case. We do not obtain a maximum now, however, since the denominator of $\partial f\tilde{f}/\partial z$ also vanishes; it can be shown that the limiting value of the derivative as these conditions are approached is $-8K^2kn_2$, not zero at all. Of course, $\partial f\tilde{f}/\partial z$ will vanish for other z, t values, corresponding to the secondary maxima of (4), but the required relations for these involve K and so do not lead to characteristic speeds.

Various attempts have been made by the present author to obtain reasonable group speeds from (9) by various artificial processes. Some of these are outlined immediately below, together with their results. They are included here only for completeness.

(*i*) Expand (9) as a power series in K (which has been assumed small). To the second order, (9) becomes $4K^2\epsilon^{-2kn_2z}$, which has no maximum. If any higher order is considered, maxima will obtain, but their positions are dependent on K, so do not give a characteristic speed.

(*ii*) Consider z large, disregarding the cos term in (9) relative to the cosh term. A maximum appears at time $-t_1 \equiv -|s/2kn_2kn_2c|$ at the plane $z_1 = -(kn_1/s)ct_1 - (1/2kn_2)$, and disappears at time t_1 at the plane $z_2 = (kn_1/s)ct_1 - (1/2kn_2)$. Here $s = (kn_1)^2 + (kn_2)^2$. Whenever $|t| > t_1$, the amplitude monotonically decreases from infinity to zero as z runs from $-\infty$ to $+\infty$. The mean speed of the maximum, while it exists, is $z_2 - z_1/2t_1 = (kn_1/s)c$. This reduces to the group speed c/kn when no absorption occurs, and so is a possible expression for the group speed in the absorbing case. The derivation requires the two conditions $K|kn_1/kn_1| \gg 1 \gg K|kn_2/kn_2|$ to be fulfilled for validity.

(*iii*) Disregard the ϵ^{-2kn_2z} factor in (9), and expand the remainder as a power series in K. The first two terms of this expansion are $2K^2 + (2K^4/3)[(kn_2z)^2 - (kn_1z - ct)^2]$, which have a z-maximum at the plane given by

$$z = \frac{kn_1}{(kn_1)^2 - (kn_2)^2}ct \quad \ldots\ldots\ldots\ldots (10)$$

This yields another possibility for the group speed in dissipative media.

3—*The time maximum*

The results obtained in (*ii*) and (*iii*) above, while themselves acceptable, have been obtained by devious means which are in no wise satisfying. The method of

(*ii*), incidentally, has no counterpart in non-absorbing media. A new approach will now be introduced which has the two advantages of being physically sound—indeed, more in accord with experimental practice than the previous methods—and mathematically unique and direct. Its application will carry through from simple, homogeneous, non-absorbing media to cases of propagation through a slab of anisotropic dissipative media, giving reasonable, simple, unique results.

It will be noticed that in all the preceding work we have been seeking the z-maximum of the pulse. For physical application, this would require knowledge of the fields existing at all points in a certain region at a certain instant or, to determine speed, at more than one instant. While such a procedure might be possible, it is certainly not common. The usual experimental practice is for the observer to remain at one spot and observe the fields as the time progresses. He would consider the pulse to be passing when the time derivative of the amplitude vanishes.

Using (9) again, and setting $(\partial/\partial t) f\tilde{f} = 0$, we obtain

$$[(\dot{kn}_2 z)^2 + (\dot{kn}_1 z - ct)^2]\, 2Kc \sin\,[2K(\dot{kn}_1 z - ct)]$$

$$= 2c\{\cosh\,[2K\dot{kn}_2 z] - \cos\,[2K(\dot{kn}_1 z - ct)]\}[\dot{kn}_1 z - ct] \quad \ldots\ldots (11)$$

This condition is satisfied if

$$\dot{kn}_1 z - ct = 0 \quad \ldots\ldots (12)$$

which leads to the group speed

$$U = c/\dot{kn}_1 \quad \ldots\ldots (13)$$

This is the general formula, valid for both dissipative and non-dissipative media; it is the generalization of (6); it is the speed which would be obtained by the stationary phase rule if the real part of $knz - kct$ is taken as "the phase."

By setting $\dot{kn}_1 z - ct = 0$ and expanding the cosh term in $\partial^2 f\tilde{f}/\partial t^2$, it may be verified that a maximum is always obtained. While the condition (12) is sufficient for a maximum, it is not necessary, and secondary maxima will occur as in the non-dissipative case. However, if (11) is expanded as a power series in K, and only the lowest order non-vanishing terms be kept, then (12) does become necessary.

4—*Criticism*

We shall now proceed to investigate the basic steps taken in deriving the group speed for non-absorbing media. In so doing, we shall correct a common error and lay the ground for future development.

It will be seen that the step from (1) to (2) was made on the basis of the approximation

$$\Phi \approx \Phi_0 + \dot{\Phi}\kappa \quad \ldots\ldots (14)$$

where $\Phi_0 = \Phi(k_0)$, $\Phi = k(nz - ct)$, $\cdot = (\partial/\partial k)_{z,t\ \text{const.}}$, and $\kappa = k - k_0$. This is a legitimate first-order approximation and is valid for κ sufficiently small. However, the first-order approximation to

$$\epsilon^{i\Phi} \equiv \epsilon^{i\Phi_0}(1 + i\dot{\Phi}\kappa + \tfrac{1}{2}[i\ddot{\Phi} - \dot{\Phi}^2]\kappa^2 + \cdots) \quad \ldots\ldots (15)$$

is $\epsilon^{i\Phi_0}(1 + i\dot{\Phi}\kappa)$, not

$$\epsilon^{i(\Phi_0+\dot{\Phi}\kappa)} \equiv \epsilon^{i\Phi_0}(1 + i\dot{\Phi}\kappa - \tfrac{1}{2}\dot{\Phi}^2\kappa^2 - \cdots) \quad \ldots\ldots\ldots\ldots\ldots\ldots(16)$$

No error would be involved if only the first-order approximation to (16) is used, but this is not the case: in integrating (2) to produce (3), the whole of (16) is used.

If we were to keep only the first two terms of (16), we would obtain $f \approx 2\epsilon^{i\Phi_0}K$, and this is the correct approximation to F as far as the second order in K. However, it gives no maximum of $f\tilde{f}$ and so is of no use in determining the position of the group. Before a maximum of $f\tilde{f}$ can be obtained, we must include at least three terms of (16), giving $f \approx 2\epsilon^{i\Phi_0}(K - \frac{1}{6}\dot{\Phi}^2K^3)$, which is a correct approximation for f as far as the third order in K. This is not, however, the correct third-order expression for F, which is properly $2\epsilon^{i\Phi_0}(K + \frac{1}{6}[i\ddot{\Phi} - \dot{\Phi}^2]K^3)$. Fortunately, though, the two squares of the amplitudes are equal, as far as the fourth order, as follows:

$$f\tilde{f} \approx 4(K^2 - \tfrac{1}{3}\dot{\Phi}^2K^4) \approx F\tilde{F} \quad \ldots\ldots\ldots\ldots\ldots\ldots(17)$$

Hence the maxima of $f\tilde{f}$ and $F\tilde{F}$ do occur together, at $\dot{\Phi} = 0$, so long as only terms up to and including the fourth order are considered and n is real.

If terms of higher order are considered, then the condition $\dot{\Phi} = 0$ continues to give a maximum of $f\tilde{f}$, but fails to give a maximum of $F\tilde{F}$, and so fails to determine the position of the group. Hence, if we continue to support $\dot{\Phi} = 0$ as determining the position of the group, we are compelled to limit ourselves to the consideration of only the lowest-order terms in the expansion of $F\tilde{F}$. The validity of the group speed rests, not on the validity of the first-order expansion (14) for Φ, but on the validity of the fourth-order expansion (17) for $F\tilde{F}$.

In all future generalizations of the group speed, our methods will be based on expansions similar to those just considered. By analogy, we shall keep only the lowest-order terms in the expansion, and just enough of them to provide a maximum. If any more terms were included, a maximum still could be found, but its position and speed would depend on the variable of the expansion (K here) and so would not be characteristic of the medium.

A slight generalization of the group concept may be obtained by allowing the amplitude factor to vary with frequency, say

$$A(k) = A_0 + A_k\kappa + \tfrac{1}{2}A_{kk}\kappa^2 + \cdots \quad \ldots\ldots\ldots\ldots\ldots\ldots(18)$$

for $|\kappa| < K$, and $A(k) = 0$ otherwise. The subscript k indicates $\mathrm{d}/\mathrm{d}k$. Then

$$\begin{aligned} F &= \int_{k_0-K}^{k_0+K} A(k)\epsilon^{i\Phi}\,\mathrm{d}k \\ &= \epsilon^{i\Phi_0}\int_{-K}^{K} [A_0 + (i\dot{\Phi}A_0 + A_k)\kappa \\ &\qquad + (\tfrac{1}{2}A_{kk} + i\dot{\Phi}A_k + \tfrac{1}{2}[i\ddot{\Phi} - \dot{\Phi}^2]A_0)\kappa^2 + \cdots]\,\mathrm{d}\kappa \\ &= 2\epsilon^{i\Phi_0}[A_0K + \tfrac{1}{3}[\tfrac{1}{2}A_{kk} + i\dot{\Phi}A_k + \tfrac{1}{2}(i\ddot{\Phi} - \dot{\Phi}^2)A_0]K^3 + \cdots] \quad \ldots\ldots\ldots\ldots(19) \end{aligned}$$

and

$$F\tilde{F} = 4[A_0\tilde{A}_0K^2 + \tfrac{1}{3}\{A_0[\tfrac{1}{2}\tilde{A}_{kk} - i\dot{\Phi}\tilde{A}_k - \tfrac{1}{2}\dot{\Phi}^2\tilde{A}_0] + \tilde{A}_0[\tfrac{1}{2}A_{kk} + i\dot{\Phi}A_k - \tfrac{1}{2}\dot{\Phi}^2A_0]\}K^4 + \cdots] \quad \ldots\ldots(20)$$

the terms in $\ddot{\Phi}K^4$ again disappearing. The principal maximum now occurs where

$$2A_0\tilde{A}_0\dot{\Phi} = i(A_k\tilde{A}_0 - \tilde{A}_kA_0) \quad \ldots\ldots(21)$$

The inclusion of A_{kk} thus has made no change in the location of the maximum; the inclusion of A_k changes the location, but not the speed, of the maximum. Since experimental pulses approximate to (19) more closely than to (1), this result is of interest. The displacement of the maximum due to A_k has an analogue, which will appear in section 5, for propagation through a slab; there it will be of importance.

Turning now to dissipative media, it will be seen that (8), (9), etc., have been invalidated. In place of them, we proceed as for (17) to deduce

$$F\tilde{F} = 4\epsilon^{-2\dot{k}n_2z}(K^2 + \tfrac{1}{6}K^4[i(\ddot{\Phi} - \ddot{\tilde{\Phi}}) - \dot{\Phi}^2 - \dot{\tilde{\Phi}}^2] + \cdots) \quad \ldots\ldots(22)$$

$$= 4\epsilon^{-2\dot{k}n_2z}(K^2 + \tfrac{1}{3}K^4[-\ddot{k}n_2z - (\dot{k}n_1z - ct)^2 + (\dot{k}n_2z)^2] + \cdots) \quad \ldots\ldots(23)$$

No z-maximum can be found from this which does not involve K. However, keeping only those terms shown explicitly in (23), a t-maximum occurs at the plane given by $\dot{k}n_1z - ct = 0$. Hence we are led again (but this time by a more correct route) to the expression $c/\dot{k}n_1$, given in (13), for the group speed.

5—*Group propagation through a dissipative slab*

In sections 2 and 3 we treated propagation in an infinite homogeneous dissipative medium. The results obtained were in many ways not satisfying. When a z-maximum was sought for, different artificial procedures led to different results. As a matter of fact, when $K \to 0$, no z-maximum exists. To escape these difficulties we were led, by physical reasoning to be sure, to locate the group by its t-maximum. This fortunately led to a reasonable solution without further artifice.

In the present section, we shall consider a concrete case in which the difficulties inherent in the complexity of the refractive index will not appear. Moreover, there will be no question as to whether the z- or t-maximum should be found, since they occur at the same plane. A further advantage of this treatment, it will be seen, lies in its closer correspondence to usual experimental conditions.

We shall consider a slab of the dissipative medium lying between the planes $z = 0$ and $z = D$, with vacuum outside this region. We shall create a group which will impinge normally on it from one side ($z < 0$), and calculate what happens. We shall not try to follow the group while it is inside the slab because of difficulties apparent from the previous treatment. We can, however, calculate the times at which the group enters and leaves the slab, and hence find its effective speed while it is inside. By eliminating the boundary effects, we shall obtain the effective group speed characteristic of the medium.

A complete solution of the wave equation is given by

$$\left.\begin{aligned}
&\mathbf{E} = E_{\mathrm{I}}\mathbf{i}, \qquad \mathbf{H} = H_{\mathrm{II}}\mathbf{j} \\
E_{\mathrm{I}} &= E_1^+ \epsilon^{ik(z-ct)} + E_1^- \epsilon^{-ik(z+ct)} && \text{for } z < 0 \\
&= e_1^+ \epsilon^{ik(nz-ct)} + e_1^- \epsilon^{-ik(nz+ct)} && \text{for } 0 \le z \le D \\
&= \mathcal{E}_1 \epsilon^{ik(z-ct)} && \text{for } D < z \\
H_{\mathrm{II}} &= E_1^+ \epsilon^{ik(z-ct)} - E_1^- \epsilon^{-ik(z+ct)} && \text{for } z < 0 \\
&= ne_1^+ \epsilon^{ik(nz-ct)} - ne_1^- \epsilon^{-ik(nz+ct)} && \text{for } 0 \le z \le D \\
&= \mathcal{E}_1 \epsilon^{ik(z-ct)} && \text{for } D < z
\end{aligned}\right\} \quad \ldots\ldots(24)$$

Here $\mathbf{E}$ is the electric field, $\mathbf{H}$ the magnetic field (Heaviside-Lorentz units), $\mathbf{i}$ and $\mathbf{j}$ are unit vectors in the x- and y-directions, and $n = n_1 + in_2$ is the complex refractive index inside the slab. To satisfy boundary conditions, the amplitude factors $E_1^+ E_1^- e_1^+ e_1^-$ and $\mathcal{E}_1$ must be such that $\mathbf{E}$ and $\mathbf{H}$ are continuous across the interfaces. Hence we require

$$\left.\begin{aligned}
E_1^+ &= e_1^+ + e_1^- - E_1^- \\
E_1^+ &= ne_1^+ - ne_1^- + E_1^- \\
0 &= \epsilon^{iknD} e_1^+ + \epsilon^{-iknD} e_1^- - \epsilon^{ikD} \mathcal{E}_1 \\
0 &= n\epsilon^{iknD} \epsilon_1^+ - n\epsilon^{-iknD} e_1^- - \epsilon^{ikD} \mathcal{E}_1
\end{aligned}\right\} \quad \ldots\ldots(25)$$

Solving this simultaneous set, we obtain

$$\mathcal{E}_1 = \frac{4n}{\Delta} E_1^+ = 4\mathcal{R}(k)\, E_1 \quad \text{say} \ldots\ldots(26)$$

where the determinant of the coefficients on the right of (25) is

$$\Delta = (n+1)^2 \epsilon^{-ik(n-1)D} - (n-1)^2 \epsilon^{ik(n+1)D} \ldots\ldots(27)$$

and $\mathcal{R}$ is defined by (26) itself.

Two omissions from (24) may require comment. No term in $\epsilon^{-ik(z+ct)}$ was included in the region $D < z$, in order that the solution should contain only outgoing waves there. Nor were components $E_{\mathrm{II}}\,\mathbf{j}$ and $H_{\mathrm{I}}\,\mathbf{i}$ included, since they may be superimposed at will, and only add unnecessary complications.

Due to the linearity of Maxwell's equations and of the boundary conditions, any superposition of solutions (24) for various k's will be a solution. We shall build up the usual incident group

$$\left.\begin{aligned}
F_1^+ &= E_1^+ \int_{-K}^{K} \epsilon^{i(k_0+\kappa)(z-ct)}\, d\kappa && z < 0 \\
&= 2E_1^+ \epsilon^{ik_0(z-ct)} \frac{\sin[K(z-ct)]}{z-ct} && z < 0
\end{aligned}\right\} \quad \ldots\ldots(28)$$

where the integration is done accurately, no question of approximations arising. The principle maximum is at $z = ct$ and enters the slab (at $z = 0$) at time $t = 0$.

Corresponding to this group, there must be a reflected group

$$F_1^- = \int_{-K}^{K} E_1^-(k_0 + \kappa)\, \epsilon^{-i(k_0+\kappa)(z+ct)}\, d\kappa \qquad z < 0 \quad \ldots\ldots\ldots (29)$$

and a transmitted one

$$\mathfrak{F}_1 = \int_{-K}^{K} \mathcal{E}_1(k_0 + \kappa)\, \epsilon^{i(k_0+\kappa)(z-ct)}\, d\kappa \qquad D < z \quad \ldots\ldots\ldots (30)$$

The amplitude factors are to be found from (25) with E_1^+ held constant. If we expand the functions concerned as power series in K, (27) becomes

$$\mathfrak{F}_1 = 4E_1\, \epsilon^{ik_0(z-ct)} \int_{-K}^{K} [\mathcal{R} + \mathcal{R}_k\kappa + \tfrac{1}{2}\mathcal{R}_{kk}\kappa^2 + \cdots] \times$$

$$[1 + i(z - ct)\kappa - \tfrac{1}{2}(z - ct)^2\kappa^2 + \cdots]\, d\kappa$$

$$= 8E_1\, \epsilon^{ik_0(z-ct)}[\mathcal{R}K + \tfrac{1}{3}[\tfrac{1}{2}\mathcal{R}_{kk} + i\mathcal{R}_k(z - ct) - \tfrac{1}{2}\mathcal{R}(z - ct)^2]K^3 + \cdots] \ldots\ldots (31)$$

Here the subscript k denotes differentiation with respect to k; $\mathcal{R}$ and its derivatives are evaluated at $k = k_0$. The group has amplitude squared

$$\mathfrak{F}_1\tilde{\mathfrak{F}}_1 = 64E_1\tilde{E}_1\{\mathcal{R}\tilde{\mathcal{R}}K^2 + \tfrac{1}{3}[\mathcal{R}[\tfrac{1}{2}\tilde{\mathcal{R}}_{kk} - i\tilde{\mathcal{R}}_k(z - ct) - \tfrac{1}{2}\tilde{\mathcal{R}}(z - ct)^2]$$

$$+ \tilde{\mathcal{R}}[\tfrac{1}{2}\mathcal{R}_{kk} + i\mathcal{R}_k(z - ct) - \tfrac{1}{2}\mathcal{R}(z - ct)^2]]K^4 + \cdots\} \ldots (32)$$

We now let K become small, and retain only enough terms in (32) as are necessary to obtain a maximum; this requires just those terms which are given explicitly. The z- and t-maxima both occur at the plane given by

$$2\mathcal{R}\tilde{\mathcal{R}}(z - ct) = i(\mathcal{R}_k\tilde{\mathcal{R}} - \tilde{\mathcal{R}}_k\mathcal{R}) \ldots\ldots\ldots\ldots\ldots\ldots (33)$$

This maximum moves through the vacuum ($D < z$) at the speed c; it emerged from the slab (at $z = D$) at time

$$t_D = \frac{D}{c} + \frac{i}{2c}\left(\frac{\tilde{\mathcal{R}}_k}{\tilde{\mathcal{R}}} - \frac{\mathcal{R}_k}{\mathcal{R}}\right) \ldots\ldots\ldots\ldots\ldots\ldots (34)$$

From (25) and (26)

$$\frac{\tilde{\mathcal{R}}_k}{\tilde{\mathcal{R}}} - \frac{\mathcal{R}_k}{\mathcal{R}} = \frac{\tilde{n}_k}{\tilde{n}} - \frac{n_k}{n} + \frac{\Delta_k}{\Delta} - \frac{\tilde{\Delta}_k}{\tilde{\Delta}} \ldots\ldots\ldots\ldots\ldots\ldots (35)$$

$$\Delta_k = iD\Delta - ikn D[(n + 1)^2\, \epsilon^{-ik(n-1)D} + (n - 1)^2\, \epsilon^{ik(n+1)D}]$$

$$+ 2n_k[(n + 1)\, \epsilon^{-ik(n-1)D} - (n - 1)\, \epsilon^{ik(n+1)D}] \ldots\ldots\ldots\ldots\ldots\ldots (36)$$

where we have reverted to kn for dkn/dk. We may substitute from (36) into (35) and thence into (34) to obtain the exit time of the pulse. The resulting expression

for t_D is a very complicated function of D, due to the effect that the boundaries have on the group. To obtain a result characteristic of the medium, not of the slab itself, these effects must be eliminated. We might expect that this could be done by increasing the thickness of the slab indefinitely; this would increase the effect of the medium relative to that of the boundaries.

As D tends to infinity, we may neglect the first two terms on the right of (35) and the last term on the right of (36), since they become negligible compared to the others appearing. Moreover, assuming $n_2 > 0$, only the increasing exponential terms having $\epsilon^{-ik(n-1)D} \equiv \epsilon^{kn_2D}\epsilon^{-ik(n_1-1)D}$ as factors need be retained in the second term on the right of (36) and in Δ. Then we have approximately

$$\left.\begin{aligned} \Delta_k &\approx iD\Delta - ik\dot{n}D\Delta \\ \frac{\tilde{\mathcal{R}}_k}{\tilde{\mathcal{R}}} - \frac{\mathcal{R}_k}{\mathcal{R}} &\approx 2iD - i(k\dot{n} + k\dot{n})D = 2i(1 - k\dot{n}_1)D \\ t_D &\approx \frac{k\dot{n}_1}{c} D \end{aligned}\right\} \quad \ldots\ldots\ldots (37)$$

This leads immediately to the effective speed

$$U_{slab} = c/k\dot{n}_1 \quad \ldots\ldots\ldots\ldots\ldots\ldots\ldots\ldots (38)$$

of a group traversing a thick slab.

This result is quite reasonable if $n_1 > 0$, but surprising if $n_1 < 0$. These two cases correspond (since we have taken $n_2 > 0$) to an absorbing and a regenerative medium, respectively. The difficulty is again due to boundary effects. In an absorbing medium, any internally reflected wave is damped and even eliminated when $D \to \infty$, whereas in a regenerative medium an internally reflected wave is amplified and becomes of overwhelming importance as $D \to \infty$. If we are to obtain results which are to be applicable to infinite media, the internally reflected waves must be removed from consideration. This is only possible, by letting $D \to \infty$, in an absorbing medium. Expression (38) is then valid for $D \to \infty$, that is, when treating a thick slab; it may also be expected to give the proper result for an infinite absorbing medium.

Had we taken $n_2 < 0$, the approximation in (37) would be somewhat altered and would lead to $U_{slab} = -c/k\dot{n}_1$. This gives a reasonable result if $n_1 < 0$, which now corresponds to an absorbing medium. This is to be expected, since it should not matter which root of n^2 we take as $n_1 + in_2$.

For transparent media, where $n_2 = 0$, the approximations (37) are not valid. A complete treatment of this case leads to the approximation, for D large $[D(\mathrm{d}kn/\mathrm{d}k) \gg (\mathrm{d}n/\mathrm{d}k)]$,

$$U_{slab} \approx \frac{c}{k\dot{n}} \frac{4n^2 + (n^2 - 1)^2 \sin^2 (knD)}{2n(n^2 + 1)} \quad \ldots\ldots\ldots\ldots (39)$$

This oscillates between $2n/(n^2 + 1)$ and $(n^2 + 1)/2n$ times the group speed obtained for an infinite homogeneous transparent medium. It appears then that experi-

ments on thick slabs of non-absorbing media may not give the expected group speeds. The complication occurring here is due, of course, to boundary effects; multiply reflected waves are not attenuated. The approximation (39) is obtained if the slab is only slightly absorbing and many wave-lengths thick, though peculiar results may be expected also for thin slabs.

If we desire to obtain the group speed of an infinite homogeneous non-absorbing medium by the present methods, we must introduce absorption to eliminate the boundary effects. Having obtained (38), we then let the absorption tend to zero, and so obtain the usual expression.

6—*Discussion and conclusion*

We have found an expression, $c/\dot{k}n_1$, which is claimed to be the group speed for any isotropic medium, absorbing or not. This claim cannot be seriously questioned, since "group speed" itself is largely a matter of mathematical definition. Whether or not it gives (approximately at least) the speed of an experimental pulse propagated through a dissipative medium is a more relevant question.

The development given has followed as closely as possible that which is appropriate to non-absorbing media, and the result for that case is generally accepted. The new methods which were required in making the generalization were indicated by physical considerations. It appears then that we have obtained the best generalization possible, outside of performing a complete Fourier analysis of a particular pulse.

In the process we have reformulated the mathematical group concept in terms of a consistent method of approximation, correcting a common laxity in this regard. We have also developed formulae applicable to the propagation of pulses through slabs of material.

Our main conclusion may be formulated as follows: For experiments on pulses propagated in infinite media or through slabs having appreciable absorption, the speed of transmission which is to be expected is $U = c/(\mathrm{d}kn_1/\mathrm{d}k)$.

WAVE PACKETS, THE POYNTING VECTOR, AND ENERGY FLOW: PART III—PACKET PROPAGATION THROUGH DISSIPATIVE ANISOTROPIC MEDIA

BY C. O. HINES

Radio Physics Laboratory, Defense Research Board, Ottawa, Canada

(Received April 9, 1951)

ABSTRACT

This paper is the third in a series investigating electromagnetic energy flow in media of complex natures. In it, formulae are developed giving the velocity of packet propagation in dissipative anisotropic media, for both homogeneous and inhomogeneous waves.

1—*Introduction*

In Part I of this series [see 1 of "References" at end of paper], formulae for the velocity of a wave packet in non-dissipative media were found and compared (as to direction) with the mean Poynting vector. Before a corresponding comparison can be made for dissipative media, the concepts and formulae used in [1] must be generalized. The first step towards this generalization was made in Part II [4], where plane pulse (group) propagation through a dissipative medium was considered. This yields a "group speed" $U = c/(\mathrm{d}kn_1/\mathrm{d}k)$ which is the component, in the direction of phase propagation, of the group velocity. The direction of the velocity cannot be determined from the use of a plane pulse (that is, localized near one plane) however, but requires a packet (that is, localized near one point) for its evaluation.

The present paper consists of a derivation of formulae for the packet velocity. It may be considered as an extension of the treatment in [4], and will be based upon the discussion found in both [1] and [4].

2—*Infinite medium*

We shall consider first the propagation of a packet consisting of waves of varying frequencies $kc/2\pi$ and varying direction cosines $\lambda\ \mu\ \nu$ of the phase normals, through an infinite homogeneous medium of effective permittivity ϵ_{pq} (see [1]). We shall treat one mode of propagation characterised by the complex refractive index $n_1 + in_2 = n = n(k, \lambda, \mu)$ which is one solution of equation (14), Part I, with ϵ_{pq} now replacing h_{pq} . We shall compose our packet out of waves having unit amplitude if $|k - k_0| < K$, $|\lambda| < L$, $|\mu| < M$, and zero amplitude other-

wise. Thus the packet contains waves centered about frequency $k_0c/2\pi$ and having propagation directions near the z-direction. The resulting complex field is then

$$F = \int_{k_0-K}^{k_0+K} \int_{-L}^{L} \int_{-M}^{M} \epsilon^{ik[n(\lambda x+\mu y+\nu z)-ct]}\, dk\, d\lambda\, d\mu \quad \ldots\ldots(1)$$

Writing $k[n(\lambda x + \mu y + \nu z) - ct] = \Phi$ and indicating partial differentiations at $k = k_0$, $\lambda = \mu = 1 - \nu = 0$, by subscripts, (1) may be expanded as

$$F = \epsilon^{ik(nz-ct)} \int_{-K}^{K} \int_{-L}^{L} \int_{-M}^{M} \{1 + i\Phi_k\kappa + i\Phi_\lambda\lambda + i\Phi_\mu\mu + \tfrac{1}{2}[(i\Phi_{kk} - \Phi_k^2)\kappa^2$$
$$+ (i\Phi_{\lambda\lambda} - \Phi_\lambda^2)\lambda^2 + (i\Phi_{\mu\mu} - \Phi_\mu^2)\mu^2 + (\ )\kappa\lambda + (\ )\lambda\mu$$
$$+ (\ )\kappa\mu] + \cdots\}\, d\kappa\, d\lambda\, d\mu \quad \ldots\ldots(2)$$

The integration is readily carried out, term by term, yielding

$$F = 8\epsilon^{ik(nz-ct)}[KLM + \tfrac{1}{6}(i\Phi_{kk} - \Phi_k^2)K^3LM + \tfrac{1}{6}(i\Phi_{\lambda\lambda} - \Phi_\lambda^2)KL^3M$$
$$+ \tfrac{1}{6}(i\Phi_{\mu\mu} - \Phi_\mu^2)KLM^3 + \cdots] \quad \ldots\ldots(3)$$

where all terms up to the fifth order in K, L, M are included. The group then has amplitude squared

$$F\tilde{F} = 64\epsilon^{-2kn_2z}[K^2L^2M^2 + \tfrac{1}{6}(i\Phi_{kk} - i\tilde{\Phi}_{kk} - \Phi_k^2 - \tilde{\Phi}_k^2)K^4L^2M^2$$
$$+ \tfrac{1}{6}(i\Phi_{\lambda\lambda} - i\tilde{\Phi}_{\lambda\lambda} - \Phi_\lambda^2 - \tilde{\Phi}_\lambda^2)K^2L^4M^2$$
$$+ \tfrac{1}{6}(i\Phi_{\mu\mu} - i\tilde{\Phi}_{\mu\mu} - \Phi_\mu^2 - \tilde{\Phi}_\mu^2)K^2L^2M^4 + \cdots] \quad \ldots\ldots(4)$$

where all terms up to the eighth order are shown.

In agreement with the formulation given in Part II, we find the position of the packet by maximizing only those terms of $F\tilde{F}$ which appear explicitly in (4). Moreover, we shall seek the t-maximum, rather than the z-maximum for reasons (physical and mathematical) given in Part II. Examination shows that t appears in the coefficient of $K^4L^2M^2$ only, x in that of $K^2L^4M^2$ only, y in that of $K^2L^2M^4$ only, while z appears in all these. Thus the mathematical simplicity gained by using the t-maximum rather than the z-maximum is even greater here than it was in Part II.

The conditions $(\partial/\partial t)F\tilde{F} = (\partial/\partial x)F\tilde{F} = (\partial/\partial y)F\tilde{F} = 0$ for the maximum, to the eighth order of K, L, M, become

$$0 = \frac{\partial}{\partial t}[-\dot{k}n_2z - (\dot{k}n_1z - ct)^2 + (\dot{k}n_2z)^2] = 2c(\dot{k}n_1z - ct) \quad \ldots\ldots(5)$$

$$0 = \frac{\partial}{\partial x}[-2kn_{2\lambda}x - kn_{2\lambda\lambda}z + kn_{2\lambda}z - k^2(n_1x + n_{1\lambda}z)^2 + k^2(n_2x + n_{2\lambda}z)^2]$$
$$= -2kn_{2\lambda} - k^2[2(n_1^2 - n_2^2)x + (n_1^2 - n_2^2)_\lambda z] \quad \ldots\ldots(6)$$

$$0 = \frac{\partial}{\partial y}[\ \ ] = -2kn_{2\mu} - k^2[2(n_1^2 - n_2^2)y + (n_1^2 - n_2^2)_\mu z] \quad \ldots\ldots(7)$$

on substituting for the various partial derivatives. Here $\cdot = \partial/\partial k$, and applies to the product in each case. The inclusion of the second derivatives in (2) has led to an alteration in the position of the packet from that which would be obtained on a simple extension of the common packet treatment. It does not affect the velocity of the packet, however. From (5)-(7) we can obtain this velocity as

$$\mathbf{V} = \left[-\frac{(n_1^2 - n_2^2)_\lambda}{2(n_1^2 - n_2^2)}\,\mathbf{i} - \frac{(n_1^2 - n_2^2)_\mu}{2(n_1^2 - n_2^2)}\,\mathbf{j} + \mathbf{k} \right] \frac{c}{\dot{k}n_1} \quad \ldots\ldots\ldots\ldots (8)$$

where **i**, **j**, and **k** are unit vectors in the x-, y-, and z-directions.

Thus the velocity has as its z-component the usual group speed $U = c/\dot{k}n_1$ found in Part II. The direction is given by the relative components

$$(n_1^2 - n_2^2)_\lambda : (n_1^2 - n_2^2)_\mu : -2(n_1^2 - n_2^2) \quad \ldots\ldots\ldots\ldots\ldots\ldots (9)$$

or

$$n^2{}_\lambda + \tilde{n}^2{}_\lambda : n^2{}_\mu + \tilde{n}^2{}_\mu : -2(n^2 + \tilde{n}^2) \quad \ldots\ldots\ldots\ldots\ldots\ldots (10)$$

or

$$(\mathrm{R.P.}n^2)_\lambda : (\mathrm{R.P.}n^2)_\mu : -2(\mathrm{R.P.}n^2) \quad \ldots\ldots\ldots\ldots\ldots\ldots (11)$$

where $\tilde{}$ indicates the complex conjugate and R.P. denotes the "real part." This direction may be compared with that given by

$$n_\lambda : n_\mu : -n \quad \ldots\ldots\ldots\ldots\ldots\ldots\ldots\ldots\ldots\ldots (12)$$

for the non-dissipative case. Obviously they agree for such media.

3—*Dissipative anisotropic slabs*

We shall now extend the treatment of slabs of material given in Part II by considering the medium as anisotropic, having effective permittivity matrix ϵ_{pq}. We shall make up an incident packet from components proportional to $\epsilon^{ik(\lambda x + \mu y - \nu z - ct)}$ as usual. If the slab is bounded by z = const. planes (say $z = 0$ and $z = D$), then boundary conditions require that the corresponding components inside the slab shall be proportional to $\epsilon^{ik(\lambda x + \mu y + Nz - ct)}$, where N is to be found. In absorbing media $N = N_1 + iN_2$ will be complex in general, whereas λ and μ are real. This means that the waves considered in the present section are inhomogeneous while they are inside the absorbing medium, in contradistinction to the homogeneous waves (proportional to $\epsilon^{ik[n(\lambda x + \mu y + \nu z) - ct]}$) considered in Part I and in the preceding section.

If the amplitude factors of the electric field are E_q (q = 1, 2, 3 for the x-, y-, and z-directions), then Maxwell's equations [(9), Part I] lead to

$$(\epsilon_{11} - N^2 - \mu^2)E_1 + (\epsilon_{12} + \lambda\mu)E_2 + (\epsilon_{13} + \lambda N)E_3 = 0 \quad \ldots\ldots (13)$$

$$(\epsilon_{21} + \lambda\mu)E_1 + (\epsilon_{22} - N^2 - \lambda^2)E_2 + (\epsilon_{23} + \mu N)E_3 = 0 \quad \ldots\ldots (14)$$

$$(\epsilon_{31} + \lambda N)E_1 + (\epsilon_{32} + \mu N)E_2 + (\epsilon_{33} - \lambda^2 - \mu^2)E_3 = 0 \quad \ldots\ldots (15)$$

These correspond to equations (11)-(13) of Part I, from which they may be obtained by substituting λ for $n\lambda$, μ for $n\mu$, N for $n\nu$, and $\lambda^2 + \mu^2 + N^2$ for n^2. (These are the substitutions involved in changing homogeneous waves into inhomogeneous waves.) Also we now have ϵ_{pq} instead of h_{pq} since we are no longer restricted to non-absorbing media. This formal distinction will be disregarded in future comparisons.

For non-vanishing fields, the determinant of the bracketted expressions must vanish, yielding a quartic for N:

$$f(N) \equiv a_4N^4 + a_3N^3 + a_2N^2 + a_1N + a_0 = 0 \quad \ldots\ldots\ldots\ldots (16)$$

where

$$a_4 = \epsilon_{33}$$

$$a_3 = (\epsilon_{32} + \epsilon_{23})\mu + (\epsilon_{31} + \epsilon_{13})\lambda$$

$$a_2 = \epsilon_{11}\lambda^2 + \epsilon_{22}\mu^2 + \epsilon_{33}(\lambda^2 + \mu^2 - \epsilon_{11} - \epsilon_{22}) + \epsilon_{32}\epsilon_{23} + \epsilon_{13}\epsilon_{31} + (\epsilon_{12} + \epsilon_{21})\lambda\mu$$

$$a_1 = \mu^3(\epsilon_{23} + \epsilon_{32}) + \lambda^3(\epsilon_{31} + \epsilon_{13}) + \lambda\mu^2(\epsilon_{31} + \epsilon_{13}) + \mu(\epsilon_{12}\epsilon_{31} + \epsilon_{21}\epsilon_{13} - \epsilon_{11}[\epsilon_{23} + \epsilon_{32}]) + \lambda^2\mu(\epsilon_{32} + \epsilon_{23}) + \lambda(\epsilon_{12}\epsilon_{23} + \epsilon_{21}\epsilon_{32} - \epsilon_{22}[\epsilon_{31} + \epsilon_{13}])$$

$$a_0 = (\epsilon_{11} - \mu^2)(\epsilon_{22} - \lambda^2)(\epsilon_{33} - \lambda^2 - \mu^2) - (\epsilon_{11} - \mu^2)\epsilon_{23}\epsilon_{32} - (\epsilon_{22} - \lambda^2)\epsilon_{13}\epsilon_{31} + (\epsilon_{21} + \lambda\mu)\epsilon_{13}\epsilon_{32} + (\epsilon_{12} + \mu\lambda)\epsilon_{23}\epsilon_{31} - (\epsilon_{12} + \mu\lambda)(\epsilon_{21} + \mu\lambda)(\epsilon_{33} - \lambda^2 - \mu^2)$$

These may be compared with the α_r's of Part I. Inspection shows that in the case of normal incidence ($\lambda = \mu = 1 - \nu = 0$), we obtain $a_r = \alpha_r$ ($r = 0, 1, \cdots 4$). If we write $b_r = \partial a_r/\partial\lambda$, $c_r = \partial a_r/\partial\mu$, and compare these with the β_r's and γ_r's of Part I, we see that for normal incidence $b_3 = \beta_4$, $c_3 = \gamma_4$, $b_1 = \beta_2$, $c_1 = \gamma_2$, and $b_4 = b_2 = b_0 = \beta_3 = \beta_1 = \beta_0 = \cdots = 0$.

In general there will be four distinct roots $N^{\mathrm{I}}N^{\mathrm{II}}N^{\mathrm{III}}N^{\mathrm{IV}}$ of the quartic (16). In the case of normal incidence, when $a_3 = a_1 = 0$, (16) becomes a quadratic in N^2, hence two of the roots are the negatives of the other two; say $N^{\mathrm{II}} = -N^{\mathrm{I}}$, $N^{\mathrm{IV}} = -N^{\mathrm{III}}$. Moreover, these are also the roots n of the corresponding homogeneous waves. The relative components of $\mathbf{E}$ can be given by setting $E_q = P_qA$, with the P_q's being obtained from (14) and (15) say, and A being an arbitrary amplitude factor. For normal incidence,

$$P_1 = \epsilon_{22}\epsilon_{33} - \epsilon_{23}\epsilon_{32} - N^2\epsilon_{33} \quad \ldots\ldots\ldots\ldots (17)$$

$$P_2 = \epsilon_{23}\epsilon_{31} - \epsilon_{21}\epsilon_{33} \quad \ldots\ldots\ldots\ldots (18)$$

$$P_3 = \epsilon_{21}\epsilon_{32} - \epsilon_{31}\epsilon_{22} + N^2\epsilon_{31} \quad \ldots\ldots\ldots\ldots (19)$$

These are the same P's as obtained for Part I. It should be noted that, at normal incidence, the P's for N^{I} and those for N^{II} are equal, since only N^2 occurs in them; similarly for N^{III} and N^{IV}.

A complete solution of the wave equations which will satisfy the boundary conditions at the planes $z = 0$, $z = D$ can be made up as follows: Each of the x-, y-, and z-components of **E** and of **H** includes a term proportional to $\epsilon^{ik(\lambda x+\mu y+\nu z-ct)}$ and another proportional to $\epsilon^{ik(\lambda x+\mu y-\nu z-ct)}$ in the region $z < 0$, terms proportional to $\epsilon^{ik(\lambda x+\mu y+N^{\mathrm{I}}z-ct)}$, $\cdots$, $\cdots$, $\epsilon^{ik(\lambda x+\mu y+N^{\mathrm{IV}}z-ct)}$, in the region $0 \leq z \leq D$, and a term proportional to $\epsilon^{ik(\lambda x+\mu y+\nu z-ct)}$ in the region $D < z$. The omission of a term in $\epsilon^{ik(\lambda x+\mu y-\nu z-ct)}$ in this last region ensures that only waves proceeding to $z = +\infty$ occur there. The electric amplitude factors may be taken as E_q^+, E_q^-, e_q^{I}, e_q^{II}, e_q^{III}, e_q^{IV}, and $\mathcal{E}_q$ in order, with $q = 1, 2, 3$ for the x-, y-, and z-components, respectively. All told, there are 21 such factors. The amplitude factors for **H** may be derived from all of these by means of Maxwell's equations. In the regions of vacuum, we have the condition $\lambda E_1^+ + \mu E_2^+ + \nu E_3^+ = 0$ and similar relations for the E^-'s and $\mathcal{E}$'s. Inside the slab, e_2^{I} and e_3^{I} are determined from e_1^{I} by (17) (18), (19) and similarly for the e^{II}'s, etc. These yield 11 conditions which can be used to reduce the number of independent amplitude factors to 10. The boundary conditions require that the x- and y-components of **E** and of **H** should be continuous across the interfaces at $z = 0$ and $z = D$. These yield eight more conditions, leaving only two amplitude factors undetermined. If we take E_1^+ and E_2^+ as the arbitrary amplitudes, all others become functions of these two and of k, λ, μ.

We may now build up an incident packet having x-component of E given in the region $z < 0$ by

$$F_1^+ = E_1^+ \int_{k_0-K}^{k_0+K} \int_{\lambda_0-L}^{\lambda_0+L} \int_{\mu_0-M}^{\mu_0+M} \epsilon^{ik(\lambda x+\mu y+\nu z-ct)}\, dk\, d\lambda\, d\mu \ldots\ldots\ldots (20)$$

remembering $\nu = \nu(\lambda, \mu)$. A similar y-component may be built up independently. These components are made up of waves having the constant amplitude E_1^+ (or E_2^+) if $|k - k_0| < K$, $|\lambda - \lambda_0| < L$, $|\mu - \mu_0| < M$, and zero amplitude otherwise. The corresponding z-component will be

$$F_3^+ = \int_{k_0-K}^{k_0+K} \int_{\lambda_0-L}^{\lambda_0+L} \int_{\mu_0-M}^{\mu_0+M} E_3^+\, \epsilon^{ik(\lambda x+\mu y+\nu z-ct)}\, dk\, d\lambda\, d\mu \ldots\ldots\ldots (21)$$

Here $E_3^+ = E_3^+(k, \lambda, \mu) = -(\lambda/\nu)E_1^+ - (\mu/\nu)E_2^+$, with E_1^+ and E_2^+ staying constant (that is, independent of k, λ, μ). Corresponding reflected and transmitted pulses will also occur.

We could find the time and point at which the incident packet enters the slab and the time and point at which the transmitted packet leaves it, thus obtaining an effective velocity of the packet while it is inside. This would be a very complicated analysis in the general case, and the results would depend on E_2^+/E_1^+, k_0, λ_0, μ_0, and D, as well as the various quantities usually appearing. For our present purposes, such a complete analysis is not worth the trouble; we want results which are dependent only on the medium and k_0, not on the packet or thickness of the slab. To eliminate the extraneous quantities we will introduce

	E_1^-	E_2^-	e_1^{I}	e_1^{II}	e_1^{III}	e_1^{IV}	$\mathcal{E}_1$	$\mathcal{E}_2$
E_1^+	-1	0	1	1	1	1	0	0
E_2^+	0	-1	π_2^{I}	π_2^{II}	π_2^{III}	π_2^{IV}	0	0
$\frac{\lambda\mu}{-\nu}E_1^+ - \frac{\mu^2+\nu^2}{\nu}E_2^+$	$\frac{\lambda\mu}{-\nu}$	$\frac{\mu^2+\nu^2}{-\nu}$	$\mu\pi_3^{\mathrm{I}} - N^{\mathrm{I}}\pi_2^{\mathrm{I}}$	$\cdots$	$\cdots$	$\cdots$	0	0
$\frac{\nu^2+\lambda^2}{\nu}E_1^+ + \frac{\lambda\mu}{\nu}E_2^+$	$\frac{\nu^2+\lambda^2}{\nu}$	$\frac{\lambda\mu}{\nu}$	$N^{\mathrm{I}} - \lambda\pi_3^{\mathrm{I}}$	$\cdots$	$\cdots$	$\cdots$	0	0
0	0	0	$\epsilon^{ikN^{\mathrm{I}}D}$	$\epsilon^{ikN^{\mathrm{II}}D}$	$\epsilon^{ikN^{\mathrm{III}}D}$	$\epsilon^{ikN^{\mathrm{IV}}D}$	$-\epsilon^{ik\nu D}$	0
0	0	0	$\pi_2^{\mathrm{I}}\epsilon^{ikN^{\mathrm{I}}D}$	$\cdots$	$\cdots$	$\cdots$	0	$-\epsilon^{ik\nu D}$
0	0	0	$(\mu\pi_3^{\mathrm{I}} - N^{\mathrm{I}}\pi_2^{\mathrm{I}})\,\epsilon^{ikN^{\mathrm{I}}D}$	$\cdots$	$\cdots$	$\cdots$	$\frac{\lambda\mu}{\nu}\epsilon^{ik\nu D}$	$\frac{\mu^2+\nu^2}{\nu}\epsilon^{ik\nu D}$
0	0	0	$(N^{\mathrm{I}} - \lambda\pi_3^{\mathrm{I}})\,\epsilon^{ikN^{\mathrm{I}}D}$	$\cdots$	$\cdots$	$\cdots$	$\frac{\nu^2+\lambda^2}{-\nu}\epsilon^{ik\nu D}$	$\frac{\lambda\mu}{-\nu}\epsilon^{ik\nu D}$

$\}$ . . . . . (22)

various conditions from time to time. These invariably make our analysis much simpler.

In the first place, it may be noted that in general all modes of propagation within the slab are excited. If we restrict our consideration to characteristic modes, we must excite these modes individually. This can only be accomplished by having the incident waves propagated normally to the interface, hence we take $\lambda_0 = \mu_0 = 0$. The "nearby" waves, having $0 < |\lambda| < L$, $0 < |\mu| < M$, will excite the unwanted modes to some extent, but the effect of this will be negligible, as will be seen shortly. The normal incidence condition is not in itself sufficient for our requirement; we must also have the correct ratio E_2^+/E_1^+. This consideration will be introduced later, however.

For the normally incident packet ($\lambda_0 = \mu_0 = 0$), the field given by (20) becomes a special case of (1) and so the equations of motion (5)-(7) can be used. Setting $n = 1$ in these, we find that the packet moves along the z-axis, its position being given by $z = ct$. It therefore enters the slab at the origin $x = y = z = 0$ at time $t = 0$.

To find the transmitted packet, we must derive the functional form of $\mathcal{E}_1 = \mathcal{E}_1(k\lambda\mu)$. This is obtained from the conditions previously mentioned. Setting $E_3^+ = -(\lambda/\nu)E_1^+ - (\mu/\nu)E_2^+$, $E_3^- = (\lambda/\nu)E_1^- + (\mu/\nu)E_2^-$, $\mathcal{E}_3 = -(\lambda/\nu)\mathcal{E}_1 - (\mu/\nu)\mathcal{E}_2$, $e_2^{\mathrm{I}} = (P_2^{\mathrm{I}}/P_1^{\mathrm{I}})e_1^{\mathrm{I}} = \pi_2^{\mathrm{I}}e_1^{\mathrm{I}}$ say, $e_3^{\mathrm{I}} = (P_3^{\mathrm{I}}/P_1^{\mathrm{I}})e_1^{\mathrm{I}} = \Pi_3^{\mathrm{I}}e_1^{\mathrm{I}}$ say, and similarly for $e_2^{\mathrm{II}} \cdots e_3^{\mathrm{IV}}$, the boundary conditions (continuity of tangential components of electric and magnetic fields at $z = 0$ and $z = D$) become [see page 212 for (22)] in matrix form. The missing components may be readily inserted by comparison.

The set of equations represented by (22) may be solved by the use of determinants in the usual way, obtaining $\mathcal{E}_1 = \mathfrak{D}_1/\Delta$, etc. It will turn out that we only require $\mathcal{E}_{1o} \equiv \mathcal{E}_1(k_0, 0, 0)$ and the first order partial derivatives $\mathcal{E}_{1k}$, $\mathcal{E}_{1\lambda}$, $\mathcal{E}_{1\mu}$ at $k_0, 0, 0$ for the derivation of the packet velocity. These may be obtained by means of

$$\mathcal{E}_1 = \frac{\mathfrak{D}_1}{\Delta} = \frac{\mathfrak{D}_{1o}}{\Delta_0} + \frac{\mathfrak{D}_{1k}\Delta_0 - \mathfrak{D}_{1o}\Delta_k}{\Delta_0^2}\kappa + \frac{\mathfrak{D}_{1\lambda}\Delta_0 - \mathfrak{D}_{1o}\Delta_\lambda}{\Delta_0^2}\lambda + \frac{\mathfrak{D}_{1\mu}\Delta_0 - \mathfrak{D}_{1o}\Delta_\mu}{\Delta_0^2}\mu + \cdots \quad (23)$$

from $\mathfrak{D}_{1o}$, $\mathfrak{D}_{1k}$, $\cdots$, Δ_μ. These, in turn, may be found by expanding every functional component of (22) as a series in κ, λ, μ, calculating the determinants as series, and extracting the relevant coefficients. In the various expansions there will, of course, be zero-order terms and terms in first partial derivatives; only these need be considered in finding the necessary quantities.

The first partial derivatives may be divided into two types: those that contain D as a factor (arising from differentiating the exponentials) and those that do not. As in Part II, we shall eventually have to let $D \to \infty$ in order to eliminate the boundary effects and so obtain a result characteristic of the medium. In view of this, derivatives of the second type will become negligible in comparison with those of the first, hence the values of the amplitude factors $E_1^- \cdots \mathcal{E}_2$ appearing in any final result will be those obtained on keeping only zero-order terms and

$$
\begin{array}{cccccccc}
E_1^- & E_2^- & c_1^{\mathrm{I}} & c_1^{\mathrm{II}} & c_1^{\mathrm{III}} \quad c_1^{\mathrm{IV}} & \mathcal{E}_1 & \mathcal{E}_2 & \\
-1 & 0 & 1 & 1 & \cdots \quad \cdots & 0 & 0 & \\
0 & -1 & \pi_2^{\mathrm{I}} & \pi_2^{\mathrm{I}} & \cdots \quad \cdots & 0 & 0 & \\
0 & -1 & -N^{\mathrm{I}}\pi_2^{\mathrm{I}} & N^{\mathrm{I}}\pi_2^{\mathrm{I}} & \cdots \quad \cdots & 0 & 0 & \\
1 & 0 & N^{\mathrm{I}} & -N^{\mathrm{I}} & \cdots \quad \cdots & 0 & 0 & \\
0 & 0 & (1+iD\delta^{\mathrm{I}})\,\epsilon^{ikN^{\mathrm{I}}D} & (1+iD\delta^{\mathrm{II}})\,\epsilon^{-ikN^{\mathrm{I}}D} & \cdots \quad \cdots & -(1+iD\kappa)\,\epsilon^{ikD} & 0 & \\
0 & 0 & (1+iD\delta^{\mathrm{I}})\pi_2^{\mathrm{I}}\,\epsilon^{ikN^{\mathrm{I}}D} & (1+iD\delta^{\mathrm{II}})\pi_2^{\mathrm{I}}\,\epsilon^{-ikN^{\mathrm{I}}D} & \cdots \quad \cdots & 0 & -(1+iD\kappa)\,\epsilon^{ikD} & \\
0 & 0 & -(1+iD\delta^{\mathrm{I}})N^{\mathrm{I}}\pi_2^{\mathrm{I}}\,\epsilon^{ikN^{\mathrm{I}}D} & (1+iD\delta^{\mathrm{II}})N^{\mathrm{I}}\pi_2^{\mathrm{I}}\,\epsilon^{-ikN^{\mathrm{I}}D} & \cdots \quad \cdots & 0 & (1+iD\kappa)\,\epsilon^{ikD} & \\
0 & 0 & (1+iD\delta^{\mathrm{I}})N^{\mathrm{I}}\,\epsilon^{ikN^{\mathrm{I}}D} & -(1+iD\delta^{\mathrm{II}})N^{\mathrm{I}}\,\epsilon^{-ikN^{\mathrm{I}}D} & \cdots \quad \cdots & -(1+iD\kappa)\,\epsilon^{ikD} & 0 &
\end{array}
\qquad \cdots\cdots(24)
$$

derivative terms proportional to D in (22). Assuming commutability of the limiting and solving processes, we are then justified in keeping only these terms in our array before attempting a solution, thus minimizing the work required. Wherever λ or μ appears explicitly in (22) we may set it equal to zero, since the term involved is not of zero order, nor does it have D as a factor.

It may be noted in passing that the limiting processes $D \to \infty$ (to eliminate boundary effects) and $K, L, M \to 0$ (to validate our maximizing procedures) must be carried out in such a way that $KD, LD, MD \to 0$. Otherwise we should have to retain terms of all orders in the expansions being made.

If we set $\delta^{\mathrm{I}} = d(kN^{\mathrm{I}}) = (kN^{\mathrm{I}})_{\kappa}\kappa + kN^{\mathrm{I}}_{\lambda}\lambda + kN^{\mathrm{I}}_{\mu}\mu$ and similarly for δ^{II}, δ^{III}, δ^{IV}, then the set (22) is equivalent, for our purposes, to [see page 214 for (24)] where we have been able to write $-N^{\mathrm{I}}$ and π_2^{I} for N_2^{II} and π_2^{II}, respectively, since these quantities are now to be evaluated at k_0, 0, 0.

Now it can be seen that there is a fairly simple solution of this set. The assumptions $E_2^+ = \pi_2^{\mathrm{I}}E_1^+$, $E_2^- = \pi_2^{\mathrm{I}}E_1^-$, $\mathcal{E}_2 = \pi_2^{\mathrm{I}}\mathcal{E}_1$, $e_1^{\mathrm{III}} = e_1^{\mathrm{IV}} = 0$, will be made, and will be proved to be consistent with (24). Under them, the E_2^- column (multiplied by π_2^{I}) may be combined into the E_1^- column, and similarly with the $\mathcal{E}_2$ and $\mathcal{E}_1$ columns; the e_1^{III} and e_1^{IV} columns do not appear. We are then left with eight equations in the four dependent variables E_1^- e_1^{I} e_1^{II} and $\mathcal{E}_1$, and the independent variable E_1^+. These equations are not, however, independent; the second is π_2^{I} times the first, the third $-\pi_2^{\mathrm{I}}$ times the fourth, and so too with the fifth and sixth, seventh and eighth. Thus we have only four independent equations in the four unknowns, hence our assumptions are valid. The array which now remains is

$$\left.\begin{array}{cccccc}
 & E_1^- & e_1^{\mathrm{I}} & e_1^{\mathrm{II}} & \mathcal{E}_1 & \\
E_1^+ & -1 & 1 & 1 & 0 & \\
E_1^+ & 1 & N^{\mathrm{I}} & -N^{\mathrm{I}} & 0 & \\
0 & 0 & (1+iD\delta^{\mathrm{I}})\epsilon^{ikN^{\mathrm{I}}D} & (1+iD\delta^{\mathrm{II}})\epsilon^{-ikN^{\mathrm{I}}D} & -(1+iD\kappa)\epsilon^{ikD} & \\
0 & 0 & (1+iD\delta^{\mathrm{I}})N^{\mathrm{I}}\epsilon^{ikN^{\mathrm{I}}D} & -(1+iD\delta^{\mathrm{II}})N^{\mathrm{II}}\epsilon^{-ikN^{\mathrm{I}}D} & -(1+iD\kappa)\epsilon^{ikD} &
\end{array}\right\} \qquad (25)$$

where, for convenience, the equations independent of π_2^{I} have been retained. A complete solution of the set (24) can be obtained, but if we choose $E_2^+ = \pi_2^{\mathrm{I}}E_1^+$, such a solution reduces to the one derived here. It is this choice that is necessary (in addition to the normal incidence condition) to obtain fields in which the N^{III} and N^{IV} modes are not excited. Similarly, the N^{I} and N^{II} modes could be eliminated by choosing $E_2^+ = \pi_2^{\mathrm{III}}E_1^+$.

The solution of (25) leads to the approximations, which are valid only to the first order in κ, λ, μ, and for $D \to \infty$,

$$\left.\begin{aligned}
\mathfrak{D}_1 &\approx 4E_1^+N^{\mathrm{I}}(1+iD\delta^{\mathrm{I}})(1+iD\delta^{\mathrm{II}}) \\
\Delta &\approx (1+iD\kappa)\{(N^{\mathrm{I}}+1)^2(1+iD\delta^{\mathrm{II}})\epsilon^{-ik(N^{\mathrm{I}}-1)D} \\
&\quad -(N^{\mathrm{I}}-1)^2(1+iD\delta^{\mathrm{I}})\epsilon^{ik(N^{\mathrm{I}}+1)D}\}.
\end{aligned}\right\} \qquad (26)$$

At normal incidence $N^{II} = -N^{I}$ so $(kN^{II})_k = -(kN^{I})_k$,

$$N_\lambda^{II} = -\frac{\partial f(N^{II})}{\partial \lambda}\Big/\frac{\partial f(N^{II})}{\partial N^{II}} = -\frac{b_3 N^{II^3} + b_1 N^{II}}{4a_4 N^{II^3} + 2a_2 N^{II}}$$

$$= -\frac{b_3 N^{I^3} + b_1 N^{I}}{4a_4 N^{I^3} + 2a_2 N^{I}} = -\frac{\partial f(N^{I})}{\partial \lambda}\Big/\frac{\partial f(N^{I})}{\partial N^{I}} = N_\lambda^{I} \quad \ldots\ldots(27)$$

and similarly $N_\mu^{II} = N_\mu^{I}$. Thus δ^{II}, as well as δ^{I}, can be expressed in terms of N^{I} and its derivatives, hence all of (26) can be expressed in terms of these. Obviously similar relations hold for N^{III} and N^{IV}, hence the superscripts will become superfluous. In terms of any one of the roots N, (26) give

$$\left.\begin{aligned}
\mathfrak{D}_1 &\approx 4E_1^{+}N(1 + i2DkN_\lambda\lambda + i2DkN_\mu\mu) \\
\Delta &\approx (N+1)^2\epsilon^{-ik(N-1)D} - (N-1)^2\epsilon^{ik(N+1)D} \\
&\quad - iD[(N+1)^2(N + kN_k - 1)e^{-ik(N-1)D} \\
&\quad - (N-1)^2(N + kN_k + 1)\epsilon^{ik(N+1)D}]\kappa \\
&\quad + iD[(N+1)^2\epsilon^{-ik(N-1)D} - (N-1)^2\epsilon^{ik(N+1)D}]kN_\lambda\lambda \\
&\quad + iD[(N+1)^2\epsilon^{-ik(N-1)D} - (N-1)^2\epsilon^{ik(N+1)D}]kN_\mu\mu
\end{aligned}\right\} \quad \ldots.(28)$$

valid to the first order in κ, λ, μ. As in Part II, only those terms in $\epsilon^{-ik(N-1)D}$ need be retained as $D \to \infty$ (assuming $N_2 > 0$), hence we get the further approximation

$$\Delta \approx (N+1)^2\,\epsilon^{-ik(N-1)D}[1 - iD(N + kN_k - 1)\kappa + iDkN_\lambda\lambda + iDkN_\mu\mu] \quad \ldots(29)$$

In deriving the packet velocity we shall require expressions for $\mathcal{E}_{1k}/\mathcal{E}_{1o}$, $\mathcal{E}_{1\lambda}/\mathcal{E}_{1o}$, $\mathcal{E}_{1\mu}/\mathcal{E}_{1o}$ only. These may now be obtained from (23), (28), and (29):

$$\left.\begin{aligned}
\frac{\mathcal{E}_{1k}}{\mathcal{E}_{1o}} &= \frac{\mathfrak{D}_{1k}}{\mathfrak{D}_{1o}} - \frac{\Delta_k}{\Delta_0} = iD(N + kN_k - 1) \\
\frac{\mathcal{E}_{1\lambda}}{\mathcal{E}_{1o}} &= \frac{\mathfrak{D}_{1\lambda}}{\mathfrak{D}_{1o}} - \frac{\Delta_\lambda}{\Delta_0} = iDk_0N_\lambda \\
\frac{\mathcal{E}_{1\mu}}{\mathcal{E}_{1o}} &= \frac{\mathfrak{D}_{1\mu}}{\mathfrak{D}_{1o}} - \frac{\Delta_\mu}{\Delta_0} = iDk_0N_\mu
\end{aligned}\right\} \quad \ldots\ldots\ldots\ldots(30)$$

We are now in a position to find the transmitted pulse. The x-component of **E** in the region $D < z$ is given by

$$\mathfrak{F}_1 = \int_{-K}^{K}\int_{-L}^{L}\int_{-M}^{M} \mathcal{E}_1(k_0 + \kappa, \lambda, \mu)\,\epsilon^{i\Phi}\,d\kappa\,d\lambda\,d\mu \quad \ldots\ldots\ldots\ldots(31)$$

with

$$\mathcal{E}_1(k_0 + \kappa, \lambda, \mu) = \mathcal{E}_{1o} + \mathcal{E}_{1k}\kappa + \mathcal{E}_{1\lambda}\lambda + \mathcal{E}_{1\mu}\mu + \tfrac{1}{2}\mathcal{E}_{1kk}\kappa^2 + \tfrac{1}{2}\mathcal{E}_{1\lambda\lambda}\lambda^2 + \tfrac{1}{2}\mathcal{E}_{1\mu\mu}\mu^2 + \mathcal{E}_{1k\lambda}\kappa\lambda + \cdots$$

$$\epsilon^{i\Phi} = \epsilon^{i\Phi_0}(1 + i\Phi_k\kappa + i\Phi_\lambda\lambda + i\Phi_\mu\mu + \tfrac{1}{2}(i\Phi_{kk} - \Phi_k^2)\kappa^2 + \tfrac{1}{2}(i\Phi_{\lambda\lambda} - \Phi_\lambda^2)\lambda^2 + \tfrac{1}{2}(i\Phi_{\mu\mu} - \Phi_\mu^2)\mu^2 + \cdots$$

$$\Phi = k(\lambda x + \mu y + \nu z - ct) \qquad \Phi_0 = k_0(z - ct)$$

$$\Phi_k = z - ct \qquad \Phi_{kk} = 0$$

$$\Phi_\lambda = \left[k_0\left(x - \frac{\lambda}{\nu}z\right)\right]_{\lambda=\mu=0} = k_0 x \qquad \Phi_{\lambda\lambda} = \left[-k_0\frac{\nu^2 + \lambda^2}{\nu^3}z\right]_{\lambda=\mu=0} = -k_0 z$$

$$\Phi_\mu = k_0 y \qquad \Phi_{\mu\mu} = -k_0 z$$

Then the integrand of (31) is, to the second order,

$$\epsilon^{i\Phi_0}\{\mathcal{E}_{1o} + [\ \ ]\kappa + [\ \ ]\lambda + [\ \ ]\mu + [\tfrac{1}{2}\mathcal{E}_{1kk} + i(z - ct)\mathcal{E}_{1k} - \tfrac{1}{2}(z - ct)^2\mathcal{E}_{1o}]\kappa^2 + [\tfrac{1}{2}\mathcal{E}_{1\lambda\lambda} + ik_0 x\mathcal{E}_{1\lambda} + \tfrac{1}{2}(-ik_0 z - k_0^2 x^2)\mathcal{E}_{1o}]\lambda^2 + [\tfrac{1}{2}\mathcal{E}_{1\mu\mu} + ik_0 y\mathcal{E}_{1\mu} + \tfrac{1}{2}(-ik_0 z - k_0^2 y^2)\mathcal{E}_{1o}]\mu^2 + [\ \ ]\kappa\lambda + [\ \ ]\lambda\mu + [\ \ ]\kappa\mu\}$$

and (31) becomes, to the fifth order,

$$\left.\begin{aligned}\mathcal{F}_1 \approx 8\epsilon^{i\Phi_0}\{&\mathcal{E}_{1o}KLM + \tfrac{1}{3}[\tfrac{1}{2}\mathcal{E}_{1kk} + i(z - ct)\mathcal{E}_{1k} - \tfrac{1}{2}(z - ct)^2\mathcal{E}_{1o}]K^3LM\\ &+ \tfrac{1}{3}[\tfrac{1}{2}\mathcal{E}_{1\lambda\lambda} + ik_0 x\mathcal{E}_{1\lambda} + \tfrac{1}{2}(-ik_0 z - k_0^2 x^2)\mathcal{E}_{1o}]KL^3M\\ &+ \tfrac{1}{3}[\tfrac{1}{2}\mathcal{E}_{1\mu\mu} + ik_0 y\mathcal{E}_{1\mu} + \tfrac{1}{2}(-ik_0 z - k_0^2 y^2)\mathcal{E}_{1o}]KLM^3\}.\end{aligned}\right\} \quad \ldots\ldots(32)$$

The amplitude squared is, to the eighth order,

$$\left.\begin{aligned}\mathcal{F}_1\tilde{\mathcal{F}}_1 \approx 64[&\mathcal{E}_{1o}\tilde{\mathcal{E}}_{1o}K^2L^2M^2\\ &+ \tfrac{1}{3}\{\tfrac{1}{2}(\mathcal{E}_{1o}\tilde{\mathcal{E}}_{1kk} + \tilde{\mathcal{E}}_{1o}\mathcal{E}_{1kk}) - i(z - ct)(\mathcal{E}_{1o}\tilde{\mathcal{E}}_{1k} - \tilde{\mathcal{E}}_{1o}\mathcal{E}_{1k})\\ &\quad - (z - ct)^2\mathcal{E}_{1o}\tilde{\mathcal{E}}_{1o}\}K^4L^2M^2\\ &+ \tfrac{1}{3}\{\tfrac{1}{2}(\mathcal{E}_{1o}\tilde{\mathcal{E}}_{1\lambda\lambda} + \tilde{\mathcal{E}}_{1o}\mathcal{E}_{1\lambda\lambda}) - ik_0 x(\mathcal{E}_{1o}\tilde{\mathcal{E}}_{1\lambda} - \tilde{\mathcal{E}}_{1o}\mathcal{E}_{1\lambda}) - k_0^2 x^2\mathcal{E}_{1o}\tilde{\mathcal{E}}_{1o}\}K^2L^4M^2\\ &+ \tfrac{1}{3}\{\tfrac{1}{2}(\mathcal{E}_{1o}\tilde{\mathcal{E}}_{1\mu\mu} + \tilde{\mathcal{E}}_{1o}\mathcal{E}_{1\mu\mu}) - ik_0 y(\mathcal{E}_{1o}\tilde{\mathcal{E}}_{1\mu} - \tilde{\mathcal{E}}_{1o}\mathcal{E}_{1\mu}) - k_0^2 y^2\mathcal{E}_{1o}\tilde{\mathcal{E}}_{1o}\}K^2L^2M^4].\end{aligned}\right\} \quad \ldots(33)$$

In accordance with previous treatments, we find the position of the packet by maximizing those terms appearing in (33). It may be noticed that, while z appears

by itself in (32), it and t only appear in the combination $(z - ct)$ in (33), hence the z-maximum and t-maximum occur at the same points.

The equations of motion of the transmitted packet are, then

$$\left.\begin{aligned} z - ct &= \frac{i}{2}\left(\frac{\mathcal{E}_{1k}}{\mathcal{E}_{1o}} - \frac{\tilde{\mathcal{E}}_{1k}}{\tilde{\mathcal{E}}_{1o}}\right) \\ x &= \frac{i}{2k_0}\left(\frac{\mathcal{E}_{1\lambda}}{\mathcal{E}_{1o}} - \frac{\tilde{\mathcal{E}}_{1\lambda}}{\tilde{\mathcal{E}}_{1o}}\right) \\ y &= \frac{i}{2k_0}\left(\frac{\mathcal{E}_{1\mu}}{\mathcal{E}_{1o}} - \frac{\tilde{\mathcal{E}}_{1\mu}}{\tilde{\mathcal{E}}_{1o}}\right) \end{aligned}\right\} \quad \ldots\ldots\ldots\ldots\ldots\ldots (34)$$

Substituting from (30), these yield

$$\left.\begin{aligned} z - ct &= D - D\frac{\partial kN_1}{\partial k} \\ x &= -D\frac{\partial N_1}{\partial \lambda} \\ y &= -D\frac{\partial N_1}{\partial \mu} \end{aligned}\right\} \quad \ldots\ldots\ldots\ldots\ldots\ldots (35)$$

The packet, therefore, emerges from the slab at $-D(\partial N_1/\partial\lambda)$, $-D(\partial N_1/\partial\mu)$,$D$ at time $t_D = (\partial kN_1/\partial k)D/c$. Since it entered the slab at 0, 0, 0 at time $t = 0$, it had an effective velocity while inside the slab

$$\mathbf{V}_{slab} = \left(-\frac{\partial N_1}{\partial \lambda}\,\mathbf{i} - \frac{\partial N_1}{\partial \mu}\,\mathbf{j} + \mathbf{k}\right)\frac{c}{(\partial kN_1/\partial k)} \quad \ldots\ldots\ldots\ldots (36)$$

Thus the velocity has as its z-component the value $c/(\partial kN_1/\partial k)$ which, in virtue of the equality of N and n at normal incidence, is the same as the group speed $c/(\mathrm{d}kn_1/\mathrm{d}k)$ found in Part II and in section 2 [equation (8)] of the present paper. The direction of the velocity is given by the relative components

$$N_{1\lambda} : N_{1\mu} : -1 \quad \ldots\ldots\ldots\ldots\ldots\ldots (37)$$

By equation (27) and another similar to it, (37) is equivalent to

$$\text{R.P.}\,\frac{b_3N^3 + b_1N}{4a_4N^3 + 2a_2N} : \text{R.P.}\,\frac{c_3N^3 + c_1N}{4a_4N^3 + 2a_2N} : 1 \quad \ldots\ldots\ldots\ldots (38)$$

By virtue of the relations $N = n$, $b_3 = \beta_4$, etc., existing at normal incidence, (38) is equivalent to

$$\text{R.P.}\,\frac{\beta_4n^3 + \beta_2n}{4\alpha_4n^3 + 2\alpha_2n} : \text{R.P.}\,\frac{\gamma_4n^3 + \gamma_2n}{4\alpha_4n^3 + 2\alpha_2n} : 1 \quad \ldots\ldots\ldots\ldots (39)$$

or

$$\text{R.P.}\,\frac{n_\lambda}{n} : \text{R.P.}\,\frac{n_\mu}{n} : -1 \quad \ldots\ldots\ldots\ldots\ldots\ldots (40)$$

This may be compared with the direction found in the infinite homogeneous medium, given by

$$(\text{R.P. } n^2)_\lambda : (\text{R.P. } n^2)_\mu : -2(\text{R.P. } n^2) \quad \ldots\ldots\ldots\ldots\ldots\ldots (11)$$

The two are not the same except when $n_2 = 0$. The difference can be explained by the fact that, in the present section, inhomogeneous waves go to make up the packet, whereas in section 2 homogeneous waves were used.

With extreme difficulty, we could construct wave packets of the proper inhomogeneity in vacuum to produce homogeneous waves inside the slab, and so compare speeds obtained for homogeneous waves by the two methods. The complimentary procedure of building an inhomogeneous packet in the infinite medium of section 2 is, however, quite simple. The amplitude squared would still be given by (4), but now we would have $\Phi = k(\lambda x + \mu y + Nz - ct)$, $\Phi_\lambda = k(x + N_\lambda z)$, $\Phi_{\lambda\lambda} = kN_{\lambda\lambda}z$, etc. The x-maximum of (4) is then located where

$$0 = \frac{\partial}{\partial x}(i\Phi_{\lambda\lambda} - i\tilde{\Phi}_{\lambda\lambda} - \Phi_\lambda^2 - \tilde{\Phi}_\lambda^2) = -2k[2x + 2N_{1\lambda}z] \quad \ldots\ldots\ldots (41)$$

This, together with a similar expression giving the y-maximum, yield as direction of the packet velocity

$$N_{1\lambda} : N_{1\mu} : -1 \quad \ldots\ldots\ldots\ldots\ldots\ldots\ldots\ldots (42)$$

in agreement with (37). This confirms the result obtained there, and serves as an indirect confirmation of (8) for homogeneous waves.

4—*Conclusions*

We have now obtained expressions for the velocity of a packet in an anisotropic dissipative medium. Two results have been obtained, depending on whether the waves making up the packet are homogeneous or not.

For homogeneous waves having normals near $\lambda = \mu = 1 - \nu = 0$, the packet velocity is

$$\mathbf{V}_{hom} = \left[-\frac{(\text{R.P. } n^2)_\lambda}{2(\text{R.P. } n^2)}\mathbf{i} - \frac{(\text{R.P. } n^2)_\mu}{2(\text{R.P. } n^2)}\mathbf{j} + \mathbf{k} \right] c \Big/ \frac{\partial k n_1}{\partial k} \quad \ldots\ldots\ldots (43)$$

while for inhomogeneous waves of the type considered it is

$$\mathbf{V}_{inhom} = [-N_{1\lambda}\mathbf{i} - N_{1\mu}\mathbf{j} + \mathbf{k}]c \Big/ \frac{\partial k N_1}{\partial k}$$

$$= \left[-\text{R.P.}\frac{n_\lambda}{n}\mathbf{i} - \text{R.P.}\frac{n_\mu}{n}\mathbf{j} + \mathbf{k} \right] c \Big/ \frac{\partial k n_1}{\partial k} \quad \ldots\ldots\ldots (44)$$

In the case of non-dissipative media, these two are equal.

The present investigation was proposed by Mr. J. C. W. Scott, and is proceeding under his supervision at the Radio Physics Laboratory, Defence Research Board, Ottawa.

References

[1] C. O. Hines, J. Geophys. Res., **56**, 63-72 (1951).
[2] J. A. Stratton, Electromagnetic theory, McGraw-Hill Book Co., Inc., New York (1941).
[3] H. G. Booker, Phil. Trans. R. Soc., A, **237**, 411-451 (1938).
[4] C. O. Hines, J. Geophys. Res., **56**, 197-206 (1951).

THE MECHANISM OF *F*-LAYER PROPAGATED BACK-SCATTER ECHOES*

BY ALLEN M. PETERSON

Electronics Research Laboratory, Stanford University, Stanford, California

(Received March 2, 1951)

ABSTRACT

An analysis of the mechanism of *F*-layer propagated (2*F*) back-scatter is given, together with the results of multifrequency experimental observations. It is shown that when scattering is assumed to occur at the surface of the earth (rather than in the *E*-region, as some have thought) theory agrees very well with the experimental evidence. The behavior of back-scatter for transmission near the critical frequency confirms the ground-origin hypothesis and is particularly difficult to explain in terms of *E*-region origin. It is shown that the leading edge of the echo corresponds to energy returned from scattering centers beyond the edge of the skip-zone. Energy from the skip-zone edge is returned with greater delay, the time-differential becoming larger as the *F*-layer vertical-incidence critical frequency is approached. Great care is clearly needed if meaningful skip-distance information is to be obtained from back-scatter observations. The rapid build-up in echo amplitude which follows a sharply-defined minimum time-delay is explained in terms of a time-delay focusing phenomenon.

I—*Introduction*

The term "scatter echoes" has been used by ionosphere investigators to designate a variety of anomalous reflections observed in the high-frequency region. By far the most numerous of such echoes fall into two categories, which have been called by Eckersley "1*E*" scatter and "2*F*" scatter. The numeral signifies the number of encounters with the reflecting region and the letter indicates the ionospheric region involved. These two types of scatter are indicated in Figure 1. "1*E*" scatter occurs at short range and is generally quite intermittent and irregular. The majority of these echoes result from direct scattering from centers in the *E*-region which are of meteoric origin. "2*F*" scatter echoes appear at much longer range and occur for transmission on frequencies up to approximately three times the vertical-incidence critical frequency. These echoes branch off from the first

*Presented at joint IRE-URSI meeting held at San Diego, April 4, 1950.

multiple (2*F*) vertical-incidence ionosphere trace at a frequency below the critical frequency and appear as a sort of extension to this trace when sufficiently sensitive equipment is used. Other anomalous reflections which involve the *F*-layer but which should not be confused with "2*F*" scatter are the so-called "spread echoes" and "1*F*" scatter. These types occur infrequently in temperate latitudes and are associated with direct back-scattering from the *F*-region.

Experimental observation of "2*F*" back-scatter using pulsed transmission has been undertaken by a number of workers [see 1, 2, 3, 4, 5, 6 of "References" at end of paper]. As a result of these experiments, there has emerged the rather general belief that the mechanism of production of the echoes involves propagation *via* *F*-layer reflection and then scattering from centers either in the *E*-region or on the ground, with return over the same path. Eckersley's observations at several frequencies showed quite well the frequency dependence of the echoes. In inter-

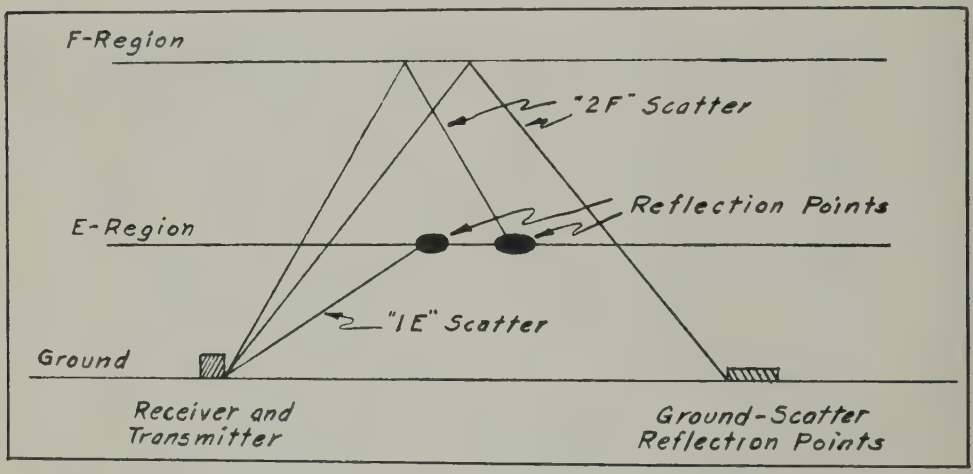

FIG. 1—SCATTER SOURCES

preting his results, Eckersley concluded that the echoes resulted from scattering centers in the *E*-region. Most other investigators have tended to favor ground-scattering.

It is the purpose of this paper to study the mechanism of *F*-layer propagated "2*F*" back-scatter echoes. Calculations are made in order to obtain theoretical time-delay *versus* frequency curves for comparison with experimental data. Variable-frequency techniques are used in the experimental work, with particular attention being given to scatter occurring in the vicinity of the vertical-incidence critical frequency. It is shown that scattering from the ground explains very well the observed data, whereas "*E*"-scattering does not.

The observed scatter echoes have been associated by some workers with the edge of the skip-zone; it is shown, however, that this is not in general the proper interpretation. For transmission at a frequency near the vertical-incidence critical frequency, there is a large difference between the minimum time-delay at which scattered energy is received and the time-delay corresponding to scattering at the

edge of the skip-zone. Energy which arrives back first corresponds to transmission at a more oblique angle than that which reaches the edge of the skip-zone. This energy is scattered back at a greater distance along the surface of the earth than the edge of the skip-zone. Nevertheless, due to the nature of the transmission process, the time-delay for the round trip is less than for that energy which has followed a more vertical path and reached the edge of the skip-zone. Experimentally it is found that when the transmission frequency is very near to the vertical-incidence critical frequency, no part of the composite echo has sufficient time-delay to correspond to scattering at the edge of the skip-zone. Instead, the leading edge of the echo is made up of energy returning with the theoretical minimum time-delay; the echo reaches peak amplitude shortly thereafter and usually drops into the noise level well before the time-delay is reached which corresponds to energy scattered from the edge of the skip-zone.

II—*Theoretical echo-delay calculations*

By making use of the Breit-Tuve theorem and of "Martyn's equivalence theorem" [7, 8], we may relate group time-delay, virtual height of reflection, and ground distance at oblique incidence to virtual-height records made at vertical

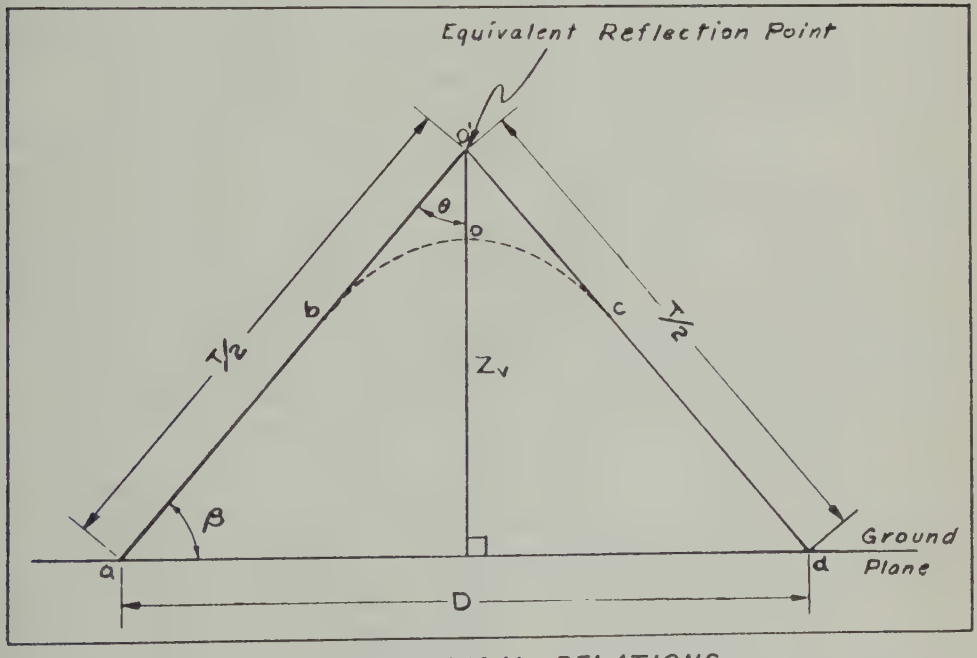

FIG. 2—GEOMETRICAL RELATIONS

incidence. The Breit-Tuve theorem states that the time τ for transmission of the group along the curved path, *abocd* in Figure 2, is the same as the time required to traverse the equivalent triangular path, *abo'cd*, at the constant light velocity c. Martyn's theorem states that the equivalent height of reflection of a wave of

frequency f_{ob} incident at an oblique angle θ is the same as that of a wave of frequency f_v at vertical incidence, where

$$f_v = f_{ob} \cos \theta \quad \ldots\ldots (1)$$

Corrections must be made to these theorems if the effects of curved earth and curved ionosphere are to be taken into account. For simplicity, the following discussion will be based upon the assumption of a plane earth and a plane ionosphere. The starting point for the analysis is the vertical-incidence virtual height *versus* frequency (Z_v , f_v) relationship. This curve may be obtained directly from vertical-incidence ionosphere records or alternatively by considering the reflecting layer to be one having an idealized parabolic electron-distribution. (The geometry of the reflection process is shown in Fig. 2.) Z_v is the virtual height at the reflection point. D is the distance to the scattering point measured along the ground. The distance T is the equivalent group-path; its length is a measure of the time-delay τ in accordance with the relation $\tau = T/c$. From the geometry of Figure 2

$$T = \frac{2Z_v}{\cos \theta} \quad \ldots\ldots (2)$$

and

$$D = T \sin \theta = 2Z_v \tan \theta \quad \ldots\ldots (3)$$

Now making use of Martyn's theorem (equation 1), we obtain from 2 and 3

$$T = 2Z_v \frac{f_{ob}}{f_v} \quad \ldots\ldots (4)$$

and

$$D = 2Z_v \sqrt{\frac{f_{ob}^2}{f_v^2} - 1} \quad \ldots\ldots (5)$$

More universal relationships are obtained if frequencies are in all cases normalized with respect to vertical-incidence critical frequency f_c . The final form is then

$$T = 2Z_v \frac{\rho}{\left(\frac{f_v}{f_c}\right)} \quad \ldots\ldots (6)$$

$$D = 2Z_v \sqrt{\frac{\rho^2}{\left(\frac{f_v}{f_c}\right)^2} - 1} \quad \ldots\ldots (7)$$

in which $\rho = f_{ob}/f_c$ is a constant for a given oblique transmission frequency. These relations used in conjunction with a Z_v , f_v curve yield the desired (T, D) curve. It should be understood that for this analysis the required Z_v , f_v information may be obtained from experimental sweep-frequency records, or from the assumption of a parabolic or some other layer distribution. If a parabolic layer is assumed then, as shown by Appleton [9]

$$Z_v = Z_1 + \frac{h}{2}\frac{f_v}{f_c} \ln \left(\frac{1 + \frac{f_v}{f_c}}{1 - \frac{f_v}{f_c}} \right)$$

$$Z_v = Z_1 + \frac{h}{2} \rho \cos \theta \ln \left(\frac{1 + \rho \cos \theta}{1 - \rho \cos \theta} \right) \quad \ldots\ldots\ldots\ldots\ldots\ldots (8)$$

Z_1 is height to the lower limit of the layer, and h is the half-thickness. It can then be shown that

$$T = \frac{2Z_1}{\cos \theta} + h\rho \ln \left(\frac{1 + \rho \cos \theta}{1 - \rho \cos \theta} \right) \quad \ldots\ldots\ldots\ldots\ldots\ldots\ldots\ldots (9)$$

and

$$D = 2Z_1 \tan \theta + h\rho \sin \theta \ln \left(\frac{1 + \rho \cos \theta}{1 - \rho \cos \theta} \right) \quad \ldots\ldots\ldots\ldots\ldots (10)$$

The variation of Z_v, T, and D with frequency and with angle of incidence for this situation can be shown conveniently by the curves of Figure 3. T is given by the radial distance from the origin, while θ is the angle of incidence measured from the vertical. In this presentation, ground distance D is given by the horizontal projection of T, and $2Z_v$ by the vertical projection. The variation with frequency is shown by plotting contours for different values of ρ. In Figure 3 the skip-distance for a given frequency appears as the minimum D from which a vertical projection will be just tangent to the contour for a given value of ρ. Above $\rho = 1$, it may be seen that there is always a skip-zone. At $\rho = 1$, which corresponds to transmission at the vertical-incidence critical frequency, the skip-zone has receded to 0 and for all frequencies lower than this, there is no skip-zone. Of perhaps more interest for the back-scatter process is the minimum value of T for a given frequency. This corresponds to the minimum radial distance from the origin to the contour for a given ρ. This minimum is important, since it gives the minimum time-delay τ at which echoes of ground-scattered origin may be expected to return to the transmission point, for the given transmitting frequency ρ. In Figure 3, the T_{min} points are all seen to fall along a horizontal straight line. This corresponds to the statement that the virtual height of reflection of the minimal time-delay ray is a constant independent of frequency for a given layer. This may be shown to be true for a parabolic layer. To find the minimum T for given ρ, we take the derivative of T with respect to θ and set equal to zero. This may be done conveniently using T from equation (9).

$$\frac{dT}{d\theta} = 2 \sin \theta \left[\frac{Z_1}{\cos^2 \theta} - \frac{h}{\frac{1}{\rho^2} - \cos^2 \theta} \right] \quad \ldots\ldots\ldots\ldots\ldots (11)$$

from which

$$\cos \theta = \frac{1}{\rho} \sqrt{\frac{Z_1}{Z_1 + h}} \quad \ldots\ldots\ldots\ldots\ldots\ldots\ldots\ldots (12)$$

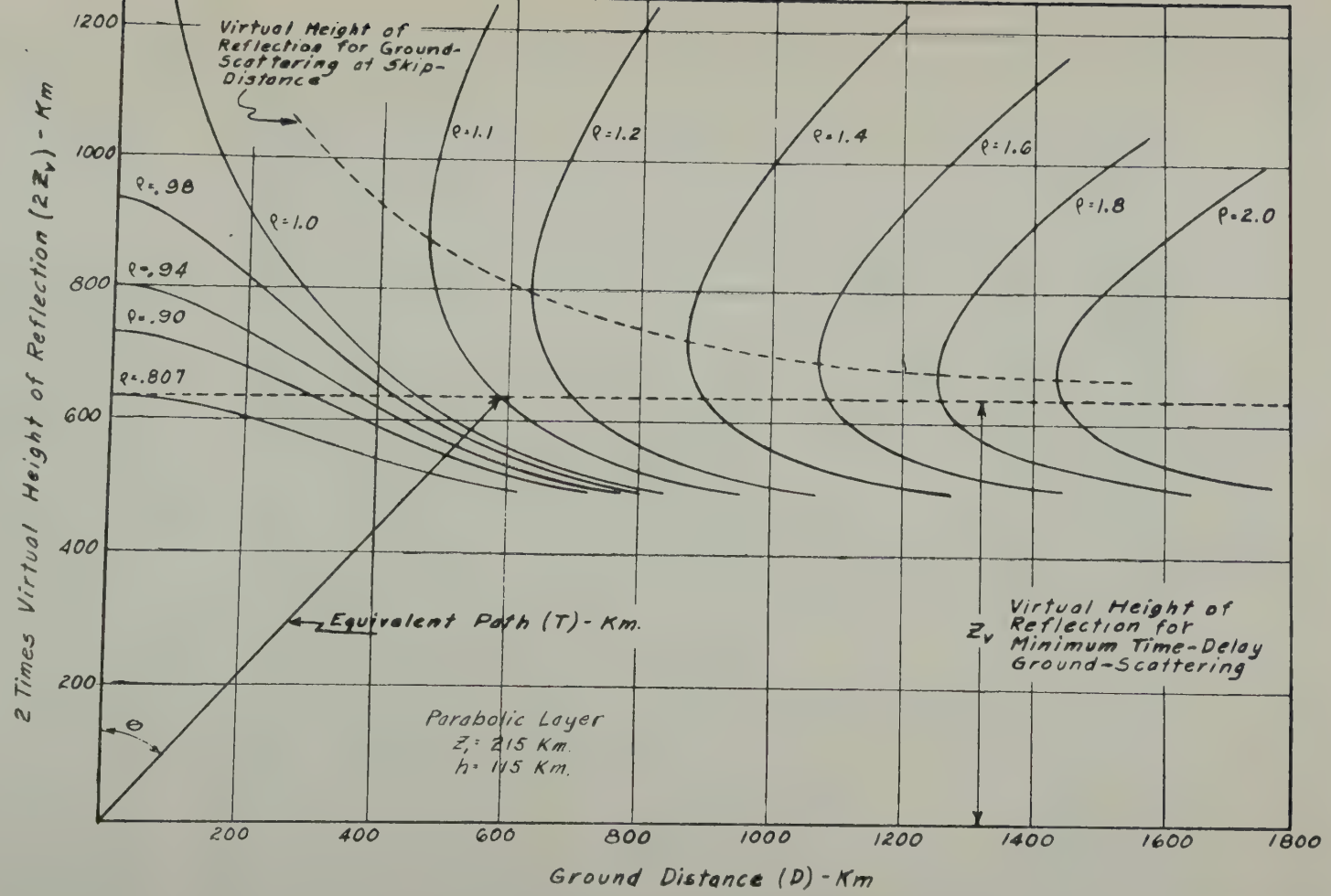

FIG. 3—VARIATION OF Z_V, T, AND D WITH FREQUENCY AND WITH ANGLE OF INCIDENCE, IF PARABOLIC LAYER IS ASSUMED

This gives the angle of incidence for the minimum T. Then we know by the equivalence theorem that the virtual height of reflection at oblique incidence at a frequency ρ is the same as that at vertical incidence at a frequency $\rho \cos \theta$. Now no matter what ρ we have chosen, we see that $\rho \cos \theta$ is a constant, as follows:

$$\rho \cos \theta = \sqrt{\frac{Z_1}{Z_1 + h}} \quad \ldots\ldots\ldots\ldots\ldots\ldots\ldots\ldots (13)$$

Hence, Z_v at oblique incidence for the minimum T is constant corresponding to a vertical-incidence virtual height Z_v^* at the frequency

$$f^* = f_c \sqrt{\frac{Z_1}{Z_1 + h}} \quad \ldots\ldots\ldots\ldots\ldots\ldots\ldots\ldots (14)$$

T_{min} as a function of frequency may readily be calculated from the above relations, as follows:

$$T_{min} = \frac{2Z_v^* \rho}{\sqrt{\frac{Z_1}{Z_1 + h}}} \quad \ldots\ldots\ldots\ldots\ldots\ldots\ldots\ldots (15)$$

It is desirable to calculate the time-delay for transmission along the skip-distance ray in order that we may compare it with the experimental echoes. Time-delay *versus* frequency for transmission along the skip-distance ray is given in Figure 3 by the radial distance from the origin to the crosses on the parametric curves for ρ. Alternatively, if no such curves as those of Figure 3 are available, we may adapt to our purposes a method presented by Appleton and Beynon [9] for calculating the skip-distance at any given transmitting frequency. The method involves finding the minimum D as a function of θ from the parabolic layer approximations. To do this, we take the derivative of D with respect to θ, using equation (10), and set equal to zero. The result is a transcendental equation for D_{min} or rather, what is equivalent, for maximum usable frequency ρ_{max} as a function of θ. Though the method yields no simple relation such as the linear one which was obtained for T_{min} , it is possible to obtain a plot for D_{min} as a function of frequency which holds for a given parabolic layer. Then knowing D_{min} , it is simply a geometrical problem to obtain the desired skip-distance group-path T_{skip} as a function of frequency.

In Figure 4, the results of calculations based on the parabolic layer are given in an equivalent range *versus* frequency presentation. Frequency on this plot is shown as a linear scale rather than the more common logarithmic scale, since it shows more clearly the linear dependence of T_{min} upon frequency. The curve for T_{min} is seen to merge with the vertical incidence "2F" trace at the frequency f^*, given by equation (14). The curve for T_{skip} increases for decreasing frequency, becoming infinite at the vertical-incidence critical frequency f_c . At this point the skip-distance has diminished to zero and transmission is vertical. However, T_{min} in this region is much less than either T_{skip} or the vertical incidence "2F" trace. It corresponds to transmission at a more oblique angle, and scattering back from a greater ground distance.

Figure 4 shows a further interesting feature of T_{min} as calculated for a parabolic

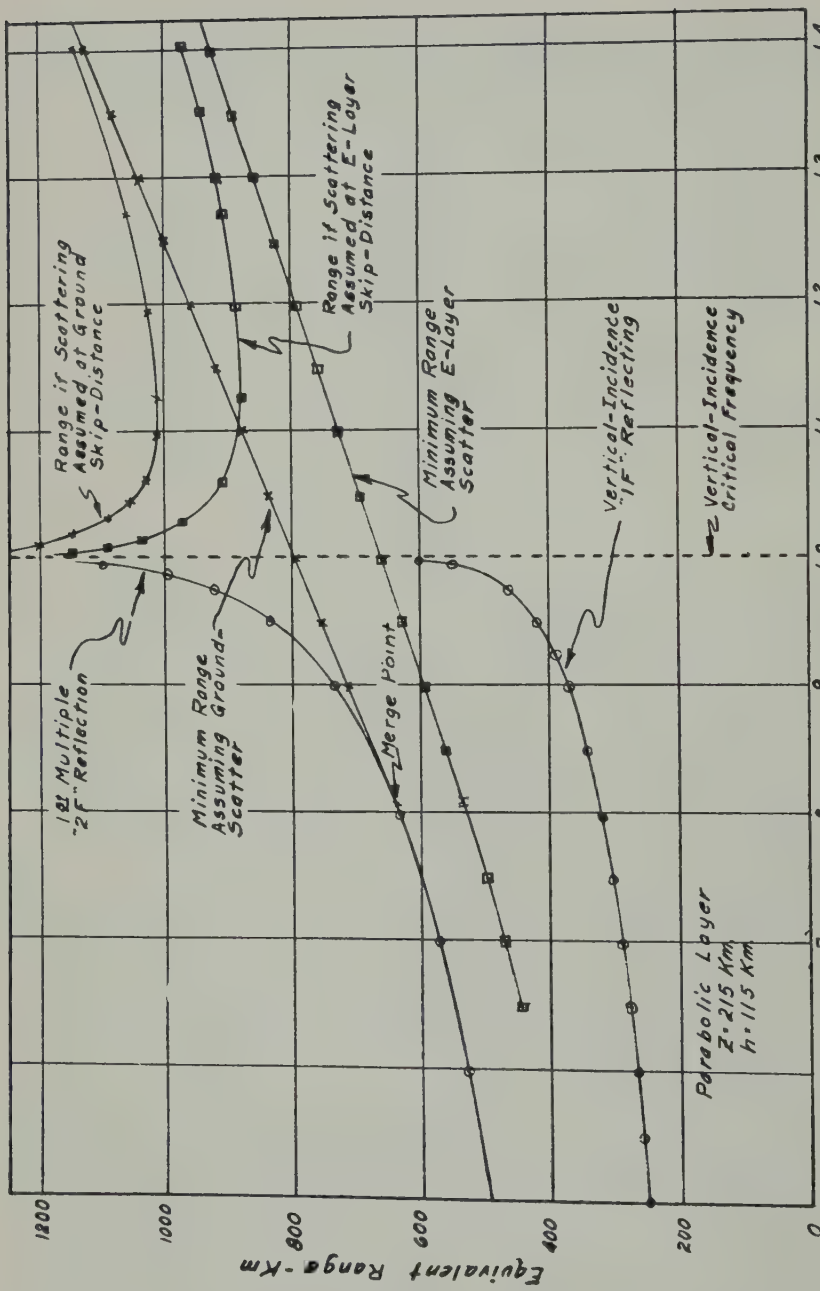

FIG. 4—SHOWING FEATURE OF T_{MIN} AS CALCULATED FOR A PARABOLIC LAYER, AND CURVES TO DEMONSTRATE THE EFFECTS OF ASSUMING SCATTERING CENTERS IN THE E-REGION

layer. T_{min} is given by the tangent from the origin to the vertical-incidence "2F" trace. Above the tangent point, the minimum possible time-delay is given by the tangent line and corresponds to transmission at an oblique angle. Below the tangent point, the minimum time-delay is given by the "2F" trace itself and corresponds to vertical-incidence transmission.

Also shown in Figure 4 are curves to demonstrate the effects of assuming scattering centers in the E-region. The method of calculation for this case is exactly parallel to that given above for the case of ground-scattering, the only change being a geometrical correction necessitated by the height above ground of the E-layer. Two features should be noted in this case. First, the curve for T_{min} when "E"-scattering is assumed never merges with the "$2F$" vertical-incidence trace. Secondly, the curve for T_{skip} still recedes to infinity when the frequency of transmission is reduced towards the critical frequency f_c .

Martyn's theorem [8] and the geometry of the reflection process enable one to show that the minimum time-delay properties which have just been obtained for a parabolic layer are not limited to layers with this distribution, but are true more generally. That is, the minimum time-delay for the scatter echo corresponds quite generally to the tangent line from the origin to the $2F$ vertical-incidence trace, when plotted on a linear frequency scale. This then shows that the virtual height of reflection for the minimal time-delay ray is a constant given by the value Z_v^* at the tangent point.

The required relations are given by equation (4) which was obtained by eliminating the cos θ from equation (2) by making use of Martyn's theorem as given by equation (1).

$$T = 2f_{ob}\frac{Z_v}{f_v} \qquad \ldots\ldots\ldots\ldots\ldots\ldots\ldots\ldots\ldots\ldots (4)$$

Now, for a given transmitting frequency, f_{ob} is a constant. The functional dependence of scatter echo range T upon angle of incidence at oblique incidence is then fixed by the vertical-incidence Z_v *versus* f_v trace. Equation (4) says that we divide the equivalent height Z_v by the frequency f_v at which Z_v is measured and then multiply the result by the constant $2f_{ob}$ to obtain the range at which scattered energy returns which was reflected at the height Z_v . For the minimum possible range T_{min} , we must according to equation (4) make $2Z_v/f_v$ a minimum. Equation (4) may be written in the following manner:

$$\frac{T}{f_{ob}} = \frac{2Z_v}{f_v}$$

Geometrically, this equation defines two proportional right-triangles OAB and $OA'B'$ on an equivalent range *versus* frequency plot (Fig. 5). To correspond to a possible transmission condition, the point A must lie upon the $2Z_v$ trace. The point A' is then obtained by extending the line OA till it intersects the vertical line at the oblique-incidence transmission frequency f_{ob} . T is given by the length of the side $A'B'$. From the geometrical construction it may be seen that the minimum scatter range T_{min} corresponds to a minimum value for the angle α. The minimum α for which there is an intersection of the line through the origin with the $2Z_v$ trace occurs for the tangent to the $2Z_v$ trace. As the transmitting frequency is varied, echoes of all equivalent ranges above the tangent line are possible, but the minimum range is given by the tangent line.

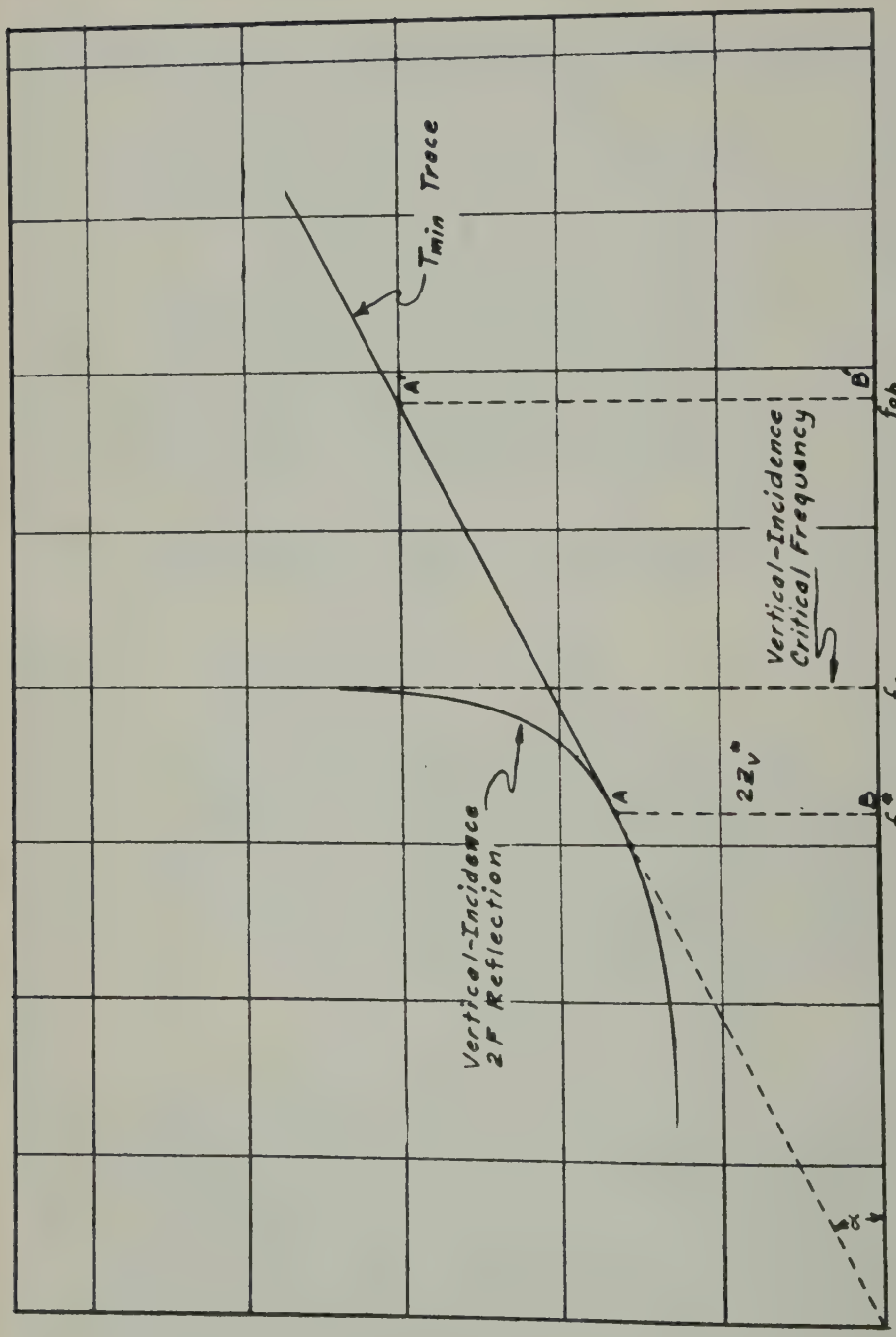

FIG. 5—EQUIVALENT RANGE VERSUS FREQUENCY PLOT

III—*Experimental observation and comparison with theory*

Observation of back-scatter echoes has been made at Stanford University using pulse transmitters whose frequency could be varied manually between 3 and 30 megacycles. The peak power was of the order of a few kilowatts on all frequencies. The equipment was so arranged that it was possible to vary the pulse width between 50 μ sec and 3000 μ sec. With the equipment used, it was possible to check experimentally the behavior of scatter-echo range as a function of frequency. The antennas used were for the most part horizontal dipoles of essentially non-directional characteristics. The vertical-incidence "1*F*" and "2*F*" traces were obtained from the Stanford sweep-frequency ionosphere equipment. This equipment was of too low sensitivity to be useful for the observation of the scatter echoes themselves. Some typical curves showing the leading edge of the scatter pattern as a function of frequency are shown in Figures 6 and 7. All of the curves are found to merge with the vertical incidence "2*F*" trace as frequency was decreased below the critical frequency. Between the merge point and vertical-incidence critical frequency, the leading edge of the scatter pattern is found to occur at shorter time-delay than the "2*F*" vertical-incidence reflection.

The echoes behave in a regular predictable manner, following the linear tangent line as frequency is raised above the critical frequency. The time-delay to the echo increases continuously with increasing frequency, though deviating from the linear relation for the higher frequencies due to earth and ionosphere curvature. With sufficient system sensitivity the echo may be followed out to the limiting range for one-hop transmission in the neighborhood of 4,500 km. It is also common to observe multiple echoes corresponding to consecutive reflections at the ionosphere and ground.

The crosses on curves of Figures 6 and 7 are experimental points, and the straight solid lines are calculated curves for T_{min} . Agreement is, in general, quite good. The dotted T_{min} curves for *E*-layer scattering do not fit the experimental data. Also, calculated curves for the skip-distance ray do not fit the experimental observations for frequencies near the critical frequency. In fact, for this region no part of the observed echo occurs at great enough delay to correspond to the skip-distance ray. T_{skip} and T_{min} , as shown in Figure 4, become more nearly equal for frequencies sufficiently above f_c and in all likelihood some portion of the echo then corresponds to scatter from the edge of the skip-zone.

The occurrence of scatter echoes at less than the vertical incidence "2*F*" time-delay when transmitting below f_c has been interpreted by Eckersley as proof that the scattering centers were in the *E*-region rather than on the ground. This conclusion followed from his argument that for ground-scattering the range of the echo with the smallest delay for frequencies below the critical must be greater than "2*F*". However, as is shown by the analysis of section II, echoes of less than the "2*F*" delay should in reality be accepted as the natural behavior of ground-scattering. The excellent agreement between experiment and theory when ground-scattering is assumed and the failure when *E*-layer scattering is assumed seems to be conclusive.

Experiment shows that the leading edge of the scatter echo is sharp and rather

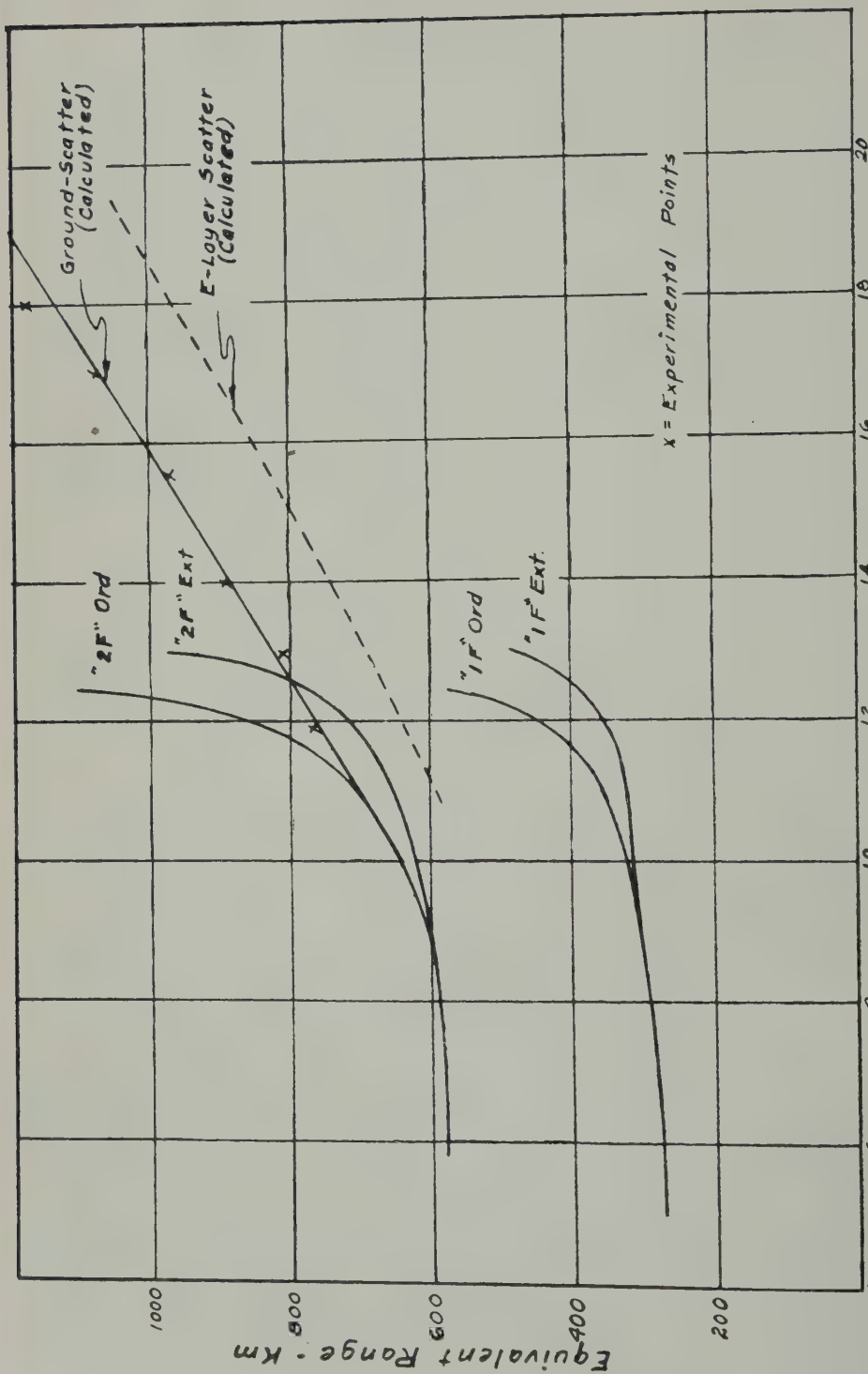

FIG. 6—EXPERIMENTAL RECORD—NOVEMBER 26, 1949; TIME: 15^h30^m

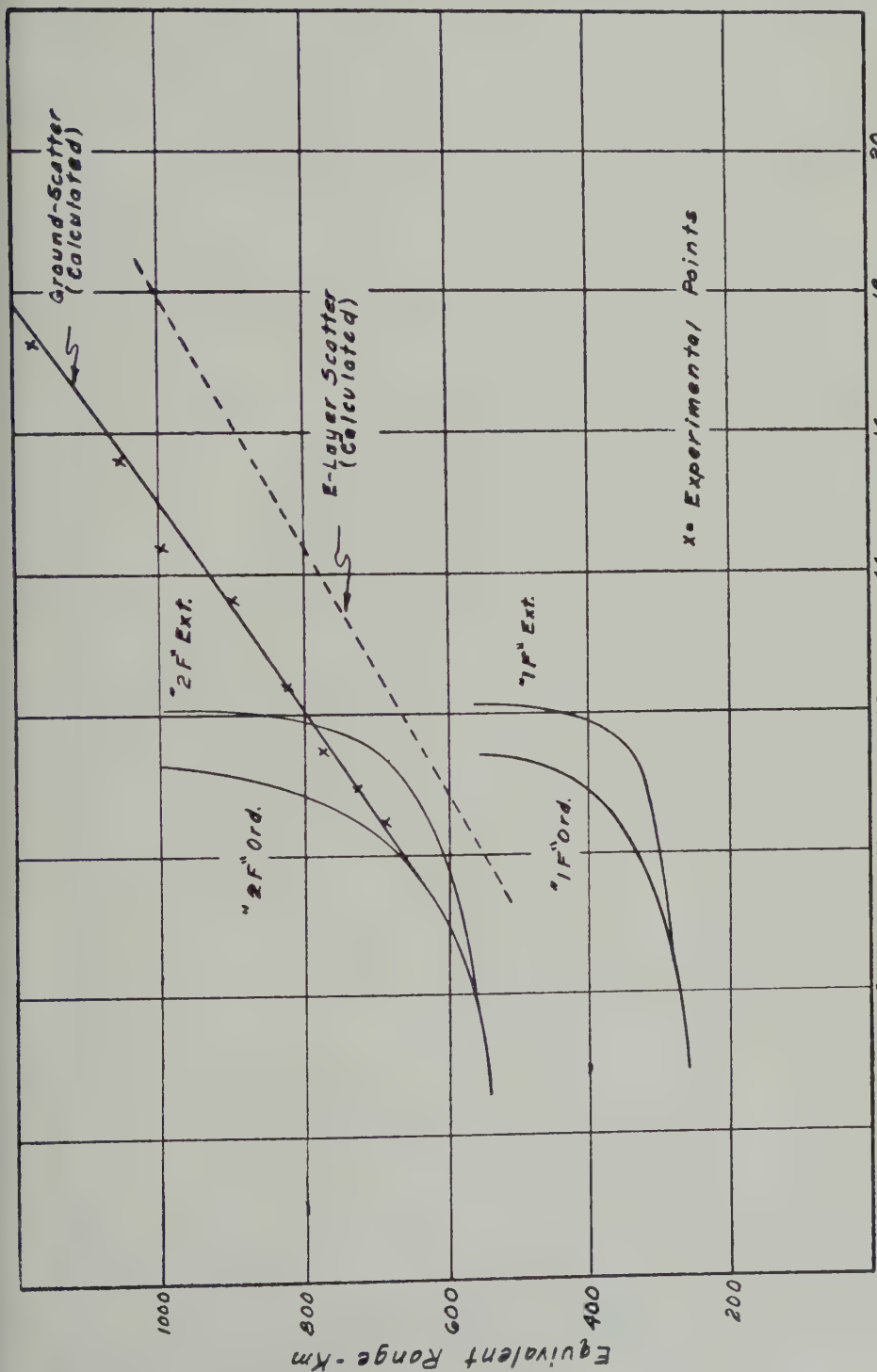

FIG. 7—EXPERIMENTAL RECORD — MARCH 3, 1950; TIME: 13^h02^m

well defined, building up to good amplitude quite quickly. This can be explained in terms of a sort of "time focusing" by extending the analysis of section II, and can be visualized by examining the curves of Figure 3. The T_{min} point may be seen to be the central point in the region in which T is changing most slowly with variations in angle of incidence θ. Energy transmitted through a range of angles in this region all tends to arrive back at nearly the same time.

The returned echo is first observed at the time-delay τ_{min} . As time progresses, energy continues to arrive back which was sent out at the angle of incidence θ_{min} (corresponding to the time-delay τ_{min}) until one transmitted pulse width $\Delta\tau$ after τ_{min} . During the time $\Delta\tau$, additional energy starts to arrive back which originally left the transmitting location at angles of incidence both greater and less than θ_{min} . Until the time $\Delta\tau$ has passed, energy continues to be added to the θ_{min} energy, increasing the strength of the returned echo. At time $\tau_{min} + \Delta\tau$, energy which left the transmitter at the angle θ_{min} ceases to arrive. The range of angles which are contributing energy to the scatter echo at time $\tau_{min} + \Delta\tau$, that is, at the end of one transmitted pulse width, may be obtained by striking an arc of radius $T + \Delta T$ (Fig. 8). Then energy, transmitted at angles between the two points of intersection of the tip of this radius with the contour for the particular frequency ρ, is contributing to the echo at time $\tau_{min} + \Delta\tau$. For time-delays greater than this, angles of incidence greater than θ_2 and less than θ_1 are commencing to add energy, while angles near θ_{min} are ceasing to contribute energy. The returned echo reaches a maximum amplitude at a time about one pulse duration after τ_{min} . For increasing pulse lengths, the echo builds up in amplitude. Due to the shape of the reflection contours, pulse lengths greater than 500 to 1000 μ secs do not appreciably increase the echo amplitude. This effect can be observed experimentally by varying the transmitted pulse width. The echo amplitude is found to build up quite rapidly in amplitude at first with increasing pulse length and then to level off.

If the proper range of frequencies is used, echoes are observed nearly 100 per cent of the time. Hence, the occurrence of scatter echoes must be considered as the usual rather than the extraordinary condition. The behavior of back-scatter with frequency has been found to be largely governed by the ratio of actual transmitting frequency to the vertical-incidence critical frequency.

A most attractive possibility for practical utilization of back-scatter echoes is the determination of skip-distance for transmission at oblique incidence. The theory developed in this paper shows the care which must be used in interpreting the scatter echoes if meaningful skip-distance information is to be obtained. The leading edge of the echo has been shown to be fixed by the "minimal time-delay" ray. Transmission at an angle of incidence corresponding to this ray results in scattering back from the ground at greater ground distance than the edge of the skip-zone. When utilizing a frequency near the vertical-incidence critical frequency, there is a great deal of difference between the minimum time-delay and the time-delay corresponding to scattering at the edge of the skip-zone. For such frequencies, using the leading edge of the scatter pattern as a means of calculating skip-distance would result in large error. Examination of the curves of Figure 4 shows that, as frequency of transmission is raised above the vertical-incidence critical frequency f_c , the minimum time-delay τ_{min} and the skip-time delay τ_{skip} approach one

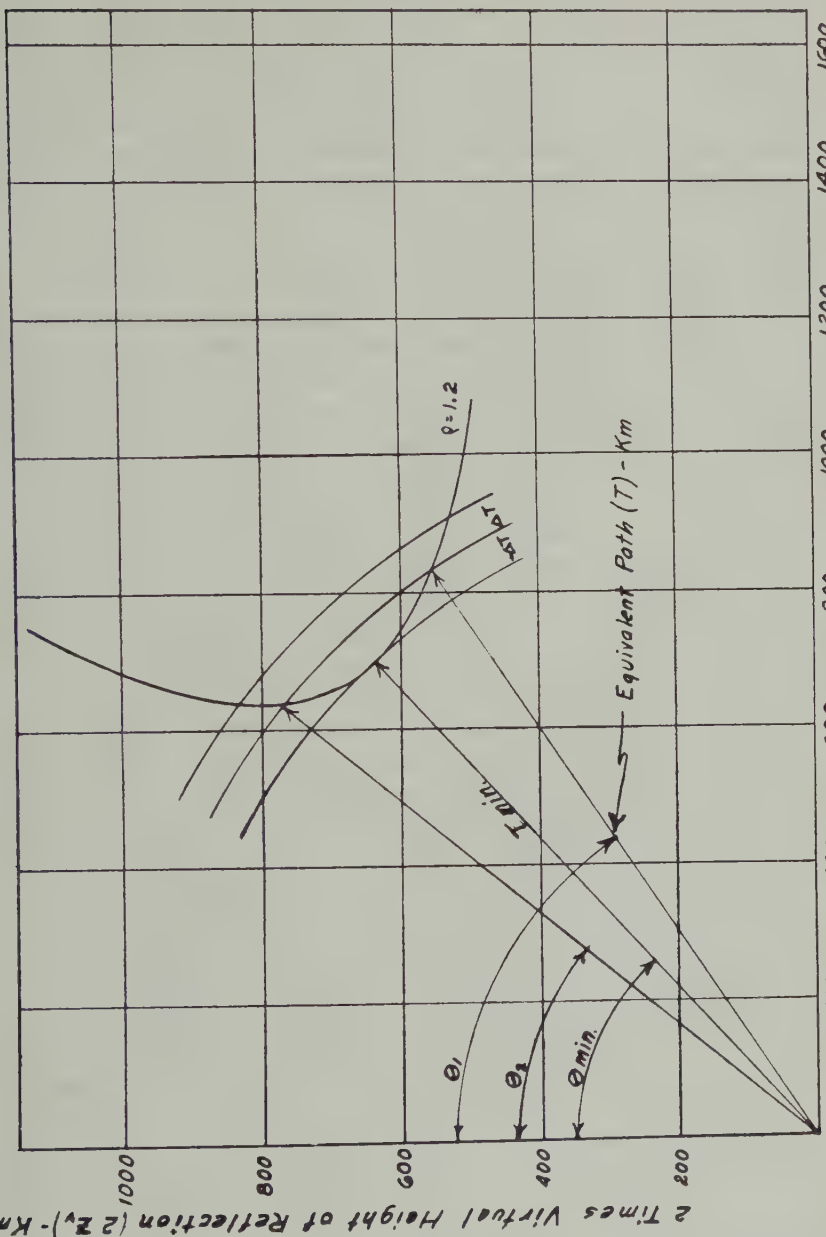

FIG. 8—RANGE OF ANGLES CONTRIBUTING ENERGY TO THE SCATTER ECHO AT THE END OF ONE TRANSMITTED PULSE WIDTH

another. At a transmission frequency of 1.3 f_c or 1.4 f_c, the two time-delays are sufficiently close so that the leading edge could be used as an index of skip-distance if care is used in interpreting the results. In the example plotted (typical parabolic layer), the difference in ground distance obtained by using τ_{min} instead of τ_{skip} for $f_{ob} = 1.4\ f_c$ is less than 25 km for a skip-distance of 880 km. This is the case if the proper virtual height is assumed for each ray-path. The proper virtual height to use with the minimal time-delay ray has been shown to be a constant Z_v^*,

given by the tangent to the $2F$ trace. To obtain the virtual height to be used with the skip-distance ray, one must make use of the overlay technique of Smith [10] or the parabolic layer approximations of Appleton and Beynon [9]. The simplicity gained by using the minimal time-delay ray with its constant virtual height Z_v^*, along with the range to the leading edge of the scatter pattern T_{min}, to obtain a ground distance may justify the error which results from such procedure. More serious errors would usually occur due to not having vertical-incidence data at the mid-point of the path.

Shortly after the range at which it becomes permissible to use the leading edge of the scatter pattern as an index of skip-distance, it also becomes necessary to take into account earth and ionosphere curvature. This destroys the simplicity of the analysis which holds for the plane earth case, since the equivalence relations become much more complicated. A first correction to the plane-earth plane-ionosphere case may be made by allowing geometrically for a curved earth while at the same time maintaining a plane ionosphere. This correction retains the simple plane ionosphere concepts, but makes computation more lengthy due to the curved earth geometry. Nomographs may be constructed which help to overcome this difficulty. For still longer transmission distances, the curvature of the ionosphere should be taken into account. Suitable approximations must be made, since an exact solution of the relation between time of transmission and distance of transmission measured along the earth D becomes very complicated.

An experimental study which tends to emphasize the regularity present in the back-scatter echo pattern is the observation of the echoes on apparatus suitable for detecting Doppler frequency shifts. At times when F-layer conditions are changing, the range at which scatter echoes are received is also changing. Consequently, one would expect the motion of the equivalent reflecting surface to produce a Doppler shift of the returned scatter energy. Experimentally, this is found to be true. The amount of shift is in accordance with the observed slow rate of change of range of the back-scatter echoes as measured on a pulse-ranging equipment, while the direction of the shift checks with the direction of the change in range. If back-scatter echoes are used to determine skip-distance, the addition of Doppler measurements would permit an instantaneous estimate of the stability of the transmission path. A low Doppler shift would indicate that transmission conditions over the given path for the frequency involved were remaining relatively fixed. A large shift would indicate rapid changes over the transmission path, an unsatisfactory condition for communication purposes. The direction of the Doppler shift would give information helping one to choose the proper operating frequency.

IV—*Conclusions*

Back-scatter of the "$2F$" type should not be considered an unusual or sporadic phenomena. When sufficient system sensitivity and proper antennas are used, the echoes are obtained nearly 100 per cent of the time. The echo behavior with time or frequency follows in a manner predictable from vertical-incidence virtual height *versus* frequency information. The leading edge of the scatter pattern is sharply defined and is given by the minimal time-delay analysis. The time-delay to the leading edge of the echo increases linearly with frequency, following the tangent

to the "2*F*" trace as transmitting frequency is raised above the vertical-incidence critical frequency. This edge of the pattern remains fixed as transmitter power or pulse width is varied. The observed increase in peak amplitude of the scatter echo with increasing transmitted pulse width may be explained by a sort of "time focusing." Great care must be taken in interpreting the results if meaningful skip-distance information is to be obtained from back-scatter measurements.

V—*Acknowledgment*

The author wishes to express his thanks to the members of the research staff at Stanford University, and in particular to Dr. L. A. Manning and Dr. O. G. Villard, Jr., for their guidance and encouragement during this investigation.

The research reported in this paper was supported by the Office of Naval Research and the United States Army Signal Corps.

References

[1] T. L. Eckersley, Analysis of the effect of scattering in radio transmission, J. Inst. Elec. Eng., **86**, 548-567 (1940).

[2] T. L. Eckersley, G. Millington, and J. W. Cox., Ground and cloud scatter of electromagnetic radiation, Nature, **153**, 341 (1944).

[3] A. H. Taylor and L. C. Young, Studies of echo signals, Proc. Inst. Radio Eng., **17**, 1491 (1929).

[4] C. F. Edwards and K. G. Jansky, Measurement of the delay and direction of arrival of echoes from near-by short wave transmitters, Proc. Inst. Radio Eng., **29**, 322-329 (1941).

[5] S. M. Hartsfield, S. M. Ostrow, and R. Silberstein, Back-scatter observations by the Central Radio Propagation Laboratory, Report No. CRPL-5-5 (Oct. 7, 1948).

[6] A. H. Benner, Predicting maximum usable frequency from long-distance scatter, Proc. Inst. Radio Eng., **37**, 44-47 (1949).

[7] S. K. Mitra, The upper atmosphere, The Royal Asiatic Society of Bengal, Calcutta, 1st ed., 204 (1947).

[8] D. F. Martyn, The propagation of medium radio waves in the ionosphere, Proc. Phys. Soc., **47**, 323-339 (1935).

[9] E. V. Appleton and W. J. G. Beynon, The application of ionospheric data to radio communication problems, Pt. I, Proc. Phys. Soc., **52**, 518-533 (1940).

[10] N. Smith, The relation of radio sky-wave transmission to ionosphere measurements, Proc. Inst. Radio Eng., **27**, 332-347 (1939).

JOURNAL OF GEOPHYSICAL RESEARCH VOLUME 56, No. 2 JUNE, 1951

SOME OBSERVATIONS OF THE VARIABLE 205 MC/SEC RADIATION OF CYGNUS A*

BY CHARLES L. SEEGER

Formerly, School of Electrical Engineering, Cornell University, Ithaca, N. Y.; now, Research Laboratory for Electronics, Chalmers, Gothenburg, Sweden

(Received March 18, 1951)

ABSTRACT

A 205 Mc/sec signal coming from the direction of the discrete radio source Cygnus A was observed on about 200 nights during the period of October 1948 to May 1950. Individual runs were from two to ten hours duration. This paper is an account of these observations.

Somewhat contrary to the results reported by Bolton and Stanley for 200 Mc/sec, the intensity of the radiation has been found to be quite variable. The mean period of the variations was about three-quarters of a minute, which is in agreement with mean periods observed at much lower radio frequencies. Strong variations have been observed at all altitude angles of the source. The signal appears to rise above the undisturbed value much more than it falls below it, the upward excursions being several times the probable value of the undisturbed signal.

A marked dependence of the variability of the signal on the altitude of the source was observed The signal was always variable at source altitude angles less than 15°. This must mean that an important part of the variability of the radiation received from Cygnus A arises in the earth's atmosphere, presumably due to scattering by random inhomogeneities. Order of magnitude calculations indicate ionospheric scattering may be a cause of fading of incoming radiation from outer space.

It is suggested that for frequencies below about 500 Mc/sec the stronger radio stars are the most suitable sources of radio frequency radiation for use in studies of the through transmission properties of the earth's atmosphere and should be of particular help in determining the physics of that part of the upper atmosphere inaccessible to normal ionospheric sounding techniques.

INTRODUCTION

The existence of a strong and apparently variable discrete source of radio frequency radiation in the direction of the constellation Cygnus was first reported

*Presented at the ninth General Assembly of URSI, Zurich, September, 1950.

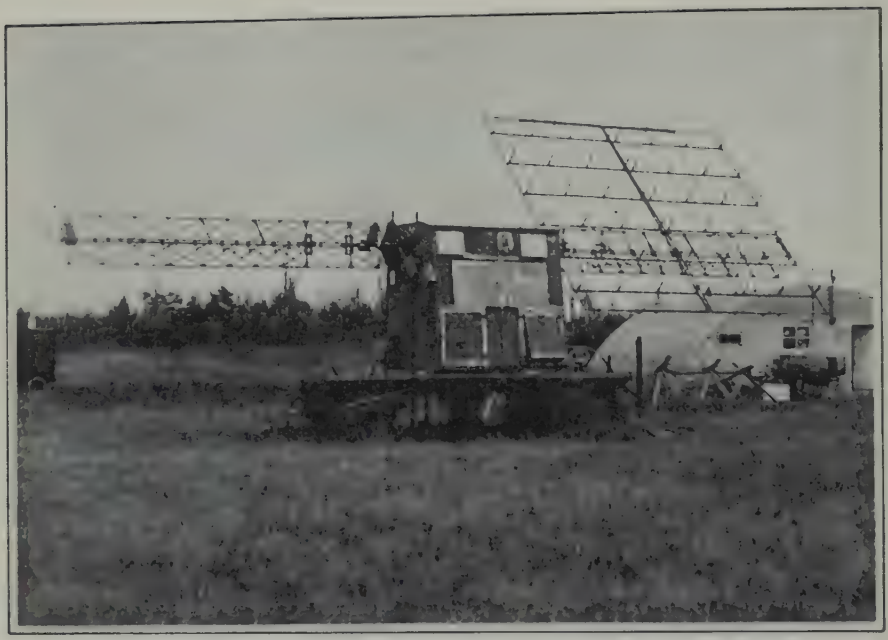

FIG. 1—ANTENNA AND ALT-AZIMUTH MOUNT USED FOR PART ONE AND PART TWO OBSERVATIONS

FIG. 2—EQUATORIALLY MOUNTED AUTOMATIC ANTENNA USED FOR PART THREE OBSERVATIONS

by Hey, Parsons, and Phillips [see 1 of "References" at end of paper]. Subsequent observations by other investigators [2, 3, 4, 5] have verified this discovery and added considerable detail to our knowledge concerning the characteristics and position of this radio star without, however, proving whether or not it is an intrinsically variable phenomenon. The purpose of this paper is to describe a series of observations, performed over an 18-month period, which indicate that, at least in the neighborhood of 200 Mc/sec, the earth's atmosphere is the chief cause of the variation in the flux received from this radio star, Cygnus A.

APPARATUS

Two different receivers and antennas were used for the observation of Cygnus A. All observations obtained before 1 June 1949 employed the 48 dipole array and manually operated alt-azimuth mechanism of Figure 1. The beam-width of this antenna (between half-power points) was 15° ± 0°.5 in both the electric and the magnetic planes. Vertical polarization was used in order to minimize reflection effects when observing at low altitude angles.

The 17.5-foot parabolic reflector of Figure 2 was employed in observations performed after 1 June 1949. This equatorial mount could be set to start, track, and stop automatically. The half-power beam-width of this antenna was approximately 23° and the polarization was essentially vertical for low altitude settings.

The general characteristics of the two receivers used with these antennas are given in Table 1. Before the beginning of any observing period, the receiver input was connected to a reference resistor and the gain of the receiver adjusted to produce an average detector output noise voltage of 2.0 volts. When the receiver

TABLE 1—*Receiver characteristics*

Particular	Receiver No. 1, used with dipole array	Receiver No. 2, used with parabolic reflector
Center frequency	205 ± 1 Mc/sec	205 ± 1 Mc/sec
Frequency band-width (Δf)	4.5 ± 0.5 Mc/sec	4.8 ± 0.2 Mc/sec
Noise figure (F)	12 − 30[a]	11 ± 1
Recording time constant	~ 1/2 sec	~ 1/2 sec
Receiver gain	(Adjusted to give a second detector output of 2.0 volts with zero antenna input signal.)	
Average apparent gain variation		
Over *10-minute* interval,	< 0.1 per cent	< 0.05 per cent
Over *2-hour* interval[b]	< 1.0 per cent	< 0.1 per cent

[a]The noise figure of this receiver increased during the period it was used in the observations of Cygnus A.

[b]These values include the slow gain-drift due to large (±15°F) changes in the ambient temperature of the equipment. No temperature control was used.

was reconnected to the antenna, any difference between the detector noise output voltage and the potential of a 2.0 volt back-bias battery was amplified and recorded on a 0-5 ma Esterline-Angus recording galvanometer. After correct adjustment of

the value of the reference resistor, the indication on the recording galvanometer with the receiver reconnected to the antenna was directly proportional to the power of the signal delivered by the antenna. Because a linear voltage detector was used at the output of the receiver, this direct proportionality was true only for signals which were small when compared to the equivalent-receiver-input noise [6]. In the observations of Cygnus A with these receivers and antennas, the signal output noise voltage was never more than 5 per cent of the total receiver output noise voltage.

This back-bias method of measuring small signal powers requires exceptional receiver gain stability. As indicated in Table 1, a satisfactory stability was achieved. In terms of the records reproduced here, where full scale corresponds to a change in the detector output voltage of 0.1 volt, a change in gain of 0.1 per cent would produce a deflection of one small division, or 2 per cent of the full scale deflection.

OBSERVING PROCEDURES

Occasional observations of the Cygnus region were performed between May and October 1948, but the first evidence of any large variations in the 205 Mc/sec galactic radio frequency radiation from this direction appeared on the night of 18 October 1948, while obtaining data for a galactic survey at this frequency [9]. Attempts to locate the source of this variable radiation, by adjusting the position of the antenna for a maximum of variability, indicated this radiation was coming from within an area of the sky about 10° in diameter and centered roughly at right ascension 20^h and declination +40°. Thus the center of this region coincided very nearly with the position of the radio "point" source, Cygnus A, as reported by Bolton and Stanley [3]. Figure 3 shows portions of the records taken on the nights of 18, 19 and 20 October 1948. The reference resistor deflection, marked *D.L.* (for Dummy Load), represents approximately zero input power to the antenna. The antenna was stationary, except as indicated. In the absence of any variations, the total signal from Cygnus A and about 180 square degrees of the surrounding region produced a deflection equal to about 50 per cent of the full scale deflection on these records.

It is convenient to divide these observations of Cygnus A into three groups on the basis of the three different observing methods employed. *Part One* and *Part Two* observations were performed with the dipole array antenna of Figure 1. *Part Three* observations were made with the antenna of Figure 2.

Part One observations—These observations were obtained between 22 November 1948 and 9 February 1949 inclusive. The half-hour observing period which occurred shortly after local sunset time was divided into three 10-minute intervals. Antenna pointing coordinates were computed for each interval on the basis of the mean position of Cygnus A. The recording tape speed was three-quarters of an inch per minute. An observer was present at all times to monitor the performance of the equipment, as well as to change the position of the antenna at the beginning of each new time interval. Figure 4 shows three typical *Part One* observations.

Part One observations are summarized in Table 2. Besides the Greenwich date and times of each observation the mean antenna coordinates for the half-hour

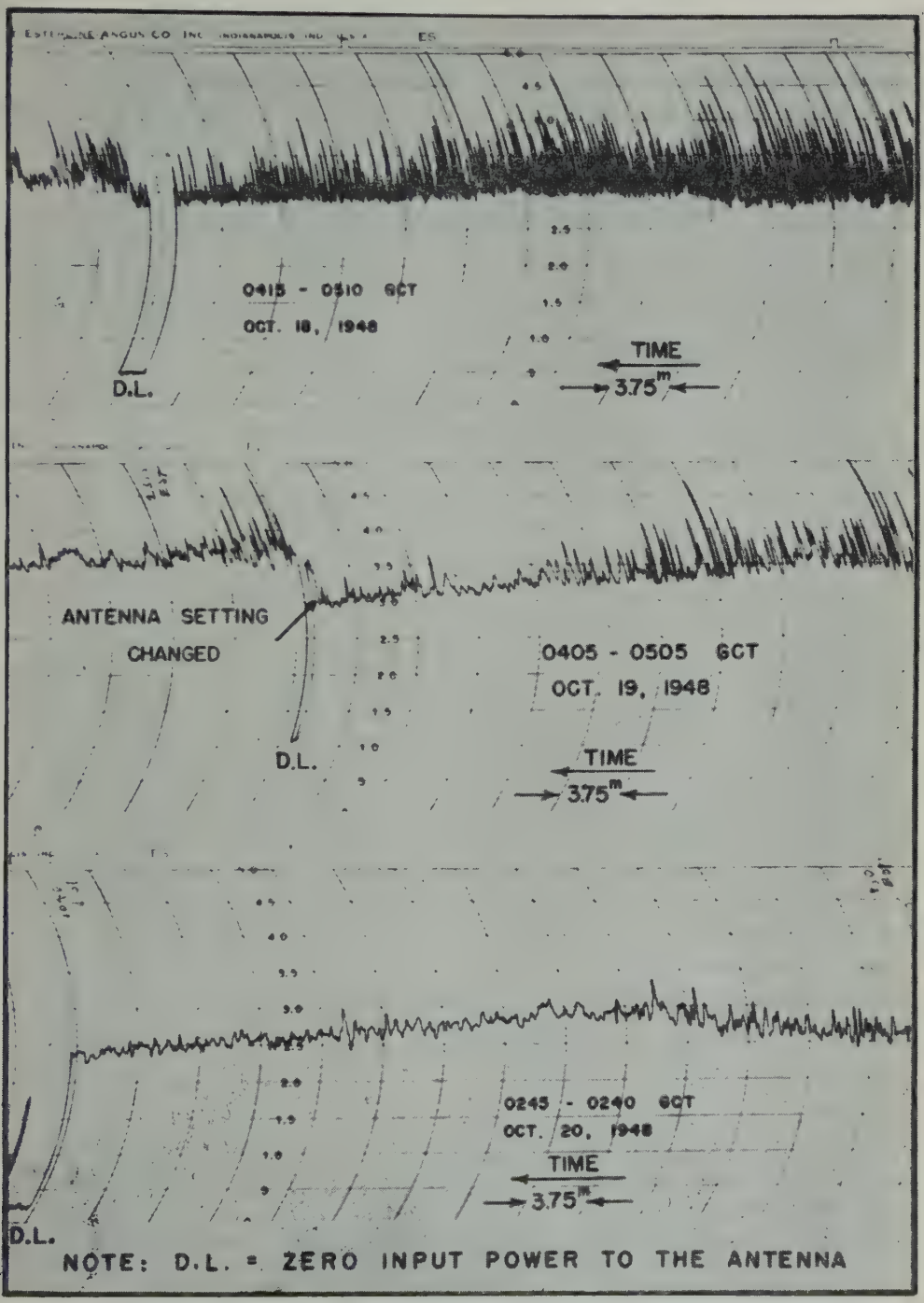

FIG. 3-RECORDS OF THE VARIABLE RADIATION RECEIVED FROM THE GENERAL DIRECTION OF CYGNUS ON THREE SUCCESSIVE NIGHTS

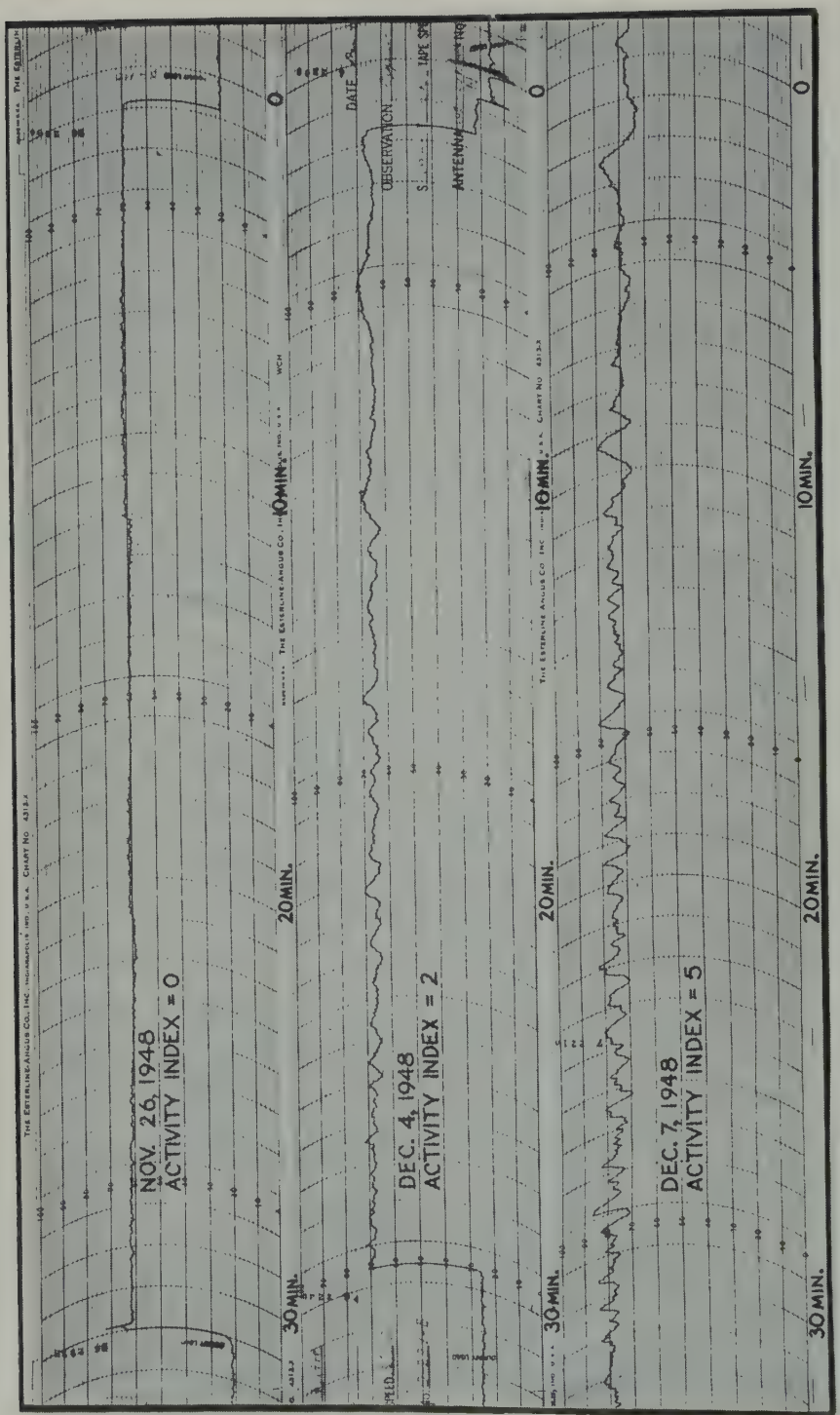

FIG. 4 – PORTIONS OF THREE TYPICAL PART ONE OBSERVATIONS

TABLE 2—*Part One observations*

Greenwich date	GCT		Average alt/az	Relative variability index
	From	To		
1948	*h m*	*h m*	° °	
Nov. 22	22 10	22 40	74/272	1–3
Nov. 24	22 00	22 30	73/273	1
Nov. 26	22 00	22 30	72/273	0
Nov. 27	22 00	22 30	71/274	0
Nov. 28	22 00	22 30	71/274	0
Nov. 29	22 03	22 30	71/274	0
Nov. 30	22 00	22 30	69/275	0
Dec. 1	22 01	22 30	69/276	0
Dec. 2	22 02	22 29	68/276	0
Dec. 3	22 00	22 30	67/277	1
Dec. 4	22 01	22 30	66/277	2–4
Dec. 5	22 00	22 30	66/278	0
Dec. 7	21 42	22 40	66/278	5
Dec. 8	21 40	22 10	67/277	1
Dec. 9	21 40	22 15	66/277	2
Dec. 10	21 40	22 10	65/278	0
Dec. 11	21 30	22 15	65/278	0
Dec. 12	21 50	22 21	62/280	0
Dec. 13	22 00	22 30	60/281	0
Dec. 14	21 40	22 10	63/279	0
Dec. 15	21 40	22 10	62/280	3
Dec. 16	21 40	22 10	61/280	1–2
Dec. 17	21 40	22 10	61/280	1
Dec. 18	21 40	22 10	60/280	0
Dec. 19	21 40	22 10	59/281	1
Dec. 20	21 40	22 10	58/282	0
Dec. 21	21 40	22 10	58/282	5
Dec. 22	21 40	22 10	57/283	2
Dec. 23	21 40	22 10	56/283	1
Dec. 26	21 40	22 10	54/284	0
Dec. 27	21 40	22 10	53/285	1
Dec. 28	21 40	22 10	53/285	0
Dec. 29	21 40	22 10	52/285	0
Dec. 30	21 40	22 10	51/286	0
1949				
Jan. 2	21 40	22 10	48/291	0
Jan. 3	21 40	22 10	48/291	0
Jan. 4	21 40	22 10	47/290	—
Jan. 26	21 40	22 10	32/300	2
Jan. 27	21 47	22 10	32/300	0
Jan. 28	21 40	22 10	31/300	0
Jan. 29	21 51	22 10	30/301	2
Feb. 8	11 35	12 05	46/69	1
Feb. 9	11 31	12 05	47/70	0

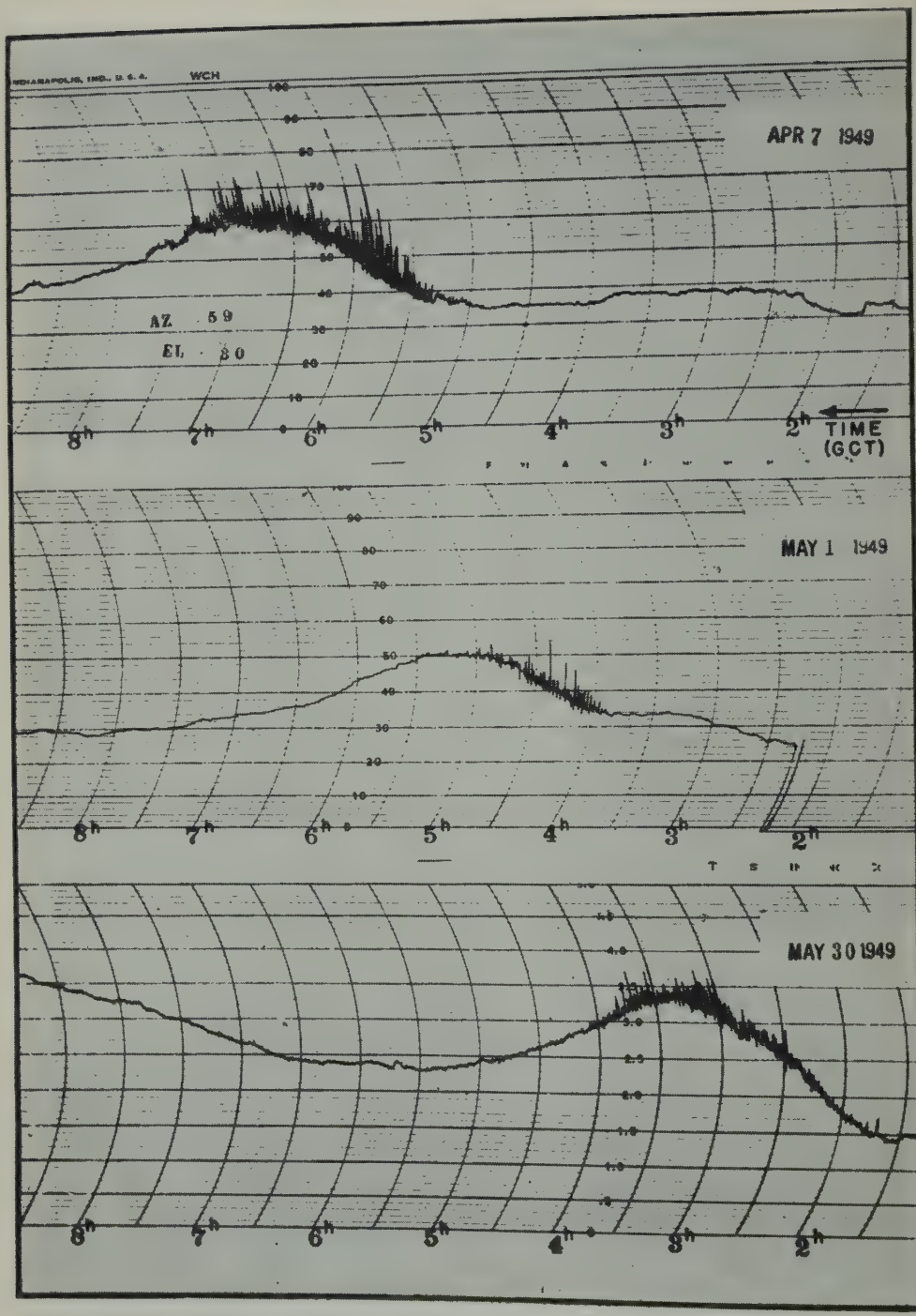

FIG. 5 — THREE TYPICAL "DRIFT" OBSERVATIONS OF THE CYGNUS REGION

TABLE 3—*Part Two observations*

Greenwich date	GCT		Average alt/az	Relative variability index
	From	To		
1949	*h m*	*h m*	° °	
Apr. 2–3	18 30	10 45	30/59	2
Apr. 3–4	13 30	10 45	30/59	3
Apr. 4–5	20 30	11 00	30/59	1–3
Apr. 5–6	20 00	11 00	30/59	2–4
Apr. 6–7	21 30	10 30	30/59	1–4
Apr. 7–8	20 30	10 30	30/59	2–15
Apr. 8–9	21 30	14 30	30/59	2–5
Apr. 9–10	19 00	10 30	30/59	3–10
Apr. 10–11	18 30	10 00	30/59	3
Apr. 12	04 00	11 00	30/59	0
Apr. 13–14	22 00	09 30	30/59	7
Apr. 14–15	21 30	10 30	30/59	5
Apr. 15–16	22 30	10 30	30/59	0
Apr. 16–17	18 30	10 30	30/59	2
Apr. 17–18	18 30	10 00	30/59	3
Apr. 18–19	18 30	10 30	30/59	3
Apr. 19–20	18 30	10 00	30/59	3
Apr. 20–21	18 30	03 00	30/59	0.5
Apr. 21–22	20 30	10 00	30/59	—
Apr. 23	02 30	18 00	60/77	0
Apr. 24	02 30	12 00	30/59	0.5
Apr. 25–26	18 30	10 00	30/59	2–3
Apr. 26–27	21 00	10 00	30/59	3–5
Apr. 27–28	21 00	18 00	30/59	3–6
Apr. 28–29	21 00	10 00	30/59	2–3
Apr. 29–30	19 00	10 05	30/59	2
Apr. 30–May 1	20 00	10 00	30/59	2–8
May 1–2	19 00	13 30	30/59	2–7
May 3–4	21 30	11 00	30/59	2
May 8	02 30	09 30	30/59	2–4
May 8–9	23 15	09 50	30/59	1–2
May 9–10	19 00	11 00	30/59	0
May 11–12	21 00	09 30	30/59	1
May 12–13	21 30	09 20	30/59	4–10
May 13–14	21 00	09 30	30/59	1–2
May 15	02 00	12 00	30/59	2–7
May 16	02 00	08 20	30/59 & 60/77	2–4
May 18	03 45	04 30	30/59	—
May 19	02 30	08 30	30/59	2
May 25–26	21 15	09 15	60/77	5
May 27–28	19 00	09 00	30/59	1
May 28–29	18 30	09 00	30/59	3
May 29–30	18 30	09 30	30/59	2
May 30–31	18 30	11 30	30/59	4

period are given.* The relative variability index is a somewhat qualitative estimate of the degree of variability observed, with 0.5 as the minimum certainly detectable value. The scale of relative variability is linear in power and two values indicate the range for occasions when, during one observation, there was a significant change in the degree of activity. A dashed line entry (——) indicates occasions when the activity was low but the observations were too poor to allow a variability determination to the usual minimal value.

Part Two observations—These observations, running from 2 April 1949 through 31 May 1949, were obtained by leaving the antenna of Figure 1 in a fixed position for a long period of time and allowing Cygnus A to rise through the antenna pattern. The basic recording speed was $1\frac{1}{2}$ inches per hour, but on many occasions, particularly in May 1949, a number of additional, parallel (that is, equal scale reading) records were made at tape speeds of 12 inches per hour and $\frac{3}{4}$ inch per minute. An observer was present during approximately one-third of these runs. The lack of personal attention to the majority of the observations was deemed to present no difficulty because of the distinctive record obtained with this "drift" technique and because Cygnus A rose through the antenna pattern during the early morning hours when local ignition interference was practically absent.

Three typical *Part Two* observations are reproduced in Figure 5. The hump in each record is due to the passage of the Milky Way through the antenna pattern. Most of this hump represents energy accepted by the 15° antenna beam from other sources in the same general direction as Cygnus A. The difference between sidereal and solar time accounts for the lateral shift of the humps in Figure 5. Also evident in this Figure are some differences in the sensitivity of the receiver for the three observations.

Table 3 summarizes the *Part Two* observations. Despite the appreciable receiver gain changes which occurred during the period of these observations, it was possible to maintain a consistent activity index because the ratio of the activity to the amplitude of the background hump depended chiefly on the antenna pattern and this was constant throughout all the *Part One* and *Part Two* observations.†

The greatest difficulty with the unsupervised drift observing technique arose as a result of the large ambient temperature changes experienced by the equipment because of the onset of spring weather conditions. Temperature control was not in use, so that most of the days for which no observations are listed in Table 3 are accounted for by the recorder drifting off scale. This sensitivity to ambient temperature was greatly minimized in the design of the second receiver used for the *Part Three* observations.

Part Three observations—After the completion in November 1949 of the automatic equatorial mount and parabolic antenna shown in Figure 2, Cygnus A was under fairly intensive observation for over six months, either from sunset to Cygnus A set or from Cygnus A rise to sunrise. Figure 6 shows two typical Cygnus

*The antennas used in these observations were situated at latitude 42° 29′.3 north and longitude $5^h\ 05^m\ 48^s.6$ west.

†This implies, of course, the additional observation that at 205 Mc/sec, and using the above equipment, there is as yet no evidence of any variation in the average intensity of the gross background radiation associated with the plane of our galaxy.

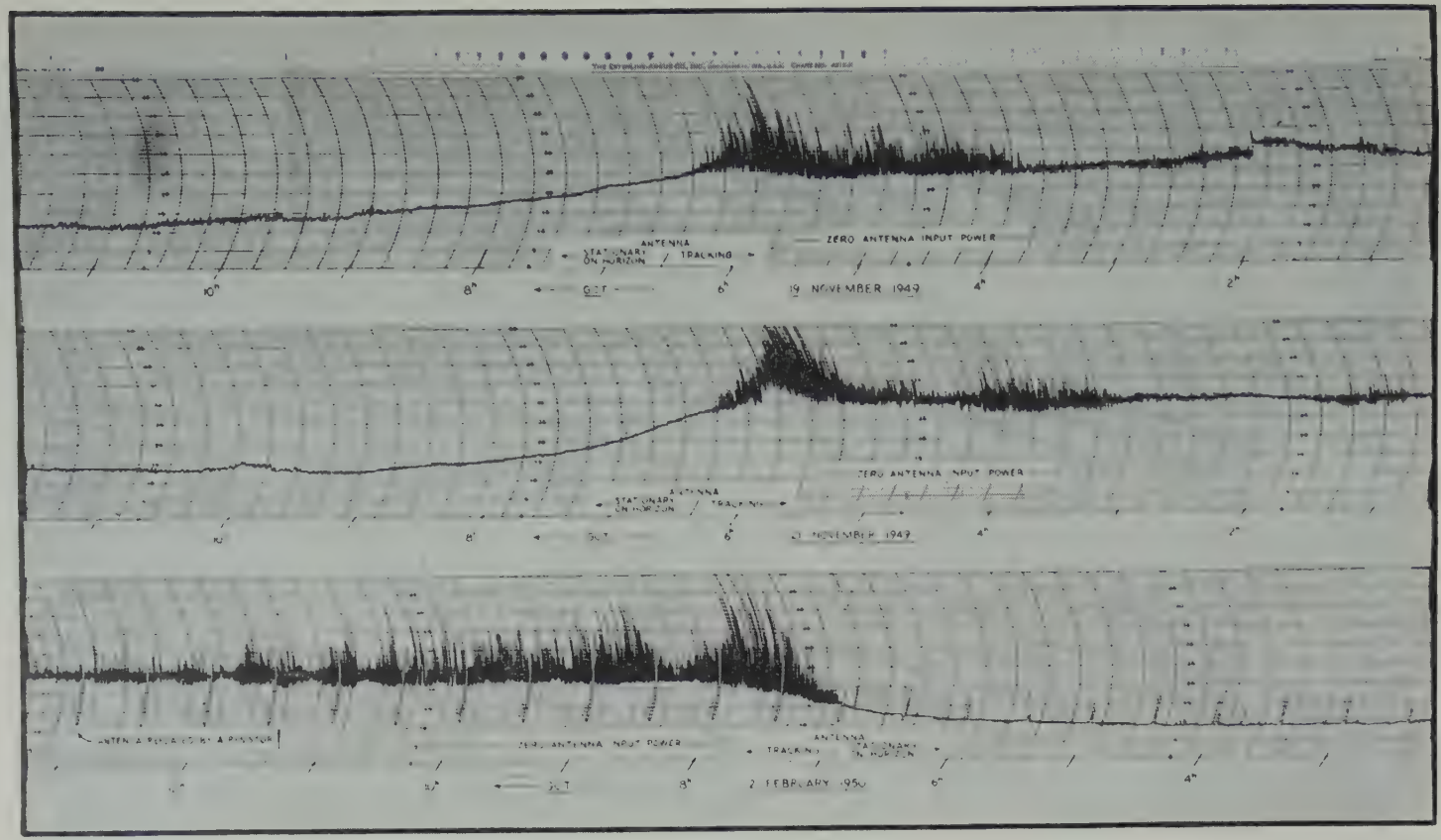

FIG. 6 — THREE RECORDS SHOWING TYPICAL VARIATION WITH TIME AND ALTITUDE OF THE 205 MC RADIATION RECEIVED FROM THE CYGNUS A "POINT" SOURCE

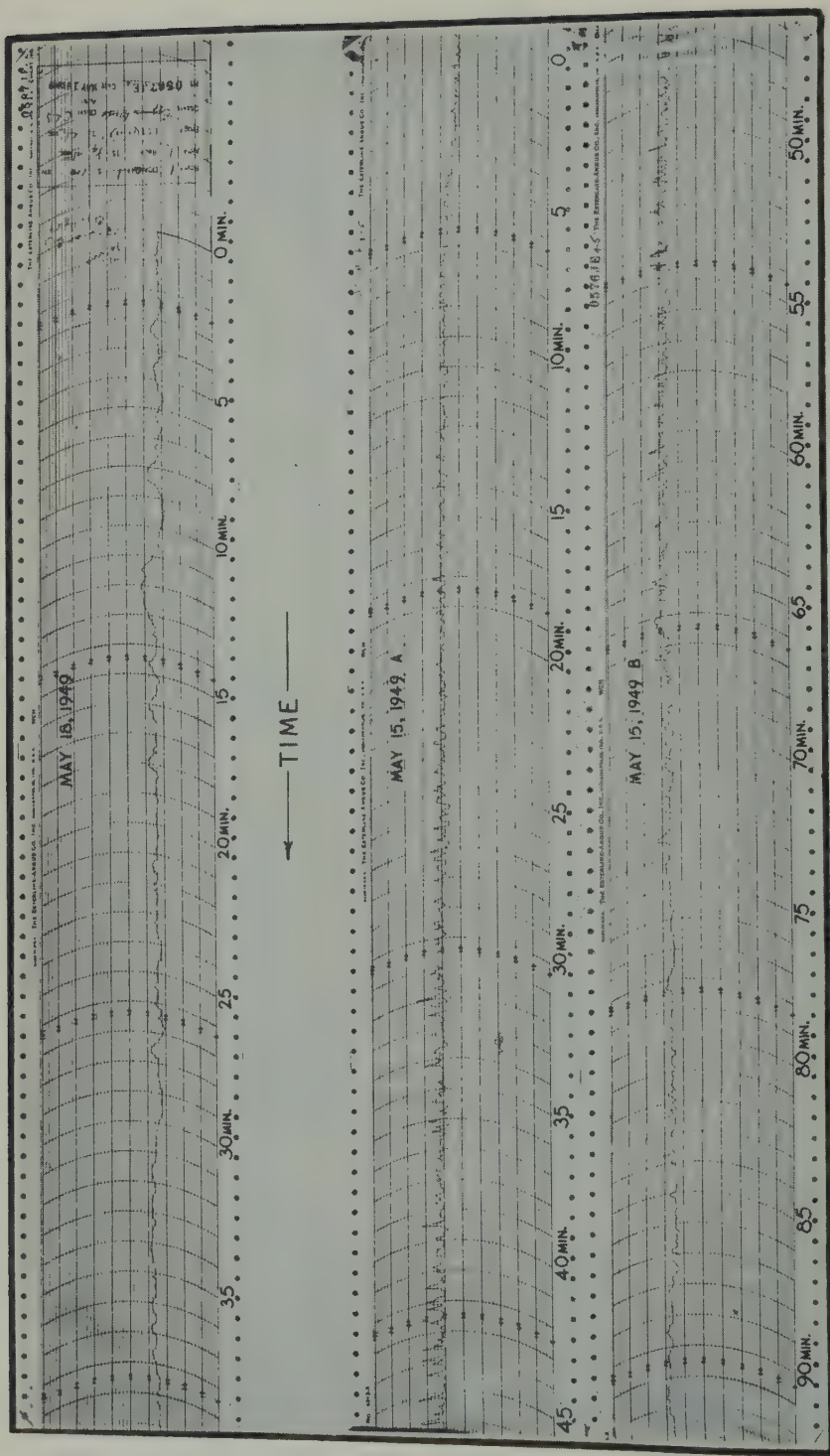

FIG. 7—TYPICAL EXAMPLES OF THE VARIABLE CYGNUS RADIATION AT 205 MC

A setting observations and one rise observation. The greatly improved stability of the second receiver can be seen in the bottom record of this Figure. In this run, the input of the receiver was switched automatically from the antenna to an arbitrary resistance for one minute every half-hour.

RESULTS

Identification of Cygnus A—All the *Part Two* observations have shown that, as in Figure 5, the center of the variable component on the records is always displaced from the peak of the hump in the direction of positive galactic latitude. The amount of the displacement agrees well with the difference between the galactic latitude of Cygnus A (approximately +5°) and the mean galactic latitude (approximately +1°.5) of the steady galactic radiation for galactic longitude 44°. Since no other comparably strong point sources have been observed within a 10° radius of the position given for Cygnus A, and since the general nature of the variations at 205 Mc sec is quite similar to that reported for Cygnus A on much lower radio frequencies, it is felt that the identification of Cygnus A as the source of the radiations responsible for these observations of variability at 205 Mc/sec is satisfactory.

Form and rate of variations—The general form of the variations of the Cygnus A radiation at 205 Mc/sec is illustrated by the records reproduced in Figure 7. These records were taken at a rate of one division ($\frac{3}{4}$ of an inch) per minute. The record for 18 May 1949 is typical of the slower rates of variation, while the record for 15 May 1949 is an example of the more rapid variations.

On a number of occasions, during the *Part Two* observations, recordings were taken at a tape speed of 12 inches per hour. An attempt was made to determine from these records the rate of variation of the Cygnus A radiation by counting the number of crests per unit time. A crest, or maximum, was counted only if its magnitude was greater than four times the minimum detectable power. A unit time interval of 7.5 minutes was chosen for convenience and to provide a reasonable number of crests per interval. Figure 8 shows typical examples of the records used in this crest counting procedure. The top record is included for comparison. It was obtained two hours after the record just below it and shows the steadiness both of the receiver and of the radiation from that part of the sky which followed the passage of Cygnus through the antenna beam. Table 4 lists the crest counts for each time interval in 14 observing periods. The high counting rate of 12-13 May has been observed on other occasions, but it is distinctly unusual. Figure 9 is a plot of the data in Table 4. The most common period between crests is about one minute, and the average period is about three-quarters of a minute. Thus the average period observed at 205 Mc/sec appears to agree with the average period reported [3, 5, 7] for the variations of Cygnus A at lower frequencies.

While periods as low as 0.1 times and as great as 10 times the average period have been observed, both extremes have never been found to occur within the same two-hour period. The most extreme change of rate observed occurred on 17 May 1949. The crest count for this observation is given in Table 4 and the record is reproduced in Figure 8.

A prominent feature of every observation of moderate to high variability is

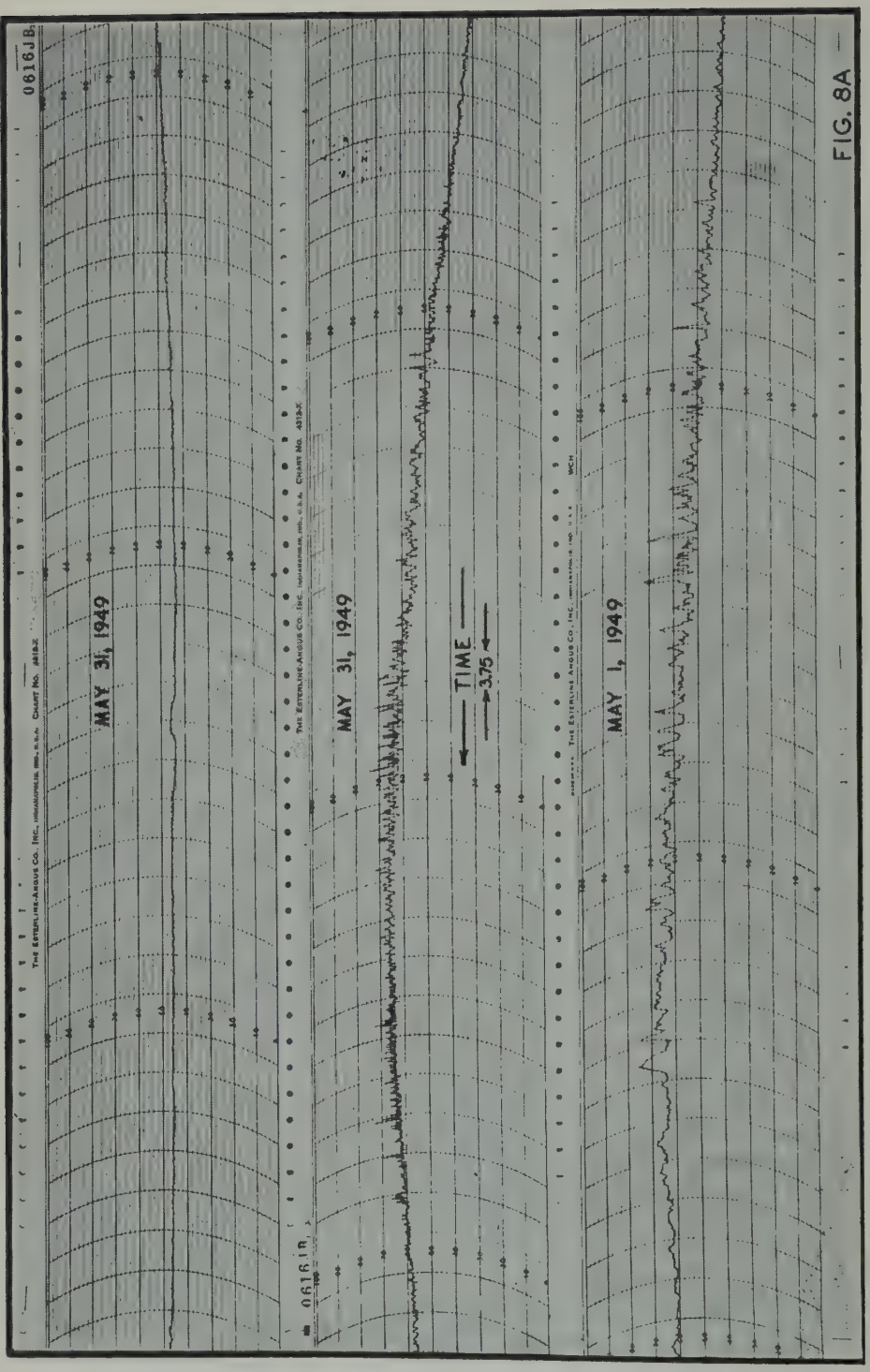

FIG. 8A —

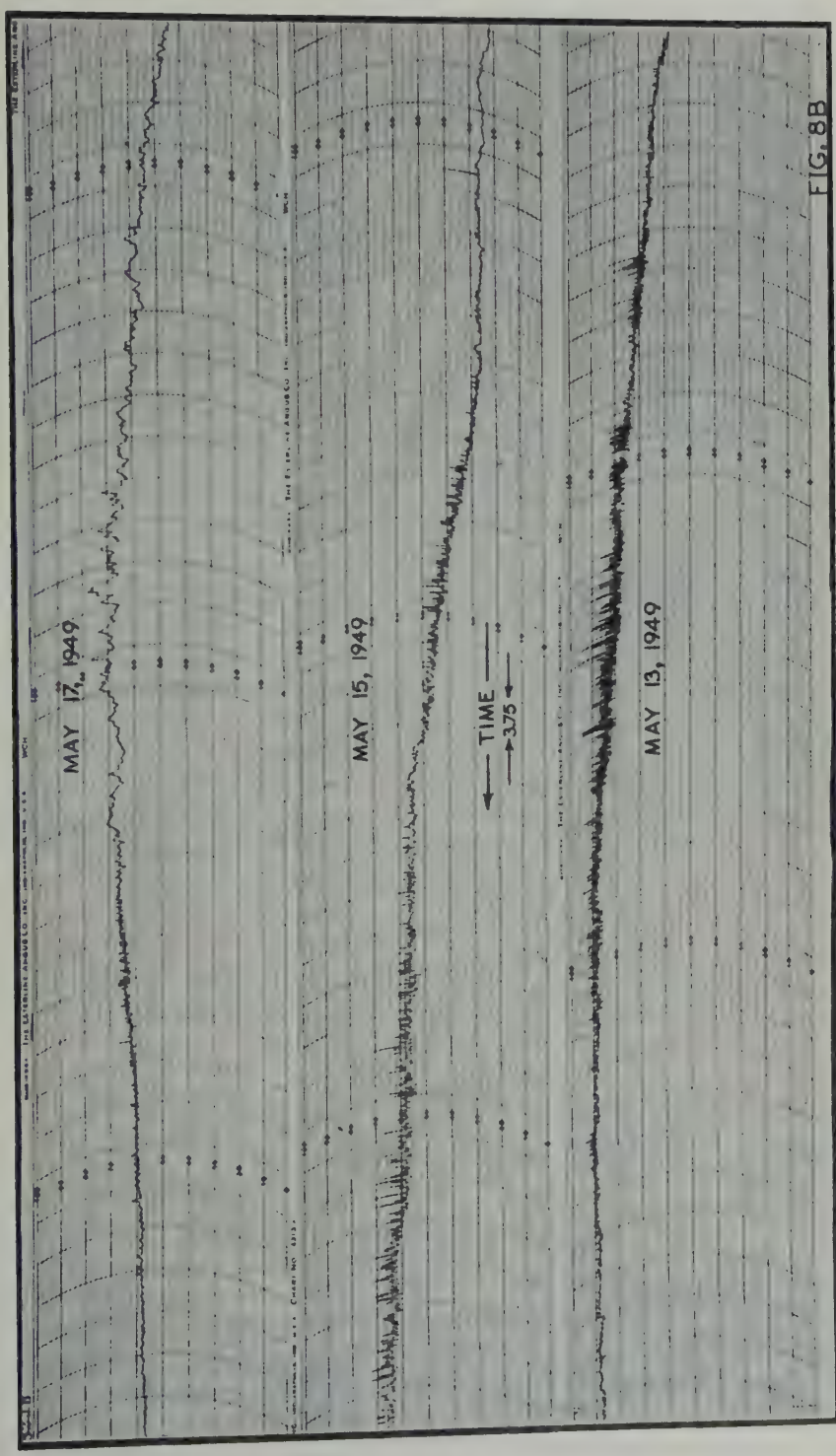

FIG. 8 — TYPICAL RECORDS FOR CREST COUNT

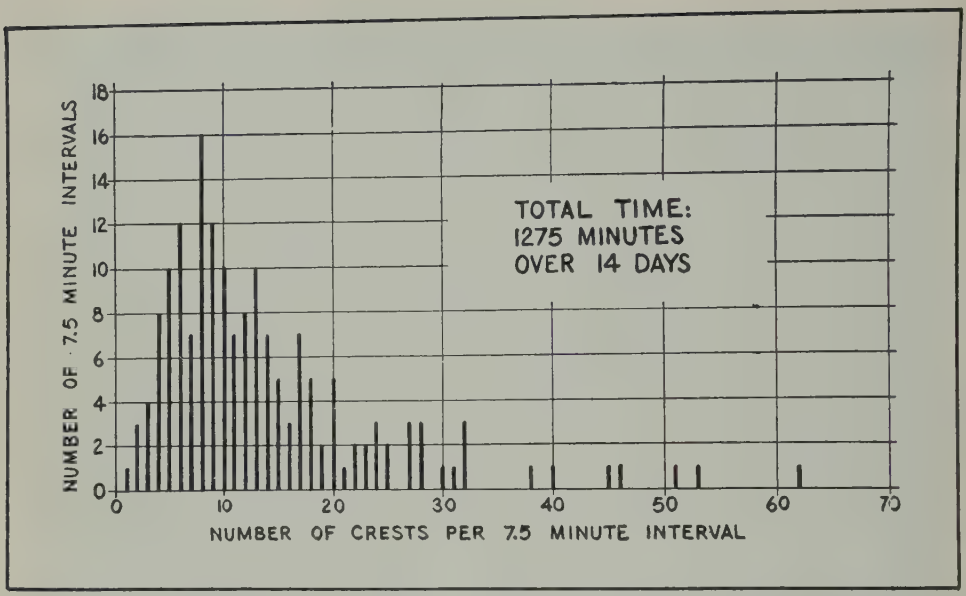

FIG. 9—DISTRIBUTION OF NUMBER OF CRESTS PER UNIT TIME INTERVAL

TABLE 4—*List of crest counts for each time interval in 14 observing periods*

Greenwich date	Number of crests per successive 7. 5 minute interval
1949	
4/27–28	4, 7, 7, 12, 9, 12, 13, 11, 12, 13, 11, 18, 17, 11
4/28–29	9, 8, 3, 6, 8, 5, 9, 10, 9, 3, 7, 6
4/30–5/1	9, 8, 10, 8, 13, 11, 12, 6, 8, 8, 8, 9, 4, 2, 4, 2
5/7–8	10, 11, 8, 8, 12, 9, 7, 13, 11, 8, 8, 14, 14
5/8–9	15, 14, 14, 24, 17, 17, 15, 10, 13, 6, 3
5/12–13	40, 25, 46, 45, 51, 62, 53
5/13–14	27, 24, 25, 20, 21, 22, 20, 15, 13, 17, 12, 9, 7
5/15	28, 32, 30, 17, 16, 20, 28, 27, 32, 31, 32, 24, 18, 10, 16
5/17	9, 6, 8, 4, 9, 7, 11, 9, 8, 5, 10, 27, 22
5/18	7, 5, 6, 6, 5, 6
5/19	9, 6, 5, 5, 3, 4, 4, 5, 4, 5, 4, 1, 2
5/28–29	10, 12, 17, 13, 13, 14, 14, 20, 18, 17, 16, 12, 6, 5
5/29–30	6, 8, 5, 8, 6, 13, 15, 10, 8, 10, 10, 6
5/30–31	13, 14, 20, 18, 19, 23, 18, 15, 23, 38, 28, 19

Total 7.5 minute intervals = 171
Total days = 14

the asymmetry of the variations. When there is considerable activity present, a definite minimum value is observed, while the amplitudes of the maxima vary over a wide range. This property of the variations can be seen in Figures 3 and 5 to 8. If it is postulated that Cygnus A is intrinsically constant and that this minimum represents a complete fade-out of just the Cygnus A radiation, the in-

tensity of the broad galactic background remaining constant, then one may estimate the undisturbed flux of Cygnus A by comparing quiet records with records showing strong variability. Such a procedure applied to the *Part Three* observations indicates the undisturbed flux of Cygnus A was about one-fifth of the galactic background flux, and that on many occasions the peak received flux from Cygnus A was five times or more as great as the undisturbed value.

The nature of the records did not permit a precise determination of the mean value of the Cygnus A flux during times of great variability. It is believed, however, that a two-to-one enhancement in the average flux over a half-hour period would not have escaped notice.*

Frequency of occurrence of variability—The most striking difference between *Part One* and *Part Two* observations is in the frequency of occurrence of variability. The 43 *Part One* observations showed significant variability to be present 42 per cent of the time, while in the 44 *Part Two* observations variability was present 86 per cent of the time in spite of a poorer receiver sensitivity. Furthermore, the average amplitude of the variations (counting only variable observations) is approximately twice as great for the *Part Two* observations as for the *Part One* observations. This suggested that perhaps both the frequency of occurrence of variability and the intensity of the variations were, to a great extent, inverse functions of the altitude of Cygnus A. This altitude dependence has been verified by more than 150 *Part Three* tracking observations. Not one example of very low activity has been observed, so far, when Cygnus A was below about 15° altitude.

Partly because of the great difference in the characteristics of the two antennas, it was not feasible to carry over to the *Part Three* observations the same activity index employed for *Part One* and *Part Two* observations. A new index was arranged which classified the activity into the following four groups:

Q = quiet

A = small amplitude variations
(1 to 5 scale divisions)

B = medium amplitude variations
(6 to 14 scale divisions)

C = large amplitude variations
(15 or more scale divisions)

A considerably greater minimum variable flux was required for definite recognition of activity in a *Part Three* observation than in the *Part One* and *Part Two* observations.†

*The characteristics of 205 Mc/sec solar radiation are completely different from the characteristics of the radiation from Cygnus A at the same frequency. This may or may not be important evidence with respect to whether Cygnus A is or is not a star, because there is no reason to believe the characteristics of solar radio radiation are typical of other stellar atmospheres.

†Whether or not variability is apparent depends on the sensitivity of the radio telescope. There is reason to believe that if the sensitivity of the equipment used in these observations was improved by a factor of ten then the Cygnus A radiation would be definitely variable most of the time, even when at high altitude angles.

Table 5 shows the result of applying this new activity index to 46 *Part Three* observations obtained between 13 November and 28 February 1950. Each number represents the number of times a particular degree of average activity was observed

TABLE 5—*Summary of the degree of activity observed in 46 Part Three observations, which were continuous over the altitude range 0° to 65°*

Activity index	Source altitude angle		
	0°–10°	25°–35°	55°–65°
C (> 15 div.)	20	0	0
B (6–14 div.)	17	3	1
A (1–5 div.)	9	14	7
Q	0	29	38
Total	46	46	46

for a particular range of source altitude angle. Averaging accomplished a first-order correction for the variation of the antenna pattern when the source was below 10° altitude.

The possibility that an appreciable part of these low altitude, rapid signal variations could be caused by the simultaneous reception of both direct and variable, ground-reflected waves was considered and found to be extremely unlikely because of the known antenna pattern, the proximity of the antenna to the ground, the nature of the local terrain and, particularly, the consistent characteristics of the records themselves.

With respect to the frequency of occurrence of variability and the average intensity of the variations, the observations described here may be summarized as follows:

(1) The probability that a given degree of activity will be observed during any half-hour of the night increases rapidly with decreasing altitude angle of the source. While high activity has been observed on a few occasions with altitude angles of 60° to 90°, it is a rare occurrence.

(2) There is an irregular variation in the activity which appears to be superimposed on the systematic increase of activity with decreasing source altitude.

(3) No sudden onsets or cessations of activity have been observed so far. Thirty minutes would appear to be a significant time interval with respect to changes in the degree of the general activity.

(4) During a particular observation there is a tendency for high amplitude variations to occur somewhat more rapidly than low amplitude variations.

(5) When a high degree of variability has been present with Cygnus A at altitude angles greater than 20°, many other parts of the sky often show definite, but generally weaker, variations of the same type. On two occasions the region of the sky containing another strong discrete source, Cassiopeia A, has shown as great a variability as that ever observed for Cygnus A.

(6) There is no reason at present to suspect any difference in the nature of

variability of the Cygnus A radiations, whether Cygnus A is rising in the northeast or setting in the northwest.

DISCUSSION

From these observations it is clear that at 205 Mc/sec the radiation from Cygnus A does vary over a wide range. Furthermore, these variations are not particularly difficult to observe at this frequency. The fact that the degree of variation increases with a decrease in the altitude of the source seems to be established beyond doubt. This must mean that an important part of the variability of Cygnus A arises in the earth's atmosphere, presumably as a result of scattering by random inhomogeneities. Calculations of the order of magnitude of atmospheric scattering have been made by H. G. Booker, and it appears that scattering in the ionosphere is quite a likely cause of fading of incoming radiation from outer space.

There is only one other published report of observations of Cygnus A at a frequency as high as 200 Mc/sec. In the first presentation of the results of their multifrequency, Lloyd's mirror observations of Cygnus A, Bolton and Stanley [2] report they operated "during three months . . . . mainly on 100 Mc, but also occasionally on 60, 85, and 200 Mc." They found no variations at 200 Mc. The discrepancy between their observations and those reported here may be a matter of chance or equipment sensitivity. Otherwise, since Cygnus A never attains a very great altitude in Australia, one is led to suspect the possible existence of an important difference in the radio frequency properties of the earth's atmosphere for the two observing stations.

The variability observed at 205 Mc/sec appears to be quite similar in nature and about equivalent in mean periodicity to the variability reported for the lower radio frequencies. This suggests that perhaps much of the variability of the Cygnus A radiation on lower frequencies may be due to the earth's atmosphere. To prove that any of the variations of the radiation from Cygnus A are not just atmospheric modulations will require simultaneous observations by at least two, and preferably three, geographically well-separated stations which employ nearly identical receiving equipment.

D. K. Bailey [8] has called attention to the importance of signals arriving from outside the earth's atmosphere as a tool for analyzing the electromagnetic wave-propagation characteristics of the atmosphere. Of the three available types of extraterrestrial sources, the radiations from Cygnus A and some of the other radio stars appear to be the most suitable for such atmospheric studies at frequencies below 500 Mc/sec. Radiation from the enhanced sun is much more easily observed than the radiation from the radio stars, but its behavior is generally unpredictable, both in intensity and in apparent source position and size. Moon radar involves additional, expensive transmitting equipment and the echo analysis is complicated by the double passage through the atmosphere, as well as by the complex reflection from the lunar surface. Though the flux from the stronger radio stars is low, yet these point sources are easy to observe, are probably quite steady in intensity most of the time (certainly when compared to the variability of "spot" solar radiation) and so far no change in their celestial positions has been observed.

A detailed study of the radio transmission properties of the earth's atmosphere

is of particular importance to radio astronomy, because without a sound knowledge of the "radio seeing" an understanding of the radio star phenomena will be extremely difficult to achieve.

ACKNOWLEDGEMENTS

The work reported here was carried out while the author was a member of the Radio Astronomy Project of the School of Electrical Engineering, Cornell University. This work was sponsored jointly by Cornell University and the Office of Naval Research.

The author is particularly happy to record his thanks to H. G. Booker (Cornell), to D. A. MacRae (Warner and Swasey Observatory), and to R. E. Williamson (David Dunlap Observatory) for their many helpful discussions and criticisms.

S. M. Colbert performed many of the observations, besides constructing much of the equipment, and was also largely responsible for the maintenance of the observations under difficult conditions.

References

[1] J. S. Hey, S. J. Parsons, and J. W. Phillips, Nature, **158**, 234 (1946).
[2] J. G. Bolton and G. J. Stanley, Nature, **161**, 312-313 (1948).
[3] J. G. Bolton and G. J. Stanley, Aust. J. Sci. Res., A, **1**, 58-69 (1948).
[4] J. G. Bolton, Nature, **162**, 141-142 (1948).
[5] M. Ryle and F. G. Smith, Nature, **162**, 462-463 (1948).
[6] H. T. Friis, Proc. Inst. Radio Eng., **32**, 419-422 (1944); and correction, **32**, 729 (1944).
[7] J. S. Hey, S. J. Parsons, and J. W. Phillips, Proc. R. Soc., A, **192**, 425-445 (1948).
[8] D. K. Bailey, Terr. Mag., **53**, 41-50 (1948).
[9] C. L. Seeger and R. E. Williamson, Astroph. J., **113**, 21-49 (1951).

JOURNAL OF GEOPHYSICAL RESEARCH VOLUME 56, No. 2 JUNE, 1951

THE DAILY MAGNETIC VARIATIONS IN EQUATORIAL REGIONS

BY A. T. PRICE AND G. A. WILKINS

Imperial College of Science and Technology, London, England

(Received April 7, 1951)

ABSTRACT

A new analysis of the *Sq*-field for the Polar Year 1932-33 indicates that the maximum daily variation of H in equatorial regions is to be found between the magnetic and dipole equators in South America and Africa, but occurs to the south of both these equators in the Far East. It also appears that the line of maximum variation varies in position with the season, its movement being in the direction opposite to that of the sun.

In the course of a detailed analysis of the *Sq*-field for the three seasons of the "Polar Year," 1932-33, we have noticed some features of the field which are of interest in connection with the study of the large daily variations of H in equatorial regions. Chakrabarty [see 1 of "References" at end of paper], Egedal [2], Chapman [3], and Martyn [4] have all pointed out that the field in these regions is subject to considerable geomagnetic control, and Martyn has suggested that the maximum daily variation of H is to be found along a "mean equator," lying midway between the magnetic and geomagnetic (dipole) equators. These discussions have necessarily been based on observations made at many different times, and, though corrections have been applied to reduce the data to a common epoch, considerable uncertainties as to the precise distribution of the field must remain, since reduction factors applicable to one station are not necessarily suitable for another. This difficulty will be removed to some extent by the widespread observations now being made at many temporary equatorial stations, but it seems unlikely that it will be removed entirely until a fair number of *simultaneous* observations at different stations become available. This is because the seasonal changes in the range of H are remarkably large at some stations, and may differ considerably in character or time of occurrence at different stations. For example, the range decreases appreciably at Huancayo between October and November; a similar decrease apparently occurs a month earlier at Tatuoca.

It therefore seems worth while endeavouring to extract the maximum possible amount of information about the field from an entirely homogeneous set of data, such as that afforded by the Polar Year observations. Though the number of equatorial stations for that epoch is not large, there are several which have not

previously been considered; the data for these (as well as for many other stations) have been kindly supplied to us by Dr. V. Laursen of the Commission for the Liquidation of the Polar Year. By using the observations (when available) of all three components H, D, and Z, and considering the field over the range of latitude $\pm 60°$, it is possible to interpolate the field with a good deal more certainty than would be the case if the data for H alone were used. In particular, the observed value of ΔD, used in conjunction with the criterion that the surface field must have a potential, has proved of considerable assistance in deciding the most probable values of ΔH. Also, the vertical variation ΔZ can be used to some extent to help decide whether the ionospheric currents associated with the field are concentrated into a narrow band (for example, near the equator) or spread over a wider area. This again helps to remove some of the uncertainty in the interpolation of the field.

The first step in the interpolation involves finding those positions on the earth's surface where the *type* of daily variation (taking into consideration all three components) is more or less the same. The loci of these positions are represented by the full curves in Figure 1, which also shows the Polar Year stations used in the analysis. If the daily variations depended purely on local time, these curves would be circles of latitude, and the variations would have the same amplitude along each circle. In the actual case, the curves are clearly influenced considerably by the geomagnetic field; also it is found that there is usually some change in the amplitude of the variations along each curve, though *it is less in that direction than in any other*. These curves will be referred to as lines of "corresponding" latitude.

A preliminary version of Figure 1 was obtained simply by linking those observatories for which the records have obviously similar characteristics. It will be seen that the observatories fall rougnly into three groups, centred about the meridians 80° west, 20° east, and 120° east, respectively. Within each group it was found that the records of stations in similar latitudes were in reasonable agreement, but this was not true for stations in different groups. In particular, stations in America invariably corresponded to stations considerably further north in Europe or Africa.

A corrected and more detailed version of Figure 1 (as shown) was then obtained in the course of the main analysis in the following way. The values of the north, east, and vertical deviations (ΔX, ΔY, ΔZ) over the earth's surface were determined for several different epochs G.M.T. by graphical interpolation, proceeding on the assumption that the *local time* changes at any particular observatory can be taken as typical of the changes at all points on a *limited segment of the line of "corresponding" latitude passing through the observatory*. Now the horizontal component (ΔX, ΔY) is the gradient of a potential function, and must therefore satisfy the condition that the line integral round any closed circuit is zero. A new method (which will be described in detail in a forthcoming paper) was developed for correcting the original estimates of ΔX and ΔY to ensure that this condition is satisfied, while keeping them in satisfactory accord with the observed data. These corrected estimates of ΔX and ΔY (for the various epochs) were then used to obtain the final version of Figure 1.

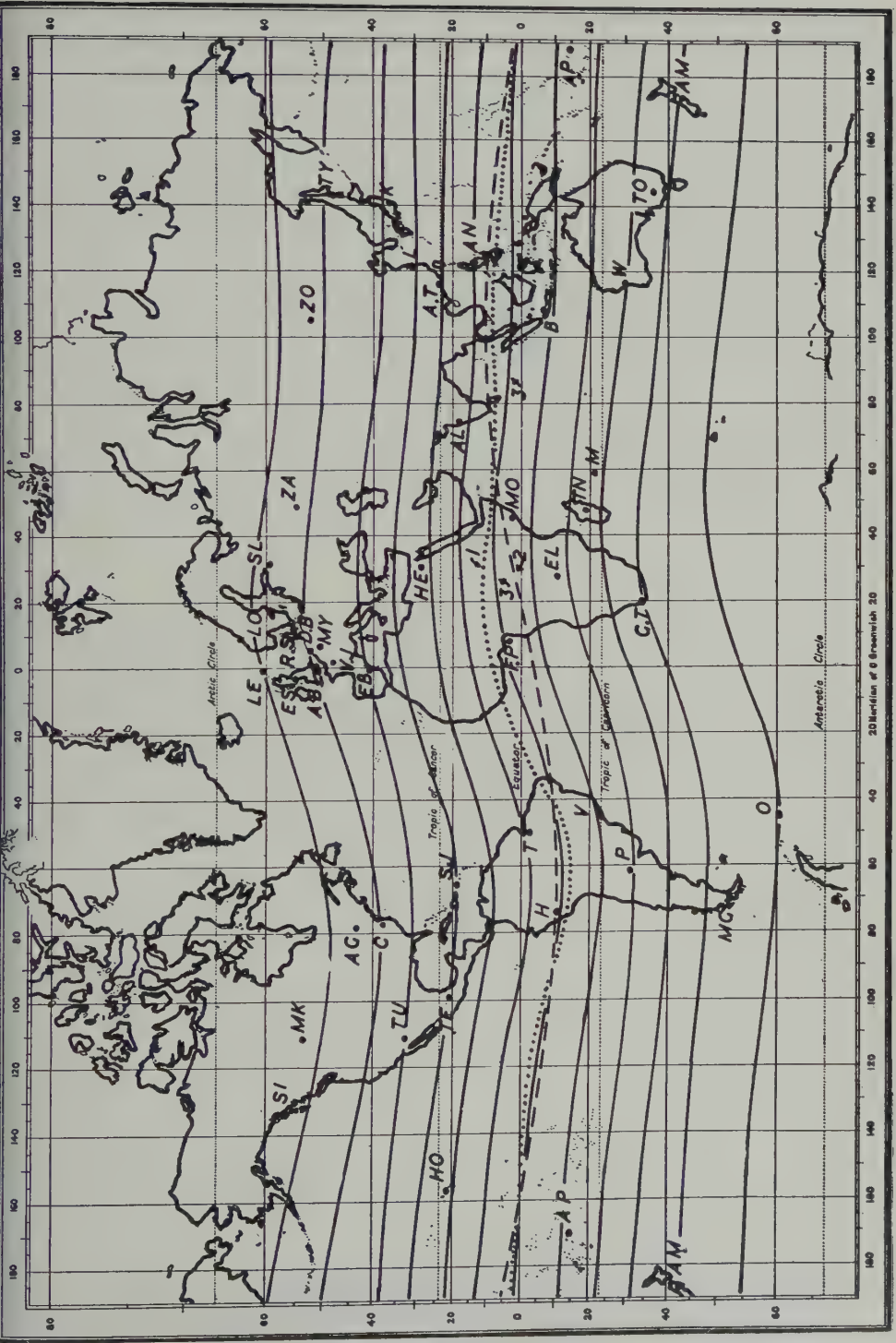

FIG. 1—LINES OF "CORRESPONDING" LATITUDES AND EQUATORS
1 = MAGNETIC EQUATOR, 2 = DIPOLE EQUATOR, AND 3 = LINE OF MAXIMUM ΔH

The Figure shows clearly that the "longitudinal effect" in the *Sq*-field is not confined to the equatorial region but extends throughout the region between latitudes ±60°. The line marked 3 in the Figure is the estimated position of the line of maximum range of ΔH, regarded as a function of latitude. The maximum range is not, however, necessarily the same all along this line; at Fernando Po it is comparable with that at Huancayo (especially during the equinoctial months), but it is not certain whether the same large value is reached elsewhere. The lines marked 1 and 2 are the magnetic equator and dipole equator, respectively. It will be seen that between 100° west and 60° east the line 3 is midway between 1 and 2, that is, it coincides with the mean equator in agreement with Martyn's suggestion referred to above. But between 60° east and 160° east, line 3 is south of this mean equator and much nearer the geographic equator. That this is so is suggested by the relatively large variation at Batavia, which is approximately equal to that at Antipolo, though this station is much nearer both the magnetic equator and the dipole equator, which are close together in this region. Moreover, if the assumption *is* made that the maximum range occurs at the mean equator (so that the field is unsymmetrical about this maximum), it is found impossible to obtain a potential function which agrees tolerably well with *both* the ΔX and ΔY components at these stations.

The above results refer generally to all the months of the Polar Year, but some small though nevertheless significant differences were found between the results for the three "Lloyd" groups of months (*J*, *E*, and *D*). In particular, it appears that the line of maximum range of ΔH is not a fixed line but *varies in position with the season*, its movement being in the *direction opposite to that of the sun*. Its position is evidently associated with (though it does not exactly coincide with) the dividing line between the northern and southern current systems, its movement corresponding to the expansion of the summer system. The observatories are too widely spaced to afford an accurate determination of the extent of this movement, but it appears to reach a value of order 5° of latitude at some places.

The results also showed that the range of ΔH at equatorial stations is decidedly greatest during the *E*-months. This suggests an increased intensity of the ionospheric currents in low latitudes for these months. It is difficult to determine whether this is due to an over-all increase in the total current flow, or to a greater concentration of current near the equator, but an examination of the variations of the east-component in the latitudes of the foci of the northern and southern current systems suggests that there is some increase in the *total* current flow during the *E*-months.

The above discussion is based solely on data obtained during the Polar Year, but observational results for other epochs have been examined to check where possible the above conclusions. The observations made by A. Walter [5] in Uganda in 1941, and the recent observations made by L. Pontier [6] in Togoland, support the assumption that there is a large range of ΔH in these localities which is comparable with that at Huancayo. The method adopted by Pontier for reducing the Togoland results to a common epoch, based on the seasonal variations at Huancayo, appears to us, however, to be open to objection for reasons we have already indi-

cated. This, we feel, throws some doubt on the conclusion reached by Pontier that a decided maximum of ΔH is reached at the *magnetic* equator.

The results of other recent observations are not yet available, but the earlier result quoted by Egedal for Kodaikanal (10°.2 north, 77°.5 east) giving a mean range of 82.5 γ for ΔH derived from all days of September 1913 and September 1918, compared with an estimated range of 125 γ at Huancayo, is consistent with our assumption that the maximum range in this part of the world occurs to the south of both the magnetic and the dipole equators. The ranges given by Egedal for Batavia (52.3 γ) and Antipolo (49.5 γ) also tend to support our assumption that the line of maximum range passes about midway between them. On the other hand, our Figure suggests that Singapore (1° north, 104° east) should be practically on the line of maximum range, but Chapman has already pointed out that the observations made at this station in 1841-45 gave an average range in April (when it was greatest) of only 37 γ.

It appears, therefore, that there is as yet no positive evidence that large variations of H, comparable with those in South America and Africa, occur anywhere in the Far East or in the Pacific. The observations now being made, or about to be made, in these areas will therefore be of particularly great interest.

References

[1] S. K. Chakrabarty, Current Science, **15**, 246 (1946).
[2] J. Egedal, Terr. Mag., **52**, 449 (1947).
[3] S. Chapman, Terr. Mag., **53**, 247 (1948).
[4] D. F. Martyn, Letter in Nature, **163**, 685 (April 30, 1949).
[5] A. Walter, Preliminary results of a magnetic survey in Uganda Protectorate, February–March 1941.
[6] L. Pontier, Ann. Géophys., **6**, 238 (1950).

JOURNAL OF GEOPHYSICAL RESEARCH VOLUME 56, No. 2 JUNE, 1951

EVIDENCE FOR IONOSPHERE CURRENTS FROM ROCKET EXPERIMENTS NEAR THE GEOMAGNETIC EQUATOR*

BY S. FRED SINGER**

Applied Physics Laboratory, Johns Hopkins University, Silver Spring, Maryland

AND

E. MAPLE AND W. A. BOWEN, JR.***

Naval Ordnance Laboratory, White Oak, Maryland

(Received April 10, 1951)

ABSTRACT

Records of magnetic field as a function of altitude have been obtained from total-field magnetometers mounted in two Aerobee sounding rockets which were fired from the seaplane tender USS *Norton Sound* in March 1949. The flights were made 60 miles apart at approximately 89° west longitude, 11° south latitude, or geomagnetic longitude 341°, geomagnetic latitude −1°. The first rocket, Aerobee Round A-10, was fired on March 17 at $17^h\ 20^m$ 90th meridian time; Round A-11 was fired on March 22 at $11^h\ 20^m$ 90th meridian time. In Aerobee A-10 the field decreased between 20 and 105 km in accordance with the simple dipole field, while in Aerobee A-11 a discontinuity of 4 ± 0.5 milligauss was observed in the altitude range of 93 to 105 km.

These results (1) establish experimentally the existence of a current system in the *E*-region of the ionosphere which is responsible for the diurnal variation of the earth's magnetic field at sea level; and (2) lend strong support to the dynamo theory of the daily magnetic variation which was originally proposed by Balfour Stewart and Schuster.

INTRODUCTION

The discovery of a diurnal variation of the terrestrial magnetic field was one of the first observed instances of the magnetic influence of the upper atmosphere.

*Supported by the U. S. Navy Bureau of Ordnance and the Office of Naval Research.

**Now with the Office of Naval Research, London Branch, England.

***Now at the U. S. Navy Civil Engineering Research Laboratory, Port Hueneme, California.

It led to the investigation of the electrical properties of the atmosphere and to the discovery of ionized layers in the Breit-Tuve and Appleton experiments of 1925.

In 1889, harmonic analysis of the diurnal magnetic variation on a world-wide basis by Schuster showed that it could be represented as the field produced by a current system. Further analysis showed that the diurnal variation was due mainly

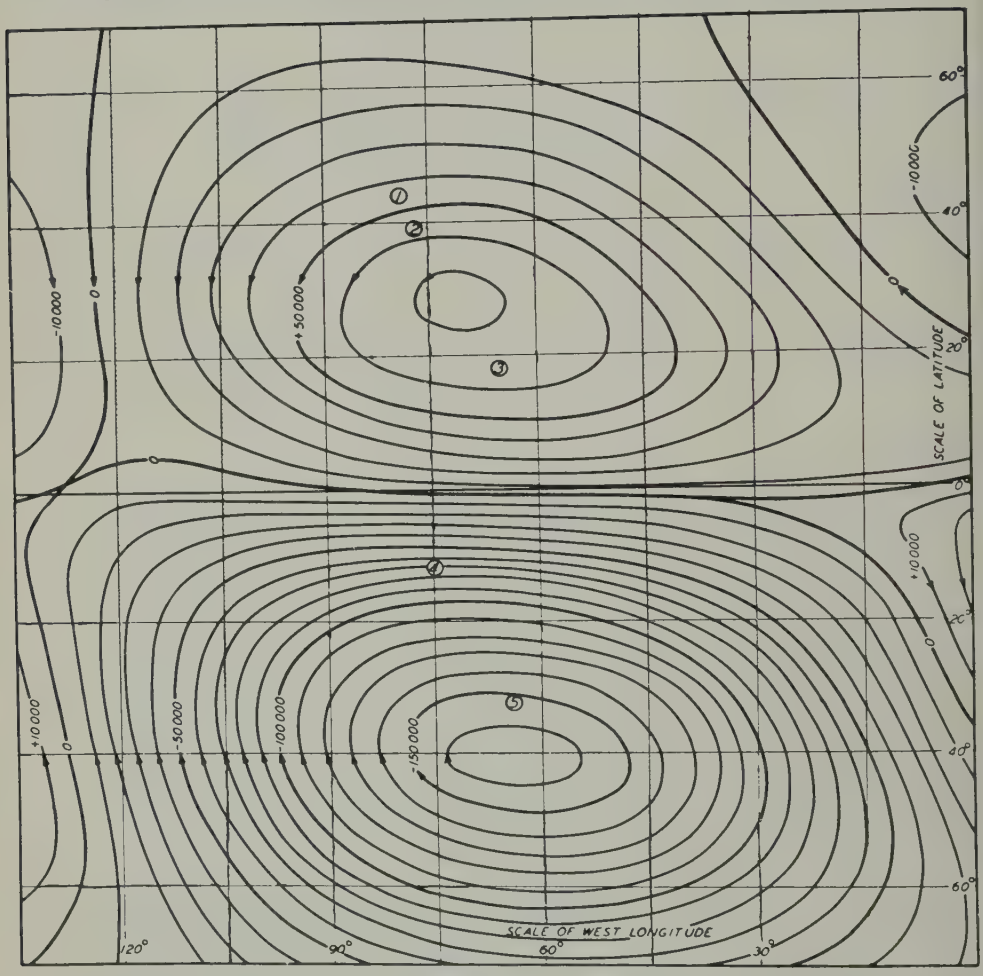

ISOMETRICS OF EXTERNAL CURRENT-FUNCTION, WESTERN HEMISPHERE
AMPERES AT 11h 75° WEST MERIDIAN MEAN TIME, INTERNATIONAL QUIET DAYS, EQUINOX 1923
DEDUCED FROM MAGNETIC DIURNAL-VARIATIONS AT AGINCOURT (1), CHELTENHAM (2), VIEQUES (3), HUANCAYO (4), AND PILAR (5)

FIG. 1—S_q CURRENT SYSTEM IN THE WESTERN HEMISPHERE (AFTER McNISH)

to an external source, presumably a current system in the upper atmosphere. This supposition, although never experimentally verified, has nevertheless been generally accepted. There has been no universal agreement, however, on the mechanism which produces this current system in the upper atmosphere. The first theory

proposed was that of Balfour Stewart—the so-called dynamo theory—which assumes that these currents are due to tidal and thermal motions of the upper atmosphere in the presence of the earth's magnetic field. Later theories have assumed that the diurnal variation is due to diamagnetic effects and drift currents in the upper layers of the ionosphere where the collision frequency is very small [see 1 of "References" at end of paper]. At our present state of knowledge concerning the ionosphere, the dynamo theory, which predicts a current system in the *E*-region, is the one which is most favored. It derives further support from the fact that magnetic disturbances are sometimes associated with radio fade-outs, which are due to an increase of ionization in the lower portions of the ionosphere (*D*-layer) [1].

It was hoped that a direct experiment which would measure the height of the current layer in the atmosphere would not only confirm its existence but also decide on the relative merits of the various theories proposed. In addition, it would determine the thickness of the layer and the variation of the current through the layer. The experiment would involve measuring the ambient magnetic field as a function of altitude by means of a rocket-borne magnetometer. A previous rocket flight at White Sands, New Mexico [2], had demonstrated the practicability of this method of investigation. That location was, however, unfavorable for detection of the current sheet with a total-field magnetometer which measures the magnitude of the ambient field without regard to direction.

The situation is much more favorable near Huancayo, Peru (longitude 75° west, latitude 12° south). The S_q-field is not only large there ($\sim$2 mG), but is also roughly parallel to the main field. This location was, therefore, the most favorable for use of a total-field magnetometer which would, under these conditions, measure the entire field of the current sheet through which it passed. An ionosphere current pattern which could account for the diurnal variations (S_q) observed at five magnetic observatories in the western hemisphere has been computed by McNish [1] and is reproduced in Figure 1. This pattern shows a large current density near the magnetic equator, which gives rise to a large magnetic field parallel to and enhancing the earth's main field in the region below the current.

Two rocket flights were made to obtain direct experimental evidence of these current sheets. Aerobee Round A-11 was launched at $11^h\ 20^m$ 90th meridian time, near the time of maximum expected current density, while Aerobee A-10, at $17^h\ 20^m$ 90th meridian time, was launched at a time when the current density was small. The expected results from the current sheet were, therefore, a decrease in field in addition to that due to the dipole field of the earth for the A-11 magnetometer as it passed through the current sheet, and little if any effect for the A-10 magnetometer.

INSTRUMENTATION

The instrumentation used for these flights, shown in Figure 2, has been discussed in detail in reference [2]. The NOL Aerobee Magnetometer (NAM), shown in Figure 3, is a total-field device which measures the magnitude of the magnetic field and is nearly independent of orientation with respect to the field. This type of instrumentation was chosen so as to make the magnetometer output independent of the roll and precession of the rocket during flight. However, a slight mismatching

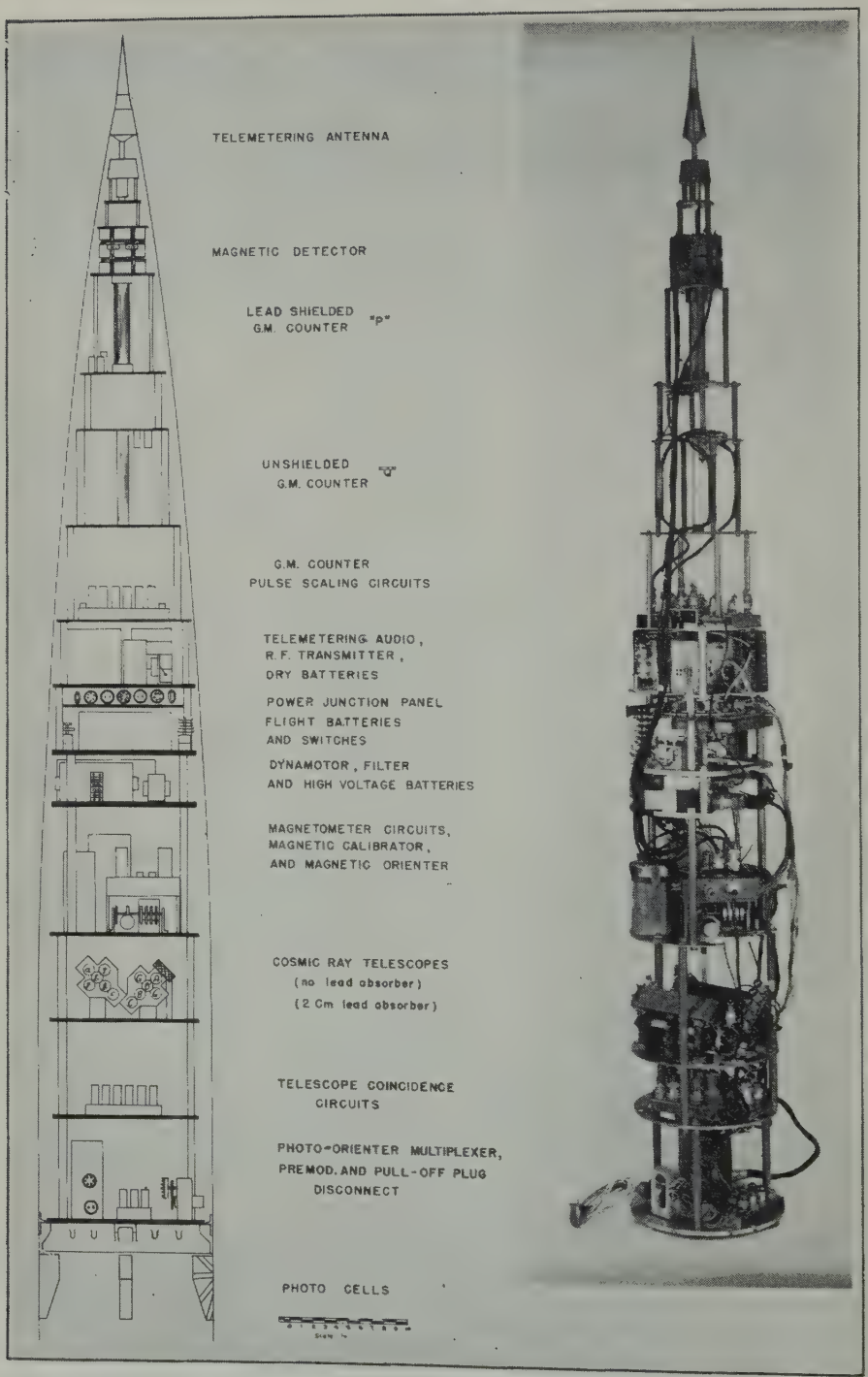

FIG. 2—INSTRUMENTATION OF AEROBEE A-11

of circuit elements is unavoidable and causes a small variation of output voltage as the magnetometer is rotated in a constant field. If its orientation is known, this variation may be corrected in analysis of the data. A total-field magnetometer was particularly suited for these flights because of its simplicity. A single com-

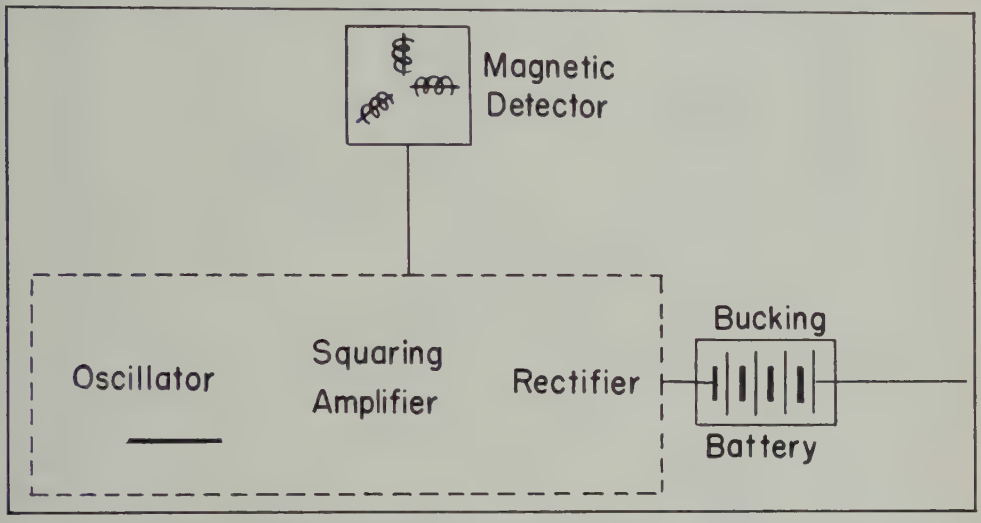

FIG. 3—BLOCK DIAGRAM OF NOL AEROBEE MAGNETOMETER

ponent detector would have required a very precise stabilization system and would not have essentially improved the precision of measurement, since the field discontinuity to be measured was parallel to the main magnetic field.

The magnetic field of the rocket itself was negligible. However, dynamotors in the rocket power supply produced a field of a few milligauss at the position of the magnetometer. These fields were compensated by winding three mutually perpendicular coils around the magnetic detector and adjusting the currents in the coils for best compensation when the power supply was energized. Two coils were also wound on the detector to supply calibration signals during flight. The zenith calibration coil had its axis parallel to that of the missile. At regular intervals a known current was applied, producing a known field H_t, first in a positive direction, immediately followed by a field H_t in a negative direction. The magnetometer then read the scalar value of the vector sum of H_t and the ambient field H, as shown in Figure 4. The cosine law gives two simultaneous equations which are used to compute the magnetometer sensitivity and the angle between the missile axis and the earth's field from the known values of the applied field and the recorded changes in magnetometer output. These computations furnish an over-all calibration of magnetometer, telemetering, and recording systems. The azimuthal calibration coil had its axis perpendicular to that of the rocket. A known field was applied immediately before the zenith calibration and served to define the angle of rotation of the missile. The rocket was also equipped with a photo-orienter system which indicated the aspect of the missile with respect to the sun. The combination of magnetometer and photo-orienter data completely define the space orientation of the missile.

IN-FLIGHT MAGNETIC CALIBRATION

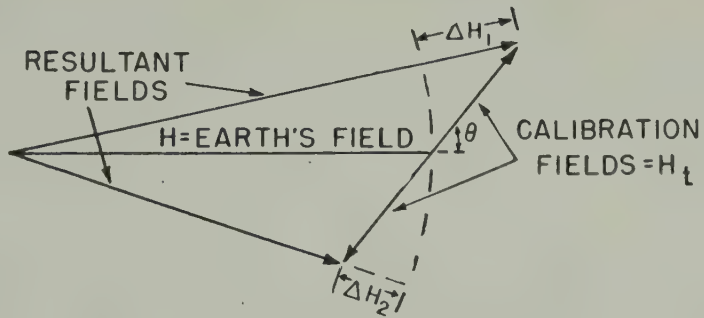

ΔH_1 AND ΔH_2, ARE QUANTITIES MEASURED

θ = ANGLE BETWEEN ROCKET AXIS AND EARTH'S MAGNETIC FIELD

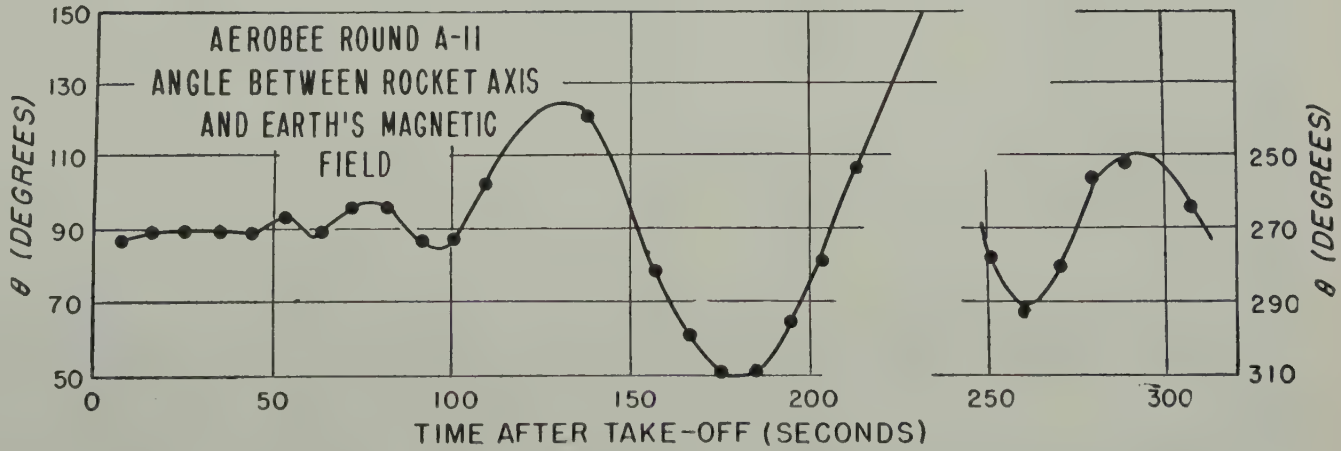

FIG. 4—MAGNETIC CALIBRATION METHOD AND ANGLE BETWEEN MISSILE AXIS (AEROBEE A-11) AND EARTH'S MAGNETIC FIELD, AS OBTAINED FROM IN-FLIGHT CALIBRATIONS

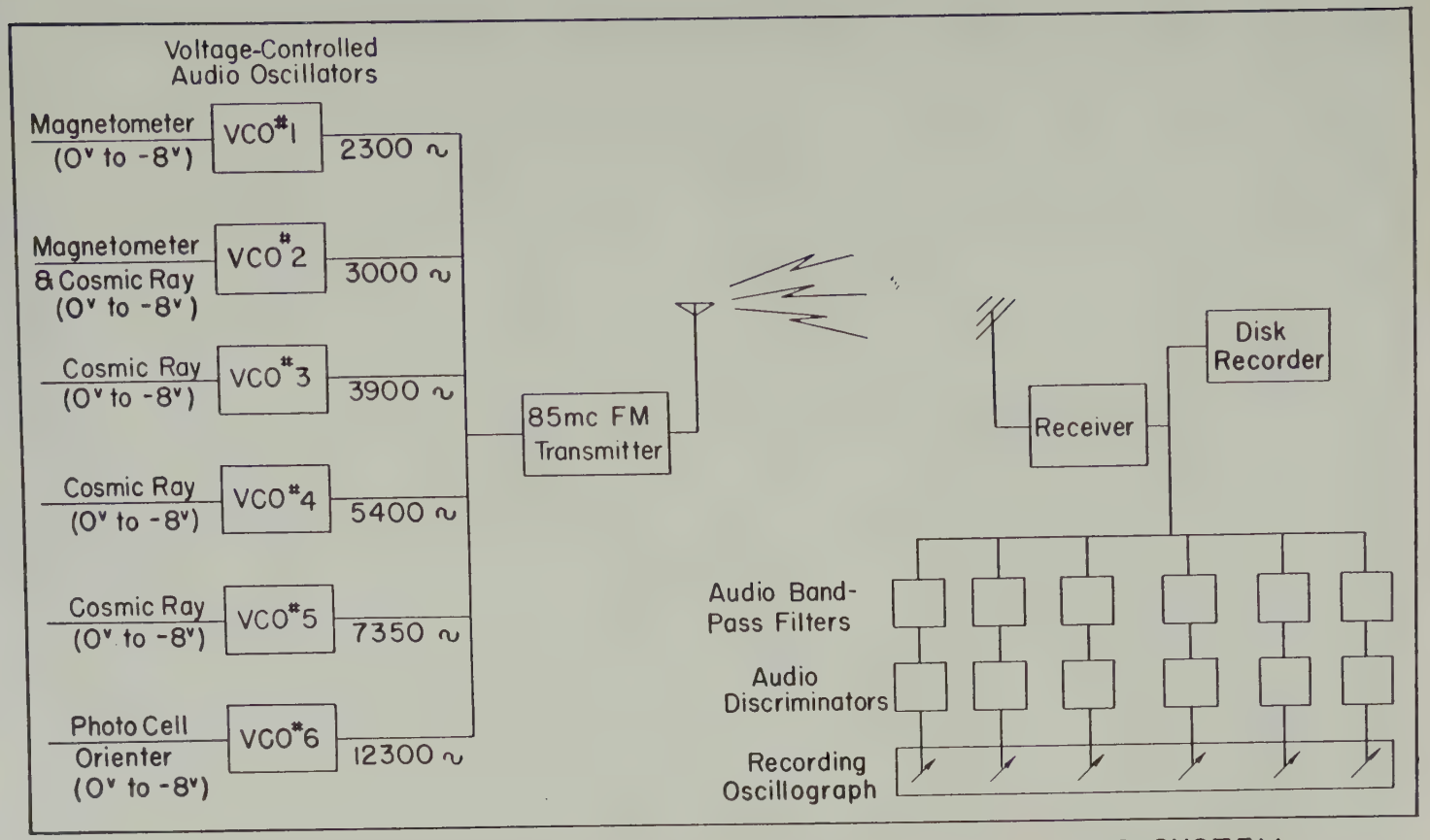

FIG. 5—BLOCK DIAGRAM OF APL AEROBEE TELEMETERING SYSTEM

The APL Aerobee telemetering system (Fig. 5) was used to transmit all intelligence from the rocket to the shipboard receiving stations. It is an FM/FM audio sub-carrier system. Variations in the D.C. output voltage of the magnetometer varied the audio frequency of voltage-controller oscillators (VCO), which in turn frequency-modulated the radio frequency carrier. The telemetered data were independently received and recorded at two stations located on two accompanying U. S. Navy destroyers. The composite audio signal was recorded on disks; at the same time it was passed through a set of audio filters and audio discriminators, after which the six channels were separately recorded on D.C. string oscillographs. In addition, optical and radar tracking was carried on from the destroyers.

FLIGHT HISTORY

Aerobee A-10 was fired at 17^h 20^m 90th meridian time, 17 March 1949, at 89° 14′ west longitude, 10° 48′ south latitude. The optical tracking to time of

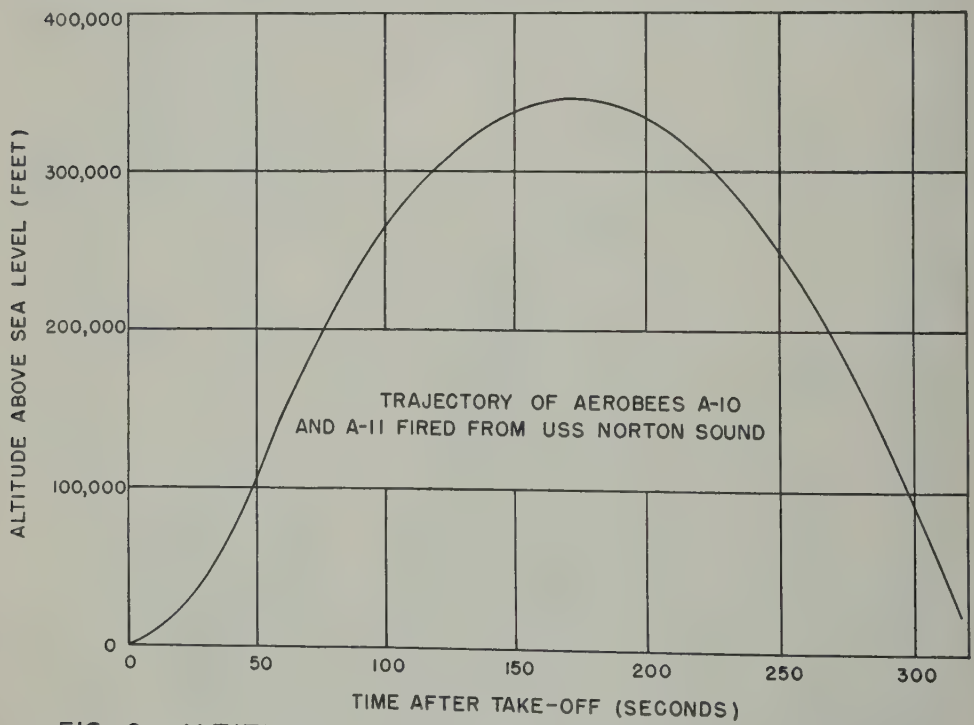

FIG. 6—ALTITUDE VS TIME PLOT OF AEROBEE ROUNDS A-10 AND A-11

burn-out and radar tracking were satisfactory. The calculated maximum altitude was 345,000 ± 5,000 feet. The estimated point of impact was 89,000 feet east and 53,000 feet south of the firing point.

Aerobee A-11 was launched at 11^h 20^m 90th meridian time on 22 March 1949 at 88° 26′ 30″ west longitude, 11° 06′ south latitude, about 60 miles southeast of

the A-10 launching site. The tracking data were unsatisfactory for this flight. The A-10 trajectory was used, since the two flights were quite similar as checked against both the magnetic and cosmic-ray data from the two flights. Two other trajectories with peaks three seconds before and three seconds after that for the A-10 flight were computed; a three-second variation in peak time corresponds to about a 10,000 foot change in peak altitude. Both of these trajectories were inconsistent with the cosmic-ray data and with the magnetic data. (The times of the cosmic-ray maxima on the upward and downward portions of flight must correspond to the same altitude, about 50,000 feet.) The peak altitude for the A-11 was, therefore, taken to be 345,000 ± 5,000 feet. The estimated point of impact was 45,000 feet south of the launching site. The altitude *vs.* time plot for the Aerobee Rounds A-10 and A-11 is shown in Figure 6.

METHOD OF ANALYSIS

The oscillograph data were reduced to a graph of magnetic field *vs.* time using the pre-flight calibration curves for the magnetometer, telemetering system, and ground recording equipment. The over-all sensitivity of the system (magnetometer, telemetering, and recording) was then computed from the in-flight calibrations and checked against the pre-flight calibration, and the reduced magnetic field data were corrected on the basis of the in-flight calibrations.

The same method of analysis of the reduced data has been used for both of the present flights and for the flight of reference [2]. It consists of correcting for the orientational and drift errors of the magnetometer. The ripple caused by the orientation error of the magnetometer and the spinning of the rocket is easily averaged out graphically. The ripple is approximately sinusoidal, the spin period being between one and two seconds. The magnetic field *vs.* time plot is next converted to a magnetic field *vs.* altitude curve by means of the time trajectory of the flight. A drift correction, linear with time, is then applied to make the data for the upward and downward portions of the flight agree, that is, give the same field reading for the same altitude. The matching is done for the upper third of the flight; in this region the effect of local surface anomalies is small, and the lateral motion of the rocket in flight would not cause an appreciable change in field between the upward and downward paths. Also, when the rocket reenters the denser atmosphere, it turns nose down (at approximately 250,000 feet), and after turn-over is subject to rather violent oscillations, which may cause physical damage; on the last portion of flight it is also subject to considerable heating due to air friction which may change the drift rate of the magnetometer. The final correction is made for the precession angle of the rocket, which is obtained from the in-flight magnetic calibrations. The angle between missile axis and earth's field for the A-11 flight is shown in Figure 4. Knowledge of missile aspect and magnetometer orientation error (that is, change in reading when rotated in a uniform field) permits correction of the precession error.

ANALYSIS OF THE A-10 FLIGHT

The chief purpose of the A-10 flight was to obtain cosmic-ray data. For this flight the magnetometer sensitivity was reduced so that its voltage output could

easily be kept within the limited input voltage range of the telemetering equipment. The drift correction required was 0.026 mG/sec. The precession correction was (2.5 cos θ) mG, where θ is the angle between rocket axis and earth's field. The magnetometer for this flight was not compensated for the permanent field due to other rocket instrumentation; the addition of the small error field (2.5 mG max.) to the earth's field (300 mG) causes a change of magnitude very nearly proportional to the cosine of the angle between the fields. The precession correction for this flight stayed at a small value (0.7 mG or less) for the upward flight and down to

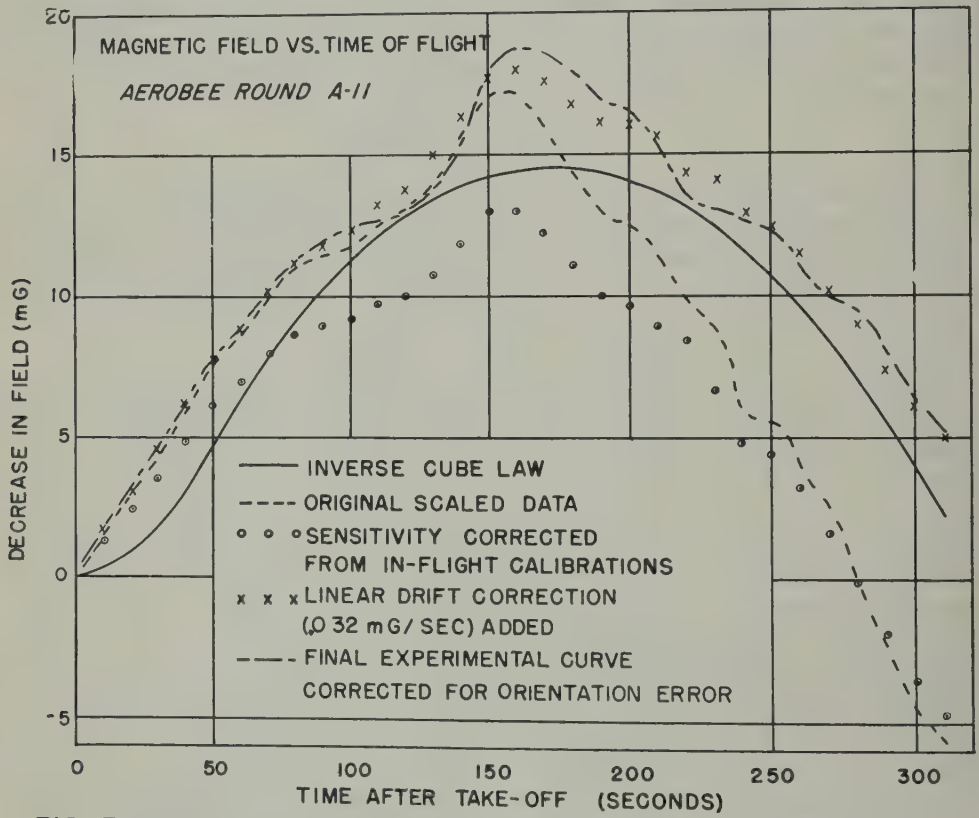

FIG. 7—MAGNETIC FIELD VS TIME PLOT SHOWING CORRECTIONS APPLIED TO THE ORIGINAL DATA

about 300,000 feet on the downward flight, θ being near 90°. At turn-over and afterwards the correction was somewhat larger.

ANALYSIS OF THE A-11 FLIGHT

The magnetic data were the chief objective of the A-11 flight, although cosmic-ray apparatus was also mounted in the rocket. The magnetometer was set at the highest sensitivity which would keep its output within the input voltage range (0 to −8 volts) of the telemetering equipment throughout the flight. An error in setting the voltage level, however, caused the voltage input to the VCO to go

positive early in the flight. The frequency of the resulting audio signal was out of range of the shipboard oscillograph recording equipment during most of the flight. The signal was, however, recorded on the wax disk (*cf.* Fig. 5). It was later possible to transfer the signal to an oscillograph record by playing back the disk at a reduced speed.

The in-flight calibrations showed a sensitivity considerably different from that obtained by extrapolation of the pre-flight calibrations. One of the contacts for the zenith calibration coil failed to operate, so that the calibration field was applied in one direction only. It was possible, by use of this signal and that of the azimuth calibration coil, to obtain values for the over-all sensitivity of the system and the aspect angle of the rocket (Fig. 4), although the accuracy was not quite as good as usual. The drift correction was 0.032 mG/sec.

In this flight the magnetometer was compensated for the fields of the other instrumentation in the rocket. The residual orientation error was that due to the magnetometer itself, which is a cos $(2\theta - 90°)$ function, θ being the angle between the rocket axis and the earth's field. The maximum correction for this precession error was ± 1 mG. The magnetic field *vs.* time plots at various stages of this analysis are shown in Figure 7.

RESULTS

The magnetic field *vs.* altitude curves for the A-10 and A-11 flights are shown in Figures 8 and 9. The solid curves show the decrease in field calculated from the inverse cube law for a centered dipole representing the earth's main field. The squares at altitudes of 0 and 100 km above sea level indicate values interpolated from the results of spherical harmonic analysis of the earth's field [3]. The experimental data are indicated by points, while the departure of the dashed curves from the inverse cube law indicates fields which can be accounted for by *assumed* dipole surface anomalies. This represents the simplest explanation of the deviation at low altitudes. No information about local anomalies in this region, other than that obtained from the present flights, is available. However, calculations assuming simple dipole anomalies show that, for a total field magnetometer, these results are reasonable and are consistent with anomalies observed on aerial surveys in other parts of the Pacific [4]. The calculations indicate that different sources are required for the two flights. The Navy Hydrographic Office charts show a "high" in the ocean bottom near the flight locations, which would indicate a possible local anomaly.

The A-10 experimental curve, representing conditions at $17^h\ 20^m$ when the ionospheric currents are small, shows the same rate of change as the computed dipole curve above 30 km. The accuracy of the total recorded decrease in field for the A-10 flight is estimated at ± 1 mG.

The A-11 experimental curve, for a 90th meridian time of $11^h\ 20^m$, when the diurnal variation of the earth's field is near a maximum and large currents are flowing in the ionosphere, shows a rather sharp upward break at 93 km. The shape of the curve above this point could not be accounted for by sources within the earth. The decrease in field between 93 and 105 km is attributed to the passage of the rocket through a current layer in the ionosphere. The rocket may not have

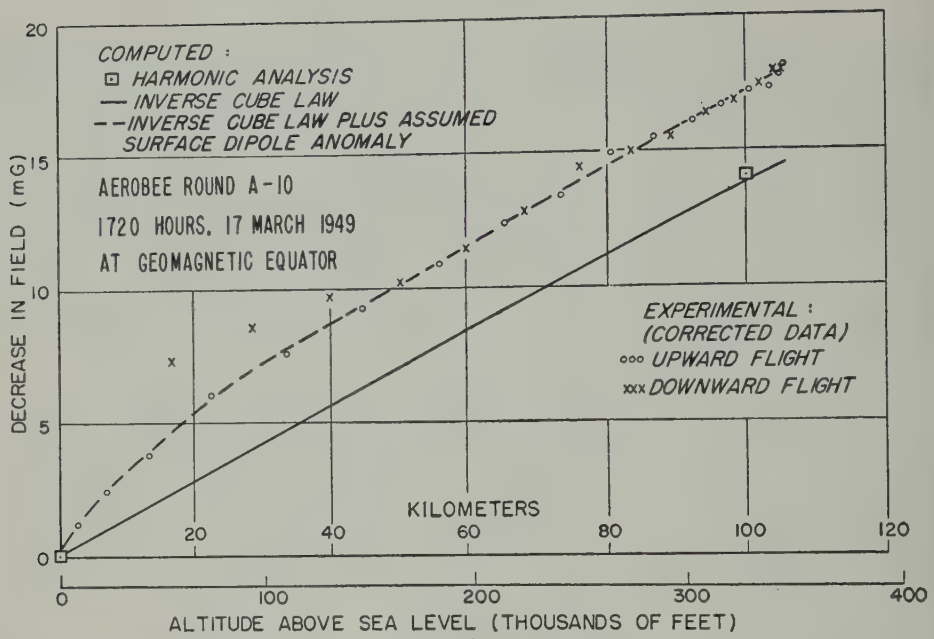

FIG. 8—DECREASE OF EARTH'S MAGNETIC FIELD (FROM ACTUAL FIELD AT SEA LEVEL) VS ALTITUDE ABOVE SEA LEVEL FOR AEROBEE A-10 FLIGHT

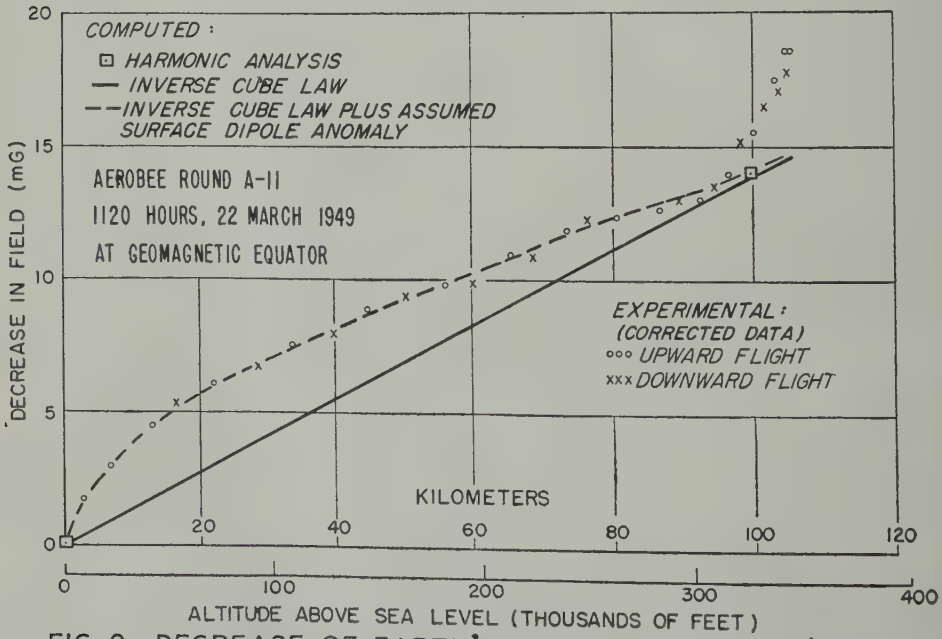

FIG. 9—DECREASE OF EARTH'S MAGNETIC FIELD (FROM ACTUAL FIELD AT SEA LEVEL) VS ALTITUDE ABOVE SEA LEVEL FOR AEROBEE A-11 FLIGHT

passed completely through the layer, since the slope of the curve did not again drop to that of the computed dipole curve. The accuracy of the total decrease in field up to 93 km is estimated at ± 1.5 mG, while the decrease of field in the region between 93 and 105 km is estimated at 4 ± 0.5 mG. The possible error in sensitivity is greatest in this region, and, as shown in Figure 4, the aspect of the missile relative to the earth's field was changing rapidly near the peak of the flight (at 172 seconds). The orientation correction increased the apparent value of the magnetic field discontinuity in this region; this correction also altered the shape of the curve to bring the upward-flight and downward-flight data into better agreement. It is apparent from Figure 7 that the sum of the various corrections had no great influence on either the altitude or the magnitude of the discontinuity.

SEA-LEVEL OBSERVATIONS

According to information furnished by the Central Propagation Laboratory of the National Bureau of Standards, no unusual ionospheric or related phenomena occurred on the firing days. World-wide magnetic observations, however, indicate that both days were magnetically disturbed, but that conditions were less disturbed toward the magnetic equator. The magnetic *C*-indices for March 17 and 22 were 1.4 and 1.8, respectively.

An examination of field intensity recordings made at Huancayo, Peru, on a number of frequencies for different transmission paths revealed no unusual effects. Also, no sudden ionosphere disturbances or unusual solar effects were observed on the two days. The only ionosphere station near enough to the location of the rocket firings for the records to to be of assistance is that at Huancayo. A careful examination of the Huancayo ionosphere records revealed no unusual effects at the times of interest. Unfortunately, the Huancayo equipment does not give as good detail as do modern ionosphere equipments. Also, it is not possible to make reliable *E*-region virtual height measurements on these records.

The diurnal variations of *H*, the horizontal component of the earth's field, recorded at the magnetic observatory at Huancayo, Peru, for the days of the flights are shown in Figure 10. These data were furnished through the Instituto Geofísico de Huancayo. A magnetic storm was in progress during the week of the rocket firings, and the traces are unusually low and very irregular.

The reference times for the rocket flights are shown at $17^h\ 20^m$, 17 March, and $11^h\ 20^m$ hours, 22 March, on the Huancayo (75th meridian) time-scale. The flights occurred at the same hours 90th meridian time. These reference times would be valid for quiet days when smooth diurnal-variation curves would be obtained. Under quiet conditions it would be expected that surface measurements at the site of the flights would produce approximately the same curves when plotted for 90th meridian time.

For the present flights, with a magnetic storm in progress, correlation with the magnetograms is more doubtful. It is questionable whether the same short-time variations recorded at Huancayo (due, perhaps, to local conditions in the ionosphere) would appear at the site of the flights, about 1,000 miles away. If the short-time variations are correlated, however, they would appear at the same instant at both locations; that is, the short-time variations to be considered for the flights

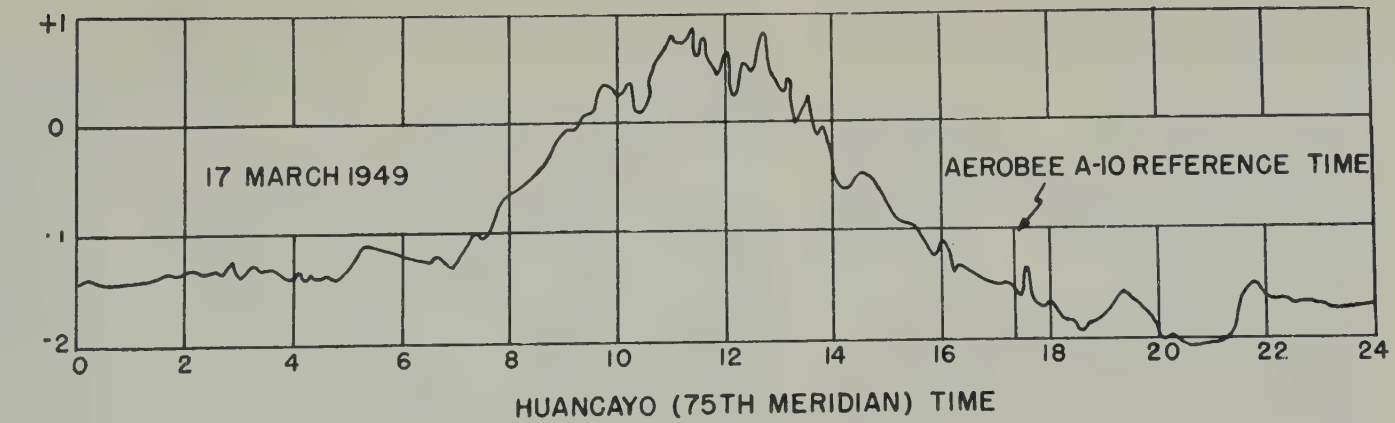

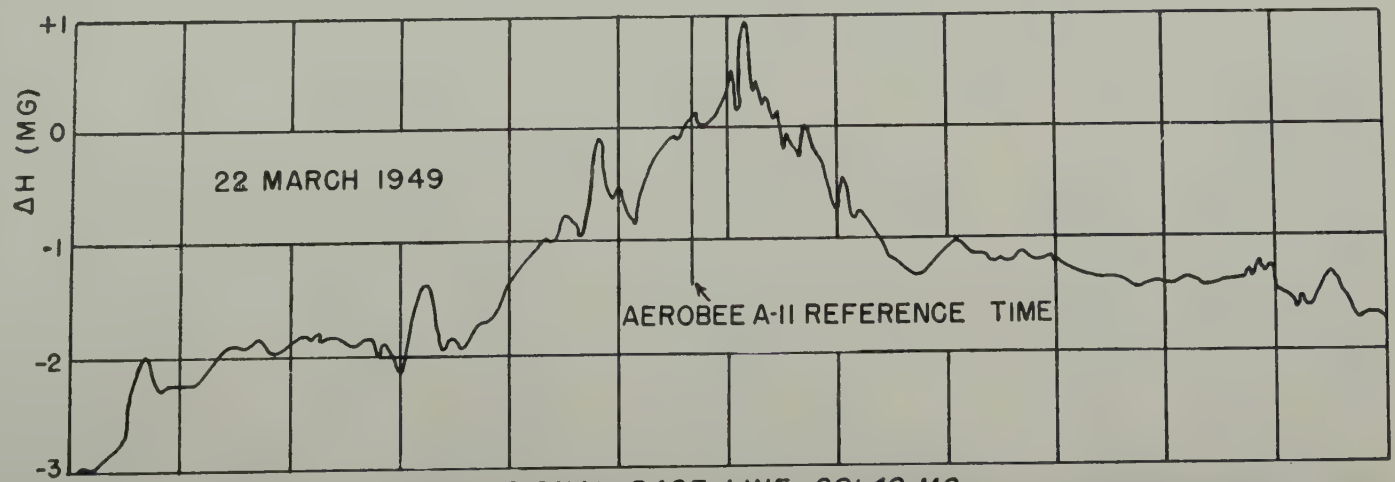

FIG. 10—MAGNETOGRAMS OF THE HUANCAYO MAGNETIC OBSERVATORY

would be those appearing one hour later on the Huancayo time-scale than the reference times shown.

The best approximation seems to be to take the height of a smooth curve drawn through the magnetogram as representative of the strength of the ionosphere currents at the times of the flights. This value is itself in doubt, since there is no very definite value on these days for the lower limit of the diurnal-variation curves.

The best base-line for these measurements is still under consideration. The averaging techniques used to determine storm-time curves yield fairly smooth base-lines; however, these lines are displaced upward by the average value of the diurnal variation, and the average values to be subtracted are uncertain for these disturbed days.

The height of the magnetogram at $17^h\ 20^m$ 75th meridian time for 17 March 1949, the date of the A-10 flight, is very near the "average minimum" value for the 24-hour period. The experimental curve for the A-10 flight shows no evidence of a current layer in the altitude range covered.

On March 22, the day of the Aerobee A-11 flight, the maximum on the magnetogram occurred at $12^h\ 20^m$ 75th meridian time, considerably later than on quiet days. The height of the curve at $11^h\ 20^m$ is about 1.7 mG above the "average minimum" value for the day. The flight actually occurred during the brief increase of 0.5 mG at $12^h\ 20^m$ 75th meridian time; this may indicate that the value of 1.7 mG should be increased somewhat.

DISCUSSION

The following considerations affect the results which might be predicted for the A-11 flight from surface measurements:

(1) Harmonic analysis of the records from a number of observatories has indicated that about two-thirds to three-quarters of the diurnal variation is caused by external sources, the remainder being produced by sources inside the earth. However, the effect of the ocean-land boundary near Huancayo would be to decrease the contribution of the internal sources to the variation of the north component of field.*

(2) The ionospheric current pattern is not an infinite sheet. Computations indicate that, at Huancayo, the north component of field produced by the pattern of Figure 1 would be about 10 per cent larger just below the current than at the earth's surface. The calculation of such a pattern for the entire hemisphere involves a great deal of smoothing and cannot include rapid local variations. It is probable that the actual pattern has a larger local concentration of current than that indicated; this would cause a greater discrepancy between the field at the surface and that just below the currents.

(3) Since the flight location was about 1,000 miles from Huancayo, the

*In general, the internal sources are assumed to be currents induced in a conducting spherical shell within the earth, of approximately the same pattern but of opposite polarity. However, the South Pacific (average depth 5,000 feet) forms a good conducting layer, and part of the currents are induced in the ocean. At midday near the South Atlantic coast, the currents in the ocean would close along the coast, and the currents in the earth would also be distorted.

diurnal variation at the surface might be different there. There is no apparent reason, however, for assuming that it would be larger at the flight location.

(4) Magnetic conditions were disturbed on the day of the A-11 flight. A short-time increase in field of 0.5 mG at the time of the flight is shown on the Huancayo magnetogram. This increase may have also occurred at the flight location and may have been even larger there.

Items (1) and (2) above indicate that the discontinuity on passing through the current layer would be between 3 and 3.5 mG.* Consideration of item (4) would increase this figure. If the 0.5 mG increase at Huancayo is assumed to apply to the flight location, the figure would be increased to about 4 mG.

The magnetic field discontinuity of 4 ± 0.5 mG obtained in the A-11 flight seems rather large, since there is no evidence that the current layer was completely surmounted. To provide agreement between the flight results and the sea-level observations, it must be assumed that one or more of the following factors is involved:

(1) The accuracy of measurement indicated is based on the consistency of the in-flight calibrations for the A-11 flight and on experience gained from the other two flights. It is possible, although it does not seem probable, that a greater error occurred.

(2) A larger local short-time variation than that indicated on the Huancayo magnetogram might have occurred at the flight location.

(3) The rocket did penetrate practically all of the current layer, and, therefore, the current density decreases rapidly above 105 km.

The latter assumption would indicate a rapid decrease in the conductivity of the ionosphere. To provide the conductivity required by the dynamo theory, the *E*-region, or at least the lower portion of the region, must be predominantly ionic. If this were true throughout the region, the decrease of conductivity as the mean free path of the ions increases with altitude would not be sufficiently rapid. The data of the A-11 flight could be interpreted more reasonably, however, if a rapid transition from ionic to electronic ionization occurred above 105 km.

The features of the A-11 curve (Fig. 9) below 90 km have been interpreted in terms of an assumed surface anomaly. At our present state of knowledge of the lower regions of the ionosphere, an interpretation in terms of a current does not appear justified.

CONCLUSIONS

The results obtained from these flights substantiate the predictions of the dynamo theory. The present data establish the existence of a current layer in the *E*-region of the ionosphere but are insufficient for detailed conclusions. The observed decrease in field on the A-11 flight attributed to penetration of the rocket into the ionosphere current layer is 4 ± 0.5 mG in the altitude range of 93 to 105

*Assuming that 80 per cent of the surface variation is due to external currents and that the field of these currents is 15 or 20 per cent larger just below the currents than at the surface.

km. Since the rocket may not have passed completely through the layer, the observed effect in the altitude range covered seems rather large when compared with surface measurements. This result implies that a very small part of the current flows at altitudes higher than 105 km; however, it may be the result of the disturbed magnetic conditions on the day of firing. It is hoped that additional flights which penetrate the entire current layer will help to clear up this question.

ACKNOWLEDGMENTS

This work was made possible by the support of the U. S. Navy Bureau of Ordnance which sponsored the development of the Aerobee sounding rocket under contract NOrd 7386 and the development of the magnetometer at the NOL and the Bell Telephone Laboratories under contracts NOrd 632 and 7541. The work at the NOL on these flights was done under the Office of Naval Research contract NR-081-017. The Aerobee was developed and built by the Aerojet Engineering Corporation and the Douglas Aircraft Company, under the technical direction of APL/JHU. We are indebted to Captain T. A. Ahroon, USN, and the other officers and men of the USS *Norton Sound* who were responsible for the conduct of the expedition and the rocket firings. The Physical Science Laboratory of the New Mexico College of Agriculture and Mechanic Arts has carried a major share of the technical field-work for the Aerobee in the conduct of pre-flight telemetering tests, flight telemetering, and in the reduction of the telemetered data.

We are greatly indebted to Dr. E. H. Vestine, of the Department of Terrestrial Magnetism, Carnegie Institution of Washington, for helpful advice on problems relating to the geomagnetic field; to Mr. A. Giesecke, Jr., Director of the Huancayo Geophysical Institute; and to Mr. S. M. Ostrow, of the Central Radio Propagation Laboratory, National Bureau of Standards.

Finally, we would like to express our appreciation to Dr. J. A. Van Allen and Mr. L. R. Alldredge for their active encouragement of this project; to our associates at the Naval Ordnance Laboratory, in particular to Dr. E. A. Schuchard for much helpful advice on magnetometer problems, and to Mr. C. J. Aronson; and at the Applied Physics Laboratory to Messrs. L. W. Fraser and A. V. Gangnes.

References

[1] For a comprehensive discussion of problems of the geomagnetic field and the upper atmosphere, see Terrestrial Magnetism and Electricity, edited by J. A. Fleming, McGraw-Hill Book Company, Inc., New York (1939); Geomagnetism, by S. Chapman and J. Bartels, Oxford, Clarendon Press (1940); and The Upper Atmosphere, by S. K. Mitra, Calcutta, R. Asiatic Soc. of Bengal (1947).

[2] S. F. Singer, E. Maple, and W. A. Bowen, Jr., Phys. Rev., **77**, 398 (1950); and E. Maple, W. A. Bowen, and S. F. Singer, J. Geophys. Res., **55**, 115 (1950).

[3] E. H. Vestine, I. Lange, L. Laporte, and W. E. Scott, The Geomagnetic Field, Its Description and Analysis, Dept. Terr. Mag., Carnegie Inst. Washington, D. C., Pub. 580 (1947).

[4] L. R. Alldredge and F. Keller, Jr., Trans. Amer. Geophys. Union, **30**, 494 (1949).

INTERNATIONAL DATA ON MAGNETIC DISTURBANCES, FOURTH QUARTER, 1950

Preliminary report on sudden commencements

S.c.'s given by five or more stations are in italics. Times given are mean values, with special weight on data from quick-run records.

1950 October 01d 09h 29m: Es.—01d 12h 39m: Va.—03d 19h 15m: Tl SF El.—04d 18h 06m: Tl.—04d 19h 11m: Do.—05d 18h 26m: Do.—05d 20h 52m: Tl.—06d 17h 12m: El.—06d 22h 27m: El.—09d 11h 50m: El.—10d 22h 58m: Wn.—11d 19h 15m: El.—12d 18h 00m: Wn.—13d 02h 24m: Tl.—14d 02h 38m: Sw Ap Am.—14d 20h 12m: Do.—16d 06h 00m: Sw.—17d 06h 27m: Sw.—17d 21h 11m: Tl El.—17d 21h 26m: El.—20d 18h 07m: Wn.—20d 19h 19m: Wn.—20d 22h 17m: Wn.—21d 20h 02m: So.—22d 21h 19m: So Sw Wn El.—23d 00h 16m: El.—23d 04h 23m: El.—23d 21h 48m: Wn.—24d 21h 02m: Wn.—25d 22h 35m: Wn.—26d 01h 18m: Am.—26d 02h 25m: Am.—26d 18h 06m: So.—28d 01h 09m: Ap.—28d 12h 08m: Tl, Do.—28d 12h 56m: Tl.—28d 19h 07m: Tl.

1950 November 01d 05h 30m: Sw.—*01d 18h 34m:* Wn Ma CF Tl El.—04d 16h 35m: El.—05d 20h 37m: Wn.—09d 08h 51m: Hr.—10d 07h 00m: Sw.—11d 19h 18m: Wn.—11d 21h 01m: Wn.—12d 19h 43m: Wn.—12d 22h 13m: Wn El.—13d 15h 04m: Tl.—14d 19h 47m: So Wn.—15d 06h 45m: Am.—16d 18h 50m: El.—21d 20h 35m: So Wn.—21d 22h 09m: Tl El.—22d 12h 07m: El Hr.—22d 15h 02m: Ma.—22d 18h 44m: Tl Te El Hr.—22d 21h 58m: Do Wn.—23d 21h 48m: Wn.—24d 17h 04m: Wi Ma.—25d 00h 37m: Tl El.—26d 03h 45m: So.—26d 08h 32m: Si.—26d 18h 57m: Wn.—27d 21h 25m: Tl.—28d 13h 52m: Tl.—*28d 19h 31m:* eight.—29d 20h 43m: Wn Tl.

1950 December 02d 15h 20m: Pi SJ.—02d 16h 05m: Wn.—03d 20h 48m: So Wn.—07d 01h 52m: Wn.—07d 18h 06m: So Wn.—07d 22h 20m: Wn.—10d 20h 23m: So Wn Fu.—*12d 05h 26m:* thirty.—13d 17h 48m: Wn.—13d 18h 07m: Fu SF.—13d 22h 47m: Wn.—14d 05h 41m: Am To.—14d 16h 29m: Wn Ma.—14d 18h 17m: So.—14d 18h 55m: Sw Fu Tl.—15d 10h 31m: Tl.—18d 10h 00m: Te.—18d 18h 17m: Wn.—18d 18h 45m: Sw Fu.—19d 00h 01m: Wn.—19d 17h 25m: Fu.—20d 22h 26m: Wn Fu Tl.—21d 20h 33m: Wn.—22d 11h 15m: Te.—23d 00h 20m: Tl Ap.—24d 15h 15m: Fu.—27d 19h 59m: So Wn.—29d 23h 54m: Wn Ma Tl.—30d 20h 47m: Wn.

Preliminary report on solar-flare effects

Effects confirmed by ionospheric or solar observations are in italics.

1950 October 09d 15h 22m-16h 16m: Tu.—10d 11h 33m: Do.—*11d 17h 17m:* Hu.—*11d 17h 30m:* Hu.—12d 18h 27m: Pi.—17d 21h 14m: Pi.—18d 05h 48m-56m: Eb.—19d 21h 39m-48m: Tu.—23d 04h 23m-33m: Eb.—23d 13h 13m: Va.—23d 13 h 33m: Va.—27d 01h 07m-21m: ZS.—27d 06h 02m-12m: Tu.—28d 06h 26m-36m: Eb.

1950 November 01d 18h 29m-59m: Eb.—05d 15h 19m-33m: Tl Tu.—06d 16h 03m-17m: Tu.—10d 12h 25m-30m: Eb.—15d 06h 45m-07h 00m: Hr.—15d 08h

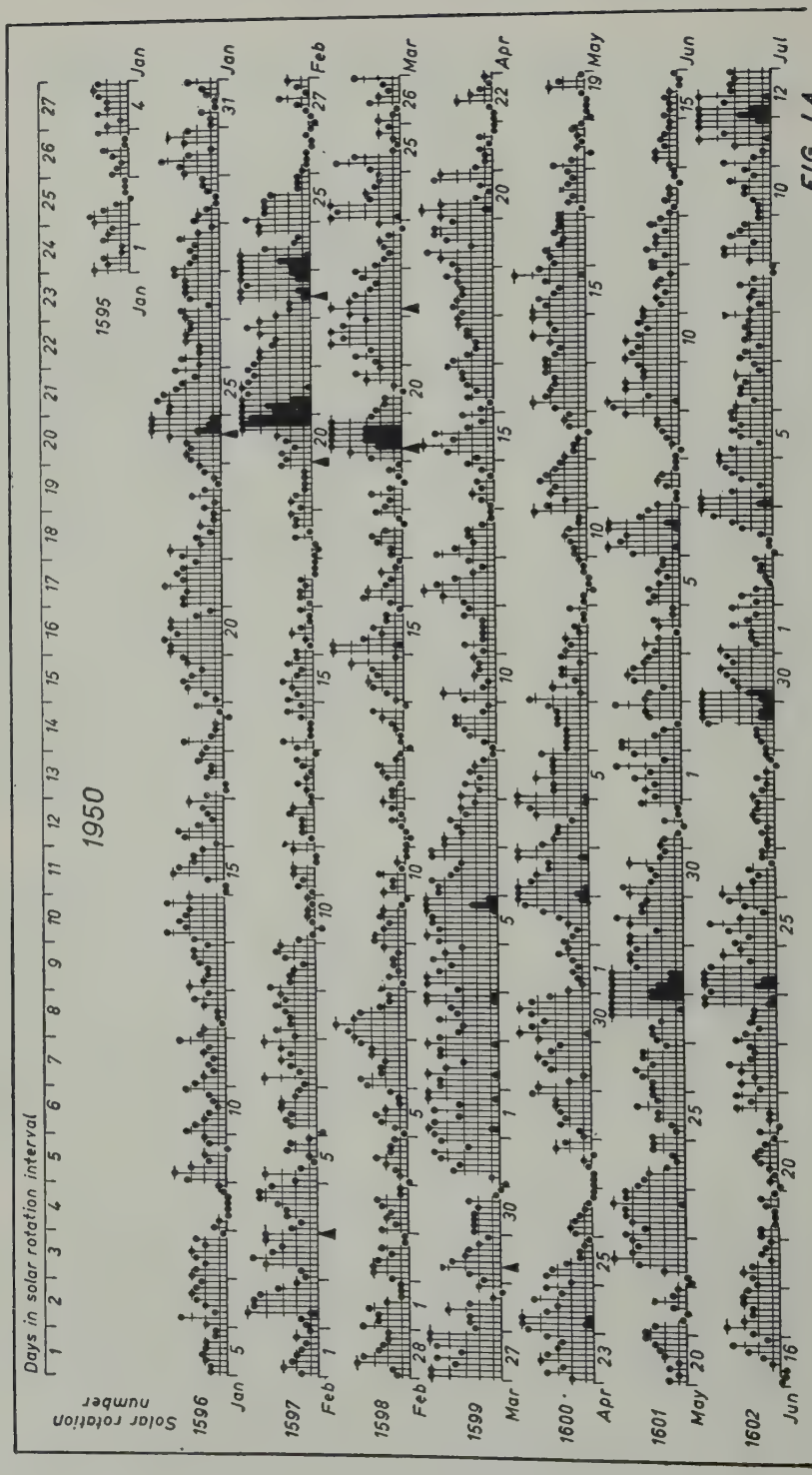

Planetary magnetic three-hour-range indices Kp for the year 1950

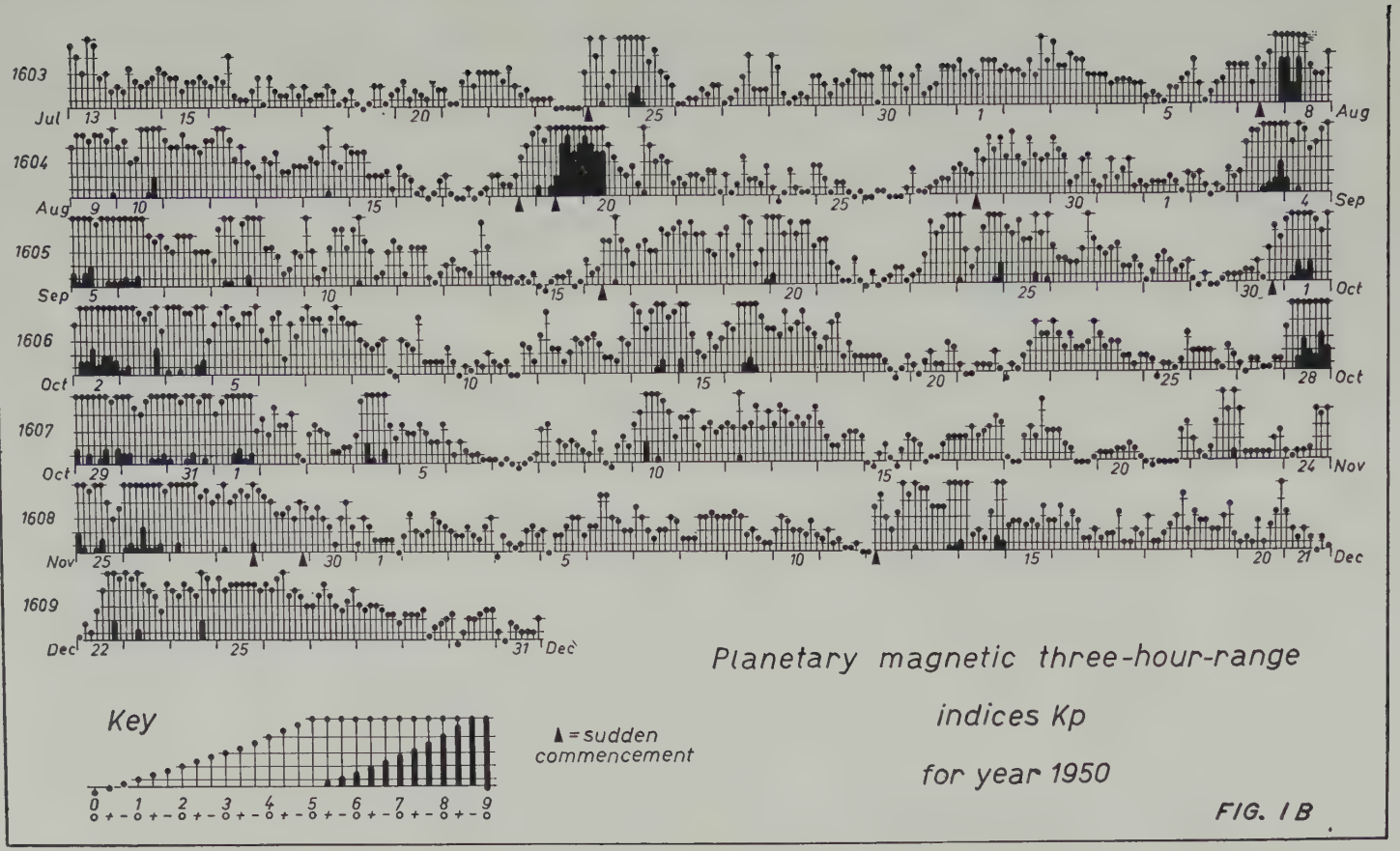
1603
Jul 13 15 20 25 30 1 5 8 Aug
1604
Aug 9 10 15 20 25 30 1 4 Sep
1605
Sep 5 10 15 20 25 30 1 Oct
1606
Oct 2 5 10 15 20 25 28 Oct
1607
Oct 29 31 1 5 10 15 20 24 Nov
1608
Nov 25 30 1 5 10 15 20 21 Dec
1609
Dec 22 25 31 Dec
Key
0 + - 1 + - 2 + - 3 + - 4 + - 5 + - 6 + - 7 + - 8 + - 9
▲ = sudden commencement
Planetary magnetic three-hour-range indices Kp for year 1950

FIG. 1B

Geomagnetic planetary three-hour-range indices Kp, preliminary magnetic character-figures, and final selected days, October to December, 1950

October 1950									
E	1	2	3	4	5	6	7	8	Sum
1	5 −	5 +	6 +	6 −	6 +	5 −	4o	5o	42o
2	4o	6o	6o	7 −	6 −	6 +	6 +	6o	47o
3	5 +	6 −	5o	5 −	4 +	5 −	7 −	4 −	40o
4	5 +	5o	5 +	5 −	5 −	6 −	6o	3o	40 −
5	4o	5 −	5o	4 +	4o	5 −	5 −	5o	36 +
6	4 −	3o	4 +	5 −	2 −	4o	3 +	4 +	29o
7	5o	4 +	4 +	4 −	4 +	5o	4 +	4o	35o
8	4o	3o	3 −	2 +	3 −	3o	1 −	0 +	19 −
9	3o	3 −	2 +	4 +	1 +	1 +	1 +	1 +	18 −
10	2 +	1 +	0 +	1o	1 −	1 +	1o	2o	10o
11	1 +	1o	1 +	0 +	0 +	3 −	2 +	1 +	11 −
12	3 +	5 −	2 +	2 +	1 +	2o	3o	3 −	22 −
13	3o	3 +	3 −	2 −	2 −	1 +	3o	3 −	19 +
14	5o	5 −	4 −	5 −	5 +	6o	4 +	5 −	38 +
15	6o	5o	3 +	2o	2 −	3 +	2 +	3o	27 −
16	4o	4 −	5o	6 −	6o	5 +	4 +	4 −	38 −
17	4 −	3 +	5 −	4 −	4o	5 −	4 −	3 +	31o
18	2 +	3o	4o	4 +	2 −	3 −	2 −	2 −	21 +
19	2 −	2 −	2 −	1 +	1 −	0o	1 −	2 −	9 +
20	1o	0 +	1 +	2o	1o	1o	3 −	2 +	12 −
21	1o	0 +	0 +	1o	1o	1o	2o	1 −	7 +
22	0o	1o	1 −	2 −	3 −	4o	3 +	3 +	17 −
23	4o	3 +	2 +	3 +	2 +	2 +	3 −	4o	24 +
24	3 +	2 +	3 −	3 −	2 −	2 −	1o	2 −	17o
25	2 −	1 +	0o	1o	1o	1 −	1 +	3 +	10 +
26	2o	2o	2o	2o	1o	1 −	2 +	2 −	14 −
27	1o	0 +	1 +	1 +	1 −	1 −	1 +	1 +	8o
28	4 −	5o	6o	7o	6 +	6o	7 +	7 −	48o
29	6o	5o	6 −	5o	5 +	6o	5 −	6o	44 −
30	6 −	6 −	4 +	4o	5 −	5 +	5 +	6 −	41 −
31	5 +	5o	5 −	5 +	6 −	5 −	5 +	5o	41o

November 1950									
1	2	3	4	5	6	7	8	Sum
4o	5 −	5o	6 −	6o	5 +	6 −	3o	39 +
4 −	3 −	4 +	3 +	3 +	4o	1o	1 −	23o
3 −	3 +	3o	3 −	1 +	1 +	2 −	2 −	18 −
3 −	5 −	6 +	5 +	5o	6o	3 +	2 +	36 −
3 +	3 −	3 −	3 +	3 −	2o	2o	3 +	22o
2o	1o	2o	1 +	1o	1o	1 −	1 −	10 −
1 −	0 +	1 −	0 +	0o	0 +	1 −	1o	4o
3o	3 +	0 +	2o	2 −	2o	2 −	1 +	15 +
1o	3 −	1 +	0 +	0o	2 −	2 +	2 −	11o
3 +	4o	6 +	5o	5 +	5 −	4o	2 +	35o
4 −	4 −	4o	2 −	3o	3 +	3 −	3o	25o
3 +	3o	5 +	3o	3 +	4 +	3o	4o	29 +
3 +	4 +	4o	3 +	4 −	3 +	4 −	4 +	30o
3 +	2 +	2 −	2 −	2 +	3 −	3 −	2 +	19o
0 +	0o	1o	2 −	1 −	0o	1 +	2 +	7 +
2o	2 −	0 +	1 −	1 −	2 −	2 +	2 +	12 −
2 +	2 +	3o	2 +	3 −	3o	4 −	3 +	23 −
1 −	0 +	0 +	2 +	3o	2 +	5 −	3 −	16 +
3 −	3 −	2 −	1 +	0 +	0 +	0 +	1 −	10o
1o	1o	1o	1 +	1 +	2 −	1 +	1 −	9 +
0 +	0o	0 +	0 +	0 +	0 +	3 −	3 +	8 −
2o	1o	1 −	1 +	3 +	5o	4o	6 −	23o
4o	1o	1o	1o	1o	1o	2o	3 −	14 −
1o	1 −	1o	1o	1 +	4o	4 −	4o	17 −
6 +	5 +	5 −	5 +	6o	4o	3o	4 −	38 +
5 +	6 −	5 +	7 −	5 +	5 +	6 −	5 −	44o
5o	6 −	5o	5o	5o	4 +	5 −	4o	39 −
4 +	5 +	4o	4 +	5 −	4 +	6 −	5 −	37 +
4 +	4o	3 +	3 +	4 −	3o	4o	4 −	29 +
3o	4 −	3o	2 +	1o	3o	4o	2 +	22 +

December 1950									
E	1	2	3	4	5	6	7	8	Sum
1	1o	3o	2 +	1 +	1 +	1 +	1 +	0 +	12o
2	2 −	3 +	2o	2 −	2o	3 +	3 −	2 +	19o
3	2o	2 −	2 −	2 +	2 −	1 +	2 +	3o	16o
4	0o	2 −	1o	1 −	1o	2o	2 +	2 −	10 +
5	2o	0 +	2 −	2 −	2 +	3o	3o	2 −	16 −
6	2 +	2 +	4 +	4 +	3o	3 −	2o	2o	23o
7	4 −	3o	2o	1 +	2o	2o	3o	3 −	20 −
8	1 +	1 +	1 +	3o	3o	3 +	3o	3o	19 +
9	3o	3 +	3o	2 −	2o	1 +	1o	1o	16 +
10	2o	3o	3 −	2o	2o	2 −	3 −	2 −	18 −
11	1 +	2o	1o	1 +	1 −	1 −	1o	0 +	8 +
12	0 +	4 −	4 +	3o	2o	3 +	5o	4 +	26o
13	5 +	5 −	5 −	4 −	4 −	4 −	5 +	5 +	36 +
14	6 −	5o	2 −	2o	1 +	3 +	6o	6 −	31 −
15	2 +	3 −	3 −	2 +	3 −	2 +	4 −	3 −	21 +
16	3 −	4 −	2 +	3 +	3 −	1 +	1 +	2o	19 +
17	1 +	2 −	2 −	3 +	1o	1o	2o	2 −	14 −
18	3o	1o	1o	2 −	2 +	3o	4 +	2o	18 +
19	3 +	3 −	3 −	2o	2o	3o	4 −	2 −	21o
20	1o	1 +	1o	3 −	1o	2 +	3 +	5o	18 −
21	3 +	2o	1 +	2o	1 +	0 +	1 +	1 −	12 +
22	1 −	2 −	1o	3 −	4o	5o	6 +	5 −	26o
23	5o	5 −	6 −	4 +	4o	4 −	3 −	4 +	34 +
24	4o	4 −	4 +	4o	4 −	6 +	5 −	4o	35 −
25	5 −	4o	4 +	4 +	4 +	4 +	4 +	4o	34 +
26	4 +	4o	5 −	5o	4 −	4o	4 −	3o	32 +
27	3o	4 −	4 +	4 −	3o	3 −	3 +	4o	28 −
28	3o	3 −	3o	3o	3 −	2 +	2 +	2 −	21 −
29	2 +	2 +	2 +	3 −	1 −	1 +	2 −	2o	15 +
30	2 +	0o	1o	2o	2o	2 +	3 −	3 −	15o
31	1o	0 +	2 −	1 +	1o	1o	1o	2o	9 +

Final *C*, 1950		
Oct.	Nov.	Dec.
1.6	1.5	0.1
1.7	0.7	0.7
1.5	0.4	0.5
1.5	1.5	0.2
1.4	0.6	0.7
1.0	0.0	0.9
1.1	0.0	0.6
0.7	0.3	0.8
0.6	0.2	0.3
0.2	1.5	0.5
0.3	0.9	0.1
0.7	1.1	1.4
0.6	1.0	1.6
1.6	0.6	1.4
1.0	0.2	0.7
1.5	0.3	0.4
1.1	0.7	0.3
0.6	0.8	0.8
0.1	0.1	0.7
0.3	0.0	0.8
0.0	0.3	0.2
0.7	1.2	1.5
0.7	0.3	1.3
0.5	0.9	1.5
0.2	1.6	1.3
0.2	1.6	1.2
0.1	1.4	0.9
1.9	1.4	0.5
1.7	1.0	0.2
1.6	0.7	0.4
1.6		0.1

Final selected days

Oct.	Nov.	Dec.
Five quiet		
10	6	1
19	7	4
21	15	11
25	19	21
27	20	31
Five disturbed		
1	1	13
2	4	14
14	25	22
28	26	23
29	27	24
Ten quiet		
9	6	1
10	7	3
11	8	4
19	9	9
20	15	11
21	16	17
24	19	21
25	20	29
26	21	30
27	23	31

44m-09h 10m: Tl.—17d 15h 24m-50m: Tl.—19d 16h 43m-17h 20m: Tl.—21d 15h 20m-25m: Tu.—22d 18h 40m-19h 20m: Ch Eb Te Pi.—24d 17h 04m: Pi.—25d 12h 35m: Va.—27d 10h 25m-30m: Eb.—28d 11h 30m-36m: CF ion.—28d 19h 40m-50m: Te.—30d 05h 41m: Eb.

1950 December 02d 15h 22m-52m: Hu Va.—05d 12h 41m-52m: Va.—06d 07h 40m: Eb.—06d 11h 55m-12h 20m: Hr.—07d 18h 30m: Pi.—09d 13h 24m-42m: Tl.—14d 16h 27m: Eb.—17d 10h 08m-11h 10m: Tl.—18d 16h 09m: Pi.—20d 17h 41m-45m: Tu.

The usual diagram showing the *Kp*-indices for the year 1950 (see Figs. 1*A* and 1*B*), arranged according to 27-day solar rotations, exhibits growing recurrence-tendencies typical for the declining phase of the 11-year cycle. A complete collection of such diagrams has been published in Abhandlungen Akad. Wiss. Göttingen, Math.-Phys. Klasse, Sonderheft, 1951. For current continuations of such diagrams, see the Note (p. 138) in the March number of this JOURNAL.

IATME Bulletin No. 12e, containing all *C*- and *K*-data for the year 1950, will be distributed in July 1951, it is hoped. It will also contain a paper, "An attempt to standardize the international magnetic character-figures."

COMMITTEE ON CHARACTERIZATION OF MAGNETIC DISTURBANCES

J. BARTELS, *Chairman*
University
Göttingen, Germany

J. VELDKAMP
Kon. Nederlandsch Meteorologisch Instituut
De Bilt, Holland

PROVISIONAL SUNSPOT-NUMBERS FOR JANUARY TO MARCH, 1951

(Dependent on observations at Zurich Observatory and its stations at Locarno and Arosa)

Day	Jan.	Feb.	March
1	32	97	74
2	22	84	62
3	32	62	50
4	42	53	45
5	42	40	38
6	64	35	50
7	71	43	55
8	75	53	54
9	60	60	33
10	57	69	26
11	54	74	40
12	25	66	61
13	17	62	43
14	26	59	36
15	12	51	26
16	14	54	31
17	20	50	26
18	25	38	26
19	43	36	38
20	39	41	49
21	38	44	59
22	38	51	60
23	60	55	83
24	80	61	110
25	100	67	108
26	104	72	97
27	101	80	84
28	106	65	74
29	112		70
30	124		65
31	111		52
Means.....	56.3	57.9	55.6
No. days.....	31	28	31

Mean for quarter: 56.6 (90 days)

M. Waldmeier

Swiss Federal Observatory
Zurich, Switzerland

CHELTENHAM THREE-HOUR-RANGE INDICES K FOR JANUARY TO MARCH, 1951

[$K9 = 500\gamma$; scale-values of variometers in γ/mm: $D = 5.3$; $H = 2.6$; $Z = 4.2$ (January-February) and 4.1 (March)]

Gr. day	January 1951		February 1951		March 1951	
	Values K	Sum	Values K	Sum	Values K	Sum
1	2222 2232	17	4343 1133	22	4313 3222	20
2	3442 3233	24	2210 0111	8	0121 3222	13
3	3522 2223	21	1110 0221	8	1343 2221	18
4	3310 0122	12	0013 2222	12	0431 2222	16
5	2212 1132	14	1322 4343	22	1221 0111	9
6	2211 1120	10	5634 2113	25	1343 3223	21
7	0122 0121	9	3421 1222	17	4423 5444	30
8	2133 2121	15	2133 2433	21	4235 4444	30
9	2332 1100	12	4332 4444	28	4433 3335	28
10	1110 1343	14	4442 2234	25	4652 3333	29
11	5242 2233	23	5342 2334	26	4453 2332	26
12	5234 3322	24	5533 2344	29	4334 4232	25
13	4442 1132	21	4433 3223	24	4335 5445	33
14	3232 3223	20	3222 2232	18	5453 4353	32
15	4432 3233	24	2111 1002	8	5332 2121	19
16	2123 3324	20	0000 0001	1	1444 3332	24
17	4331 0121	15	1000 0022	5	2155 2333	24
18	1111 1112	9	2123 2232	17	2335 2333	24
19	4211 2234	19	1323 2223	18	4342 1221	19
20	3211 1111	11	2212 1020	10	1114 4221	16
21	0013 4434	19	3233 3233	22	1131 1123	13
22	6443 4555	36	4455 4345	34	4334 4455	32
23	5243 3333	26	5564 4445	37	3433 4344	28
24	1332 3222	18	5553 3433	31	4323 3223	22
25	2222 1121	13	4412 3224	22	3413 3223	21
26	1212 2342	17	2432 2233	21	3333 2223	21
27	3542 1333	24	6542 3354	32	3632 1111	18
28	4323 3233	23	5664 4333	34	2110 1023	10
29	1333 2223	19			0454 4334	27
30	3222 2333	20			3332 2222	19
31	4455 2333	29			1132 2322	16

Ralph R. Bodle
Observer-in-Charge

Cheltenham Magnetic Observatory
Cheltenham, Maryland, U.S.A.

PRINCIPAL MAGNETIC STORMS

(Advance knowledge of the character of the records at some observatories as regards disturbances)

Observatory (Observer-in-Charge)	Greenwich date	Storm-time GMT of begin.	Storm-time GMT of ending[1]	Sudden commencement Type[2]	Sudden commencement Amplitudes[3] D	H	Z	C-figure, degree of activity[4]	Maximal activity on K-scale 0 to 9 Gr. day	Gr. 3-hr. period	K-index	Ranges D	H	Z
(1)	(2)	(3)	(4)	(5)	(6)	(7)	(8)	(9)	(10)	(11)	(12)	(13)	(14)	(15)
	1951	*h m*	*d h*		′	γ	γ					′	γ	γ
llege	Jan. 10	16 00	17 06	.....	....	....	....	ms	12	4	6	115	1100	480
. L. Cleven;									16	5	6			
A. Thomas	Jan. 21	10 15	24 00	.....	....	....	....	ms	21	6	7	240	1420	780
ing month	Jan. 26	08 40	1 14	.....	....	....	....	ms	31	4	7	230	1350	1100
March)	Feb. 4	08 00	6 14	.....	....	....	....	ms	4	4	6	144	1130	780
									6	4	6			
	Feb. 8	08 00	14 00	.....	....	....	....	ms	8	6,7	6	150	1260	920
									9	6	6			
									11	6	6			
									12	4	6			
									13	4,5	6			
	Mar. 22	06 00	1 20	.....	....	....	....	ms	23	4,5	7	345	1880	890
	Mar. 7	09 30	12 18	.....	....	....	....	ms	7	5	7	290	1430	1280
	Mar. 13	07 15	15 08	.....	....	....	....	ms	13	4	7	365	1630	1320
	Mar. 22	10 20	25 16	.....	....	....	....	ms	25	4	7	250	1420	970
ka	Jan. 11	18 ..	13 11	.....	....	....	....	m	12	4	5	38	150	175
H. Nelson)								m	13	3	5			
	Jan. 21	10 57	23 21	.....	....	....	....	ms	21	6	6	84	495	430
									22	3,5	6			
	Jan. 31	00 ..	1 12	.....	....	....	....	ms	31	3,4	7	102	710	645
	Feb. 4	08 ..	4 20	.....	....	....	....	ms	4	4	6	22	209	260
	Feb. 5	08 04	6 14	.....	....	....	....	ms	6	2,4	6	56	598	525
	Feb. 8	07 00	10 09	.....	....	....	....	ms	9	6	6	55	340	290
	Feb. 11	15 00	13 15	.....	....	....	....	m	12	4,6	5	40	232	305
									13	4,5	5			
	Feb. 22	04 ..	25 15	.....	....	....	....	s	23	4	8	126	1110	550
	Feb. 26	13 ..	1 17	.....	....	....	....	s	27	3	8	111	1010	655
	Mar. 7	09 ..	12 18	.....	....	....	....	s	7	5	8	88	1070	485
	Mar. 13	07 ..	15 08	.....	....	....	....	ms	13	4,5,6	6	99	510	510
									14	4,5	6			
	Mar. 16	07 ..	16 21	.....	....	....	....	m	16	4	5	31	220	225
	Mar. 17	07 ..	17 19	.....	....	....	....	s	17	3	8	116	890	485
	Mar. 18	08 ..	19 09	.....	....	....	....	ms	18	4	7	91	565	285
	Mar. 22	00 ..	25 14	.....	....	....	....	ms	22	4,6	6	53	440	415
									23	4	6			
									25	4	6			
	Mar. 29	03 ..	30 10	.....	....	....	....	ms	29	5	6	29	325	420
ittevеen	Jan. 16	09 30	17 09	s.c.	−4	+19	−1	m	16	7,8	5	25	125	30
.van Sabben)	Jan. 21	10 58	23 24	s.c.	−2	+10	−1	ms	22	7,8	6	50	195	70
	Jan. 30	05 50	1 24	s.c.	+1	+10	0	ms	31	3	6	30	170	100
	Feb. 5	03 00	6 12	.....	....	....	....	ms	6	1	6	30	100	65
	Feb. 8	12 00	14 24	.....	....	....	....	ms	8	7	6	40	225	75
									10	8	6			
									12	7	6			
	Feb. 21	14 00	26 24	.....	....	....	....	ms	23	7,8	7	40	255	105
	Feb. 27	00 27	1 15	s.c.	−7	+76	−3	ms	27	1	7	50	200	90
	Mar. 6	07 50	15 18	s.c.	−2	+28	−3	ms	13	7	7	50	310	145
	Mar. 22	14 49	25 12	s.c.	−3	+19	−1	ms	24	7	6	30	165	105

[1]Approximate time of ending of storm construed as the time of cessation of reasonably marked disturbance movements in the ces; more specifically, when the *K*-index measure diminished to 2 or less for a reasonable period.

[2]s.c. = sudden commencement; s.c.* = small initial impulse followed by main impulse (the amplitude in this case is that of the *in impulse only*, neglecting the initial brief pulse); .... = gradual commencement.

[3]Signs of amplitudes of *D* and *Z* taken algebraically; *D* reckoned positive if towards the east and *Z* reckoned positive if ver- lly downwards.

[4]Storm described by three degrees of activity: *m* for moderate (when *K*-index as great as 5); *ms* for moderately severe (when = 6 or 7); *s* for severe (when *K* = 8 or 9).

PRINCIPAL MAGNETIC STORMS—Continued

Observatory (Observer-in-Charge)	Greenwich date	Storm-time: GMT of begin.	Storm-time: GMT of ending[1]	Sudden commencement: Type[2]	Sudden commencement: Amplitudes[3] D	H	Z	C-figure, degree of activity[4]	Maximal activity on K-scale 0 to 9: Gr. day	Gr. 3-hr. period	K-index	Ranges: D	H	
(1)	(2)	(3)	(4)	(5)	(6)	(7)	(8)	(9)	(10)	(11)	(12)	(13)	(14)	
	1951	h m	d h		′	γ	γ					′	γ	
Cheltenhem (R. R. Bodle)	Jan. 22	01 ..	24 00	.....	.....	.....	.....	ms	22	1	6	23	28	
	Jan. 31	03 ..	1 09	.....	.....	.....	.....	m	31	3	5	20	64	
	Feb. 6	00 ..	6 07	.....	.....	.....	.....	ms	6	2	6	26	66	
	Feb. 9	14 ..	11 08	.....	.....	.....	.....	m	9	8	4	13	48	
	Feb. 12	00 00	13 06	s.c.	16	31	14	m	12	2	5	18	74	
	Feb. 22	00 ..	25 06	.....	.....	.....	.....	ms	23	3	6	24	72	
	Feb. 27	00 ..	1 05	s.c.	35	62	4	ms	28	3	6	31	214	1
	Mar. 7	00 ..	10 08	.....	.....	.....	.....	ms	10	2	6	26	92	
	Mar. 12	00 42	12 15	s.c.	6	48	12	m	12	1	4	6	48	
	Mar. 22	10 ..	24 01	.....	.....	.....	.....	m	22	7,8	5	20	125	
	Mar. 27	03 15	27 05	s.c.	12	69	33	ms	27	2	6	14	69	
	Mar. 29	04 ..	30 02	.....	.....	.....	.....	m	29	3	5	17	48	
Tucson (J. B. Campbell)	Jan. 21	10 57	24 15	s.c.	+1	−20	....	ms	22	8	6	18	157	..
	Jan. 31	01 ..	1 23	.....	.....	.....	.....	ms	31	3	6	16	122	..
	Feb. 5	04 ..	6 11	.....	.....	.....	.....	ms	6	2	6	15	155	
	Feb. 8	07 ..	13 24	.....	.....	.....	.....	m	11	1	5	13	78	..
									12	2	5			
	Feb. 21	14 ..	26 09	.....	.....	.....	.....	m	22	3,4	5	15	121	..
									23	1,3,4,8	5			
									24	1,2,3	5			
	Feb. 27	00 27	1 17	s.c.	−1	+36	+3	ms	27	1	6	16	140	
									28	2,3	6			
	Mar. 6	03 ..	20 16	.....	.....	.....	.....	ms	17	3	6	18	147	..
	Mar. 21	21 ..	27 09	.....	.....	.....	.....	m	22	6,8	5	16	107	
									27	2	5			
San Juan (P. G. Ledig)	Feb. 27	00 27	28 11	s.c.	0	33	−7	ms	27	1	6	10	133	
									28	2	6			
Honolulu (R. F. White)	Jan. 21	10 30	23 15	.....	.....	.....	.....	m	22	3	4	7	86	
	Jan. 30	19 00	1 13	.....	.....	.....	.....	m	31	2	5	6	157	
	Feb. 5	03 00	6 12	.....	.....	.....	.....	m	6	2	5	6	150	
	Feb. 21	19 30	25 04	.....	.....	.....	.....	m	23	3	5	7	104	
	Feb. 27	00 27	1 12	s.c.	0	22	12	ms	27	1	6	8	166	
(*Note:* March generally disturbed but no outstanding storms)														
Instituto Geofísico de Huancayo (A.A.Giesecke)	Jan. 22	10 48	24 00	.....	.....	.....	.....	m	22	5,6,7,8	5	12	322	
	Jan. 26	03 28	27 09	p.s.c.	0	+12	+1	ms	26	7	6	8	405	
	Jan. 29	04 32	1 03	p.s.c.	0	+14	+2	m	31	3,4	5	9	364	
	Feb. 4	10 50	06 09	.....	.....	.....	.....	m	5	5,6,7	5	7	319	
	Feb. 21	06 11	25 04	s.c.	0	+11	+1	m	23	5,6,7	5	9	320	
	Feb. 27	00 25	1 14	s.c.	−1	+57	+10	ms	28	2	6	7	284	
	Mar. 6	07 51	11 20	s.c.	0	+45	+7	ms	7	5	6	9	268	
	Mar. 13	13 12	15 19	.....	.....	.....	.....	m	13	5	5	7	234	
(*Note:* Report stated that p.s.c. = pulsation s.c., in accordance with January 1951 commun tion of the International Association of Terrestrial Magnetism and Electricity)														
Elisabethville (G. Heinrichs)	Feb. 27	00 27	1 04	s.c.	....	+44	+3	m	28	2,3	.....	14	200	
Apia (G.A.M. King)	Jan. 1	12 30	3 13	.....	.....	.....	.....	m	3	2	5	7	77	
	Jan. 18	22 08	20 04	.....	.....	.....	.....	m	19	8	5	6	58	
	Jan. 21	10 55	24 00	(s.c.)	....	−16	....	m	22	7	5	7	69	
	Jan. 26	03 30	28 14	.....	.....	.....	.....	m	26	7	5	7	63	
	Jan. 30	06 42	2 05	(s.c.)	0	+9	....	m	31	2	5	8	143	
	Feb. 21	20 12	24 20	.....	.....	.....	.....	m	23	4	5	7	133	
	Feb. 27	00 27	28 12	s.c.	+1	+22	−9	ms	28	2	6	7	188	
	Mar. 7	07 10	10 13	.....	.....	.....	.....	m	10	1	5	5	80	
	Mar. 12	04 ..	15 07	.....	.....	.....	.....	m	13	7	5	4	85	
									14	1	5			
	Mar. 29	03 04	30 01	.....	.....	.....	.....	m	29	2,4	5	5	100	

PRINCIPAL MAGNETIC STORMS—Concluded

servatory bserver- Charge) (1)	Green-wich date (2)	Storm-time GMT of begin. (3)	Storm-time GMT of ending[1] (4)	Sudden commencement Type[2] (5)	Amplitudes[3] *D* (6)	*H* (7)	*Z* (8)	*C*-figure, degree of activity[4] (9)	Maximal activity on *K*-scale 0 to 9 Gr. day (10)	Gr. 3-hr. period (11)	*K*-index (12)	Ranges *D* (13)	*H* (14)	*Z* (15)
	1951	*h m*	*d h*		′	γ	γ					′	γ	γ
anus	Jan. 10	12 ..	13 10	.....	....	....	....	m	10	6	5	23	89	119
M.	Jan. 21	9 ..	24 00	.....	....	....	....	ms	22	5	6	18	119	103
Vijk)	(*Note:* Large oscillation in all three elements 10^h55^m–11^h15^m, January 21)													
	Jan. 26	3 ..	2 06	.....	....	....	....	m	31	2	5	24	124	110
									1	1,2	5			
	Feb. 5	4 ..	6 13	.....	....	....	....	m	5	7	5	22	111	96
									6	1	5			
	Feb. 8	14 ..	14 22	.....	....	....	....	m	8	6,7	5	20	98	105
									10	8	5			
									12	7	5			
	Feb. 21	14 ..	25 06	.....	....	....	....	m	22	5,7,8	5	23	144	91
									23	4,7,8	5			
	Feb. 27	00 28	1 16	s.c.	+5	+37	+36	ms	27	1	6	24	182	114
									28	2,3	6			
	Mar. 6	07 50	15 12	s.c.	−3	+19	+8	ms	7	5,7	6	24	194	128
									13	7,8	6			
									14	7	6			
	Mar. 17	04 ..	19 11	.....	....	....	....	m	17	4	5	16	61	53
	Mar. 21	20 ..	25 16	.....	....	....	....	ms	22	6,8	6	19	124	123
	Mar. 29	02 ..	30 15	.....	....	....	....	m	29	4,5	5	19	114	106
	1950													
eroo	Sep. 30	17 47	3 22	s.c.	+1	+12	−6	ms	2	4	6	19	145	135
. Prior)	Oct. 14	02 38	14 23	s.c.	+1	+3	−4	m	14	5,6	5	16	107	155
	Oct. 16	10 00	16 20	.....	....	....	....	ms	16	5	6	16	124	119
	Oct. 28	08 00	31 22	.....	....	....	....	ms	28	7	7	21	128	160
	Nov. 10	07 00	10 20	.....	....	....	....	ms	10	4,5	6	20	130	150
	Nov. 25	00 00	28 24	.....	....	....	....	m	25	1,2	5	15	110	137
	Nov. 25	15 05	.. ..	s.c.	+2	+5	−10	(Activity included in preceding entry)						
	Dec. 10	14 39	.. ..	s.c.	+1	+5	−4	(No appreciable activity followed)						
	Dec. 12	05 26	14 08	s.c.	+2	+5	−3	m	12	2,3	5	18	144	133
	Dec. 22	12 00	23 18	.....	....	....	....	ms	22	6	6	19	63	116
	1951													
	Jan. 21	10 56	23 06	s.c.	−1	−6	+4	m	22	1,5	5	13	85	96
	Jan. 31	01 00	1 16	.....	....	....	....	m	31	3,5,6	5			
	Feb. 22	05 00	24 22	.....	....	....	....	m	23	3,4	5	23	128	150
	Feb. 27	00 29	28 16	s.c.*	−5	−15	+22	ms	28	3	6	23	140	132
	Mar. 6	07 50	6 19	s.c.	+2	+20	−8	m	6	3	4	8	62	62
	Mar. 7	10 00	8 03	.....	....	....	....	m	7	4,5,6	5	10	132	94
erley	Jan. 21	00 05	24 14	.....	....	....	....	m	22	3,5,8	5	18	154	62
. Beagley)	Jan. 30	02 00	1 16	.....	....	....	....	m	31	3	5	17	150	90
	Feb. 21	22 12	25 06	.....	....	....	....	ms	23	3,4	6	29	217	83
	Feb. 27	00 27	28 12	s.c.*	−1	+39	+8	ms	28	2	7	30	281	75
	Mar. 6	07 51	7 03	s.c.	−1	+50	−4	m	6	3	5	10	95	28
	Mar. 7	07 11	15 16	s.c.?	0	+18	−2	m	7	5	5	23	186	75
									10	1,3	5			
									13	5	5			
	Mar. 16	10 04	19 12	.....	....	....	....	m	17	3	5	21	108	45
									18	4	5			
	Mar. 21	21 11	24 09	.....	....	....	....	m	23	4	5	18	144	42
	Mar. 29	03 14	30 15	.....	....	....	....	m	29	5	5	18	106	51

REVIEWS AND ABSTRACTS

HANS G. MACHT: *Die Potential-Anteile 2. und höherer Ordnung des Erd-Magnetfeldes—I.* Beitr. Geophysik, **62**, Heft 2, 127–153 (1950).

This theoretical paper, consisting of three parts, deals with the second- and higher-order potential constituents of the earth's magnetic field. After having reviewed the fundamentals concerned (geomagnetic potential expansion in spherical harmonics), the physico-analytical interpretation of (geo)magnetic potential coefficients as abstract multipoles is considered first in the present Part I. The special importance of the whole second-order potential part, already pointed out in previous papers [references 6 to 9], is emphasized again; a certain (geo)physical meaning should be attributed to its magnetic coefficients (quadrupole components) in connection with the terrestrial dipole components.

The representation of (geo)magnetic potential terms by an eccentric dipole, according to J. Bartels [reference 5], is investigated further. Whereas the second-order terms still are approximated in part, the terrestrial third- and higher-order terms (coefficients) cannot be interpreted by that dipole. This fact would suggest a mainly *crustal* origin of the latter potential constituents. The complex character of the second-order potential portion becomes evident when adopting *geomagnetic* coordinates. Then the "non-sectorial" coefficients $a_2^{3\prime}$, $a_2^{1\prime}$, $b_2^{1\prime}$, together with the single dipole coefficient $c_1^{0\prime}$, determine the position of the Earth's equivalent, eccentric, dipole M, or the so-called magnetic center C_0 . The combined "sectorial" $c_2^{2\prime}$ term, however, can by no means be represented by an eccentric dipole. Being an "invariant" against translations of the geomagnetic coordinate system (the polar axis remaining parallel to itself), a particular, real, physical significance is likely to be ascribed, besides to $c_1^{0\prime}$, also to the $c_2^{2\prime}$ quadrupole coefficient. Thus the problem arises to find for that term, as well as for the further second- and, possibly, higher-order geomagnetic potential constituents, a physical interpretation which goes beyond the purely abstract conception of magnetic multipoles. This task will be treated later in Parts II and III of this paper.

AUTHOR'S ABSTRACT

LETTERS TO EDITOR

A REPLY TO THE COMMENT BY PROF. FERRARO ON MY ARTICLE "SOUTHWARD SHIFTING OF THE AURORAL ZONE"

In the December, 1950, issue of this JOURNAL, Prof. V. C. A. Ferraro gave an interesting comment on my article "The southward shifting of the auroral zone" (J. Geophys. Res., **55**, 127–142, 1950), and he showed his general picture of the process of formation of the auroral zone.

I now think that the description in my article of the way of interpreting the

phenomenon of the southward shifting of the northern auroral zone was not sufficient. However, I have never assumed that the charged particles impinging upon the upper atmosphere over the auroral zone come directly from the sun. On the contrary, it has been my belief that the neutral ionized corpuscular stream, such as suggested by Prof. Chapman and Prof. Ferraro, should be the only possible primary stream which is emitted from the sun and travels toward the earth.

The assumption I made was that the behavior of the charged particles which escape from the front surface of the neutral ionized stream and impinge on the auroral zone can be approximated by that of a single charged particle. The main point of my article was that the trajectory of those particles should be fairly affected by the D_{st}-field. As a matter of fact, the outer boundary of the auroral zone should be determined by the combination of the earth's main field and D_{st} , especially in the neighborhood of the earth. Mathematically speaking, the condition is given by a closing or opening of the forbidden space in the region within the assumed ring current. And, even if we assume a uniform magnetic field as D_{st} , the calculated location of the auroral zone is almost the same as that obtained by assuming an equatorial current ring, as shown in the following Table.

TABLE 1—*Magnetic colatitude of the outer boundary of the auroral zone*

H_0	$Ca^+(v = 1{,}000km/sec)$		$Ca^+(v = 2{,}000km/sec)$	
	Ring-current field	Uniform field	Ring-current field	Uniform field
γ	°	°	°	°
100	28.8	28.7	29.8	29.6
80	27.9	27.8	28.9	28.7
60	26.7	26.5	27.8	27.7
40	25.2	24.9	26.5	26.4
20	23.1	22.7	24.7	24.6
10	21.4	21.1	23.5	23.2
0	17.6	17.6	20.9	20.9

H_0 is the intensity of D_{st}-field on the magnetic equator and v the velocity of the assumed Ca^+-ion.

However, the closing or opening of the forbidden space takes place at the point about five times the earth's radius or more from the center of the earth, when the velocity of the assumed stream of Ca^+ takes the order of magnitude of 10^3 km/sec.

The only difficulty with Chapman-Ferraro's theory, which I pointed out in my article, concerns the magnitude of the radius of the equatorial current ring, and nothing else. That is to say, provided that Z is 10 earth-radii or more for a Chapman-Ferraro ring current, my way of interpretation of the formation of the auroral zone can also be applied. I am inclined to assume that the charged particles which impinge on the auroral zone come from around the two points on the front surface of the Chapman-Ferraro stream at which the retardation of propagation of the front becomes zero (Chapman and Ferraro, Terr. Mag., **36**, 171–186, 1931).

In the latter half of Prof. Ferraro's comment, he showed a possible relation between the position of the auroral zone and the magnitude of the initial phase of a

magnetic storm. But the relation I obtained is that between the position of the auroral zone and the intensity of the D_{st}-field of a magnetic storm. So far as I have studied and know, there is no definite proportionality between the initial phase and the main part of a magnetic storm. Some storms have a large initial phase, but have a very small decrease of H in their main part. Some large storms, on the contrary, have no definite initial phase. So that I am still trusting that my way is the more reasonable interpretation of the observed phenomenon.

Needless to say, the physical mechanism of the causation of magnetic storms as well as the auroral zone has not yet been fully clarified, though the examinations by Störmer, Chapman, Ferraro, Vestine, and others have given us a variety of important knowledge on that subject. My work was also a trial to get at one quantitative character of a magnetic storm, and does not pretend to give the whole picture of magnetic storms.

I hope that further studies and discussions by the specialists in the world will result in a more clear picture of magnetic storms and the auroral zone.

Takesi Nagata

Geophysical Institute, Tokyo University
Tokyo, Japan, April 16, 1951

A FORECAST OF SOLAR ACTIVITY

In the December, 1943, issue of this Journal,[1] I published some predictions for the then next sunspot-cycle, the eighteenth in the Zürich statistics. According to these predictions, a cycle having a high maximum and a steep ascent to the maximum was to be expected. In the meantime, these predictions have come true. Actually we experienced, in 1947, one of the highest maxima in sunspot-history, which was preceded by an extremely steep ascent from minimum to maximum.

The same method which yielded these successful predictions leads to the following predictions for the future course of solar activity:

It is to be expected with a probability of 0.95 (that is, of 19 to 1) that

(1) On the declining branch of the present cycle the smoothed monthly averages R of Wolf's relative sunspot-numbers will not fall below 38 before April, 1953.

(2) The coming minimum will occur within 18 months, reckoned from the month in which R has fallen below 38.

(3) R will not fall below 9 at the coming minimum.

(4) R will exceed 130 at the maximum of the next cycle.

(5) The ascent to the maximum of the next cycle will be so steep that the values of R will rise from one-quarter of their maximum value to the maximum within less than 32 months.

Prediction (1) is published here for the first time; the other predictions have been taken from previous publications.[2,3]

[1]W. Gleissberg, Terr. Mag., 48, 243 (1943).
[2]W. Gleissberg, Astroph. J., 110, 90 (1949).
[3]W. Gleissberg and A. Kiral, Zs. Astroph., 28, 17 (1950).

The above predictions indicate that the coming minimum will be unusually shallow and that the next sunspot-cycle probably again will be one of very intensive solar activity.

W. Gleissberg

Istanbul University Observatory
Bayazit, Istanbul, Turkey, February 19, 1951

NOTES

(16) *Plans for a new magnetic observatory in the south of Argentina*—The newly-established Departamento de Magnetismo Terrestre y Electricidad Atmosferica, Observatorio Astronomico, Universidad Nacional de la Plata, of which Dr. L. Slaucitajs is head, has set for its program of endeavors the building of a magnetic observatory in the south of Argentina, revision of the present network of repeat-stations, especially in regions of rapid changes, participation in magnetic surveys, examination of accumulated observatory data, and studies of global problems. As Professor of Geophysics, Dr. Slaucitajs will also educate young Argentines in terrestrial magnetism.

(17) *Fiftieth anniversary of the founding of the National Bureau of Standards*—This United States Government Bureau has completed its first fifty years of notable achievement in science and engineering, and in maintenance of precise measuring standards and techniques.

(18) *Research and development programs, Geophysical Laboratory, Toronto, Canada*—One of the principal interests is the Pre-Cambrian Shield, and many of its properties are under study. Its radioactivity, seismic properties, gravitational attractions, thermal behavior, and magnetic properties are being investigated. Broad studies in radioactivity include field and laboratory measurements. A mass spectrograph is nearing completion, to be used for age determinations by measurement of lead isotopic ratios and other geophysical problems. The study of seismic waves procured by rockbursts in mines is being continued, and the propagation of seismic waves is being studied on a laboratory model scale by electronic techniques. An airborne magnetometer for measurement of all three components of the earth's field is being developed, and flight trials have commenced. A mathematical analysis of the conditions of failure of a spherical shell was completed, and this has been correlated with existing mountain ranges, island arcs, and deep earthquake sites, thereby providing an explanation for these features.

(19) *Operation of mobile ionospheric station by the National Bureau of Standards*—In order to obtain more comprehensive data regarding the ionosphere, the Central Radio Propagation Laboratory of the National Bureau of Standards has incorporated a mobile ionospheric research unit into the existing chain of 60 world-wide ionosphere stations. With the new unit, ionospheric soundings will be made from points midway between two permanent transmitting-receiving stations. The information will be used in studies of ionospheric effects on radio waves directly above the mobile transmitter-receiver, as also as an aid in analyzing the behavior

of radio waves propagated from transmitters to distant receivers. The first recording stop of the mobile unit was 30 miles east of Cincinnati, Ohio, a point midway between the Bureau's transmitting station at Sterling, Virginia, and a leased transmitting station operated by Washington University, St. Louis, Missouri. Within a few years and after a number of midpoint locations, the Bureau expects to have sufficient information about the ionospheric radio propagation to map accurately the paths of radio waves across the country and into other parts of the world. Experiments are designed to record simultaneously both vertical and oblique incidence data, and from an analysis of the information the relation between oblique and vertical incidence reflectors will be more exactly deduced.

(20) *Formal establishment of the Office of Science Adviser*—The Office of Science Adviser under the direction of the United States Department of State was formally established on February 6, 1951, presaging evolvement of some of the recommendations contained in "Science and foreign relations," the recent report of the survey group headed by L. V. Berkner.

(21) *Indian Institute of Science, Bangalore, India*—The Indian Institute of Science is one of the premier institutions of India conducting post-graduate research in pure and applied sciences. A diploma, associateship, or fellowship conferred by the Institute compares favorably with similar technical qualifications earned elsewhere in the United Kingdom or in the United States. Various departments of the Institute cover fields of chemistry, physics, electrical technology, aeronautical engineering, metallurgy, social sciences and industrial economics, and some others. The Institute of Science has recently published a report covering the period 1938–1948 (139 pages, Bangalore Press, Rupee 1). The report describes the research contributions from various departments and the facilities provided in each. By a rare oversight, the list of the present staff of the Institute is missing from the report. However, well-known names like Sir C. V. Raman, K. S. Krishnan, Nagendra Nath, Guha, and others have been associated with the Institute. This report might be of help to American students who wish to avail themselves of the opportunity provided by the Fulbright Act for study overseas.

(22) *Mining geophysicists to organize*—The increasing use of geophysics as a tool in the search for essential metallic ores has led the Society of Exploration Geophysicists to consider the organization of a mining section, according to Dr. Sigmund Hammer, of the Gulf Research and Development Company, Pittsburgh, Pennsylvania, vice-president of the Society. Mining exploration scientists have been invited to attend a conference to be held on April 23, 1951, during the Society's annual meeting in St. Louis, Missouri. A mining geophysics section within the Society would provide a better opportunity for oil and mining geophysicists to exchange ideas and thus aid in the development of more efficient techniques in both industries.

(23) *Aurora Borealis*—The United States *Hydrographic Bulletin* (Nos. 4 and 5 of January 24 and February 3, 1951) contained the following accounts of the Aurora Borealis:

Second Officer H. Quevedo, of the Chilean S.S. *Copiapo*, Captain J. Ojeda, Master, reported that on December 12, 1950, at 23^h30^m GMT, in latitude 40°45′ north, longitude 55°00′ west, the sky over the northern horizon became exceptionally

bright with vertical columns of varying intensity extending from a bearing of 310° to 340°. The phenomenon reached to an altitude of about 15°, and disappeared entirely at 01^h 30^m GMT, December 13. The sky was clear; visibility excellent; wind SW, force 4; barometer 29.96 inches; air temperature 66° F.

Second Officer W. H. Brandt, of the American S.S. *Tramar I*, Captain K. N. Crosby, Master, reported that on December 13, 1950, at 23^h 15^m GMT, in latitude 66° 05′ north, longitude 6° 40′ east, en route from Narvik to Baltimore, an unusually brilliant display of northern lights was observed. The rainbow-like profusion of colors extended from a bearing of 270° to 080°, and resembled a multicolored veil which was drawn across the sky, at times fanning out in the shape of butterfly wings. The phenomenon lasted about 15 minutes and was finally obscured by a snow squall. Torchlike shafts of yellow-green were observed arching across the sky several hours before and after the major display. The sky was clear; wind SW, force 4; barometer 29.38 inches, rising; air temperature 31° F.

(24) *Geomagnetic activities of the United States Coast and Geodetic Survey*—Two Inter-American Geodetic Survey observers trained by the United States Coast and Geodetic Survey continued on magnetic surveys in Brazil and Chile.

In cooperation with the Central Radio Propagation Laboratory, of the National Bureau of Standards, a visual-recording magnetograph is being installed at Anchorage, Alaska, for correlated studies of the ionosphere.

Reports containing reproductions of Tucson, San Juan, and Honolulu magnetograms for the second half of 1938 have been issued.

Chart 3077, "Isogonic Chart for 1950, United States," and Chart 3069b, "Lines of Equal Magnetic Declination and of Equal Annual Change in Alaska for 1950," were issued.

(25) *New magnetic observatory in Japan*—Dr. K. Wadate, Director of the Central Meteorological Observatory, Tokyo, Japan, reports that a magnetic observatory was established in May, 1950, at Memanbetsu. The geographical position is 43° 54′.5 north and 144° 11′.6 east. Provisional work has been carried on since its establishment.

(26) *New magnetic observatory in the Philippines*—A magnetic observatory has been installed by the Coast and Geodetic Survey of the Philippine Government at Muntinlupa, Province of Rizal. The geographic coordinates are 14° 22′.5 north and 121° 00′.9 east. Construction began in October 1949, and the installation and tests of variometers were made in October, 1950. Regular, continuous records have been obtained since January 1, 1951. The officer-in-charge is Lieut.-Comdr. S. de Guzman. The buildings duplicate those at the new magnetic station of the United States Coast and Geodetic Survey at Honolulu. Much assistance has been given by the United States Coast and Geodetic Survey during the establishment of this observatory.

(27) *Conference on auroral physics to be held at London, Ontario, Canada*—A conference on auroral physics, jointly sponsored by the Physics Department of the University of Western Ontario and the Geophysical Research Directorate of the Air Force Cambridge Research Laboratories, Cambridge, Massachusetts, will be held during July 23 to 26 at the University of Western Ontario, at London, Ontario. The entire field of auroral physics will be given consideration, with important

theoretical papers to be presented by internationally known scientists. General topics to be discussed will deal with the formation of the aurora, mechanisms of solar corpuscular streams, and excitation mechanisms in the ionosphere (80-400 km) and in the mesosphere (400-1,000 km). Several papers will be presented on the identification and interpretation of the emission spectra of the ionosphere and mesosphere and other observational studies.

(28) *Personalia*—Among recent visitors at the Department of Terrestrial Magnetism, Carnegie Institution of Washington, were the following: Prof. *T. G. Cowling*, University of Leeds, Yorkshire, England, who on April 4, 1951, spoke to the staff on "Dynamo theories of the earth's main field;" Dr. *J. A. Ratcliffe*, of the Cavendish Laboratory, Cambridge University, London, who on April 11, 1951, presented a talk to the staff entitled "A physicist tries to understand the magneto-ionic theory;" and Dr. *P. G. Gane*, of the Bernard Price Institute of Geophysical Research, Johannesburg, South Africa, who on April 16, 1951, described his interesting seismic recordings of the numerous daily earth tremors occurring in the Witwatersrand gold-fields.

Of interest are the following personnel changes in the Division of Geophysics, of the United States Coast and Geodetic Survey: Dr. *H. H. Howe*, geophysicist in the Washington office, transferred to the National Bureau of Standards on March 30, 1951. Mr. *J. L. Bottum* left Washington on March 19, 1951, to take over the operation of the Barrow Magnetic Observatory, relieving Mr. *W. H. Schmieder*, who had been in charge since April 1949. Mr. Schmieder, will return to duty at the College Magnetic Observatory.

A Section of Geophysics has been approved by the National Academy of Sciences. The following men were recently elected to that Section and members of the National Academy of Sciences: Dr. *Ross Gunn*, Director of the Division of Physical Research, United States Weather Bureau, Washington, D.C.; Dr. *Columbus O'D. Iselin*, Senior Physical Oceanographer and former Director of the Woods Hole Oceanographic Institution, Woods Hole, Mass., and Dr. *Thomas G. Thompson*, Director of the Oceanographic Laboratories, University of Washington, Seattle, Wash. Drs. *Donald W. Kerst* and *Frederick Seitz, Jr.*, both professors of physics at the University of Illinois, were also elected to membership (Section of Physics) in the National Academy of Sciences.

Prof. *Vilhelm F. K. Bjerknes*, noted Norwegian physicist, died in Bergen on April 9, 1951, at the age of 89 years. A theory of electric resonance that aided in the development of wireless telegraphy was proposed by him. He was professor of geophysics for many years at Oslo and at Leipzig universities, and founded the Bergen Weather Service. In late years he was associated with the Astrophysical Institute, Oslo-Blindern, Norway. His son, Prof. J. A. B. Bjerknes, internationally known as a meteorologist, is a professor at the University of California.

LIST OF RECENT PUBLICATIONS

By. W. E. Scott

Department of Terrestrial Magnetism,
Carnegie Institution of Washington,
Washington 15, D. C.

(Received April 30, 1951)

A—*Terrestrial Magnetism*

Ambolt, N. Ergebnisse der Beobachtungen des magnetischen Observatoriums zu Lovö (Stockholm) im Jahre 1947. Stockholm, Kungl. Sjökarteverket, 32 pp. (1950). 31 cm.

Apia Observatory. Annual report for 1944. Issued under the authority of the Hon. K. J. Holyoake, Minister of Scientific and Industrial Research. Wellington, R. E. Owen, Govt. Printer, 149 pp. (1949). 24 cm.

Apia Observatory. Annual report for 1945. Issued under the authority of the Hon. K. J. Holyoake, Minister of Scientific and Industrial Research. Wellington, R. E. Owen, Govt. Printer, 145 pp. (1949). 24 cm.

Bartels, J., and J. Veldkamp. International data on magnetic disturbances, third quarter, 1950. J. Geophys. Res., **56**, No. 1, 127-129 (1951).

Beagley, J. W., and J. M. Bullen. Trends in magnetic declination at Apia and Christchurch. N. Z. J. Sci. Tech., B, **31**, No. 1, 16-26 (1950).

Blackett, P. M. S. Magnetic field of large rotating bodies. Proc. R. Inst., **34**, No. 156, 393-394 (1950). [Abstract.]

Bodle, R. R. Cheltenham three-hour-range indices *K* for October to December, 1950. J. Geophys. Res., **56**, No. 1, 130 (1951).

Chakrabarty, S. K. Sudden commencements in geomagnetic field variations. Nature, **167**, No. 4236, 31 (1951).

Copenhagen, Det Danske Meteorologiske Institut. Magnetisk aarbog, 1ste del: Danmark — Annuaire magnétique, 1ere partie: le Danemark. 1949. Köbenhaven, G.E.C. Gad, 27 pp. (1950). 32 cm.

Crichton, J. Eskdalemuir Observatory. Met. Mag., **79**, No. 942, 337-340 (1950). [Gives history and describes buildings, instrumental equipment, and observational program.]

Fanselau, G. Ergebnisse der Beobachtungen am Adolf Schmidt-Observatorium für Erdmagnetismus in Niemegk in den Jahren 1939-1944. I. Teil: Stunden-, Tages-, Monats- und Jahresmittel der erdmagnetischen Elements. Berlin, Akad.-Verlag, 114 pp. (1950). 30 cm. [Published under the auspices of the Meteorologischer Dienst der Deutschen Demokratischen Republik, Erdmagn. Jahr. 1939-1944.]

Harper, W. G. Lerwick Observatory. Met. Mag., **79**, No. 941. 309-314 (1950). [Brief history and descriptions of buildings, site, instrumental equipment, and observational programs are given.]

Ishikawa, G. On the initial phase of geomagnetic storm. Pap. Met. Geo., Tokyo, **1**, No. 2-4, 319-336 (1950).

Kawai, N. Magnetic polarization of tertiary rocks in Japan. J. Geophys. Res., **56**, No. 1, 73-79 (1951).

Koenigsfeld, L. Observations magnétiques faites à Manhay (Belgique) pendant l'année 1947. Liège, Les Presses de "Lejeunia," 4 + tables of hourly values. 23 cm. [Université de l'Liège, Institut d'Astronomie et de Géodésie, Physique du Globe, No. 5.]

Ledig, P. G., W. C. Parkinson, A. A. Giesecke, Jr., W. E. Scott, and E. Balsam. Magnetic

results from Huancayo Observatory, Peru (Department of Terrestrial Magnetism, Carnegie Institution of Washington, January 1945-June 1947; Instituto Geofísico de Huancayo, July-December 1947). Washington, D. C., Carnegie Inst. Wash. Pub. 175, vol. 10-C, v + 127 pp., 120 tables (1951). 28 cm.

Macht, H. G. Die Potential-Anteile 2. und höherer Ordnung des Erd-Magnetfeldes—I. Beitr. Geophysik, **62**, Heft 2, 127-153 (1950).

Martyn, D. F. The theory of magnetic storms and auroras. Nature, **167**, No. 4238, 92-97 (1951).

Mauritius, Royal Alfred Observatory. Results of magnetical and meteorological observations for the months January to December 1944 (new series, v. 30, pts. 1-12). Nairobi, E. A. Met. Dep. Press, 1-193 (1949). [Issued as monthly bulletins.]

Mauritius, Royal Alfred Observatory. Results of magnetical and meteorological observations for the months January to December 1947 (v. 33, pts. 1-12). Port Louis, J. E. Félix, Govt. Printer (1949). [Issued as monthly bulletins.]

Milne, E. A. Gravitation and magnetism. Mon. Not. R. Astr. Soc., **110**, No. 4, 266-274 (1950).

Olsen, J. Results of magnetic observations made at Tatuoca (Brazil), September 1933-January 1934, with an appendix "The lunar-diurnal variation of the magnetic declination at Tatuoca for the period Sept. 1933 to Jan. 1934," by J. Egedal. Copenhagen, Temporary Commission on the Liquidation of the Polar Year (TCLPY) 1932-33, International Meteorological Organization, 9 pp. with tables and appendix (1951). 32 cm.

Olsen, J. Results of magnetic observations made at Magallanes (Chile), January-August 1933. Copenhagen, Temporary Commission on the Liquidation of the Polar Year (TCLPY) 1932-33, International Meteorological Organization, 12 pp. with tables (1951). 31 cm.

Pontier, L. Amplitude de la variation de *H* au voisinage de l'équateur magnétique au Togo. Ann. Géophys., **6**, No. 4, 238-241 (1950).

Principal Magnetic Storms. Principal magnetic storms, October to December, 1950. J. Geophys. Res., **56**, No. 1, 131-133 (1951).

Rougerie, P. Variation diurne lunaire de la déclinaison magnétique et de la composante verticale du champ terrestre au Val-Joyeux. Ann. Géophys., **6**, No. 4, 300-308 (1950).

Runcorn, S. K., A. C. Benson, A. F. Moore, and D. H. Griffiths. The experimental determination of the geomagnetic radial variation. Phil. Mag., **41**, No. 319, 783-791 (1950).

Sandoval, R. O. Elementos magnéticos en la República Mexicana. Universidad Nacional de México, Instituto de Geofisica, 223 pp. (1950). 30 cm. [Contains values of magnetic elements for 1879-1946, and magnetic determinations in Mexico City between 1769 and 1868.]

Truesdell, C. Correction to the paper "On the effect of a current of ionized air upon the earth's magnetic field." J. Geophys. Res., **56**, No. 1, 134 (1951).

Tsubokawa, I., Y. Harada, and S. Amagai. Magnetic survey in the southwestern part of Japan. Bull. Geogr. Surv. Inst. Japan, **2**, Pt. 1, 77-79 (1950). [Three magnetic charts of *D*, *H*, and *I*, reduced to epoch 1950, accompany article.]

United States Coast and Geodetic Survey. Magnetograms, Honolulu, T.H., July-December 1948. Washington, D. C., U. S. Coast Geod. Surv., 56 pp. (1950). 25 cm.

United States Coast and Geodetic Survey. Magnetograms, San Juan, Puerto Rico, July-December 1948. Washington, D. C., U. S. Coast Geod. Surv., 54 pp. (1950). 25 cm.

United States Coast and Geodetic Survey. Magnetograms, Tucson, Arizona, July-December 1948. Washington, D. C., U. S. Coast Geod. Surv., 54 pp. (1950). 25 cm.

Van Vleck, J. H. Landmarks in the theory of magnetism. Amer. J. Physics, **18**, No. 8, 495-509 (1950).

Weber, A. M., and E. B. Roberts. The 1950 world isogonic chart. J. Geophys. Res., **56**, No. 1, 81-84 (1951).

Wingst Observatorium. (1) Ergebnisse der erdmagnetischen Beobachtungen im Observatorium Wingst im Jahre 1945 (O. Meyer); (2) Erdmagnetische Karten von Westdeutschland für 1950.5 (F. Errulat). D. Hydrogr. Inst., Hamburg, No. 3, 81 pp. (1951). 24 cm.

Witteveen Magnetic Observatory. Yearbook 1946. B—Geomagnetism (K. Nederlands Met. Inst. No. 98). 's-Gravenhage, v + 28 (1949). 34 cm.

Yoshimatsu, T. A classification of the types of SC of magnetic storm. Rep. Ionosphere Res. Japan, **4**, No. 4, 220 (1950). [Short note.]

B—*Terrestrial Electricity*

Barnard, V. The approximate mean height of the thundercloud charges taking part in a flash to ground. J. Geophys. Res., **56**, No. 1, 33-35 (1951).

Battan, L. J. The "Thunderstorm-Project" data. Bull. Amer. Met. Soc., **32**, No. 1, 27-29 (1951).

Burkard, O., und D. Zych. Luftelektrische Messungen mit stabilisiertem Netzgerät. Arch. Met. Geophys. Biokl., A, **3**, Heft 2, 102-108 (1950).

Gartlein, C. W., and R. K. Moore. Southern extent of aurora borealis in North America. J. Geophys. Res., **56**, No. 1, 85-96 (1951).

Goldschmidt, J. Neukonstruktion eines Einfadenelektrometers. Arch. Met. Geophys. Biokl., A, **3**, Heft 2, 98-101 (1950).

Hatakeyama, H., and K. Utikawa. The diurnal variation of the atmospheric potential gradient at the summit and the slope of Mt. Fuji. J. Met. Soc. Japan, **29**, No. 1, 28-33 (1951). [Japanese and English.]

Hess, V. F. New studies on the radioactivity of the atmosphere. Arch. Met. Geophys. Biokl., A, **3**, Heft 2, 56-63 (1950).

Hogg, A. R. Air-earth current observations in various localities. Arch. Met. Geophys. Biokl., A, **3**, Heft 2, 40-55 (1950).

Israël, H. Zur Entwicklung der luftelektrischen Grundanschauungen. Arch. Met. Geophys. Biokl., *A*, **3**, Heft 2, 1-16 (1950).

Kasemir, H. W. Studien über das atmosphärische Potentialgefälle. IV: Zur Strömungstheorie des luftelektrischen Feldes I. Arch. Met. Geophys. Biokl., A, **3**, Heft 2, 84-97 (1950).

Nolan, J. J. The control of the electrical conductivity of the lower atmosphere. Arch. Met. Geophys. Biokl., A, **3**, Heft 2, 17-28 (1950).

Norinder, H., und R. Siksna. Variationen des Ionengehaltes in der bodennahen Luftschicht. Arch. Met. Geophys. Biokl., *A*, **3**, Heft 2, 29–39 (1950).

Ohta, S. On the contents of condensation nuclei and uncharged nuclei on the Pacific Ocean and the Japan Sea. Bull. Amer. Met. Soc., **32**, No. 1, 30-31 (1951).

Rossmann, F. Luftelektrische Messung mittels Segelflugzeugen. Bad Kissingen, Ber. D. Wetterdienstes US-Zone, No. 15, 54 pp. (1950). 30 cm.

Schonland, B. F. J., and D. J. Malan. The distribution of electricity in thunderclouds. Arch. Met. Geophys. Biokl., A, **3**, Heft 2, 64-69 (1950).

Wait, G. R Measurements by airplane of electric charge passing vertically through thunderstorms to ground. Arch. Met. Geophys. Biokl., A, **3**, Heft 2, 70-76 (1950).

C—*Cosmic Rays*

Barker, K. H., and C. C. Butler. The nuclear interaction length of the particles in penetrating cosmic-ray showers. Proc. Phys. Soc., A, **64**, No. 373, 4-9 (1951).

Bergstralh, T. A., and C. A. Schroeder. A search for cosmic-ray diurnal effects at balloon altitudes. Phys. Rev., **81**, No. 2, 244-247 (1951).

Goodman, P., K. P. Nicholson, and H. D. Rathgeber. The ionization of cosmic-ray particles. Proc. Phys. Soc., A, **64**, No. 373, 96-97 (1951).

Harding, J. B. The origin of cosmic ray stars. Phil. Mag., **42**, No. 324, 63-73 (1951).

Hogg, A. R. Some time variations of cosmic rays. J. Atmos. Terr. Phys., **1**, No. 2, 114-120 (1950).

Jelley, J. V. Detection of μ-mesons and other fast charged particles in cosmic radiation, by the Čerenkov effect in distilled water. Proc. Phys. Soc., A, **64**, No. 373, 82-87 (1951).

Lord, J. J. The altitude and latitude variation in the rate of occurrence of nuclear disintegrations produced in the stratosphere by cosmic rays. Phys. Rev., **81**, No. 6, 901-909 (1951).

Pomerantz, M. A. An increase of the primary cosmic-ray intensity following a solar flare. Phys. Rev., **81**, No. 5, 731-733 (1951).

Simpson, J. A., Jr. Change of cosmic-ray neutron intensity following solar disturbances. Phys. Rev., **81**, No. 4, 639-640 (1951).

Staker, W. P., M. Pavalow, and S. A. Korff. The latitude effect of cosmic-ray neutrons. Phys. Rev., **81**, No. 5, 889-890 (1951).

Wada, M. Some problems to the study of cosmic-ray intensities during magnetic storms. Rep. Ionosphere Res. Japan, **4**, No. 4, 224-226 (1950). [Short note.]

D—*Upper Air Research*

Appleton, E. Studies of the F_2 layer in the atmosphere. I—The position of the ionospheric equator in the F_2 layer. J. Atmos. Terr. Phys., **1**, No. 2, 106-113 (1950).

Appleton, E. Magnetic and ionospheric storms. Arch. Met. Geophys. Biokl., A, **3**, Heft 2, 113-119 (1950).

Argence, E., M. Mayot, et K. Rawer. Contribution a l'étude de la distribution électronique de l'ionosphère et de l'absorption des ondes courtes. Ann. Géophys., **6**, No. 4, 242-285 (1950).

Banerjee, S. S., and R. R. Mehrotra. Location of undulations in the $F2$ region of the ionosphere. J. Sci. Industr. Res., New Delhi, **9B**, No. 12, 304-305 (1950).

Baral, S. S. Ionospheric studies at Calcutta (1944-50). J. Sci. Industr. Res., New Delhi, **10**, No. 2, 60-64 (1951).

Baral, S. S., and A. P. Mitra. Ionosphere over Calcutta (solar half-cycle January 1945-June 1950). J. Atmos. Terr. Phys., **1**, No. 2, 95-105 (1950).

Barré, M., et K. Rawer. Une perturbation ionosphérique extraordinaire observée en Terre Adélie. Ann. Géophys., **6**, No. 4, 309-317 (1950).

Becker, W. Über die Dämpfung der ausserordentlichen Komponente in der E_1-Schicht der Ionosphäre. J. Atmos. Terr. Phys., **1**, No. 2, 73-81 (1950).

Becker, W., und W. Dieminger. Über die Häufigkeit und die Struktur der E_2-Schicht der Ionosphäre. Naturwiss., **37**, Heft 4, 90-91 (1950).

Benner, A. H. Vertical incidence ionospheric absorption at 150 kc. Proc. Inst. Radio Eng., **39**, No. 2, 186-190 (1951).

Bibl, K. Methoden zur Bestimmung des Ionisationsverlaufs hinter dem Maximum der E-Schicht. Naturwiss., **37**, Heft 16, 373-374 (1950).

Booker, H. G. Studies on propagation in the ionosphere. Ithaca, Cornell University, School of Electrical Engineering, Tech. Rep. No. 2, 74 pp. (Dec. 15, 1950). [Report on the Ninth General Assembly of URSI, Zurich, Sep. 1950, Commission III—Ionospheric Propagation.]

Booker, H. G. Studies on propagation in the ionosphere. Ithaca, Cornell University, School of Electrical Engineering, Tech. Rep. No. 3, 30 pp. (Dec. 15, 1950). [Account of D. F. Martyn's theory of magnetic storms and auroras, presented at the Ninth General Assembly of the URSI, Zurich, Sep. 1950.]

Booker, H. G., J. A. Ratcliffe, and D. H. Shinn. Diffraction from an irregular screen with applications to ionospheric problems. Phil. Trans. R. Soc., A, **242**, No. 856, 579-607 (1950).

Boutet, R. A. La haute atmosphère. Paris, Office National d'Études et de Recherches Aéronautiques, Pub. No. 38, 121 pp. with 51 figs. (1950). 27 cm.

Bowe, P. W. A. The waveforms of atmospherics and the propagation of very low frequency radio waves. Phil. Mag., **42**, No. 325, 121-138 (1951).

Bramley, E. N. Diversity effects in spaced-aerial reception of ionospheric waves. Proc. Inst. Elec. Eng., **98**, Pt. 3, No. 51, 19-25 (1951).

Bricard, J., et A. Kastler. Polarisation des radiations monochromatiques du ciel nocturne et de la raie D crépusculaire. Ann. Géophys., **6**, No. 4, 286-299 (1950).

Briggs, B. H. An investigation of certain properties of the ionosphere by means of a rapid frequency-change experiment. Proc. Phys. Soc., B, **64**, No. 375, 255-274 (1951).

Budden, K. G. The propagation of a radio-atmospheric. Phil. Mag., **42**, No. 324, 1-19 (1951).

Chandrasekhar, S., and D. Elbert. Polarization of the sunlit sky. Nature, **167**, No. 4237, 51-55 (1951).

Chang, C. S. Sodium bands in the ultra-violet λλ 3100-2750. Chinese J. Phys., **7**, No. 5, 577-582 (1950). [In English.]

Chapman, S. Upper atmospheric nomenclature. J. Atmos. Terr. Phys., **1**, No. 2, 121-124 (1950).

Covington, A. E. Some characteristics of 10.7-centimetre solar noise—I. J. R. Astr. Soc. Can., **45**, No. 1, 15-22 (1951).

Dieminger, W. The scattering of radio waves. Proc. Phys. Soc., B, **64**, No. 374B, 142-158 (1951).

Elvey, C. T. Progress in studies of the airglow in upper air research. Amer. J. Physics, **18**, No. 7, 431-437 (1950).

Eyfrig, R. Zur Frage des täglichen Ganges der Elektronen Konzentration der *F*2-Schicht äquatorialer Stationen. Naturwiss., **37**, Heft 3, 67-68 (1950).

Feinstein, J. The interpretation of radar echoes from meteor trails. J. Geophys. Res., **56**, No. 1, 37-51 (1951).

Gerson, N. C. Continental sporadic *E* activity. Trans. Amer. Geophys. Union, **32**, No. 1, 26-30 (1951).

Gerson, N. C. Note concerning "The stratification of the atmosphere" by H. Flohn and R. Penndorf. Bull. Amer. Met. Soc., **32**, No. 1, 34-35 (1951).

Gherzi, E. Echoes from the *D*- and F_2-layers on a frequency of 21 Mc/s.? Nature, **167**, 412 (March 10, 1951).

Helliwell, R. A., A. J. Mallinckrodt, and F. W. Kruse, Jr. Fine structure of the lower ionosphere. J. Geophys. Res., **56**, No. 1, 53-62 (1951).

Hines, C. O. Wave packets, the Poynting vector, and energy flow: Part I—Non-dissipative (anisotropic) homogeneous media. J. Geophys. Res., **56**, No. 1, 63-72 (1951).

Huruhata, M. Photoelectric studies of the night sky light (II). Rep. Ionosphere Res. Japan, **4**, No. 3, 137-146 (1950).

Ishikawa, G. The total conductivity of the ionosphere. Rep. Ionosphere Res. Japan, **4**, No. 4, 220 (1950). [Short note.]

Jaeger, J. C., and K. C. Westfold. Equivalent path and absorption for electromagnetic radiation in the solar corona. Aust. J. Sci. Res., A, **3**, No. 3, 376-386 (1950).

Kelso, J. M. The effect of the Lorentz polarization term on the vertical incidence absorption in a deviating ionosphere layer. Proc. Inst. Radio Eng., **39**, No. 4, 412-419 (1951).

Kerr, F. J., and C. A. Shain. Moon echoes and transmission through the ionosphere. Proc. Inst. Radio Eng., **39**, No. 3, 230-242 (1951).

Knighting, E. Some meteorological aspects of radio dust formation. Proc. Phys. Soc., B, **64**, No. 373, 21-30 (1951).

Kōno, T. Experimental study on scattered echoes, Parts I and II. Rep. Ionosphere Res. Japan, **4**, No. 3, 127-135, and No. 4, 189-199 (1950).

Little, C. G., and A. Maxwell. Fluctuations in the intensity of radio waves from galactic sources. Phil. Mag., **42**, No. 326, 267-278 (1951).

Lovell, A. C. B. The new science of radio astronomy. Nature, **167**, No. 4238, 94-97 (1951).

Lovell, A. C. B. Radio astronomy. Discovery, **12**, No. 1, 7-12 (1951).

McNicol, R. W. E., and G. de V. Gipps. Characteristics of the E_s region at Brisbane. J. Geophys. Res., **56**, No. 1, 17-31 (1951).

Meinel, A. B. Doppler-shifted auroral hydrogen emission. Astroph. J., **113**, No. 1, 50-54 (1951).

Merrill, P. W. Displaced calcium lines in the spectrum of HD 190073. Astroph. J., **113**, No. 1, 55-59 (1951).

Miller, W. Effective earth's radius for radiowave propagation beyond the horizon. J. Applied Phys., **22**, No. 1, 55-62 (1951).

Minnis, C. M. Ionospheric storms and radio circuit disturbances. Wireless Eng., **28**, No. 329, 43-51 (1951).

Moore, R. K. A V.H.F. propagation phenomenon associated with aurora. J. Geophys. Res., **56**, No. 1, 97-106 (1951).

Nagata, T. The solar-flare type variation in geomagnetic field and the integrated electrical conductivity of the ionosphere (I). Rep. Ionosphere Res. Japan, **4**, No. 3, 155-172 (1950).

Nagata, T., and T. Suzuki. The solar-flare type variation in geomagnetic field and the integrated electrical conductivity of the ionosphere. II—Effect of *F*-layer. Rep. Ionosphere Res. Japan, **4**, No. 4, 201-205 (1950).

Naismith, R., and R. Bailey. An automatic ionospheric recorder for the frequency range 0.55 to 17 Mc/s. Proc. Inst. Elec. Eng., **98**, Pt. 3, No. 51, 11-18 (1951).

Nicolet, M. Propositions pour une nomenclature de la haute atmosphère. Ann. Géophys., **6**, No. 4, 318-321 (1950).

Rawer, K. Sur la répartition approximative de l'ionisation de la couche *F*2 du point de vue mondial. Paris, C.-R. Acad. sci., **232**, No. 1, 98-100 (1951).

Reber, G. Motion in the solar atmosphere as deduced from radio measurements. Science, **113**, 312-314 (March 23, 1951).

Reber, G. La radio-astronomia. Cielo e Terra, **1**, Nos. 5-6, 8 (1950); **1**, Nos. 7-8, 4-7 (1950).
Ryle, M., and A. Hewish. The effects of the terrestrial ionosphere on the radio waves from discrete sources in the galaxy. Mon. Not. R. Astr., **110**, No. 4, 381-394 (1950).
Scott, J. C. W. The gyro-frequency in the arctic *E*-layer. J. Geophys. Res., **56**, No. 1, 1-16 (1951).
Schrott, R. Ein Echolotungsgerät für Ionosphären- und Wetterforschung. Arch. Met. Geophys. Biokl., A, **3**, Heft 2, 109-112 (1950).
Seeger, C. L., and R. E. Williamson. The pole of the galaxy as determined from measurements at 205 mc/sec. Astroph. J., **113**, No. 1, 21-49 (1951).
Shaw, I. J. Some further investigations of ionospheric cross-modulation. Proc. Phys. Soc., B, **64**, No. 373, 1-20 (1951).
Standards Committee. Standards on abbreviations of radio-electronic terms, 1951. Proc. Inst. Radio Eng., **39**, No. 4, 397-400 (1951).
Stanley, J. P. The absorption of long and very-long waves in the ionosphere. J. Atmos. Terr. Phys., **1**, No. 2, 65-72 (1950).
Stephenson, G. Calculation of relative transition probabilities for first negative bands of N_2^+. Proc. Phys. Soc., A, **64**, No. 374A, 209-210 (1951).
Sumi, M. Penetration of neutral particles into the upper atmosphere. Rep. Ionosphere Res. Japan, **4**, No. 3, 147-153 (1950).
Theissen, E. Schichtdaten der *F*2-Schicht der Ionosphäre nach dem Parabelmodell. Naturwiss., **37**, Heft 14, 334-335 (1950).
Tilton, E. P. V.H.F.: Why—How—When? Parts I and II. QST, **35**, No. 1, 40, 41, 88, and **36**, No. 2, 46-49 (1951).
Waldmeier, M. Radio-Helioskopie. Naturwiss., **38**, Heft 1, 1-4 (1951).
Whale, H. A., and J. P. Stanley. Group and phase velocities from the magneto-ionic theory. J. Atmos. Terr. Phys., **1**, No. 2, 82-94 (1950).
Wild, J. P. Observations of the spectrum of high-intensity solar radiation at metre wavelengths. II—Outbursts. Aust. J. Sci. Res., A, **3**, No. 3, 399-408 (1950).
Wild, J. P., and L. L. McCready. Observations of the spectrum of high-intensity solar radiation at metre wavelengths. I—The apparatus and special types of solar bursts observed. Aust. J. Sci Res., A, **3**, No. 3, 387-398 (1950).
Yabsley, D. E. Atmospheric noise levels at radio frequencies near Darwin, Australia. Aust. J. Sci. Res., A, **3**, No. 3, 409-416 (1950).
Yonezawa, T. On the variation in the *F*2-layer thickness after sunset. Rep. Ionosphere Res. Japan, **4**, No. 4, 226-230 (1950). [Short note.]

E—*Earth's Crust and Interior*

Birch, F. Recent work on the radioactivity of potassium and some related geophysical problems. J. Geophys. Res., **56**, No. 1, 107-126 (1951).
Brooks, C. E. P. Legacy of the ice-age. Met. Mag., **79**, No. 941, 321-323 (1950).
Bullen, K. E. Theoretical travel-times of *S* waves in the earth's inner core. Mon. Not. R. Astr. Soc., Geophys. Sup., **6**, No. 2, 125-128 (1950).
Chackett, K. F. K^{40} and the age of the atmosphere. Phys. Rev., **81**, No. 6, 1057 (1951).
David, T. W. E. The geology of the Commonwealth of Australia. London, Edward Arnold, 3 vols., xx + iv + 1365 and one volume of folding maps (1950). 24 cm.
Dobrin, M. B. Dispersion in seismic surface waves. Geophysics, **16**, No. 1, 63-80 (1951).
Eardley, A. J. Structural geology of North America. New York, Harper and Bros., 620 with 16 maps (1951). 29 cm.
Ewing, M., and F. Press. Crustal structure and surface-wave dispersion. Bull. Seis. Soc. Amer., **40**, No. 4, 271-280 (1950).
Flint, R. F., and E. S. Deevey, Jr. Radiocarbon dating of late-Pleistocene events. Amer. J. Sci., **249**, No. 4, 257-300 (1951).
Geophysical discussion, Royal Astronomical Society. The granitic layer. Observatory, **71**, No. 860, 15-19 (1951).
Godwin, H. Comments on radiocarbon dating for samples from the British Isles. Amer. J. Sci., **249**, No. 4, 310-307 (1951).

GOGUEL, J. ¿Que sabemos de la constitucion interna del globe? Bol. Cien. y Tecnol., Dep. de Asuntos Culturales, Unión Panamer., Washington, D. C., Núm. 3, 30-37 (noviembre 1950).
GOGUEL, J. M. Seismic refraction with variable velocity. Geophysics, **16**, No. 1, 81-101 (1951).
GUTENBERG, B. Travel times from blasts in southern California. Bull. Seis. Soc. Amer., **41**, No. 1, 5-12 (1951).
INGHAM, W. N., AND N. B. KEEVIL. Radioactivity of the Bourlamaque batholiths, Canada. Bull. Geol. Soc. Amer., **62**, No. 2, 131-148 (1951).
JEFFREYS, H. On the radioactivity of potassium. Ann. Géophys., **6**, No. 1, 10-17 (1950).
KINGDON-WARD, F. Notes on the Assam earthquake. Nature, **167**, No. 4239, 130-131 (1951).
KULP, J. L. Origin of the hydrosphere. Bull. Geol. Soc. Amer., **62**, No. 3, 326-329 (1951).
LIGHTHILL, M. J. On the instability of small planetary cores (II). Mon. Not. R. Astr. Soc., **110**, No. 4, 339-342 (1950).
MERRELL, R. H. The distribution and frequency of Alaskan earthquakes, 1939-1948. Bull. Seis. Soc. Amer., **40**, No. 4, 267-269 (1950).
MORELLI, C. Rilievo sperimentale gravimetrico-magnetico nell'avampaese dei Colli Euganei. Ann. Geofis., Roma, **3**, No. 4, 523-566 (1950).
MUKHERJEE, S. M. Microseisms and sea waves. Bull. Seis. Soc. Amer., **41**, No. 1, 1-4 (1951).
MURPHY, L. M. United States earthquakes, 1947. Washington, D. C., U. S. Dept. of Comm., Coast Geod. Surv., Ser. No. 730, 62 pp. (1950). 25 cm.
NININGER, H. H. A résumé of researches at the Arizona Meteorite Crater. Sci. Mon., **72**, No. 2, 75-86 (1951).
OULIANOFF, N. Considérations géologiques sur l'altimétrie de la région Sierra-Montana-Sion après le séisme du 25 janvier 1946. Bull. Lab. Géol. Min. Géophys., Musée Géol., Université de Lausanne, No. 94, 20 pp. (1949).
OULIANOFF, N. Séismes d'origine proche, dans les régions a tectoniques superposées. Extract, Pub. Bur. Centrale Séismologique Internat., Ser. A (Travaux Scientifiques), Fasc. 17, 133-142 (presented at the Oslo Assembly, 1948).
PANETH, F. A. The frequency of meteorite falls. Proc. R. Inst., **34**, No. 156, 375-381 (1950).
PETTERSSON, H. Through three oceans with the *Albatross*. Proc. R. Inst., **34**, No. 156, 341-351 (1950).
RAMSEY, W. H. On the instability of small planetary cores (I). Mon. Not. R. Astr. Soc., **110**, No. 4, 325-338 (1950).
RANKAMA, K., AND T. G. SAHAMA. Geochemistry. Chicago, University of Chicago Press, xvi + 912 (1950).
RICHTER, C. F. Velocities of *P* at short distances. Bull. Seis. Soc. Amer., **40**, No. 4, 281-289 (1950).
RICH, J. L. Three critical environments of deposition, and criteria for recognition of rocks deposited in each of them. Bull. Geol. Soc. Amer., **62**, No. 1, 1-19 (1951).
TANDON, A. N. The very great earthquake of August 15, 1950. Science and Culture, **16**, No. 4, 147-155 (1950).
TILLOTSON, E. The great Assam earthquake of August 15, 1950. Nature, **167**, No. 4239, 128-130 (1951).
VERHOOGEN, J. The adiabatic gradient in the mantle. Trans. Amer. Geophys. Union, **32**, No. 1, 41-43 (1951).
WILLMORE, P. L. The theory and design of two types of portable seismograph. Mon. Not. R. Astr. Soc., **6**, No. 2, 129-137 (1951).

F—*Miscellaneous*

BABCOCK, H. W. Stellar magnetic fields. Nature, **166**, No. 4215, 249-251 (1950).
BEAGLEY, J. W. Notes on solar activity and associated geophysical effects. N. Z. J. Sci. Tech., B, **31**, No. 1, 46-47 (1950). [Solar, magnetic, auroral, and ionospheric data on the N. Z.-U. S. A. circuit during disturbance of May 10-13, 1949.]
BULLEN, K. E. Origin of the moon. Nature, **167**, No. 4236, 29 (1951).
DAVIS, L., JR. The strength of interstellar magnetic fields. Phys. Rev., **81**, No. 5, 890-891 (1950).
ELLISON, M. A. The asymmetry of the flare Hα line. Observatory, **71**, No. 860, 33 (1951).

Hutchinson, W. C. A., and J. A. Chalmers. The electric charges and masses of single raindrops. Q. J. R. Met. Soc., 77, No. 331, 85-95 (1951).

International Council of Scientific Unions. The Fifth General Assembly of the International Council of Scientific Unions, held at Copenhagen, September 14 to 16, 1949. Reports of proceedings edited by F. J. M. Stratton, General Secretary. Cambridge, University Press, viii + 249 (1950). 25 cm.

Ionosphere Research Committee. Catalogue of disturbances in ionosphere, geomagnetic field, field intensity of radio wave, cosmic ray, solar phenomena, and other related phenomena. Provisional report of solar eclipse observation, Sept. 12, 1950. Science Council of Japan, Tokyo, No. 8, 26th co-operative observation, 14 pp. (1950).

Kuiper, G. P. On the origin of the solar system. Proc. Nat. Acad. Sci., 37, No. 1, 1-14 (1951).

Kuiper, G. P., and K. O. Kiepenheuer. Solar magnetic fields. Research Reviews, ONR, Washington, D. C., 15-17 (Feb. 1951).

Righini, G., e G. Godoli. Riduzione del materiale spettroeliografico raccolto alla torre solare di Arcetri nel periodo 1932-1949. Oss. e Mem. Osservatorio Astrofy. di Arcetri, Fasc. 66, 133-146 (1950).

Righini, G. e G. Godoli. Sui numeri caratteristici dell'attività solare. Ann. Geofis., Roma, 3, No. 4, 501-513 (1950).

Ruthe, K. Geophysikalisches (Nordpolargebiet und Südpolargebiet). Polarforschung, 2, Heft 1/2, 303-306 and 312-313 (1949).

Scott, W. E. List of recent publications. J. Geophys. Res., 56, No. 1, 140-146 (1951).

Ueberreiter, K. A statistical postwar survey on the natural sciences and German universities. Washington, D. C., Library of Congress, European Affairs Division, 33 pp. with 7 charts (1950). 24 cm.

Union of South Africa, Weather Bureau. Bibliography of regional meteorological literature, Vol. 1, Southern Africa, 1486-1948 (compiled by R. J. Venter). Pretoria, Govt. Printer, W. B. 12, 412 pp. (1950). 30 cm. [A classified bibliography of the literature dealing with meteorological matters in Southern Africa.]

United Nations Educational, Scientific and Cultural Organization (Unesco). Directory of international scientific organizations. Paris, Unesco, Pub. 619, xiii + 224 (1950). 24 cm. [Gives information on international organizations whose activities deal with the various branches of science.]

Waldmeier, M. Spektral photometrische Klassifikation der Protuberanzen. Zs. Astroph., 28, Heft 2, 208-218 (1951).

Waldmeier, M. Provisional sunspot-numbers for October to December, 1950. J. Geophys. Res., 56, No. 1, 130 (1951).

Woolley, R. v. d. R., and C. W. Allen. Ultra-violet emission from the chromosphere. Mon. Not. R. Astr. Soc., 110, No. 4, 358-372 (1950).

NOTICE

When available, single unbound volumes can be supplied at $3.50 each and single numbers at $1 each, postpaid.

Charges for reprints and covers

Reprints can be supplied, but prices have increased considerably and costs depend on the number of articles per issue for which reprints are requested. It is no longer possible to publish a schedule of reprint charges, but if reprints are requested approximate estimates will be given when galley proofs are sent to authors. Reprints without covers are least expensive; standard covers (with title and author) can be supplied at an additional charge. Special printing on covers can also be supplied at further additional charge.

Fifty reprints, without covers, will be given to institutions paying the publication charge of $4.00 per page.

Alterations

Major alterations made by authors in proof will be charged at cost. Authors are requested, therefore, to make final revisions on their typewritten manuscripts.

Orders for back issues and reprints should be sent to Editorial Office, 5241 Broad Branch Road, N.W., Washington 15, D.C., U.S.A.

Subscriptions only are handled by The Johns Hopkins Press, Baltimore 18, Maryland, U.S.A.

CONTENTS—Concluded